Investigation into the roles of HP1γ, H3.3 and HIRA in gene regulation *in vivo*

By

Bing Liang

A thesis submitted in partial fulfilment of the requirement for the Degree of
Doctor of Philosophy
at Imperial College London
Department of Medicine

2019

Abstract

This thesis addresses two distinct aspects of chromatin regulation *in vivo* in mice; the chromatin remodeler HIRA and the heterochromatin binding protein HP1γ.

To date, H3.3 has been largely studied *in vitro* and reported to be enriched at promoters, bodies of active genes and some regulatory elements throughout the cell cycle by its chaperone HIRA and has been described as an 'active mark' for transcription. Moreover, H3.3 is also targeted to telomeric and pericentric heterochromatin regions by the DAXX/ATRX complex. However, the *in vivo* function of H3.3 in mammalian systems is still largely unknown.

In this thesis, we showed that in the HIRA KO compared to WT, there was an apparent abnormal presence of a memory T cell population in the mouse thymus indicated by CD44 expression on CD4 and CD8 single positive T cells, and an increased population of CD44 expressing cells in the lymph node and spleen. Thus, either CD44 gene expression is directly affected by HIRA KO or the T cell differentiation program is altered or both. Moreover, TCRα V(D)J recombination seems to be impaired by HIRA KO. This might imply that HIRA chromatin remodeling or the presence of H3.3 might be important for TCR recombination.

Recently the importance of Heterochromatin Protein 1 γ (HP1γ) in regulating sex differences was demonstrated in our lab. In this thesis, sex dimorphism in proliferation was investigated and we showed that male embryonic fibroblasts (MEFs) proliferate faster than female MEFs, which is consistent with previous observations that the embryonic growth rate is higher in male compared with female mammals. HP1γ KO completely abolished the sex difference in proliferation. To determine whether this sex-regulatory effect of HP1γ was a more general phenomenon, recently, RNA-seq analysis was performed in the lab on both male and female

MEFs, with or without HP1γ. Strikingly, males showed a higher dependency on HP1γ in maintaining their normal gene expression profile compared to females. RNA splicing analysis of the RNA-seq data suggested that the sex difference in gene expression was not a result of difference in splicing and vice versa. Similarly, HP1γ KO exerted a bigger impact in males in terms of alternative splicing where there are many more genes found to be alternatively spliced upon HP1γ KO in males than females. This was consistent with the results of Mass Spectrometry following pulldown of MEF-derived proteins with HP1γ antibody which revealed splicing factors in the male but not the female samples. Consistent for a role for HP1γ in regulating sex dimorphism in alternative splicing, HP1γ KO ameliorated this dimorphism.

The emerging evidence of an activating role of HP1γ in euchromatin brings the possibility that HP1γ and HIRA/H3.3 may interact to regulate gene expression in euchromatin. Especially with the recent observation in our lab that shows co-localization between HP1γ and H3.3 in MEFs by co-immunoprecipitation.

Therefore, it is important to further investigate the interaction of HP1γ with H3.3 and the role of HP1γ as a key epigenetic modifier in defining sexually dimorphic gene expression in males and females and its role in cellular proliferation in order to shed light on the largely unexplained sex bias previously reported in normal physiology and diseases.

Declaration of Originality

I confirm that this thesis and the research described within it is entirely my own original work. Any reference to the ideas or work of other people is fully accredited within the document.

Copyright Declaration

The copyright of this thesis rests with the author. Unless otherwise indicated, its contents are licensed under a Creative Commons Attribution-Non Commercial-No Derivatives 4.0 International License (CC BY-NC-ND).

Under this license, you may copy and redistribute the material in any medium or format on the condition that; you credit the author, do not use it for commercial purposes and do not distribute modified versions of the work.

When reusing or sharing this work, ensure you make the license terms clear to others by naming the license and linking to the license text.

Please seek permission from the copyright holder for uses of this work that are not included in this license or permitted under UK Copyright Law.

Acknowledgments

First and foremost, I would like to express my sincere gratitude to my supervisor Prof. Richard Festenstein (without whom this thesis would not have been possible) for his help and guidance throughout my PhD. I truly appreciate his patience and all the supports in the lab as well as my personal life. He was responsible and reachable during my thesis writing-up.

I would like to thank Dr Michael Jones for his supervision and support during my master study. He was reachable and considerate throughout my whole study at Imperial College London.

I would like to thank Dr Jackson Ping Kei Chan and Dr Pui Pik Law for their direct supervision, continuing encouragements and advice in the lab. I would like to extend my sincere thanks to all my colleagues in the 'Gene Control Mechanisms and Disease' team.

Many thanks to our collaborators:

Dr. Masahide Asano for providing the HP1γ knockout mice used in this study.

Dr. Buhe Nashun, Dr. Petra Hajkova and Dr. Vineet Sharma for providing the H3.3B-EGFP mouse model used in this study.

Bioinformatics core facility at the LMS for their help in transcriptomic and RNA splicing analysis.

Axel Imhof (Munich) for Mass Spectrometry proteomics analysis.

Abbreviations

APS	Ammonium persulphate
Ap1m1	Adaptor-related protein complex AP-1, mu subunit 1
A	Alanine
ac	Acetylation
AHSP	Alpha-hemoglobin-stabilizing protein
APS	Ammonium persulphate
ATRX	Alpha-thalassemia/mental retardation X-linked syndrome
Asb7	Ankyrin repeat and SOCS box containing 7
ASF	Alternative splicing factor
ASF1a	Anti-silencing function 1a
b-ac	Mouse beta actin
bp	Base pair
BSA	Bovine Serum Albumin
C	Cytosine
CAF-1	Chromatin assembly factor-1
CaCl2	Calcium Chloride
CAF1	Chromatin assembly factor 1
CABIN1	Calcineurin binding protein 1
C terminal	Carboxyl terminal
CBX	Chromobox
Cbx3	Chromobox protein homolog 3
CD	Chromo domain
CD2	Cluster of differentiation 2
CD4	Cluster of differentiation 4
CDS	Coding sequence
cDNA	Complementary deoxyribonucleic acid
Chd2	Chromodomain helicase DNA-binding domain 2
ChIP	Chromatin Immunoprecipitation
ChIP-seq	Chromatin immunoprecipitation sequencing
Ct	Cycle threshold
cm	centimeter
CO2	Carbon dioxide
CKO	Conditional knock out
CSD	Chromo-shadow domain
CTE	Carboxyl terminal extension
Ct	Cycle threshold
D	Diversity segment
DAXX	Death domain associated protein
Dax1	DSS–AHC-critical region of the X chromosome 1
DEPC	Diethyl Pyrocarbonate

DGS	DiGeorge syndrome
DHS	DNA hypersensitive site
DGKz	Diacylglycerol Kinase Zeta
DMSO	Dimethyl sulfoxide
DNA	Deoxyribonucleic acid
DNAse	Deoxyribonuclease
DNMT	DNA methyltransferase
dNTPs	Deoxynucleotide Triphosphate
DP	Double positive
dsRNA	double stranded RNA
DTT	Dithiothreitol
ES cells	Embryonic stem cells
ESCs	Embryonic stem cells
ECL	Enhanced Chemiluminescence
E13.5	Embryonic day 13.5
EDTA	Ethylenediaminetetraacetic acid
EGFP	Enhanced Green Fluorescent Protein
FACS	Fluorescent activated cell sorting
F	Female
FBS	Fetal bovine serum
FSC	Forward scatter
g	Gravity
G	Guanine
Gapdh	Glyceraldehyde 3-phosphate dehydrogenase
Gdi	Guanosine diphosphate (GDP) dissociation inhibitor 1
GFP	Green fluorescence protein
GO	Gene Ontology
GSEA	Gene Set Enrichment Analysis
H	Histone
h	Human
H3f3a	H3 histone, family 3A
H3f3b	H3 histone, family 3B
H3.3	Histone 3.3
H3K9me3	Trimethylated histone H3 lysine 9
HAT	Histone acetyltransferase
HCI	Hydrochloric Acid
HDAC	Histone deacetylase
HDM	Histone demethylase
HIRA	Histone regulator A
HET	Heterozygous
Hin	Hinge domain
HMTases	Histone methyltransferase

hnRNPs	Heterogeneous nuclear ribonucleoproteins
HKMT	Histone lysine methyltransferase
HOM	Homozygous
HP1	Heterochromatin protein 1
HRP	Horse Radish Peroxidase
HSP	Heat shock protein
IgG	Immunoglobin G
IgH	Immunoglobulin heavy chain
J	Joining segment
K	Lysine
kb	Kilobase
KCl	Potassium Chloride
kDa	Kilo Dalton
KD	Knockdown
kg	Kilo gram
KO	Knock out
M	Male
M	Molar
Magohb	Mago-nashi homolog B
Me	Methylation
me2	Di-methylation
me3	Tri-methylation
mESC	Mouse embryonic cell
mg	Mini gram
MgCl2	Magnesium Chloride
MHC	Major histocompatibility complex
min	Minute
mM	Mini molar
ml	Mini liter
mm	Millimeter
mRNA	Messenger ribonucleic acid
MNase	Micrococcal Nuclease
MS	Mass Spectrometry
MRG15	MORF-related gene on chromosome 15
MW	Molecular weight
Mtf2	Metal response element binding transcription factor 2
Neurod6	Neurogenic differentiation 6
N terminal	Amino terminal
nm	Nanometer
ng	Nanogram
NaOH	Sodium hydroxide
NaOAc	Sodium acetate

NaCl	Sodium Chloride
NFR	Nucleosome free region
ng	Nano gram
NPC	Neural Progenitor Cell
Neurod6	Neurogenic differentiation 6
Oct4	Octamer-binding transcription factor 4
P	Phosphorylation
PBS	Phosphate buffered saline
PCNA	Proliferating cell nuclear antigen
PCR	Polymerase chain reaction
Pdx1	Pancreatic and duodenal homeobox 1
PEV	Position effect variegation
Pg	Picogram
PI	Propidium iodide
PMSF	Phenylmethanesulfonylfluoride
PML-NB	Promyelocytic leukemia nuclear bodies
PTB	Polypyrimidine tract-binding protein
PTM	Post translational modification
Q	Long arm of chromosome
Q-RTPCR	Quantitative real time polymerase chain reaction
RAG	Recombination activating gene
RCAF	Replication coupling assembly factor
RIPA	Radio-immunoprecipitation assay
RNA	Ribonucleic acid
RNAP	Ribonucleic acid polymerase
RNAP II	Ribonucleic acid polymerase II
RNAse	Ribonuclease
RNAse A	Ribonuclease A
RNAi	Ribonucleic acid interference
Rnf167	Ring finger protein 167
RT	Reverse transcriptase
RPA	Replication protein A
RPM	Revolutions Per Minute
RSS	recombination signal sequence
S	Serine
SAHF	Senescence associated heterochromatin foci
SCNT	Somatic Nuclear Transfer
SD	Standard deviation
SDS	Sodium dodecyl sulphate polyacrylamide gel
SEM	Standard error of the mean
SF 2	Splicing factor 2
S phase	Synthesis phase

sec	Second
seq	Sequencing
siRNA	Small interfering ribonucleic acid
SILAC	Stable isotope labelling by/with amino acids
SP	Single positive
Srp19	Signal recognition particle 19
Sry	Sex determining region of chromosome Y
SRp20	Serine/Arginine-rich protein 20
SSC	Side scatter
SUV39h	Histone H3 lysine 9 methyltransferases Suppressor of variegation 3-9 homologue
SWI/SNF	SWItch/ Sucrose Non-Fermentable
T	Thymine
TAE	Tris/acetate/EDTA
TBE	Tris/Borate/EDTA
TBS	Tris buffered saline
Tbxa2r	Thromboxane A2 receptor
TCR	T cell receptor
TDPCR	Touch down polymerase chain reaction
TE	Tris/EDTA
TEMED	Tetramethyl ethylenediamine
TES	Transcription end site
TFBS	Transcription factor binding site
tRNA	Transfer RNA
Tris	Tris (hydroxymethyl) aminomethane
TSS	Transcription start site
U	Ubiquitination
UBN1	Ubinuclein 1
U	Unit
UTR	Untranslated region
V	Voltage
V	Variable region
vol	Volume
wt	Weight
WT	Wild type
µg	Micro gram
µl	Microliter
µm	Micro meter
µM	Micro molar
°C	Celsius

Table of Contents

List of Figures and Tables

Chapter 1

Fig 1.8.5. Antigen receptor variable exons are assembled by V(D)J recombination.

Fig 1.8.6. Schematic model of V(D)J recombination.

Fig 1.9.1. Schematic diagram of sex determination model.

Fig 1.9.2. FCG mice are produced by breeding XX gonadal females with XY−*Sry* gonadal males, producing the four genotypes shown.

Chapter 2

Chapter 3

Fig 3.3.2. Illustration of T cell development with indicated transferrin receptor CD71 expression in mouse thymus.

Fig 3.3.3. CD71 cell sorting process by FACS.

Fig 3.3.4. QRT-PCR showing the expression level of HIRA in CD71+ and CD71- thymocytes in mice.

Fig 3.3.5. Western blot showing the detection of HIRA in mouse thymocytes.

Fig 3.3.6. An illustration of TCR rearrangement during T cell development with CD44 expression.

Fig 3.3.7. V(D)J recombination of the TCRα loci in CD71- DP T cells (upper) and CD71+ DP T cells (lower).

Fig 3.3.8. Schematic diagram showing the organization of mouse *TCRα* genes.

Chapter 4

Fig 4.1.1. Volcano plot showing the differentially expressed genes in HP1γ wild-type MEFs compared to HOM MEFs.

Fig 4.1.2. Sexual dimorphic gene expression in WT MEFs and their sexual dimorphic response to HP1γ KO.

Fig 4.2.1. Growth curve of male and female HP1γ WT and HP1γ KO MEFs.

Fig 4.2.2. Bar chart showing the cell-cycle analysis in MEFs in Males and Females.

Fig 4.3.1. Tables illustrating a list of proteins found associated with HP1γ by Mass Spectrometry (MS) in each group.

Fig 4.3.2. Scatter Plot of comparison on HP1γ protein binding profiles between female and male by MS.

Fig 4.3.3. String network of proteins that were only identified in HP1γ IP but not in IgG IP.

Fig 4.3.4. Schematic diagram of the exclusion and inclusion isoforms for the five models of Alternative Splicing (AS) events that were examined in this thesis.

Fig 4.3.5. Schematic diagram showing little overlap between genes that are sexually dimorphic in expression and genes that are sexually dimorphic in alternative splicing in male and female MEFs for the five models of AS events that were investigated in this thesis.

Fig 4.3.6. Schematic diagram showing the overlap between genes that are sexually dimorphic in alternative splicing, genes that are differentially spliced upon HP1γ KO in males and genes that are differentially spliced upon HP1γ KO in females.

Fig 4.3.7. Schematic diagram showing the overlap between genes that are sexually dimorphic in alternative splicing and genes that are differentially spliced upon HP1γ KO in males compared to WT females.

Fig 4.3.8. Schematic diagram showing the overlap between genes that are sexually dimorphic in alternative splicing and genes that are differentially spliced upon HP1γ KO in females compared to WT males.

Fig 4.4.1. ChIP-seq profiles of HP1γ enrichment on *Msn* gene on Xa chromosome in HCT116 cells and immortalized MEFs.

Fig 4.4.2. ChIP-seq profiles of HP1γ enrichment on *Msn* gene on both Xa and Xi chromosomes in HCT116 cells and immortalized MEFs.

Fig 4.4.3. ChIP-seq profiles of HP1γ enrichment on *Zfx* and *Eif2s3x* genes in HCT116 cells and immortalized MEFs.

Fig 4.5. Cell cycle arrest by *Cdkn2a*.

Supplementary

Fig S1. Representative genotyping results.

Fig S2. GFP expression as measured by Flow cytometry.

Fig S3. Representative gel for sheared chromatin.

Fig S4. FACS plots showing different T cell marker expression in different cell population in mouse thymus, lymph node and spleen.

Fig S5. Validation of co-immunoprecipitation experiment.

Fig S6. Scatter Plot of comparison between HP1γ IP vs IgG IP in female sample.

Fig S7. Representative result obtained from Bioanalyzer High Sensitivity DNA Analysis for checking size and quality of ChIP sequencing library.

Fig S8. Cell-cycle analysis as assessed by PI staining using flow cytometry (FACS)

Fig S9. FACS plots showing CD4, CD8, CD71 and EGFP expression during CD71 cell sorting.

Fig S10. Gene expression level of Cdkn2a in original RNA-seq samples.

Fig S11. List of genes with either higher expression in WT male compared to WT female or *vice versa* in MEFs.

Fig S12. Average profile plot for H3.3B-EGFP enrichment of genes grouped into four tiers by expression level in HP1γ WT and HOM MEFs.

Fig S13. Schematic diagram showing the model of the regulation of CD44 splicing by H3K9me3 and HP1γ.

Fig S14. List of genes of which alternative splicing was sensitive to HP1γ KO in males and females respectively.

Fig S15. Genes that were equalized with respect to SE between the sexes in males and genes that acquired difference between the sexes in females with respect to SE upon HP1γ KO.

Fig S16. Relative enrichment of H3.3 on *Gapdh*, *Pdx1* and *Neurod6* genes in HIRA WT and HIRA HOM CKO thymocytes as revealed by ChIP.

Chapter 1 - Introduction

1.1 Epigenetics

The term '*epigenetics'* was introduced by Conrad Waddington who defined it as the interactions between the environment and the genes that leads to the development from genotype to phenotype (Waddington, 1940). Nowadays, epigenetics is generally accepted as the study of heritable changes in gene function without changing in DNA sequence (Wu and Morris, 2001). Epigenetic changes are initiated and maintained by three systems: covalent modifications of DNA bases (DNA methylation), posttranslational modifications of the amino-terminal tail of histones and small regulatory RNAs-associated gene silencing (Egger *et al*., 2004). The epigenome for each cell is distinct, which give rise to cellular differentiation under a common genome. Disruptions of the 'epigenome' have been associated with cancer, neurological disease, autoimmune disorders and imprinting disorders (Moosavi and Motevalizadeh Ardekani, 2016). In this thesis, different epigenetic factors and their roles in gene regulation will be described and discussed.

1.2 Chromatin organization

Development of specific cell types requires activation and repressing of specific genes in a highly coordinated manner. The way genes are packaged in chromatin sets up the cell-type specific epigenome facilitating differentiation of cells for specific functions. To accommodate a large amount of genetic material, DNA is packed with core histone proteins into a condensed structure called chromatin (Alberts B, 2002a). The dynamic structure of chromatin not only can condense the DNA in the nuclear compartment, but also compact the DNA for mitosis and meiosis and regulates gene expression. Nucleosomes are the basic subunit of chromatin and consist of 147bp DNA wrapped in 1.7 negatively supercoiled turns around the nucleosome core particle comprised of two H3–H4 and two H2A–H2B histone dimers (Hubner *et al*., 2013) (Fig 1.1). Nucleosomes are separated from each other by 10–80 bp linker DNA associated with linker histone H1 (Felsenfeld and Groudine, 2003). The binding of linker histone H1 to the entry/exit sites of DNA on the surface of the core particle can further compact chromatin structure into a higher-order transcriptionally inactive 30nm fiber from the smaller "beads on a string" fibers of approximately 10-11nm (Jiang and Pugh, 2009). This 30nm fiber contains 6–11 nucleosomes per turn which has been proposed to progressively form even higher order chromatin fibers in interphase (Belmont and Bruce, 1994), and larger fibers of 100–200 nm chromonema structure in mitotic chromosomes (Rattner and Lin, 1985, Widom and Klug, 1985). Each core histone protein has an unstructured amino-terminal (N-terminal) polypeptide 'tail' sticking out from the nucleosome core which allows a diversity of post translational modifications (PTMs) to happen (Loyola and Almouzni, 2007). The existence of a large variety of PTMs and multiple H1 subtypes brings about a considerable degree of complexity to the chromatin.

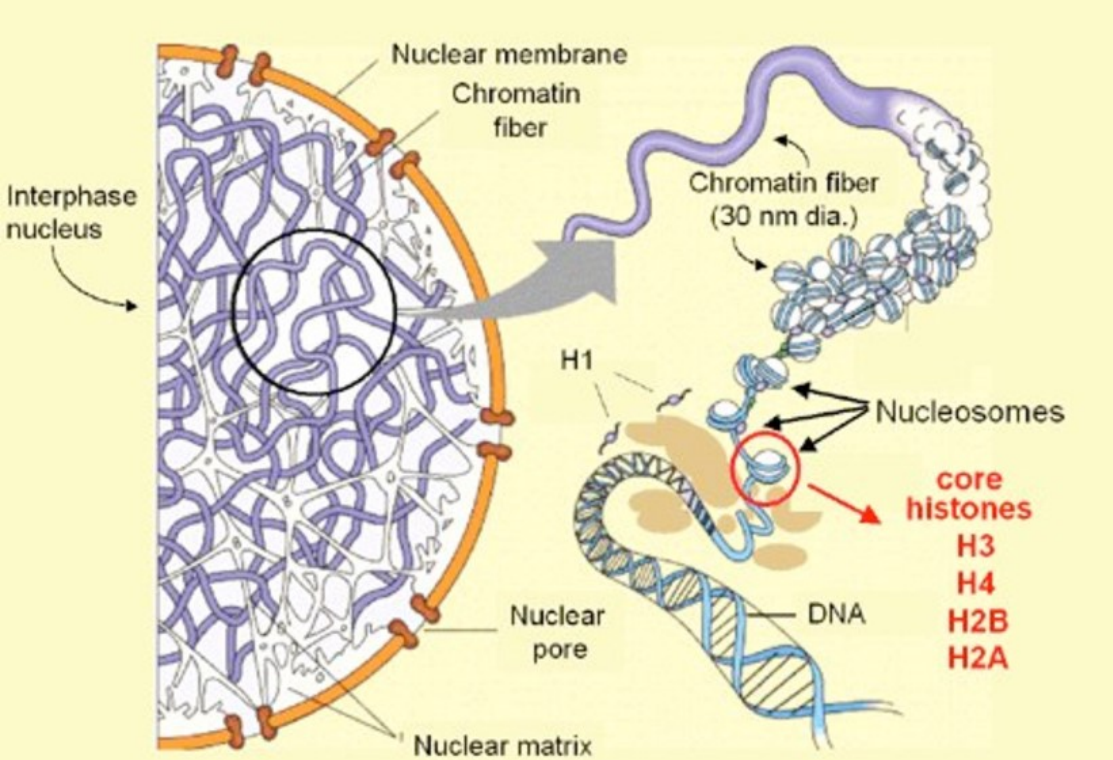

Fig 1.1. Schematic diagram of chromatin organization. *Genomic DNA is packed in the nucleus by wrapping around the nucleosomes and forms a 'beads on- a-string' organization. Linker histone H1 assists further compaction which is thought to trigger formation of the 30nm fiber. Heterochromatin is formed by fiber-fiber interaction. This figure is adapted with permission from "Role of epigenetic modifications in acute promyelocytic leukemia" Raffaella Villa (Villa, 2009).*

1.2.1 Euchromatin and Heterochromatin

Chromatin of two distinct structures was first described on the basis of cytogenetic observations that 'heterochromatin' in the nucleus remained condensed whereas 'euchromatin' underwent cycles of condensation and de-condensation throughout the cell cycle (Straub, 2003). They are located in distinct environments from a chromatin point of view (Bannister and Kouzarides, 2011). These two types of chromatin show different organizations and features which contribute to the various influences on gene regulation. The euchromatin is a relatively "open" environment which contains most of the active genes and undergoing "rise and fall" changes during cell cycle (Alberts B, 2002b). In contrast, heterochromatin, such as centromeres and telomeres, are relatively more compact structures. Placement of genes near to

these regions as a result of chromosomal rearrangement or insertion results in their silencing. This position effect variegation (PEV) phenomenon was first observed in Drosophila (Muller, 1930). Nucleosome turnover is a highly dynamic process and the turnover rate differs across the genome that are likely to have functional importance for epigenome maintenance, gene regulation, and control of DNA replication by chromatin modifications, chromatin remodelers, histone chaperones and histone variants during transcription (Venkatesh and Workman, 2015).

Euchromatin, which is actively transcribed, possesses a higher nucleosome turnover rate compared to heterochromatin which is highly compacted and inaccessible (Dion *et al*., 2007, Deal *et al*., 2010, Rufiange *et al*., 2007). In multicellular organisms, two distinct heterochromatic environments have been defined: Facultative heterochromatin (fHC) and Constitutive heterochromatin (cHC). cHC contains permanently silenced genes located at regions such as the centromeres and telomeres. It is always characterized by relatively high levels of H3K9me3 and HP1α/β (Trojer and Reinberg, 2007). fHC are genomic regions containing genes that are differentially expressed through development and differentiation. Like cHC, fHC is also transcriptionally silent but retains the potential to interconvert between heterochromatin and euchromatin. One example of fHC is the inactive X chromosome in female that becomes active when it is passed on to male child and this temporarily inactive fHC is called Barr body (Priyadharscini and Sabarinath, 2013).

Euchromatin is usually marked by the presence of active post-translational histone modifications such as histone H3 lysine 4 trimethylation (H3K4me3) and histone H3 lysine 9 acetylation (H3k9ac) (Bannister and Kouzarides, 2011). By contrast, heterochromatin is gene poor and genes within this region are frequently repressed by silencing histone marks including histone H3 lysine 9 trimethylation (H3K9me3) and histone H3 lysine 27 trimethylation

(H3K27me3) (Bannister and Kouzarides, 2011). A schematic illustration of comparison between euchromatin and heterochromatin including the major features possessed by two chromatin states is showing in Fig 1.2.

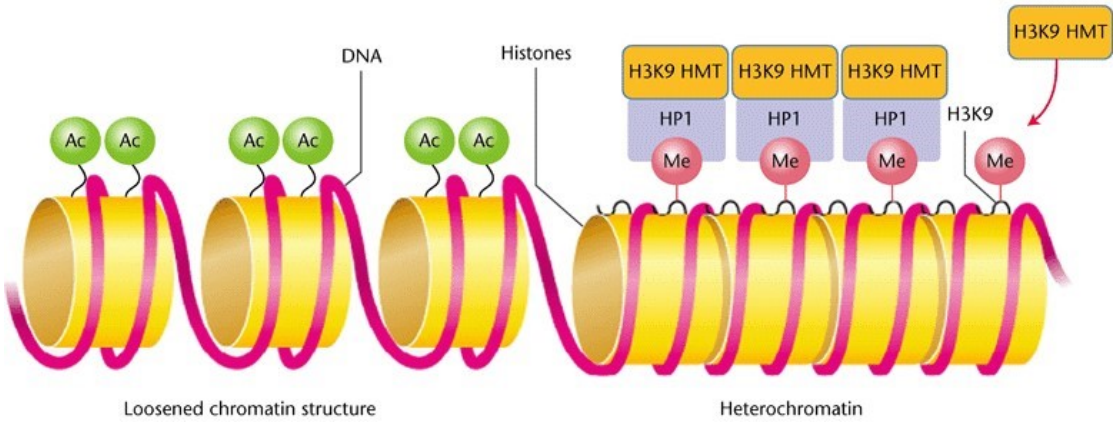

EUCHROMATIN	HETEROCHROMATIN
Low DNA density	High DNA density
Gene rich	Gene poor
Actively participate in transcription	Little or no transcriptional activity
Loosely coiled	Compactly coiled
Early replicative	Late replicative
Genetically active	Genetically inactive
Hypomethylated DNA	Enriched DNA methylation
Acetylation on H3/H4	Hypoacetylation on H3/H4
Methylated on H3K4	Methylated on H3K9 and H3K27

Fig 1.2. Schematic diagram demonstrating the organisation of Euchromatin and Heterochromatin. *Euchromatin is characterised by its relatively open structure whereas heterochromatin is tightly compacted in the nucleus. The two forms of chromatin show distinct epigenetic profile features. Key features of each form of the chromatin is summarised in the table below the diagram. This figure is adapted with permission from "Heterochromatin and Euchromatin" Joel C Eissenberg and Sarah CR Elgin (Eissenberg, 2014)*

1.3 The “epigenetic code” - Histone Modifications

Position effect variegation (PEV) occurs when a gene is abnormally close to a block of heterochromatin which results in gene silencing in a proportion of the cells that would normally express it. PEV has been intensely studied in *Drosophila* on the *white* gene (Girton and Johansen, 2008). A diagram of PEV in *Drosophila* is shown in Fig. 1.3.1. This phenomenon is highly conserved from *Schizosaccharomyces pombe* (*S. pombe*) (Allshire *et al*., 1994) to mammals (Festenstein *et al*., 1996, Festenstein *et al*., 1999). Extensive screenings for dominant mutations that suppress or enhance *white* variegation in *Drosophila* have identified many conserved epigenetic modifiers, including the histone H3 lysine 9 methyltransferase SU(VAR)3-9 and heterochromatin protein HP1 (Elgin and Reuter, 2013). HP1a binds H3K9me2/3 and interacts with SU(VAR)3-9 at pericentric heterochromatin leading to the idea of a “histone code” in the core memory system (Elgin and Reuter, 2013). A similar system operates at fHC to silence homeobox (*hox*) genes in *Drosophila* Polycomb (Pc) where the Polycomb chromodomain (CD) also recognizes a histone methylation mark, in this case, H3K27me3 (Bernstein *et al*., 2006, Fischle *et al*., 2003, Kassis *et al*., 2017).

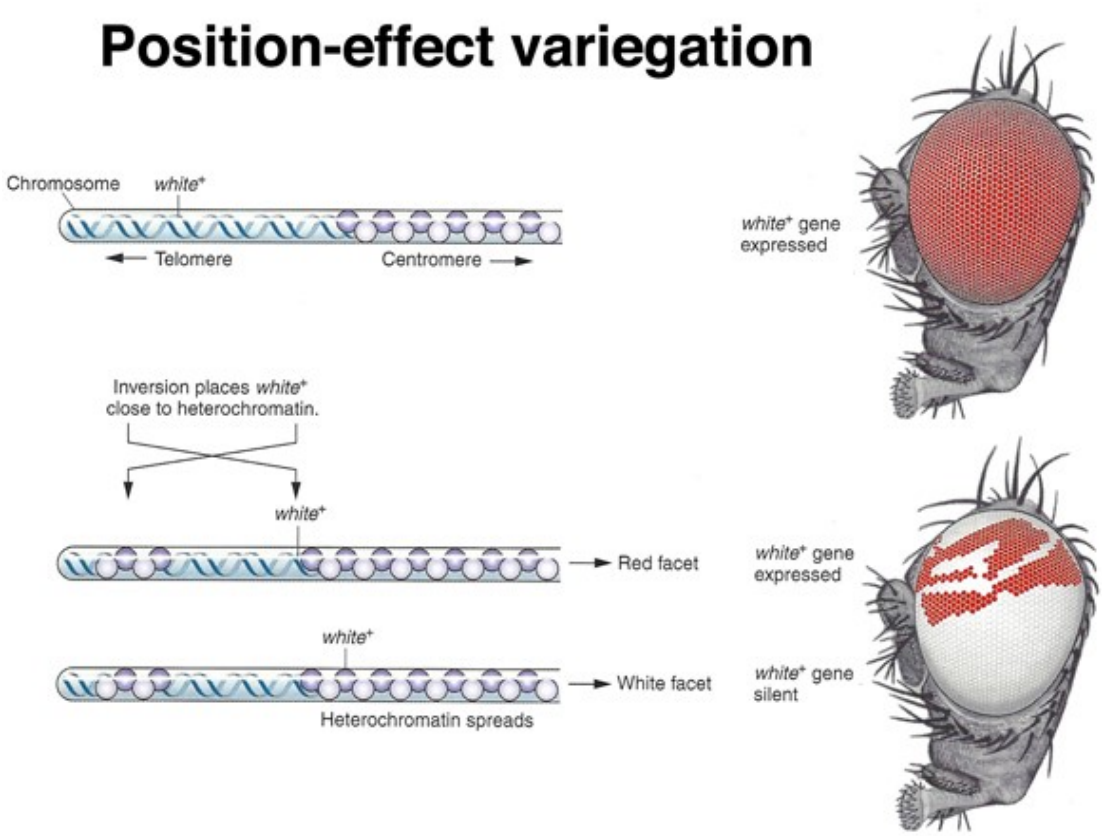

Fig 1.3.1. Model of Position effect variegation (PEV) in Drosophila. *In the chromosome, there is a barrier that marks the euchromatin-heterochromatin boundary. When a new euchromatin-heterochromatin junction is created because of the inversion, it lacks a boundary, and some of the euchromatin, including that containing the white gene, becomes heterochromatic and transcriptionally inactivated and hence the variegated red eye color in a proportion of cells in Drosophila eye. This figure is adapted with permission from http://www.discoveryandinnovation.com/BIOL202/notes/lecture18.html*

The "Histone code" hypothesis has been used to describe the consequences of different PTMs brought to enable variable DNA functions (Marino-Ramirez *et al*., 2005). To date, there are at least 8 different histone modifications (acetylation, methylation, phosphorylation, deimination, β-N-acetylglucosamine, ADP ribosylation, ubiquitylation and sumoylation, histone tail clipping and histone proline isomerization) (Bannister and Kouzarides, 2011) (Fig 1.3.2).

Chromatin Modifications	Residues Modified	Functions Regulated
Acetylation	**K**-ac	Transcription, Repair, Replication, Condensation
Methylation (lysines)	**K**-me1 **K**-me2 **K**-me3	Transcription, Repair
Methylation (arginines)	**R**-me1 **R**-me2a **R**-me2s	Transcription
Phosphorylation	**S**-ph **T**-ph	Transcription, Repair, Condensation
Ubiquitylation	**K**-ub	Transcription, Repair
Sumoylation	**K**-su	Transcription
ADP ribosylation	**E**-ar	Transcription
Deimination	**R > Cit**	Transcription
Proline Isomerization	**P-cis > P-trans**	Transcription

Fig 1.3.2. Different classes of histone modifications (PTMs) identified on histone variants. *The functions that have been associated with each modification are shown in the table. This figure is adapted with permission from "Chromatin modifications and their function" Kouzarides T. (Kouzarides, 2007)*

The chromatin-modifying enzymes that catalyze major PTMs involve histone acetyl transferases (HATs), histone deacetylases (HDACs), kinases, phosphatases, and histone lysine methyltransferases (HKMT). These enzymes can be recruited to target sites by sequence-specific DNA-binding transcription factors or more general features of the DNA such as its global CG content and DNA methylation status which can be read by the DNA-binding Zn-finger CxxC domain present in many chromatin-modifying enzymes (Voo *et al*., 2000). In reverse, factors associated with the transcriptional machinery can directly lead to the

accumulation of specific marks such as H3K4me3 and H3K36me3. HDACs and HATs acts in the opposite way, which catalyze the removal and adding of acetyl groups of lysine residues respectively. There are two major classes of HATs: type-A and type-B. The type A are nuclear HATs and type-B HATs are predominantly cytoplasmic which only acetalize free histones but not those already deposited into chromatin (Bannister and Kouzarides, 2011). Like histone acetylation, the phosphorylation of histones is highly dynamic and controlled by kinases and phosphatases that perform addition and removal of the phosphate group respectively (Oki *et al*., 2007). Phosphorylation takes place on serine (S), threonine (T) and tyrosine (Y) residues that one mainly located in the N-terminal tails (Bannister and Kouzarides, 2011). Histone methylation mainly occurs on the side chains of lysine (K) and arginine (R) residues. Unlike acetylation and phosphorylation, histone methylation does not alter the charge of the histone protein (Bannister and Kouzarides, 2011). Furthermore, di- or tri-methylation of lysine (K) residues and symmetrical or asymmetrical di-methylation of arginine (A) residues add additional level of complexity to the chromatin structure and gene regulation (Ng *et al*., 2009, Bedford and Clarke, 2009, Lan and Shi, 2009).

Transcriptionally active and silent chromatin is characterized by distinct histone posttranslational modifications (PTMs) or combinations thereof. High levels of lysine acetylation on the H3 and H4 tails, trimethylation of H3 lysine 4 and trimethylation of H3 lysine 36 are found on active genes (Zhang *et al*., 2015). In contrast, methylation of H3 lysine 9 and methylation of H3 lysine 27 and hypoacetylated forms of H3 are generally enriched at transcriptionally silent regions (Loyola *et al*., 2006) but H3K9me3 has also been suggested to be associated with some transcribed active genes (Vakoc *et al*., 2005). Lysine 9 has been shown to be the only lysine residue that pre-existed before chromatin assembly. The H3.1 and H3.3 show distinctions in K9 modifications.H3.1 contains more K9me1 whereas, H3.3

presents other modifications including K9/K14 diacetylated (Ac/K9 and K14) and K9me2 (Loyola *et al*., 2006). This is important as it defines when PTMs are imposed and also affect PTMs occurrence. For instance, although H3k9me3 was not found on both H3.1 and H3.3 prior to deposition, those pre-existed modifications on H3 variants can enhance the action of Suv39HMTase to produce H3K9me3 as found in pericentric heterochromatin after chromatin assembly (Loyola *et al*., 2006). This observation implicates that initial modifications on histone variants before assembly influence the final PTMs within chromatin.

We now know that histone modifications not only regulate chromatin structure by merely being there, but they can directly influence chromatin structure. For instance, acetylation on lysine residues can reduce the positive charge of histones, hence weakening their interaction with negatively charged DNA and increasing nucleosome fluidity (Workman and Kingston, 1998). Moreover, different modifications can cross-talk with each other (Bannister and Kouzarides, 2011) and PTMs could function as a signal platform to recruit chromatin modifiers to local chromatin, which determine the functional outcome of certain PTMs (Yun *et al*., 2011). An illustration of different histone modifications and different type of cross-talks between them is showing in Fig 1.3.3. The cross-talk provides an added level of complexity which helps to fine-tune the overall control. For example, HP1 binds to H3K9me2/3 in heterochromatin, but during mitosis, phosphorylation of serine 10 on histone H3 ejects HP1 from chromatin which allows condensins to access chromatin to promote mitotic chromatin condensation (Fischle et al., 2005, L Dormann et al., 2007). Moreover, PTMs cross-talk allows effective conversion from phosphorylation-based signals to acetylation-based actions in response to cellular stimuli (Yang and Seto, 2008). To conclude, distinct histone variant performs unique function in addition to their role in DNA packaging by two possible mechanisms: (1) Switching the

chromatin structure into an ‘active’ or ‘silencing’ state. (2) Providing a docking site for recruiting chromatin modifiers to chromatin (Turner, 2002, Jenuwein and Allis, 2001).

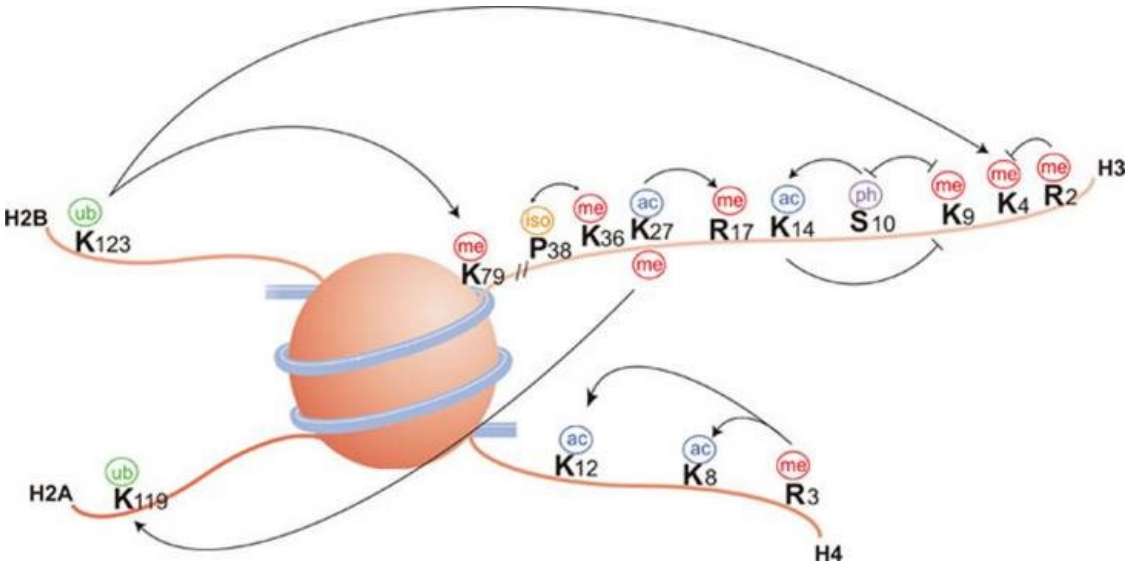

Fig 1.3.3. Schematic diagram showing different histone modifications (PTMs) and histone modification cross-talks. *Histone modifications can positively or negatively affect each other. Positive effects are indicated by arrow head and negative effects are indicated by flat head. This figure is adapted with permission from “Regulation of chromatin by histone modifications” Andrew J Bannister1 and Tony Kouzarides. (Bannister and Kouzarides, 2011)*

1.4 Heterochromatin Protein 1 (HP1) Superfamily

1.4.1 Introduction into HP1

Heterochromatin protein 1 (HP1) was originally identified in *Drosophila melanogaster* as a heterochromatin associated protein and acts as a dosage-dependent modifier of position effect variegation (PEV) (Eissenberg *et al*., 1990) (see Section 1.3). It is required for heterochromatin formation and gene silencing (Ryu *et al*., 2014). HP1 belongs to a highly conserved family of chromatin proteins, with homologues that are found in almost all eukaryotes from fission yeast (Swi6, Chp2 and Chp1) to humans (HP1α, HP1β and HP1γ) except for budding yeast (Huisinga *et al*., 2006, Singh *et al*., 1991). The genomic structure of genes encoding HP1 protein is conserved from *Drosophila* to humans in that they all contain five exons separated by four introns. In *Drosophila*, genes encoding HP1 proteins are known as *Su(var)2-5* and in mouse and human, they are named as (*Cbx5*, *Cbx1* and *Cbx3*) and (*CBX5*, *CBX1* and *CBX3*) respectively. (Jones *et al*., 2001, Norwood *et al*., 2004). A schematic diagram showing the conserved genomic structure of murine HP1-encoding gene is in Fig 1.4 (a). Each HP1 isoform plays differential roles by interacting with different factors that are involved in different aspects of euchromatin and heterochromatin structure and function (Ryu *et al*., 2014). As showing in Fig 1.4 (b), HP1 has two conserved domains, an N-terminal chromodomain (CD) and a C-terminal chromo shadow domain (CSD), connected by a flexible linker region. CD is a domain found in many chromatin-associated proteins that recognizes different histone PTMs (LeRoy *et al*., 2009). CD of HP1 specifically binds to di- and tri- methylated H3K9 (H3K9me2 and H3K9me3) (Jacobs and Khorasanizadeh, 2002). CSD is structurally similar to the CD and is responsible for HP1 dimerization and its interaction with many other proteins that possess a conserved pentapeptide motif, PXVXL (Brasher *et al*., 2000). HP1 proteins have been shown to form homo- and hetero- dimers with each other via their CSD (Nielsen *et al*., 2001). The linker region of HP1 is less conserved and accounts for the most variations in amino acid

sequence between HP1 proteins (Lomberk *et al*., 2006b). CSD has also been found to function in nuclear targeting, protein interaction as well as chromatin binding (Smothers and Henikoff, 2001, Piacentini *et al*., 2009, Zhao *et al*., 2000, Nielsen *et al*., 2001). It is till recently that, in *Drosophila*, the C-terminal extension region (CTE) has been found to be present only in HP1b and HP1c but not HP1a in *Drosophila* (Fig 1.4 b). CTE targets HP1b and HP1c to both nucleus and cytoplasm (Lee *et al*., 2019), which may indicate that the HP1b and HP1c could play a role in cytoplasm.

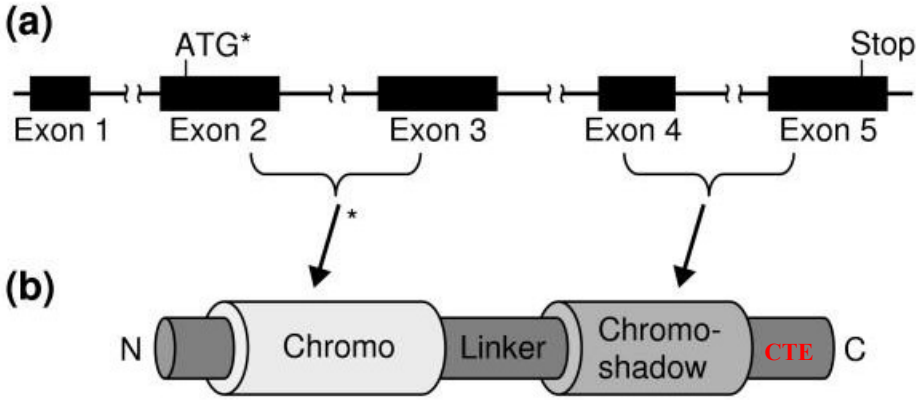

Fig 1.4. Schematic diagram showing the structure of HP1 proteins and the genes encoding them. *(a) The conserved genomic structure of genes encoding HP1 from Drosophila to humans. Each gene is made up of 5 exons and 4 introns. ATG start codon and stop codons are indicated. The exons encoding the chromo domain (CD) and the chromo shadow domain (CSD) are indicated. Asterisks mark the different arrangement in murine Cbx3 (encoding HP1γ), where ATG is in exon 3 and the CD is encoded by exons 3 and 4 of this gene. (b) The conserved structure of HP1 proteins. N, amino terminus; C, carboxy terminus. CTE (red) specifically in HP1b an HP1c isoforms in Drosophila targets these two isoforms to cytoplasm. This figure is adapted with permission from "The Heterochromatin Protein 1 family" Gwen Lomberk et al. (Lomberk et al., 2006b)*

The localization and the role of HP1 in heterochromatin environment has been well studied. However, several lines of evidence also suggested that HP1 localizes not only to heterochromatin but also to euchromatic regions and functions as a gene activator there (Kim *et al*., 2011, Piacentini and Pimpinelli, 2010) . Localization of HP1 protein appears to be

isoform-specific in both *Drosophila* and mammals. *Drosophila* HP1a mainly localizes to heterochromatin, while HP1c preferentially localizes to euchromatin and being mostly excluded from heterochromatin. HP1b is found both in euchromatic and heterochromatic domains (Smothers and Henikoff, 2001, Font-Burgada *et al*., 2008). In mammals, HP1α and HP1β are mainly heterochromatic, whereas HP1γ has been found in both heterochromatin and euchromatin (Minc *et al*., 2000, Huisinga *et al*., 2006). Localization of mammalian HP1 homologs only partially overlap and show differential dynamics during differentiation and cell-cycle progression (Minc *et al*., 1999, Hayakawa *et al*., 2003, Dialynas *et al*., 2007). The significance of this localization pattern given by three isoforms is thought to allow HP1 to perform multiple functions independently in both heterochromatin and euchromatin. For instance, in *Drosophila*, HP1c has been shown to co-localize with transcriptionally active domains of polytene chromosomes which contains zinc-finger containing transcription factors and active form of RNA Polymerase II (Pol II) (Font-Burgada *et al*., 2008) and, in mammalian cells, HP1 proteins, in particular HP1γ, have been associated with transcriptional elongation (Vakoc *et al*., 2005, Lomberk *et al*., 2006a). Therefore, these studies suggest that in addition to its function in gene silencing, HP1 also functions as an activator in euchromatin.

1.4.2 Introduction into mammalian HP1γ

There are three HP1 homologs named HP1α, HP1β, and HP1γ in mammals (Jones *et al*., 2000). Increasing evidence suggests that the role of HP1 proteins in maintaining genome stability goes beyond heterochromatic regions as they has been found to function in gene expression, DNA replication, DNA repair, cell cycle, cell differentiation, and development as well (Maison and Almouzni, 2004). Previous studies suggested that HP1α and HP1β are predominantly localized in foci of constitutive heterochromatin, by contrast, HP1γ shows an indistinct, `pan-nuclear'

distribution (Bartova *et al*., 2005, Horsley *et al*., 1996, Minc *et al*., 1999, Nielsen *et al*., 1999, Smothers and Henikoff, 2001). While HP1α and HP1β have been exactly localized in heterochromatic regions, HP1γ has been found either exclusively associated with euchromatin or present in both euchromatin and heterochromatin (Minc *et al*., 2000). HP1 proteins initiate and maintain the heterochromatin structure through their specific binding both to H3K9me3 (CD domain) and Suv39h1(CSD domain) (Bannister *et al*., 2001, Lachner *et al*., 2001). In mammals, studies on Hp1α -/-, Hp1β -/- and Hp1γ -/- MEFs showed that three HP1 isoforms have both redundant and distinct functions within pericentric heterochromatin (PCH) and they also act globally throughout the genome (Bosch-Presegue *et al*., 2017). Moreover, by targeted knockout (KO) of each isoform, it has been shown that the loss of either HP1α or HP1β did not change each other's levels but increased enrichment of HP1γ was observed in PCH. This suggests that HP1γ plays a supporter role for both isoforms (Bosch-Presegue *et al*., 2017).

Phenotypically, the newborn mice with disrupted *Cbx1* gene encoding HP1β exhibit perinatal lethality, acute respiratory failure and aberrant cerebral cortex development (Aucott *et al*., 2008). In this study, they also mentioned that HP1α wild type and deficient littermates showed no phenotypic difference. Of particular interest, mice with HP1γ-/- null mutation are infertile in both sexes (Naruse *et al*., 2007, Abe *et al*., 2011) and the chromosomes also exhibited a defect in progression of their pairing in early meiotic prophase (Takada *et al*., 2011). Taken together, these studies indicate that HP1γ is playing a role in the genome that cannot be compensated by the other two isoforms.

As mentioned before, HP1 has been widely implicated in gene silencing and recognizes the heterochromatic histone modification H3K9me3 via chromo-domain (CD). Interestingly, Vakoc and his colleagues found it to be present in the transcribed regions of all highly

expressed genes (c-kit, IL-2, β-major, Gapdh, GATA-2, c-myc, AHSP, DGKz, and Band 3) examined in that study (Vakoc *et al*., 2005). As both HP1 and H3.3 might be expected to bind to highly expressed genes, it is w orth investigating whether HP1 interacts with H3.3, as this interaction might be important for gene regulation (Kim *et al*., 2011). Moreover, HIRA (H3.3 chaperone) and HP1 have been found transiently co-localized in promyelocytic (PML) nuclear bodies in cells undergoing senescence (Jiang *et al*., 2011), which indicates that HIRA might interact with HP1 in this context. Except for the well-known repression function of HP1γ in heterochromatin, HP1γ has been also shown to interact with both initiating and elongating forms of RNAPII (Vakoc *et al*., 2005). The potential co-operation between HP1γ and H3.3 may directly regulate gene expression by facilitating and stabilizing the transcription machinery.

1.5 Histone Variants

1.5.1 Overview

Histones are a major component of chromatin, the basic unit of chromatin is the nucleosome, consisting of 147bp DNA wrapped around a core of histone proteins. The protein-DNA complex is fundamental to genome packaging, function, and regulation (Kamakaka and Biggins, 2005). DNA accessibility is essential for the vital progression of cellular processes such as DNA replication, transcription and repair, which requires a highly dynamic chromatin and nucleosome structure (Knezetic and Luse, 1986, Teves *et al*., 2014, Polo, 2015). This can be achieved through chromatin-modifiers, the posttranslational modification (PTM) of histones, and the incorporation of histone variants.

There are two classes of histone proteins. One class is named 'canonical' histones; they are expressed from tandem gene arrays during S phase for rapid deposition onto chromatin during DNA synthesis (Henikoff and Smith, 2015, Osley, 1991, Stillman, 1986). They package the newly replicated genome and can be replaced with non-canonical histones resulting in changes in nucleosome structure, stability, dynamics, and, ultimately, DNA accessibility (Weber and Henikoff, 2014). The other one is classified as non-canonical histones (replacement histones), which were originally identified as products of histone genes that were synthesized outside of S phase (Zweidler, 1984, Tagami *et al*., 2004). They, in contrast, are constitutively expressed throughout the cell cycle and are incorporated into chromatin in a replication-independent manner (Skene and Henikoff, 2013). From a structural point of view, histone variants can be grouped into homomorphous and heteromorphous families, depending on the extent of their structural difference compared to their conventional counterparts (Ausio *et al*., 2001, West and Bonner, 1980). Homomorphous group (H2A.1 and H2A.2; H3.1, H3.2 and H3.3) only harbour a small change in their amino acid sequence compared to their conventional counterparts, on the other hand, heteromorphous family (H2A.X, H2A.Z, macroH2A (mH2A), H2A Barr body-

deficient (H2A.Bbd) and centromeric protein A (CENP-A)) contain a big change that affects larger portions of the histone molecule (Ausio, 2006).

In this section, I will firstly introduce the different histone variants in mammals with highlights on histone variant H3.3.

1.5.2 Introduction into histone variant H3

To date, there are five H3 variants that have been identified in mammals: 1) two canonical variants, H3.2 and the mammalian-specific H3.1, and 2) three replacement variants, H3.3, the centromere-specific variant CenH3 (CENP-A in mammals) (Allshire and Karpen, 2008) and the testis specific histone H3t (Witt *et al*., 1996). CENP-A in mammals is crucial for proper chromosome segregation (Allshire and Karpen, 2008) and H3t is a testis-specific histone variant functioning in chromatin reorganization during spermatogenesis (Witt *et al*., 1996). There are two additional primate-specific H3 variants, H3.X and H3.Y identified at a later date, which are said to associated with the regulation of cellular responses to stress stimuli, such as nutrient starvation (Wiedemann *et al*., 2010). The sequence alignment and specific features of human H3 variants are illustrated in Fig 1.5.1.

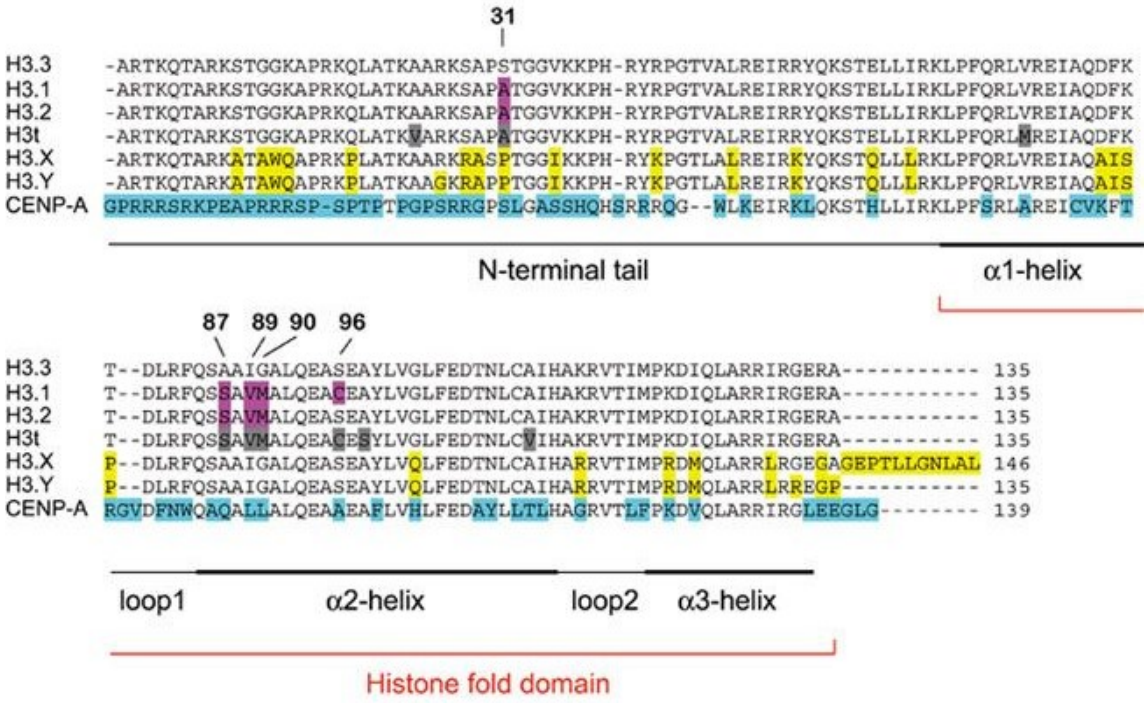

Fig 1.5.1. Alignment of amino acid sequences corresponding to human H3 variants. *The amino acid differences are highlighted. H3.1 and H3.2 differences are highlighted in purple, H3t in grey, H3.X and H3.Y in yellow, and CENP-A in light blue. The position numbers of amino acids that are different between H3.3 and H3.1/2 are indicated. The positions of the N-terminal tail and of the α-helixes of the histone-fold motif are shown. This figure is adapted with permission from "The double face of the histone variant H3.3" Emmanuelle Szenker et al., (Szenker et al., 2011)*

In this section, I will mainly focus on H3.3 to update on discoveries in this area. Regardless of the fact that H3.3 was largely considered as a mark of transcriptional activity, some studies in several organisms have also revealed the unexpected enrichment of H3.3 at silent chromatin loci such as telomeres or centromeres which prompts us to broaden our views concerning the role of this variant. Here, the nature, properties and regulated expression of H3.3 as compared with its canonical counterparts are illustrated in Fig 1.5.2. The H3.1 and H3.2 genes are organized in tandem, multi-copy clusters within the genome. In humans, the HIST1 cluster is located on chromosome 6p21, which contains histone H1 and 49 core histone genes including ten H3 genes. Canonical histone genes lack introns and their corresponding mRNAs do not have polyadenylated (Poly A) tails. H3.1 and H3.2 mRNA translation is tightly regulated by proteins that are responsible for their peak of transcription and increased mRNA processing

during S phase (Ray-Gallet *et al*., 2011b). In contrast, H3.3 mRNAs possess introns and Poly A tails and they are constitutively expressed throughout the cell cycle, which allows histone deposition and exchange in a DNA synthesis-independent manner during and outside S phase. H3.3 differs from H3.2 by only 4 amino acids at residues 31, 87, 89 and 90 with an additional residue 96 in H3.1. These specific four residues in H3.3 make up the α-helixes of the histone folding motif, which indicates that the H3.3 protein may have a distinct folding configuration compared to canonical H3 protein (Szenker *et al*., 2011). (Frank *et al*., 2003). Three of these residues (amino acids 87, 89, and 90) mediate recognition by the H3.3-specific histone chaperones HIRA and DAXX (Filipescu et al., 2013a, Ricketts and Marmorstein, 2017), and serine 31 specifically located in N-terminal of H3.3 can be phosphorylated and influence the methylation of lysine 27 (Hake *et al*., 2005, Jacob *et al*., 2014) (Fig 1.5.2).

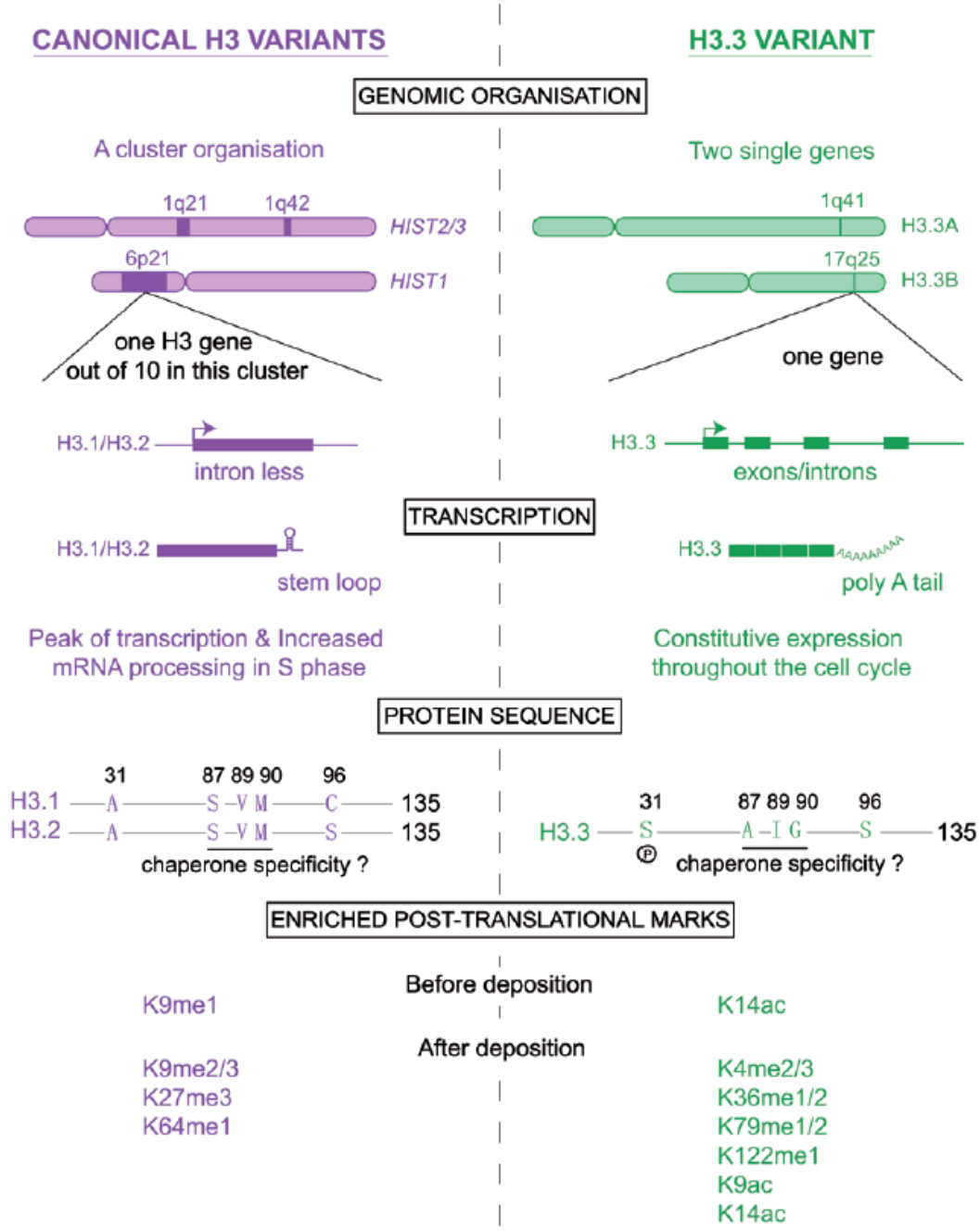

Fig 1.5.2. Histone variant H3.3 compared with canonical histone H3.1 and H3.2. *Differences between the H3.1 and H3.2 (in purple) and the histone variant H3.3 (in green) are illustrated. Genes encoding H3.1 and H3.2 are organized in tandem clusters within the genome. They lack introns and are not polyadenylated in contrast to the H3.3 genes (H3.3a and H3.3b). The amino acid differences between the canonical H3 and H3.3 are indicated. H3.3 Serine residue (S) at position 31 can be phosphorylated. The motifs SVM and AIG in H3.1/2 and H3.3 could account for chaperone specificity respectively. PTMs for each group are shown at the bottom. This figure is adapted with permission from "The double face of the histone variant H3.3" Emmanuelle Szenker et al., (Szenker et al., 2011)*

Histone H3.3 is encoded by 2 single genes, *H3f3a* and *H3f3b* (*H3.3a* and *H3.3b* in Drosophila) (Bush *et al*., 2013). A recent H3.3 study, which used an HA-tagged H3.3 targeted to the endogenous locus as well as an EGFP gene with its own IRES, showed strong HA stain (H3.3) in most cells in spleen, thymus, liver, kidney, exclusive localization in the nuclei in brain, spermatocytes and round spermatids in testis and nuclei of theca cells and oocytes in the ovary, in which H3.3A-HA and H3.3B-HA expression pattern in adult tissues was analyzed by immunohistochemistry in mouse *ex vivo* (Bachu *et al*., 2019). This implied that H3.3-HA is expressed broadly in most cells of adults' tissues. Moreover, H3.3 expression was also tested for in T and B lymphocytes and myeloid cells from thymus, spleen and bone marrow by flow cytometry in that study and they found that the majority of cells in spleen (T, B lymphocytes, and myeloid cells), thymus (CD4+ and CD8+ T cells) and bone marrow (B cells and myeloid cells) were EGFP positive in both H3f3a-HA and H3f3b-HA mice. And the EGFP signal from H3f3a-HA and H3f3b-HA mice are expressed at comparable levels in each cell type in these tissues with a narrow monophasic peak, indicating that H3.3 expression levels are largely uniform within each cell type (Bachu *et al*., 2019).

H3.3 is targeted to transcriptionally active loci including promoters, gene bodies and regulatory elements throughout the cell cycle, by its chaperone HIRA and has been described as an 'active mark' for transcription (Ahmad and Henikoff, 2002). More recently, H3.3 has also been shown to be incorporated into promoters of highly expressed genes (Lund *et al*., 2015a). In that study, it is suggested that factors putatively affecting expression of 'H3.3 occupied promoters' included spatial positioning of H3.3 on these promoters and enrichment for methylation of H3 (H3K4me3) close to the TSS (Lund *et al*., 2015a).

The minor amino acid difference between H3.3 and its conventional counterparts H3.1 and H3.2 makes it difficult to specifically identify H3.3 using antibodies hence, making it difficult to study H3.3 deposition in mammalian systems. However, in the lab, we overcome this problem by generating H3.3B-EGFP transgenic mice from ES cells in which the EGFP gene was homologously integrated into the *H3.3b* gene to create a chimeric H3.3B-EGFP protein (see Fig 2.1). In this way, we can use anti-EGFP antibody to detect or pull-down H3.3 protein.

1.5.3 Deposition pathways of histone H3 variants and their chaperones

Histone chaperones are considered as the most likely candidates that are responsible for incorporating specific histone variant into the genome (Ray-Gallet *et al*., 2011b). The incorporation of histone variants is highly dynamic, which has been associated with different aspects of DNA metabolism during development such as DNA replication, transcription, recombination, and repair. Different histone variants have specific expression, localization and distribution patterns, which confer novel structural and functional properties on the nucleosome and affect chromatin remodelling and PTMs of histones. Moreover, core histones are continuously replaced by new histones throughout the whole cell cycle and incorporation of different histone variants alters the nucleosome properties both physically and chemically. The replacement of a canonical histone by a non-canonical variant, independent of replication, is a dynamic process that can potentially change the composition of chromatin (Henikoff and Smith, 2015).

Accordingly, the incorporating pathways are grouped into two categories: replicative histones that expressed in S phase and are deposited in a DNA-synthesis coupled manner (DSC), and replacement histones, whose expression is throughout the cell cycle and are incorporated

through DNA synthesis-independent (DSI) pathways. Each identified H3 chaperone or chaperone complex contributes to a H3 variant deposition pathway as shown in Fig 1.5.3.

In higher eukaryotes, chromatin loading of H3.3 depends on the highly conserved histone chaperone HIRA or on the DAXX/ATRX complex (Filipescu et al., 2013a). The specificity of both DAXX/ATRX and HIRA to H3.3 was shown to be mediated by a conserved sequence motif in H3.3 (AAIG) that differs from canonical H3 (SAVM) (Lewis *et al*., 2010, Elsasser *et al*., 2012).

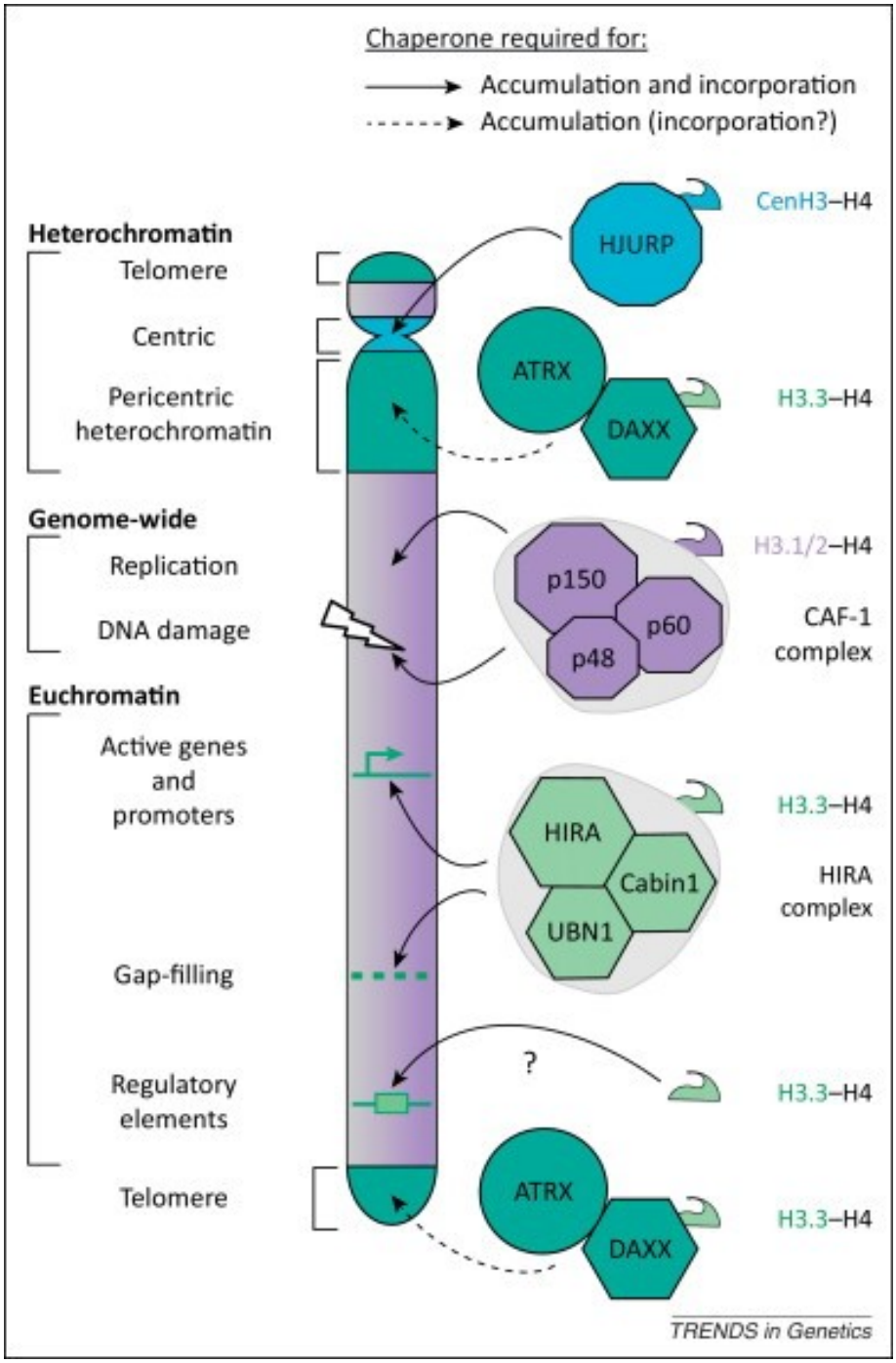

Fig 1.5.3. Local enrichment of histone H3 variants and their chaperones. *During DNA replication and DNA damage repair, incorporation of canonical histones H3.1 and H3.2 (purple) together with H4 occurs genome-wide. This DSC pathway is mediated by the CAF-1 complex. In mouse somatic and ES cells, the replacement variant H3.3 (light green) is enriched in coding regions and at specific chromatin sites. In euchromatin, this H3.3 enrichment is achieved by the HIRA complex which consists of HIRA, Cabin1 and UBN1 and it is responsible for H3.3 enrichment in the gene bodies of actively transcribed genes and at promoters of both actively transcribed or non-transcribed genes. In heterochromatin, DAXX/ATRX complex accumulates H3.3 at pericentric repeats (major satellite) and telomeres. This figure is adapted with permission from "Developmental roles of histone H3 variants and their chaperones" Dan Filipescu et al., (Filipescu et al., 2013b).*

1.5.3.1 DNA-synthesis coupled (DSC) deposition

Chromatin assembly factor-1 (CAF-1) complex

During each division cycle, as cells replicate their DNA, they must also synthesize an equal amount of histone proteins and assemble them together into nucleosomes. To meet this cyclical demand, bulk histone gene expression is tightly regulated during S phase (Osley, 1991). This replication coupled (RC) pathway involves a variety of components, including proliferating cell nuclear antigen (PCNA), chromatin assembly factors such as CAF-1 and replication-coupling assembly factor (RCAF), Hir proteins, and other histone chaperones (Mello and Almouzni, 2001, Verreault, 2000). The CAF-1 complex is the major player in this DSC deposition pathway. The CAF1 complex is made up of three subunits, p150, p60 and p48. The largest subunit p150 is said to interact directly with newly synthesized DNA and acetylated histone (Kaufman *et al*., 1995). CAF1 specifically incorporates H3.1-H4 (perhaps H3.2–H4) dimers onto newly synthesized DNA during DNA replication and DNA damage repair which involves a direct binding with proliferating cell nuclear antigen (PCNA) (MacAlpine and Almouzni, 2013, Polo and Jackson, 2011, Filipescu et al., 2013a). A schematic diagram showing the DNA replication-coupled deposition pathway is in Fig 1.5.4 (a).

1.5.3.2 DNA-synthesis independent (DSI) deposition

Histone regulator A (HIRA) complex

HIRA protein, together with calcineurin binding protein 1 (Cabin1) and ubinuclein 1 (UBN1) form a HIRA complex which is said to incorporate H3.3 onto both active and repressed genes as well as some regulatory elements in a DNA replication-independent manner (Banaszynski *et al*., 2010, Dipak Amin *et al*., 2011, Balaji *et al*., 2009). The HIRA complex has been suggested to be involved in the genome-wide deposition of H3.3 onto promoter regions of both active and repressed genes, the body of active genes, and a subset of regulatory elements

(Goldberg *et al*., 2010, Ray-Gallet *et al*., 2011b, Schneiderman *et al*., 2012). Additionally, a complex comprised of Death domain associated protein (DAXX) and alpha-thalassemia/mental retardation X-linked syndrome (ATRX) (Goldberg *et al*., 2010, Drane *et al*., 2010, Lewis *et al*., 2010) provides a dispensable way to deposit H3.3 onto actively transcribed genes just like HIRA. However, it has been shown that DAXX/ATRX is specifically required for H3.3 enrichment at telomeres in mouse ES cells and pericentric heterochromatin regions in mouse embryonic fibroblasts (MEFs) (Goldberg *et al*., 2010, Drane *et al*., 2010, Loppin *et al*., 2005, Torres-Padilla *et al*., 2006). A schematic diagram showing the DNA replication-coupled deposition pathway is in Fig 1.5.4 (b).

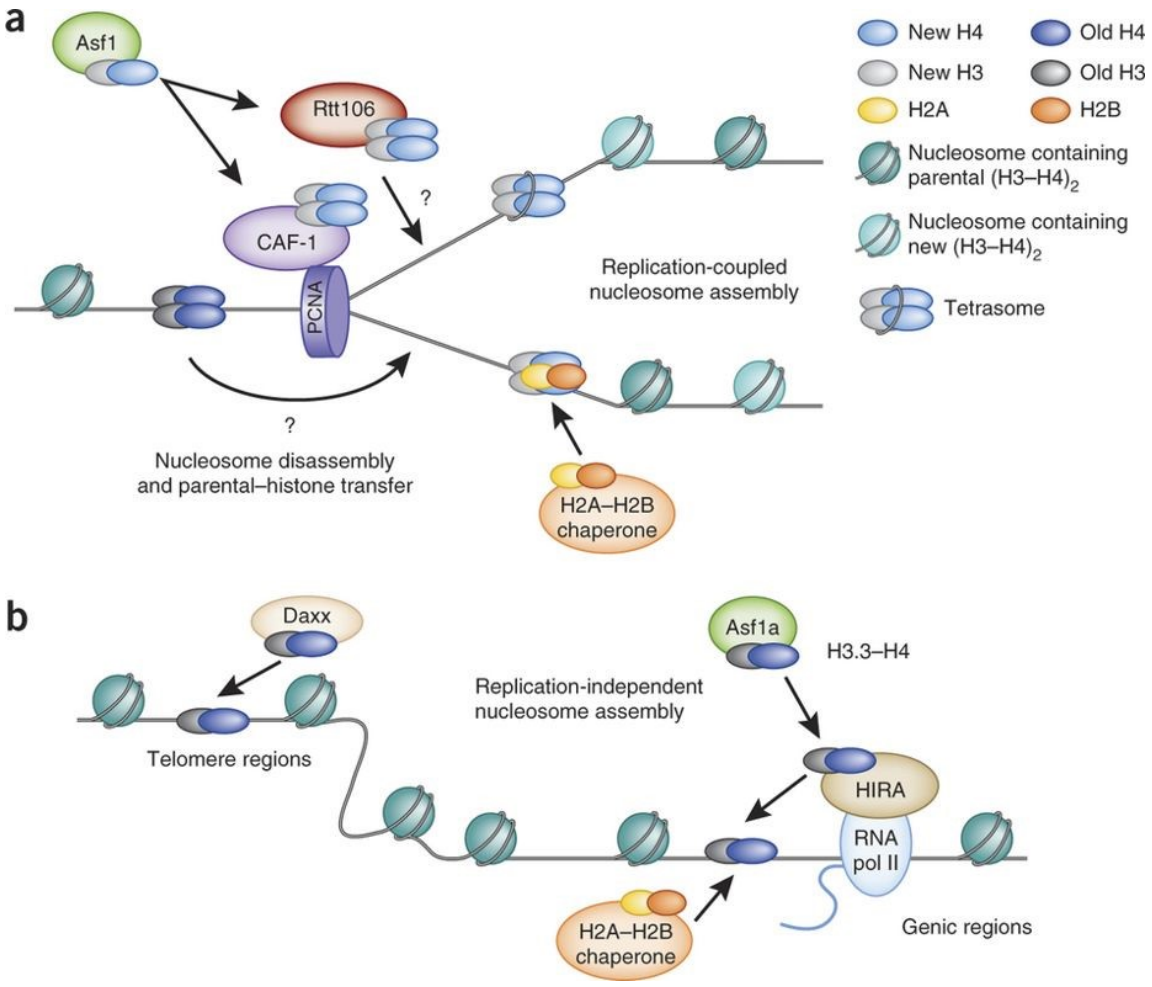

Fig 1.5.4. Histone chaperones are key regulators of replication-coupled and replication-independent nucleosome assembly. *(a) Histone chaperones coordinate to regulate replication-dependent (DSC) nucleosome assembly. Asf1 transfers the newly synthesized histone H3–H4 that was imported into the nucleus to CAF-1 and Rtt106 for (H3–H4) dimerization and deposition onto newly synthesized DNA. Deposition onto replicated DNA partially depends on the interaction between CAF-1 and PCNA. (b) HIRA and DAXX mediate replication-independent (DSI) nucleosome assembly of H3.3–H4. In human cells, Asf1a transfers H3.3–H4 to HIRA for deposition of H3.3–H4 at genic regions. DAXX/ATRX facilitate deposition of H3.3–H4 at telomere regions. This figure is adapted with permission from Review Article "Histone chaperones in nucleosome assembly and human disease" Rebecca J Burgess and Zhiguo Zhang (Burgess and Zhang, 2013)*

1.5.4 Distribution of histone H3.3

Distinct histone variants have their specifically defined deposition patterns and mark different chromatin states (Talbert and Henikoff, 2010, Kouzarides, 2007). However, the mechanisms used to achieve this remains largely unknown. In mammals, the canonical histones (H3.1 and H3.2) show an increased expression during S phase, which indicates they are the major histone source during DNA replication (Corpet and Almouzni, 2009, Groth *et al*., 2007). In contrast, the replacement histone H3.3 is constitutively expressed during and outside S phase to provide a continuous source of H3 (Wu *et al*., 1982). It has been demonstrated that H3.3 is enriched in actively transcribed genes (Jin *et al*., 2009, Mito *et al*., 2005b, Wirbelauer *et al*., 2005). While some more recent studies showed that during 'reprogramming' of the male pro-nucleus, H3.3 is also incorporated into paternal chromatin after fertilization (Drane et al., 2010, Filipescu et al., 2013b). Additionally, the deposition of H3.3 onto telomeric and pericentric heterochromatin regions by DAXX/ATRX complex is also in a replication-independent pathway (Loppin *et al*., 2005, Torres-Padilla *et al*., 2006, Goldberg *et al*., 2010, Drane *et al*., 2010). Published genome-wide H3.3 deposition profile was determined by using ChIP-sequencing in murine embryonic stem cells (ES cells) *in vitro* in which, H3.3 has been shown to not only mark actively transcribed genes in ES cells and neural progenitor cells (NPCs) but also the genic and intergenic ES transcription factor binding site (TFBS) (Chen *et al*., 2008,

Goldberg *et al*., 2010). Although H3.3 was found to be enriched nearby the transcription start sites (TSS) of both active and repressed genes, it is enriched in the body of active genes, but not repressed genes (Goldberg *et al*., 2010). The deposition profile of H3.3 at cell-type specific genes and regulatory elements changes with differentiation. However, housekeeping genes, which remain highly expressed through differentiation, retain similar enriched patterns of H3.3 occupancy. Pluripotent genes such as *Oct4* are highly active in ES cells but become inactive after differentiation. Thus, the enrichment of H3.3 at the gene body of *Oct4* largely disappeared in the differentiated NPCs. More recently, H3.3 has also been shown to be incorporated into promoters of highly expressed genes (Lund *et al*., 2015b). In that study, Lund *et al*. suggested that factors putatively affecting expression of 'H3.3 occupied promoters included spatial positioning of H3.3 on these promoters and enrichment for methylation of H3 (H3K4me3) close to the TSS (Lund *et al*., 2015b). These observations in terms of HIRA-dependent H3.3 deposition was obtained in either ES cell or adipose stem cells *in vitro*. In contrast, this PhD project set out to investigate H3.3 deposition in a somatic tissue (Thymus) in *vivo*.

1.5.5 Functions of histone H3.3

1.5.5.1 H3.3 acts as a switch for gene expression

DNA accessibility during replication and gene transcription is highly dynamic and is thought to be tightly regulated by three mechanisms, which include ATP-dependent chromatin remodeling complexes, histone post-translational modifications (PTMs), and the exchange of histone variants (Varga-Weisz and Becker, 2006). Different H3 variants have been implicated in performing distinct gene regulatory functions in addition to their fundamental role in DNA packaging. H3.3 has been found to be enriched with active marks such as H3K4me2/3, H3K9Ac and H3K14Ac (Wirbelauer *et al*., 2005), in contrast, H3.2 is always enriched with repressive H3K27me2/3 and H3K9me2 marks (Hake and Allis, 2006). When outside S phase,

H3.2 is replaced with H3.3 carrying active marks that alter chromatin state and ultimately the DNA accessibility favoring a more open structure for genes transcription. Therefore, exchange of histone variants can act as the switch of gene expression. Additionally, another study showed that H3.3 can greatly impair the higher-ordered chromatin folding and promote gene activation (Chen *et al*., 2013). This is not surprising as the H3.3-containing nucleosome is very unstable and, as shown in a previous genome-wide analysis of H3.3 dissociation study, H3.3 turn-over is very rapid at transcription start sites (TSS), with the highest rate at nucleosome-depleted regions (NDRs) just upstream of Pol II binding and dropped across gene bodies (Ha *et al*., 2014, Jin and Felsenfeld, 2007). Therefore, H3.3 is thought to act as a switch for gene expression.

1.5.5.2 Developmental role of histone H3.3

H3.3 is the major variant of histone H3 that is highly conserved among eukaryotes with only 4-5 amino acid difference from its counterparts H3.1 and H3.2 (Delaney *et al*., 2018). Most genomes contain two or more genes expressing H3.3 and loss or depletion of the H3.3 protein results in developmental defects in most organisms (Delaney *et al*., 2018). Several lines of evidence in *Drosophila* suggested that complete loss of H3.3 protein usually causes sterility or embryonic lethality, but it is not essential for viability, at least after the embryonic stage. However, H3.3 is required for male meiosis, where the loss of H3.3 leads to defects in chromosome condensation and segregation in meiotic cells of the male germline (Sakai *et al*., 2009). The importance of H3.3 is manifested in developmental defects upon loss or depletion of the protein in mammals. Deletion of both H3.3 genes (*H3f3a* and *H3f3b*) results in developmental retardation and early embryonic lethality in mice (Jang et al., 2015b). Deletion of *H3f3b* alone leads to developmental deficiencies and death at birth and deletion of *H3f3a* alone results in postnatal mortality, slowed growth, and reduced male fertility (Couldrey *et al*.,

1999, Tang *et al*., 2015). Moreover, missense mutations identified in specific cancer types, including pediatric high-grade glioblastoma (HGG) and certain types of bone tumors, preferentially occur in *H3F3A* and *H3F3B* genes encoding H3.3 protein in human (Shi *et al*., 2017). More recently, complete loss of H3.3 protein only leads to reduced fertility and viability in response to high-temperature stress in *Caenorhabditis elegans*, which suggested a role for H3.3 in the stress response (Delaney *et al*., 2018). There are some other well recognized biological processes where H3.3 appears important: it is important for embryonic stem cell differentiation (Banaszynski *et al*., 2013), neuron plasticity (Maze *et al*., 2015) and the DNA damage response (Adam *et al*., 2013, Frey *et al*., 2014). At the molecular level, depletion of H3.3 does not dramatically affect gene regulation in the developing mouse embryo, surprisingly, it disrupts heterochromatin structures at telomeres, centromeres, and pericentromeric regions of chromosomes, leading to mitotic defects (Jang et al., 2015a).

1.6 Histone chaperones

1.6.1 Introduction

Histone chaperones (HC) were firstly identified as histone carriers that facilitate proper nucleosome assembly, which is thought to be important for maintenance of genome stability. As the research of chromatin and epigenetics grew rapidly, the functional link between histone chaperones and histone post translational modifications (PTMs) were thought to be important for the establishment, maintenance, and propagation of specific chromatin states (Avvakumov *et al*., 2011). The other non-negligible function of histone chaperones is that they target free histones for degradation, for instance Nucleosome Assembly Protein 1 (Nap1) eliminates competing, non-nucleosomal histone-DNA interactions during nucleosome assembly in yeast (Andrews *et al*., 2010).

Histone chaperones not only physically interact with histone proteins, but also recruit histone modification enzymes as well as facilitate histone proteins modifications by other histone modifiers (Fillingham *et al*., 2008). For instance, in the nucleus, the association between H3-H4 and anti-silencing factor 1 (Asf1) promotes acetylation of lysine 56 of H3 (H3K56) by histone acetyltransferase Rtt109 (Adkins *et al*., 2007, Chen and Dent, 2014, Collins *et al*., 2007, Driscoll *et al*., 2007, Han *et al*., 2007), which is followed by the deposition of H3-H4 dimers onto the nascent DNA by the next set of chaperones, CAF-1 and Rtt106 (Avvakumov *et al*., 2011). This histone chaperone mediated histone recycling and propagation of post-translational modifications is required for robust re-establishment of the local chromatin structure at the DNA replication fork (Avvakumov *et al*., 2011) To date, a growing body of evidence suggest that the role of histone chaperones is not limited to processes such as DNA replication, transcription, and repair. For example, FACT (Facilitates Chromatin Transcription) has now been identified as an exchange factor that can swap the histones within existing nucleosomes

for histone variants and prevent histones from being displaced by the passage of RNA polymerases during transcription (Formosa, 2012). The importance of histone chaperones is also manifested in cancer and other human diseases upon their alterations or mutations (Lorain *et al*., 1996, Wilming *et al*., 1997, Jiao *et al*., 2011, Schwartzentruber *et al*., 2012). A list of histone chaperones and their histone cargo and function during nucleosome assembly is showing in Fig 1.6.1.

Histone chaperone	**Histone**	**Function during nucleosome assembly**
Anti-silencing factor 1 (Asf1)	H3–H4	Histone import; histone transfer to CAF-1 and HIRA; regulation of H3K56ac
Chromatin assembly factor 1 (CAF-1)	H3.1–H4	H3.1–H4 deposition; $(H3–H4)_2$ formation
Death domain–associated protein (DAXX)	H3.3–H4	H3.3–H4 deposition at telomeric heterochromatin
Histone cell cycle regulation defective homolog A (HIRA)	H3.3–H4	Deposition of H3.3–H4 at genic regions
Nuclear autoantigenic sperm protein (NASP)	H3–H4	Histone supply and turnover
Regulator of Ty transposition (Rtt106)	H3–H4	Formation and deposition of $(H3–H4)_2$ tetramer
Facilitates chromatin transcription (FACT)	H3–H4, H2A–H2B, H2A.X–H2B	Deposition and exchange of H3–H4, H2A–H2B, H2A.X–H2B
Nucleosome assembly protein 1 (Nap1)	H3–H4 and H2A–H2B	H2A–H2B nuclear import and deposition

Fig 1.6.1. List of histone chaperones that were mentioned in this thesis. *This figure is adapted with permission from Review Article "Histone chaperones in nucleosome assembly and human disease" Rebecca J Burgess and Zhiguo Zhang (Burgess and Zhang, 2013)*

1.6.2 Histone Regulator A (HIRA) mediated H3.3 deposition

The *HIRA* gene was discovered by positional cloning of the DiGeorge syndrome chromosome deletion region at human chromosome 22q11. It has been demonstrated that HIRA is essential

for mouse embryogenesis by targeted mutagenesis, in which homozygous HIRA knockout (KO) leads to embryonic lethality by day 11 (Roberts *et al*., 2002). The function of HIRA was first described based on its specific role in the DNA replication coupled (DSC) nucleosome assembly pathway in *Xenopus* egg extracts (Ray-Gallet *et al*., 2011b). Then, following its isolation with H3.3, its specific ability to deposit H3.3-H4 was demonstrated *in vitro* (Tagami *et al*., 2004).

The HIRA complex, composed of HIRA, Ubinuclein-1 (UBN1), and Calcineurin Binding Protein 1 (CABIN1), cooperates with the histone chaperone Anti-silencing function protein 1 (ASF1) to mediate H3.3-specific binding and chromatin deposition at different genic regions (Tagami *et al*., 2004, Goldberg *et al*., 2010, Ray-Gallet *et al*., 2011b). The conserved Hpc2-related domain (HRD) in UBN1 is said to confer H3.3-specific-binding by the HIRA complex. HIRA is well known as an activator of gene transcription by incorporating H3.3 onto promoters, enhancers and gene bodies of active transcribed genes (Chen *et al*., 2013). Conversely, HIRA has also been implicated in transcriptional repression, where HIRA/ASF1 spreads across heterochromatic regions via association with the Heterochromatin Protein 1 (HP1) ortholog, Swi6, to maintain a silent chromatin state in fission yeast (Wang *et al*., 2000). Recently, how HIRA deposits H3.3 on distinct genic regions has been revealed by a short hairpin RNA (shRNA) screen (Zhang *et al*., 2017c) in which, they identified a single-stranded DNA (ssDNA) binding protein Replication Protein A (RPA) as a regulator of the deposition of newly synthesized H3.3 into chromatin (Zhang *et al*., 2017c). They showed that RPA facilitates HIRA-mediated incorporation of newly synthesized H3.3 at promoters and enhancers for gene regulation (Zhang *et al*., 2017c). Moreover, previous microarray studies in *Drosophila* provided strong evidence for a correlation between transcriptional activity and H3.3 incorporation (Mito *et al*., 2005a). Because of the association of H3.3 with transcriptionally active chromatin domains, it has been suggested that there is a causal

relationship between the presence of H3.3 and the accessibility of the chromatin template for transcription. It has been noted that if H3.3-containing chromatin is more easily transcribed, increased transcription may lead to further replacement of H3 by H3.3 (Jin and Felsenfeld, 2006).

There is a human disease called DiGeorge syndrome (DGS), of which, the syndrome is comprised of: T-cell deficiency, hypoparathyroidism, cardiac malformations, and facial abnormalities (Davies, 2013). Most DGS infants develop a small thymus with low T cell numbers but there are still less than 1% of infants with DiGeorge anomalies that are athymic and consequently no T cells derived from the thymus (Naeim, 2013). It has been reported that ~90% of patients with DGS have a small deletion in chromosome number 22 at position 22q11.2 (de la Chapelle *et al*., 1981, Kelley *et al*., 1982). Interestingly, HIRA was identified as one of the candidate genes located within the q11 region of chromosome 22 that was commonly deleted in DGS patients (Farrell *et al*., 1999). This indicates that HIRA may play a role in regulating T cell development (see section 3.8). There is another known candidate gene, T-box family transcriptional regulator (TBX1) (Papaioannou and Silver, 1998), in which, rare mutations have been described leading to the DGS phenotype (Yagi *et al*., 2003, Zweier *et al*., 2007). Mice having parathyroid defects can be partially rescued by expressing a human bacterial artificial chromosome (BAC) vector containing the TBX1 gene (Merscher *et al*., 2001). Notably, extensive evidence also suggested that H3.3 and HIRA are required for reprogramming events during development in animals (Loppin *et al*., 2005, Akiyama *et al*., 2011, Santenard and Torres-Padilla, 2009) and plants (Ingouff *et al*., 2010, Nie *et al*., 2014).

1.7 Epigenetics in alternative RNA splicing

1.7.1 Introduction to RNA splicing

Alternative RNA splicing explains how protein diversity is achieved by the limited number of genes found in higher eukaryotes. The canonical protein is produced by joining exons in sequence and removing all introns during RNA splicing. But alternative splicing may drop exons or retain introns, resulting in a different protein. The importance of alternative splicing is dramatically manifested by the splicing defects found in numerous diseases such as cystic fibrosis, frontotemporal dementia, Parkinsonism, premature aging, and cancer (Luco *et al*., 2011, Caceres and Kornblihtt, 2002, Cooper *et al*., 2009).

There are five major alternative splicing events described in metazoans: skipped exon (SE), alternative 5' splice sites (A5SS), alternative 3' splice sites (A3SS), mutually exclusive exons (MXE) and retained introns (RI) (Zhou *et al*., 2014). Introns are non-coding regions within the genome and RIs may trigger nonsense-mediated decay (NMD) of mRNA or introduce mutations in the translated protein. Recently, the retention of introns by alternative splicing has been suggested as a conserved regulatory mechanism that can affect gene expression and protein function and correlate with age and age-onset of neurodegenerative diseases (Adusumalli *et al*., 2019). One example would be that the level of intron retention (RI) increased in male *Drosophila* heads as the animal aged and some differential RI genes identified from aging *Drosophila* as well as human brain tissues are revealed to be associated with Alzheimer's disease (AD)-related pathways (Adusumalli *et al*., 2019).

Traditionally, alternative RNA splicing is predominantly thought to be regulated by splicing enhancers and silencers located either in introns or exons (Chasin, 2007). They are small conserved RNA sequences that can either stimulate or inhibit the use of splice sites through

binding to regulatory proteins such as SR proteins (serine/arginine rich proteins) or heterogeneous nuclear ribonucleoproteins (hnRNPs) (Luco *et al*., 2011). As RNA splicing can occur co-transcriptionally (Beyer and Osheim, 1988), multiple layers of post- and co-transcriptional regulatory mechanisms coordinate to control this process (Kornblihtt *et al*., 2013b). There is a growing body of evidence supporting the idea that histone modifications and chromatin organization influence pre-mRNA splicing (Shukla and Oberdoerffer, 2012, Hodges *et al*., 2009, Khan *et al*., 2012, Chodavarapu *et al*., 2010). Chromatin structure contributes to the regulation of RNA splicing by affecting its coupling with transcription which include the modulation of chromatin conformation and histone marks, the recruitment of splicing factors and nucleosome positioning (Kornblihtt *et al*., 2013a). Notably, exons have a length of 140–150 nucleotides long on average, which is strikingly similar to the nucleosome (147bp) (Kornblihtt *et al*., 2009). Next-generation sequencing has been widely used to study genome-wide nucleosome positioning and it has been previously suggested that DNA sequences at intron-exon junctions promote nucleosome positioning, suggesting an essential role of nucleosome positioning in exon definition (Dhami *et al*., 2010, Kolasinska-Zwierz *et al*., 2009, Nahkuri *et al*., 2009). Moreover, it has been suggested that nucleosome density is high at strong splice sites (Spies *et al*., 2009, Tilgner *et al*., 2009), which indicates a potential role for nucleosome positioning in regulation of splicing. Similarly, RNA Pol II has also been shown to be more highly enriched at alternatively spliced exons than at constitutive ones (Brodsky *et al*., 2005). Given the ability that RNA Pol II can interact with histone modifiers, such as the histone 3 lysine 36 (H3K36) methyltransferase Set2 (Xiao *et al*., 2003), and recruit splicing regulators, such as SR proteins or U2 spliceosomal RNA (de la Mata *et al*., 2003, Listerman *et al*., 2006, Kornblihtt *et al*., 2004), nucleosome positioning may play a role in modulating RNA Pol II enrichment at exons and therefore splicing efficiency.

A mechanistic model involving direct physical crosstalk between chromatin and the splicing machinery via an adaptor complex has been suggested (Luco *et al*., 2010, Sims *et al*., 2007). Multilayered regulation by the H3K36me3 histone mark, chromatin binding factor MRG15 (MORF-related gene on chromosome 15), and splicing factor PTB (polypyrimidine tract-binding protein) establishes a 'chromatin-splicing adaptor' system (Luco *et al*., 2010) in which, MRG-15 reads high levels of H3K36me3 marks on exons and acts as an adaptor protein to further recruit PTB to its weaker binding site inducing exon skipping. Conversely, MRG-15 and PTB do not accumulate along the gene marked with H3K4me3, thus favoring exon inclusion (Fig 1.7.1).

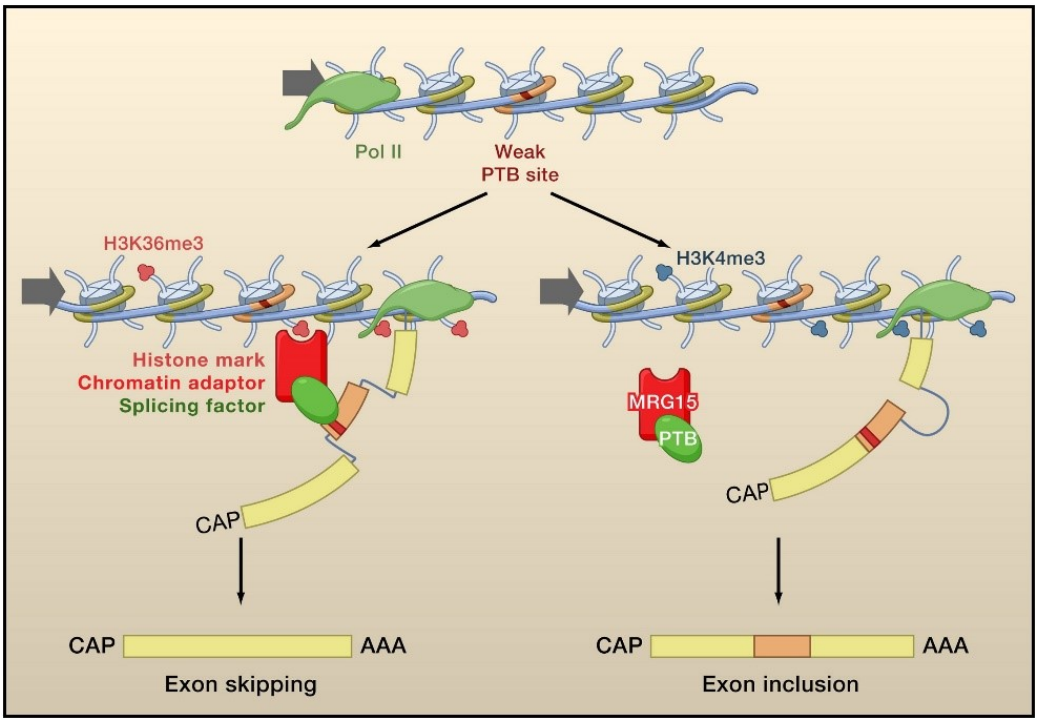

Fig 1.7.1. The chromatin-adaptor model of RNA alternative splicing. *H3K36me3 (red) along the gene determines the binding of adaptor protein MRG15 that reads H3K36me3 (red) and in turn recruits splicing factors PTB to its weaker binding site inducing exon skipping. When the PTB-dependent gene is hypermethylated in H3K4me3 (blue), MRG15/PTB does not accumulate along the gene, and thus favoring exon inclusion. This figure is adapted with permission from "Epigenetics in alternative pre-mRNA splicing" Reini F. Luco et al (Luco et al., 2011)*

1.7.2 Association between HP1γ and alternative RNA splicing

Another example of a possible chromatin-splicing adaptor system including the H3K9me3 mark and HP1 proteins appears to recruit heterogeneous nuclear ribonucleoproteins (hnRNPs) in *Drosophila* in which, co-immunoprecipitation (Co-IP) experiments confirmed HP1a interacts with hnRNP proteins (Piacentini *et al*., 2009). In humans, proteomic analysis of proteins binding to H3K9me3 identified the chromatin-binding protein HP1α/β, splicing factors Ser/Arg-rich protein (SRp20) and alternative splicing factor 1/pre-mRNA-splicing factor 2 (ASF1/SF2) as interaction partners (Loomis *et al*., 2009). It has also been shown that the inclusion of the CD44 variant exons in humans is regulated by SWI/SNF (SWItch/Sucrose Non-Fermentable) complex, suggesting that RNA splicing is also regulated by chromatin and its components (Batsche *et al*., 2006). Moreover, the enrichment of H3K9me3 was observed on the variant regions of CD44 in both HeLa cells (Batsche *et al*., 2006) as well as human T cells (Barski *et al*., 2007), which favors the inclusion of CD44 variant exons. H3K9 methylation provides the binding site for the chromodomain (CD) of HP1 proteins and HP1γ has been reported to be the only HP1 isoform on the coding region of active genes (Vakoc *et al*., 2005, Mateescu *et al*., 2008). These results point to a possible role for the H3K9me3 histone mark in the regulation of recruitment of splicing factors mediated by the chromatin-adaptor protein HP1. HP1γ may function in a way structuring chromatin and pre-mRNA to slow down RNA Pol II elongation, which in turn facilitates the recruitment of spliceosome as there is no study showing the association between HP1γ and spliceosome so far. Loomis et.al. found both HP1γ and the splicing factor SRP20 binding to the methylated H3 peptide by pull-down and mass spec (Loomis *et al*., 2009).

1.8 T-cell identity and epigenetic memory

1.8.1 T cell development

T cell lymphopoiesis takes place primarily in the thymus, which serves as a suitable home for haematopoietic stem cell (HSC)-derived lymphocyte progenitors becoming T cells (Zlotoff and Bhandoola, 2011). By contrast, B cell development occurs in bone marrow (and the liver in the foetus) in mammals. Although T and B cells might share a common lymphoid progenitor, unlike B cells of which, the development occurs in the bone marrow, T cells require exit from the bone marrow and differentiate with unique signals in the thymus (Schmitt *et al*., 2004). Fig 1.8.1 outlines the steps of T cell differentiation in the thymus, which is defined by the specific expression of different cell surface markers (Fig 1.8.1). Firstly, T cells start as CD4/CD8 double negative (DN) which then become CD4/CD8 double positive (DP), and lastly, they mature into CD4 or CD8 single positive (SP) T cells. The DN stage can be further subdivided into DN1, DN2, DN3 and DN4, which express different combinations of cell-surface markers, CD25 and CD44. As shown in Fig 1.8.1, T cells at the first two stages (DN1, DN2) are CD44+ and subsequently, CD44 is downregulated, and its expression stays low throughout the rest of T cell development. When T cells are activated through recognition of specific antigen, there is a rapid increase in the expression of CD44 on the cell surface. Memory T cells retain high CD44 expression on their cell surface (Godfrey *et al*., 1993, Berard and Tough, 2002, Butterfield *et al*., 1989). Notch signalling is said to be required during the transition of early T cell progenitor (ETP) to DN2 and ETP to DN3 (Sambandam *et al*., 2005, Tan *et al*., 2005). Under the influence of the Notch signalling pathway, T cells undergo a complex programme which leads to T cell maturation (Laky *et al*., 2006, Laky and Fowlkes, 2008). CD4+ SP “helper” cells and CD8+ SP “cytotoxic” cells are separated at an early stage within the thymus (Rothenberg and Zhang, 2012). After T cells leave the thymus, they continue to specialize in response to antigens, turning on a gene expression programme to become

distinct cytokine-producing T-cell (Th1, Th2, Th17, and Treg cells) or cytotoxic T-cells (CTLs). (Zhang *et al*., 2012). During the T cell activation process, the T cell receptor (TCR) on both CD4+ helper T cells and CD8+ cytotoxic T cells binds to the antigens presented by antigen presenting cells (APCs), which triggers initial activation of the T cells. This is followed by binding of CD4 and CD8 molecules to the major histocompatibility complex (MHC) class II and MHC class I respectively, which further stabilises the whole structure (Nakayama, 2014). Antigen presentation by MHC proteins is essential for adaptive immunity. There are also some co-stimulatory proteins on APCs involved that help to activate T cells.

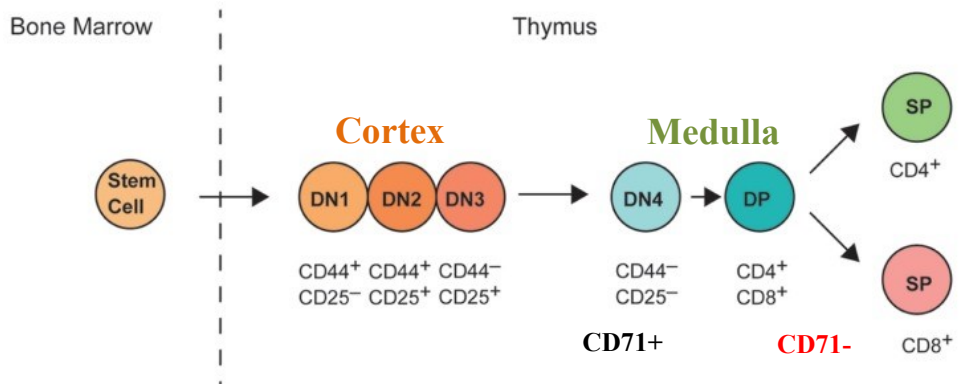

Fig1.8.1. Schematic diagram showing the intra-thymic T-cell development with well-defined differentiation cell surface markers. *Hematopoietic stem cells arise in the bone marrow and migrate to the thymus. In the thymus, T cells move from cortex to medulla. Thymocyte differentiation is characterized by the expression of well-defined cell-surface markers, including CD4, CD8, CD44 and CD25, as well as T-cell receptor (TCR). CD71 is the transferrin receptor, which is lost on mature T cells. Double negative (DN) cells are CD71+ (black) and double positive (DP) cells are CD71- (red). Early committed T cells do not express CD4 or CD8 (DN) thymocytes. DN thymocytes can be further subdivided into four stages of differentiation (DN1, CD44+CD25-; DN2, CD44+CD25+; DN3, CD44-CD25+; and DN4, CD44-CD25-). At the DN3 stage, DN cells express a pre-TCR which triggers the upregulation of CD4 and CD8 expression on the cell surface, and progression to the CD4+CD8+ DP stage. Interactions between Notch receptor-expressing thymocytes and thymic stromal cells that express Notch ligands induce a complex programme of T-cell maturation in the thymus, which ultimately results in the generation of self-tolerant CD4+ helper T cells and CD8+ cytotoxic T cells, which migrate from the thymus to peripheral. This figure is adapted with permission from "A transgenic mouse model of human T cell leukemia virus type 1-associated diseases" Takeo Ohsugi (Ohsugi, 2013).*

Previously, transferrin receptor, CD71 was suggested as a marker for immature, proliferating T cells in the thymus (Brekelmans *et al*., 1994). During early T cell development in the thymus, there is an intense proliferation phase in which T cells are expressing CD71 (CD71+) but subsequently, CD71 expression ceases when T cells become CD4/CD8 double positive (Fig 1.8.1). The sequential expression of CD71 on T cells in the thymus is shown in Fig 1.8.2. An alternative illustration of CD71 expression on T cell surface during development is in Fig 3.3.2 in section 3.8.2.

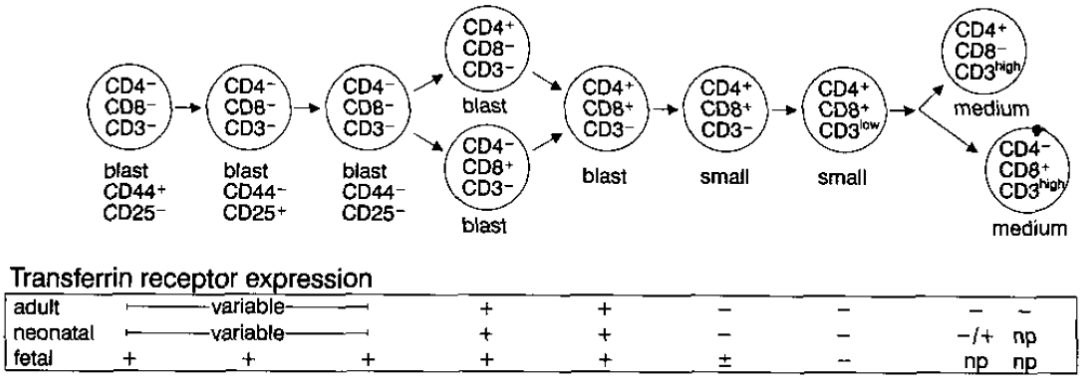

Fig 1.8.2. Transferrin receptor CD71 expression during murine T cell development in thymus. *This schematic diagram is showing the indicated expression of CD71 on T cell surface during early development (CD4/CD8 DN) and subsequently ceases when T cells become CD4/CD8 DP. Some of the mature thymocytes were not present in neonatal or fetal thymus. This figure is adapted with permission from "Transferrin receptor expression as a marker of immature, cycling thymocytes in the mouse" Pieter Brekelmans et al., (Brekelmans et al., 1994)*

1.8.2 Memory T cell

Naïve T cells are those that have never encountered and responded to a pathogen. When they recognize antigens, they undergo clonal expansion to generate massive numbers of effector T cells. More specifically, these are a type of effector T cell, called cytotoxic T cells which can then migrate into inflamed tissues and kill infected cells (Kaech and Cui, 2012). However, the majority (90-95%) of effector T cells undergo apoptosis, whilst the remaining activated cells

establish a small population of memory T cells pool (Palmer, 2003). A distinctive feature of memory T cells is that they are able to turn on a distinct cohorts of inducible gene expression programme more rapidly and at a greater level than their naïve and effector counterparts in response to re-infection (Pennock *et al*., 2013). These genes include several well-described immune-responsive genes, such as interleukin-2 (IL-2), tumour necrosis factor (TNF), and interferon-γ (IFNG). The rapid and abundant inducible gene expression program in memory T cells is termed 'transcriptional memory' (Dunn *et al*. 2015) and remarkably this transcriptional memory can be retained up to 75 years after their first encounter with an antigen (Hammarlund *et al*., 2003).

To date, memory T cells have been extensively studied and recently, two general pathways of their formation have been proposed: the memory T cells either arise from a subset of the effector cells that escape apoptosis, or descend directly from naïve T cells (Kaech and Cui, 2012) (Fig 1.8.3 a/b). In these studies, DNA accessibility and DNA methylation profile experiments in populations of naive, effector and memory T cells in human T cells and *in vivo* in mice revealed that DNA methylation profile differs from that in naïve T cells which, in effector cells, DNA methylation on genes encoding key components of the effector response is lost suggesting that these genes are turned "on" and this was catalysed by DNA methyltransferase DNMT3a (Akondy *et al*., 2017, Youngblood *et al*., 2017). Their evidence favors the model shown in Fig 1.8.3 b and it is indicated in these two studies that epigenetic regulation could play a role in T cell memory. Moreover, in memory cells, both naive-associated genes and genes encoding the effector molecules have been found to retain a low level of DNA methylation which could, in turn, be needed to maintain both the memory-cell population and the ability of memory cells to re-express effector molecules quickly to fight re-infection (Kaech and Cui, 2012) (Fig 1.8.3 c). Notably, memory T cells can be further

subdivided into central memory T cells (T_{CM} cells), effector memory T cells (T_{EM} cells) and tissue resident memory T cells (T_{RM}). Both T_{CM} cells and T_{EM} cells have an intermediate to high expression of CD44 and they both express L-selectin (CD62L) but T_{CM} cells are circulating through the body and T_{EM} cells are found in the peripheral circulation except the lymph nodes. Therefore, CD44 expression is usually used as a T cell surface marker for distinguishing naïve T cells from memory T cells in mice. T_{RM}, in contrast, only occupy tissues without recirculating. Whether these subpopulations of memory T cell arise through the same pathway needs to be investigated in the future.

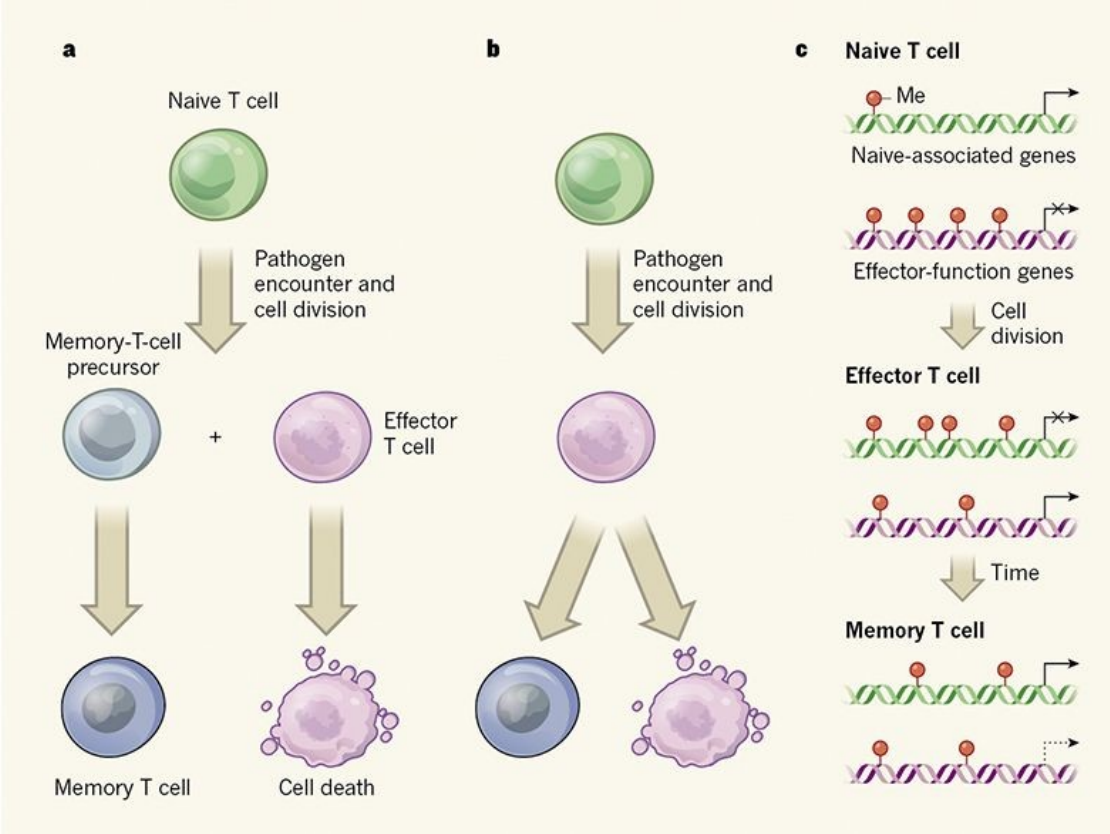

Fig 1.8.3. Two proposed pathways of memory T cells formation. a. *This model proposes that the precursor cells that give rise to memory T cells and effector T cells both arise independently from naive T cells.* ***b.*** *In another model, a subset of effector cells gives rise to memory T cells.* ***c.*** *In both Akondy et al. and Youngblood et al. studies, they analysed the methylation of genes associated with naive-cell function and effector-cell function in naive cells, effector cells and memory cells. Their evidence is consistent with the model shown in* ***b****. This figure is adapted with permission from "The origins of memory T cells" Omilusik KD and Goldrath AW (Omilusik and Goldrath, 2017).*

1.8.3 Epigenetics in T cell memory

Although signaling pathways and transcription factors are known to be the key players during our body's defense against pathogen infections, it is becoming clear that epigenetic regulation plays important roles in turning on a cell lineage-, context-specific and precise gene expression program in diverse cell types (Mehta and Jeffrey, 2015, Lau *et al*., 2018). Such precise gene expression programs allows the immune system to respond more rapidly and effectively to previously encountered pathogens which is thought to be the hallmark of adaptive immunity (J. Moticka, 2016).

Nowadays, epigenetic memory studies have been largely limited to processes such as development and metabolism, therefore, the mechanism underlying epigenetic memory for signal-dependent transcription in immune cells has remained elusive. A recent global epigenome study showed that memory IFNβ-stimulated genes (ISGs) acquired H3.3 and H3K36me3 marks after initial IFN stimulation, which further accelerated the recruitment of RNA polymerase II and transcription and chromatin factors to these genes (Kamada *et al*., 2018). This, together with emerging evidence from model organisms (Tamura *et al*., 2009, Sarai *et al*., 2013, Banaszynski *et al*., 2013, Ng and Gurdon, 2008), which provides insights into the contribution of epigenetic regulation in adaptive immunity, suggests that epigenetic mechanisms are central to establishing and maintaining transcriptional memory (Dunn *et al*., 2015). These epigenetic mechanisms are thought to be diverse and include not only classical histone modification events, but also some less well-known mechanisms involving chromatin structure, histone variants, upstream signaling pathways, and nuclear localization of genomic regions. This multi-layered epigenetic mechanism is thought to elicit transcriptional memory programs in T cells (Dunn *et al*., 2015). Although the precise mechanism of multi-layered epigenetic regulation in T cell memory remains unclear, the contribution of histone

modifications in memory T cell development has been explored extensively and are now thought to epigenetically mark genes and prime them for robust reactivation following reinfection. A summary table illustrates the known roles of variant histones and chromatin chaperone/remodeling proteins in regulating transcription in T memory cells (Fig 1.8.4).

In this thesis, I will examine the role of HIRA in regulating chromatin *in vivo* by employing mice in which the HIRA gene is deleted in T cells of the immune system. It will focus on the effect of this HIRA deficiency on T cell development including the acquisition of specific gene expression patterns and the key process of T cell receptor rearrangement and relate the perturbations in these processes to H3.3 occupancy (see result section 3.8).

Mechanism	cell type/species	role
PTMs		
Acetylation	Memory CD4+/CD8+ T cells	▪ Marks memory responsive genes for rapid reactivation
		▪ Form stable marks of transcriptional activation that are retained in memory T cells
Methylation	Memory CD4+/CD8+T cells	▪ Loss of repressive histone methylation marks at active genes are preserved in memory T cells to facilitate faster transcription of target genes
Histone variants		
H3.3	mES cells	▪ Marks gene enhancers for rapid reactivation
		▪ Primes genes for transcription by destabilizing nucleosome structure to facilitate recruitment of transcription factors
	Xenopus	▪ Required for transcriptional memory following somatic cell transfer
	pre-B cells	▪ Forms stable marks of transcriptional activity that persist through cell division
H2A.Z	Yeast/CD4+ T cells	▪ Destabilizes chromatin structure to facilitate recruitment of transcription machinery
	Yeast	▪ Regulates the localization of recently repressed genes to the nuclear periphery to facilitate transcriptional memory

Fig 1.8.4. Summary of epigenetic mechanisms and their role in memory cell development. *This table is adapted with permission from "Multi-layered epigenetic mechanisms contribute to transcriptional memory in T lymphocytes" Jennifer Dunn et al. (Zhang et al., 2005a)*

1.8.4 A potential role for HIRA/H3.3 in regulatory T cell memory

Previous proteomics data obtained in our lab by Stable Isotope Labelling of Amino Acids (SILAC), the level of proteins involved in T cell biology and V(D)J recombination were affected by Cre-loxP (Abi-Ghanem *et al*., 2015) mediated deletion of HIRA in murine peripheral T cells (Vineet Sharma PhD thesis 2014). This SILAC data also showed that CD44 (H-CAM) expression is upregulated in proliferating peripheral lymph node T cells. These two phenomena might be linked by the fact that CD44 up-regulation in the absence of HIRA could be the consequence of impaired T cell development in thymus. It has been known that T cells are able to spontaneously undergo extensive proliferation after transfer into immune-deficient hosts and in such cases upregulate CD44 (Surh and Sprent, 2000). In addition to the T cell proliferation aspect indicated by the increased CD44 level in our model system, it would be interesting to investigate if the memory T cells' induction or maintenance has been affected in the HIRA knock-out T cells. CD62 (L-selectin) and CD44 are two adhesion molecules associated with naïve and previously activated T cells respectively. It has been noted that naïve T cells express CD62LhiCD44lo phenotype, whereas previously activated T cells express CD62LloCD44hi phenotype which persists following activation and is referred to as a memory cell phenotype (Gerberick *et al*., 1997). Memory B and T cells are capable of "remembering" pathogens long after they are first encountered (Van Kaer, 2015) and reproduce a faster and stronger immune response than the first time. Taken together with the previous observation of H3.3 localization at the V(D)J recombining loci (Jones *et al*., 2011), an important functional role might be played by HIRA in regulating turnover of H3.3 at genomic regions to enable tightly regulated immune system development.

1.8.5 T cell receptor (TCR) V(D)J recombination

V(D)J recombination is the process by which lymphocytes randomly assemble different gene segments – known as variable (V), diversity (D) and joining (J), in order to generate unique receptors that recognize many different types of molecule (Roth 2014) (Fig1.8.5). V(D)J recombination is initiated and directed by the lymphoid-specific recombinase activating gene (RAG)1 and RAG2 protein complex (referred to as RAG), which work together with DNA bending factors, HMG1A or HMG1B to carry out DNA cleavage (van Gent *et al*., 1997, Oettinger *et al*., 1990). RAG can recognize recombination signal sequences (RSSs) that flank each V, D, or J segment of TCR and immunoglobin (Ig) and introduce DNA double-strand breaks between the them (Bassing *et al*., 2000). The rearrangements occur in an ordered fashion, with D to J joining proceeding followed by joining of V segment to the rearranged DJ segments (Roth, 2014) (Fig 1.8.6). V(D)J recombination is thought to be developmentally programmed through changes in chromatin structure and chromatin organization which provide RAG proteins access to RSSs (Krangel 2007, 2003; Cobb *et al*. 2006). During early T cell development in the thymus, TCRβ rearrangement occurs early in CD4/CD8 DN3 (Zuniga-Pflucker, 2012). While primary TCRα rearrangement happens after T cells become CD4/CD8 DP with secondary rearrangement in later resting DP cells to produce a mature αβTCR (Jones and Zhuang, 2007). Only DP cells with a functional TCR are capable of recognizing antigens presented by MHC molecules and receive a positive-selection signal to further differentiate to CD4+ or CD8+ single-positive (SP) cells (Jones and Zhuang, 2007).

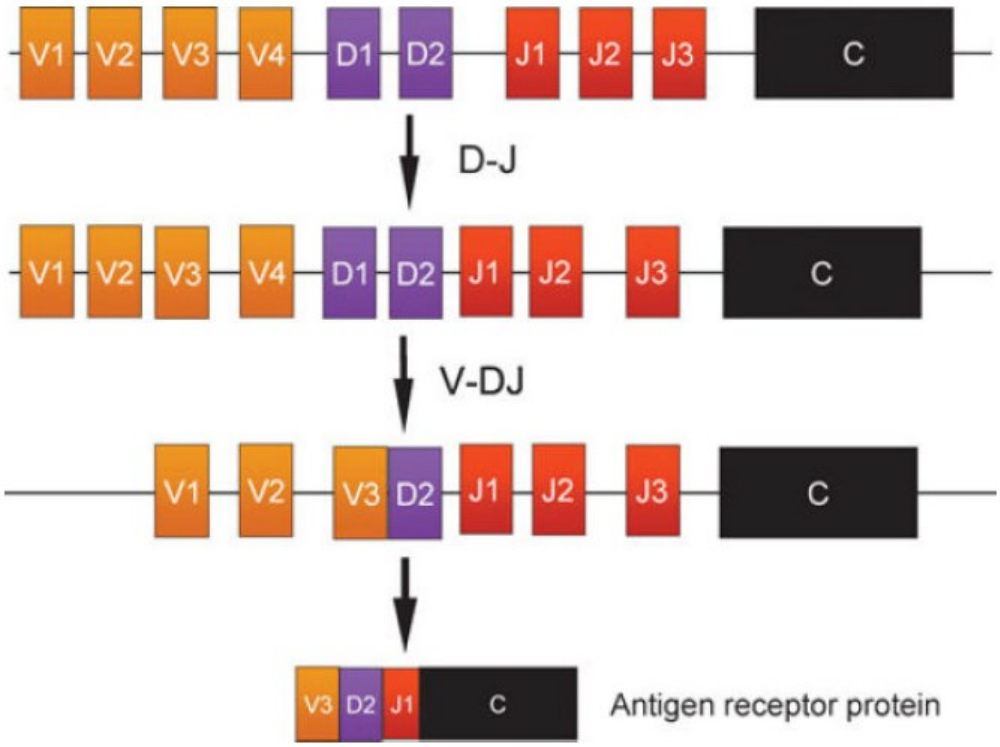

Fig 1.8.5. Antigen receptor variable exons are assembled by V(D)J recombination. *Assembly of a complete variable exon occurs in two steps. First, a D and a J segment are chosen from among several possibilities and are brought together to form a D-J rearrangement. Then a V region is selected and joined with the D-J rearrangement to form a complete V(D)J exon. Immunoglobulin light chain genes and TCR alpha and γ genes rearrange in a single step, involving V-J recombination, as D segments are absent from these loci. This figure is adapted with permission from "V(D)J Recombination: Mechanism, Errors, and Fidelity" David B. Roth (Roth, 2014).*

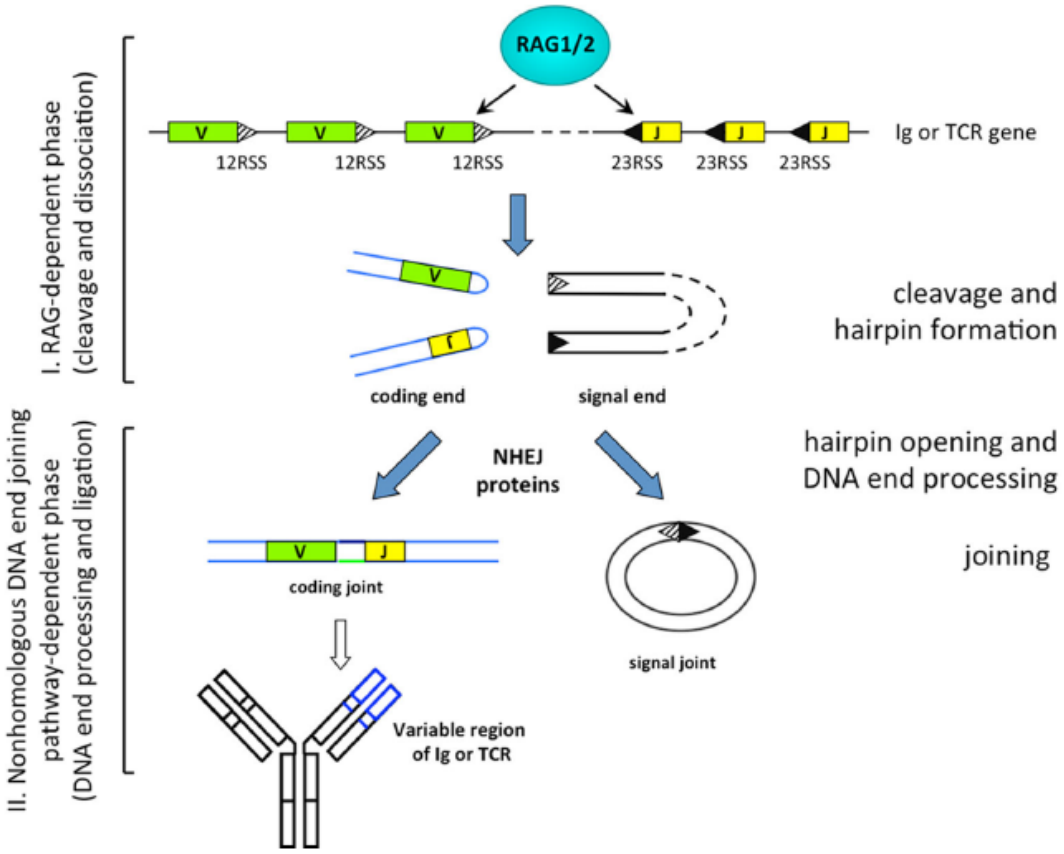

Fig 1.8.6. Schematic model of V(D)J recombination. *V(D)J recombination consists of two steps: RAG dependent cleavage phase and NHEJ-dependent joining phase. The RAG complex binds and brings two RSSs together (stripe and black triangle on 12V and 23J respectively) and introduces double-strand DNA breaks. Both coding ends and signal ends are joined by NHEJ pathway. Functional coding joint encodes variable domain of TCR. This figure is adapted with permission from "Histone methylation and V(D)J recombination" Shimazaki, N. & Lieber, M.R. Int J Hematol (Shimazaki and R Lieber, 2014)*

1.8.6 Chromatin and V(D)J recombination

V(D)J recombination generates a diversity of antigen receptor genes in a lineage- and stage-specific manner and is thought to be orchestrated through complex mechanisms within a highly complex chromatin architecture (Shimazaki and Lieber, 2014, Shih and Krangel, 2013). This process is directed by the lymphoid-specific recombinase activating gene (RAG)1 and RAG2 protein complex (referred to as RAG) (Matthews and Oettinger, 2009, Schatz and Spanopoulou, 2005, Bassing *et al*., 2002). RAG can recognize recombination signal sequences (RSSs) that flank each TCR or Ig V, D, or J gene segment. During this recombination event,

the most fundamental step is the restriction imposed by RAG protein expression, which is limited to developing pro- and pre-B cells and DN and DP thymocytes (Shih and Krangel, 2013, Kuo and Schlissel, 2009). In both the B and T cell lineages, V(D)J recombination events are thought to be developmentally programmed through changes in chromatin structure and chromatin organization that provide RAG proteins access to pairs of RSSs (Krangel, 2007, Krangel, 2003, Cobb *et al*., 2006). Recent studies revealed dynamic changes in histone modification at recombinationally active V(D)J loci which favors an open chromatin that gives the accessibility of the RAG complex to the RSSs at TCR genes. In their studies, they found that only the loci undergoing recombination have hypermethylation of lysine4 of histone H3 and acetylation of H3/H4 (Xu and Feeney, 2009, Subrahmanyam and Sen, 2010), which are thought to correlate with transcriptional activity (Bernstein *et al*., 2002).

1.9 Sexual Dimorphism

Sexual dimorphism refers to differences between males and females of a species at chromosomal, gonadal, hormonal and behavioral level (Angelopoulou *et al*., 2006). It describes a series of morphological, physiological and behavioral phenotypes that distinguishes males from females (Rigby and Kulathinal, 2015). Sex differences in human diseases including rates of disease incidence, symptoms and age of onset bring us greater interest in studying this phenomenon.

At the chromosomal level, genetic sexual dimorphism refers to the presence of two identical (XX) in females and two different (XY) sex chromosomes in males, which carry distinct content of genes and regulatory sequences (Angelopoulou *et al*., 2006). In the mouse, at embryonic day 10.5 (E10.5), the Y chromosome-specific sex-determining region Y (*Sry*), a HMG box transcription factor starts to express and causes testes development and testicular secretions in males, whereas, in the absence of *Sry*, ovaries develop in females (Rigby and Kulathinal, 2015). In addition, the presence of a nuclear hormone receptor Dax1 (DSS–AHC-critical region of the X chromosome 1) in the XX gonad represses the male developmental pathways in females (Rinn and Snyder, 2005). It has been reported that a single-base pair mutation in the *Sry* gene results an XY sex-reversed female (McElreavey *et al*., 1992). Once formed, ovaries and testes regulate the downstream sexual differential developmental processes by secreting sex-specific hormones at hormonal level (Rigby and Kulathinal, 2015).

To date, sex determination has been best explained by three factors, the organizational effects of gonadal steroids, the activational effects of hormones and the non-gonadal effects of the sexual inequality in the number and type of sex chromosomes (Arnold, 2014). Sex hormones (mainly androgens, estrogens and progestins) secreted by testes and ovaries act on many tissues to induce non-gonadal phenotypes in males and females. In hours to weeks after removal of

the gonads, these hormonal effects typically disappear, hence sex differences that are eliminated by adult gonadectomy are classified as activational effects and can be reversed (Arnold, 2014). However, those gonadal hormones acting at early stages of development lead to sex differences that do not disappear after gonadectomy is classified as the organizational effects of gonadal hormones (Phoenix *et al*., 1959). Finally, there are some sex differences that cannot be explained by either activational or organizational effects of gonadal hormones, but by direct effects of sex chromosome which, differentially expressed genes on X and Y chromosomes in each XX and XY cell act in a sex-specific manner to cause sex differences in non-gonadal phenotypes (Arnold and Chen, 2009, Arnold, 2004) (Fig 1.9.1). The "four core genotypes" (FCG) mouse model which comprises four genotypes: XX gonadal males or females and XY gonadal males or females suggested that sex chromosome complement (XX vs. XY) is unrelated to the animal's gonadal sex (*Sry* gene) (Arnold and Chen, 2009) (Fig 1.9.2). It is becoming clear that both sex chromosome effects such as dose of X genes or parental imprinting and gonadal hormones effects are thought to regulate sex differences in behavior, gene expression and susceptibility to disease. However, this difference in X-linked gene dosage between males and females is further corrected by random X chromosome inactivation (XCI) in females (Snell and Turner, 2018). The X chromosome has the potential to cause sex difference in several ways. Firstly, expression of XCI can be either from maternally derived (Xm) or paternally derived X chromosome (Xp). Secondly, a gene escaping XCI leads to a higher expression level of this gene in XX females compared to XY males. Thirdly, genomic imprinting on Xp results in differential gene expression between sexes. Moreover, the availability of heterochromatic factors on X or Y chromosomes, so that may alter the autosomal gene expression in a sex-specific manner (Snell and Turner, 2018, Wijchers and Festenstein, 2011). This sex-specific effect is supported by the studies in *Drosophila* where, the large heterochromatic Y chromosome results in genome-wide gene expression variation at distinct

loci showing position effect variegation (PEV) with altered availability of heterochromatic factors and hence the epigenetic status of specific autosomal loci (Wijchers and Festenstein, 2011, Lemos *et al*., 2010).

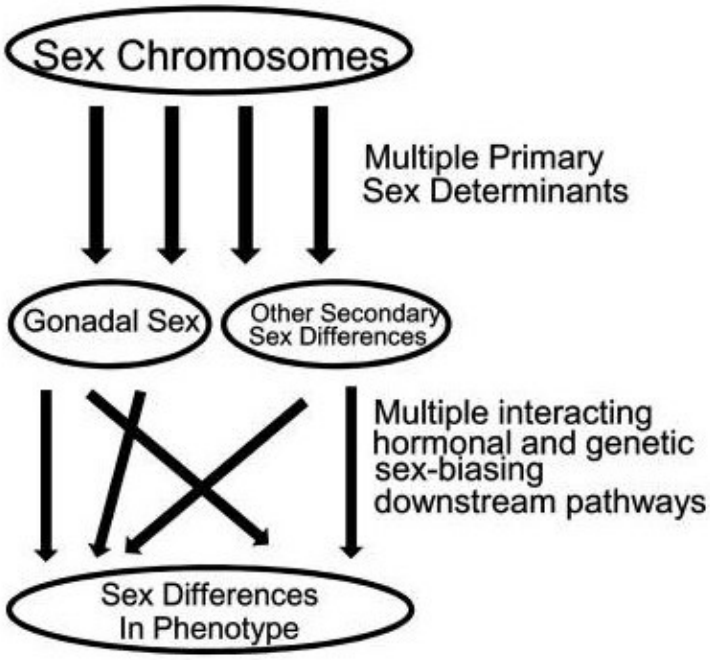

Fig 1.9.1 Schematic diagram of sex determination model. *This model illustrates multiple primary parallel-acting factors encoded by the sex chromosomes, which activate different secondary downstream pathways to cause sex differences in phenotype. In this model, sex hormones are the most important group of secondary factors causing sex differences in phenotype of mammals. This figure is adapted with permission from "Cell-autonomous sex determination outside of the gonad" Arnold et al., (Arnold et al., 2013).*

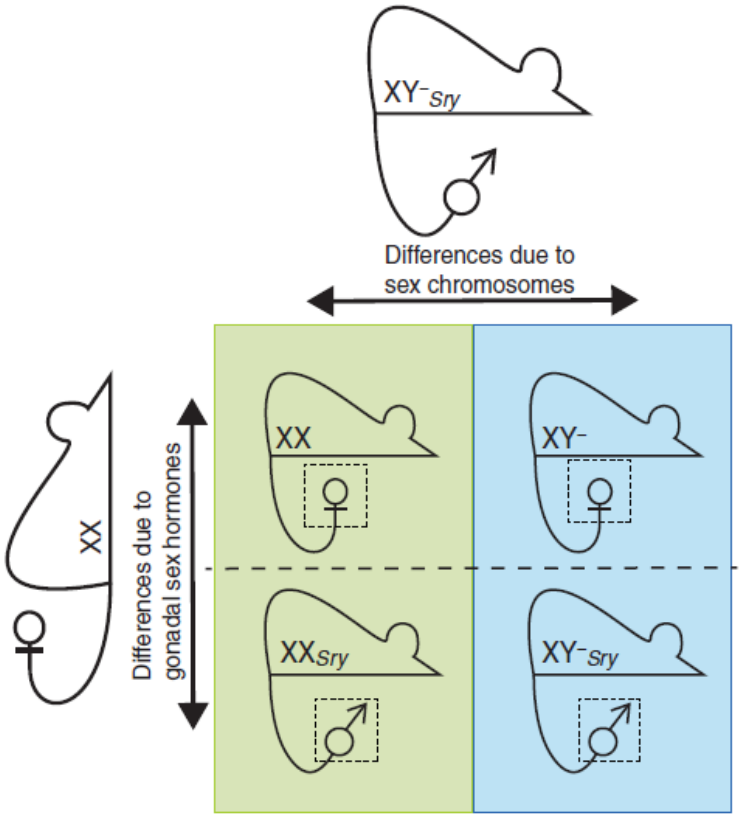

Fig 1.9.2. FCG mice are produced by breeding XX gonadal females with XY−Sry gonadal males, producing the four genotypes shown. *The figure shows the genetic differences among the four genotypes, in presence/absence of the Y chromosome and number of X chromosomes. FCG mice allow a 2 × 2 comparison to detect the phenotypic effects of sex (Sry present or absent) or sex chromosome (XX vs. XY). This figure is adapted with permission from "Sex Chromosome Effects on Male-Female Differences in Mammals" Snell DM and Turner JMA (Snell and Turner, 2018)*

A previous study in *Drosophila* showed that the depletion of HP1a resulted in male-biased lethality (Liu *et al*., 2005), which raised the question as to whether mammalian HP1 might contribute to sex dimorphism. Recently the importance of HP1γ in regulating sex differences was demonstrated in our lab. Of particular interest, RNA-seq analysis showed that males showed a higher dependency on HP1γ in maintaining their normal gene expression profile compared to females (Law *et al*., 2019). Wildtype (WT) male embryonic fibroblasts (MEFs) were shown to proliferate at a faster rate than female MEFs consistent with previous observations that the growth rate is higher in male compared with female mammals (Burgoyne

et al., 1995, Burgoyne, 1993, Thornhill and Burgoyne, 1993). HP1γ knockout (KO) completely abolished this difference in proliferation. Gene ontology analysis also revealed a sex dimorphic transcriptomic signature for cell cycle-related genes (Law *et al*., 2019). Previously, a study by our group showed a sizeable number of autosomal genes that are epigenetically regulated by sex chromosome complement (XY or XX) rather than phenotypic sex using a 'sex-reversal' mouse (four core genotype model, see above) in which the mice were either deficient or transgenic for the sex determining *Sry* gene.

1.10 Hypotheses and Aims of this project

1.10.1 Hypotheses

- HIRA mediated H3.3 incorporation regulates the transcription of a subset of genes and rearrangement of the T cell receptor locus.
- HIRA/H3.3 pathway is involved in regulating T cell development and the establishment of memory T cells.
- HP1γ is important for regulating sex dimorphism in gene expression and the cell cycle program in mouse embryonic fibroblasts (MEFs).
- HP1γ is involved in regulating sex dimorphic alternative RNA splicing in mouse embryonic fibroblasts (MEFs).

1.10.2 Aims

The overall hypotheses that this thesis addresses are 1) that HP1γ, acts *in vivo* to regulate sexually dimorphic gene expression and sex dimorphism in cellular proliferation and 2) that HIRA/ H3.3 plays a role in the development of T cells. Therefore, in this project, using mouse thymocytes, which are wild type or homozygous conditional knockout for HIRA and mouse embryonic fibroblasts, which are wild type or homozygous knockout for HP1γ, I aimed to experimentally address the following general questions:

1. What is the genome-wide distribution of H3.3 *in vivo*?
2. What is the role of HIRA in the regulation of gene expression via H3.3 and what is its role in T cell development?
3. What is the role of HP1γ in regulation of sexually dimorphic expression of genes?

4. What is the role of HP1γ in regulation of alternative RNA splicing?

The results section has been divided into distinct sections based upon these hypotheses – Chapter 3 deals with the HIRA/H3.3 investigations and Chapter 4 deals with the HP1γ /sex dimorphism investigations. In the general discussion the crossover between these two separate chapters is discussed.

Chapter 2 - Materials and Methods

2.1 Experimental mice

2.1.1 Animal handling

Animals used to fulfill the thesis were maintained and handled according to the Imperial College Subcommittee for Animal Research guidelines and the British Home Office regulations.

2.1.2 Transgenic mouse models

2.1.2.1 Transgenic H3.3B-EGFP mouse model

H3.3B-EGFP mice containing knock-in construct of H3.3B-EGFP were generated by Dr. Vineet Sharma (Imperial College London, London, U.K.) and Dr. Buhe Nashun (MRC Clinical Science Centre, London, U.K.). H3.3B-EGFP mice were generated by inserting the EGFP gene downstream of the coding sequence (CDS) of the *H3f3b* gene (encoding histone variant H3.3b) (Fig 2.1). Hence, animals containing this target knock-in will produce H3.3B-EGFP fusion proteins.

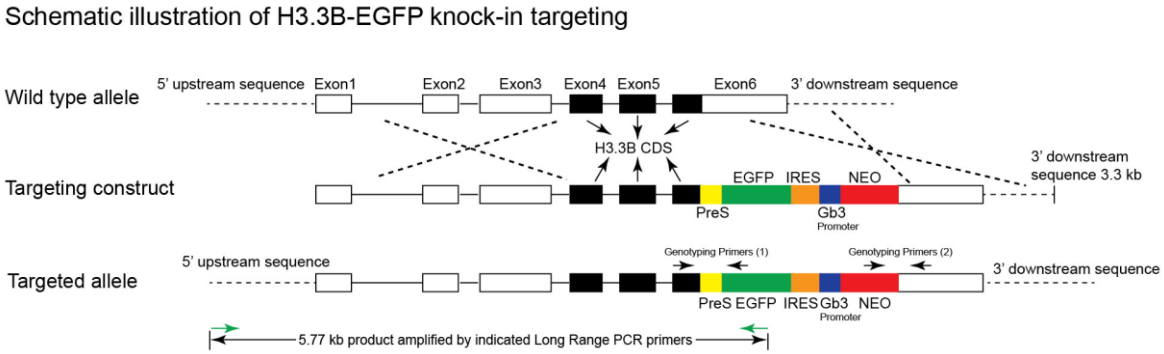

Fig 2.1. Schematic illustration of H3.3B-EGFP knock-in targeting. *The EGFP construct was inserted downstream of the coding sequence of the H3.3b gene. This figure is adapted with permission from "Continuous Histone Replacement by Hira Is Essential for Normal Transcriptional Regulation and De Novo DNA Methylation during Mouse Oogenesis" Nashun, Hill et al., (Nashun et al., 2015a)*

2.1.2.2 HIRA homozygous conditional knockout H3.3B-EGFP mice

HIRA homozygous knock-out mice are embryonic lethal (Roberts *et al*., 2002). No homozygous mutant mice survived until weaning. The breeding strategy used to obtain mice with a HIRA deletion specific for T cells was produced by Dr Philip Wise (GCMD, Imperial College London) *(Nashun et al., 2015b)* (Fig 2.2) A conventional knock out for *HIRA* (*HIRA* KO) was obtained from Prof. Peter Scambler (Roberts *et al*., 2002). Heterozygous mice for the conditional knock out allele (CKO+/-) for *HIRA* were obtained from WTSI Mouse Genetics Program. In the present project, mice with heterozygous conditional knock out of *HIRA* and heterozygous of *Cre* (*HIRA* CKO+/-, *Cre*+/-) were generated by mating the heterozygous knock out of *HIRA* with *Cre* (*HIRA* KO+/-, *Cre*+/+) mice (Cre expression is under the control of CD4 promoter) with the heterozygous conditional knockout of *HIRA* (*HIRA* CKO+/-) mice. By interbreeding these mice, mice with homozygous conditional knock out of *HIRA* (*HIRA* CKO-/-) were generated. Mice with homozygous conditional knock out of *HIRA* and expressing H3.3B-EGFP (*HIRA* CKO-/-, H3.3B-EGFP +/-) were generated by mating the *HIRA* CKO-/- mice with the H3.3B-EGFP knock in mice (H3.3B-EGFP +/-). Accordingly, it was expected that the floxed *HIRA* exon 4 would be deleted in T cells. Fig 2.3 illustrates the mating scheme of this line. Thymus, Lymph node and Spleen used were taken from 6-8 weeks old mice.

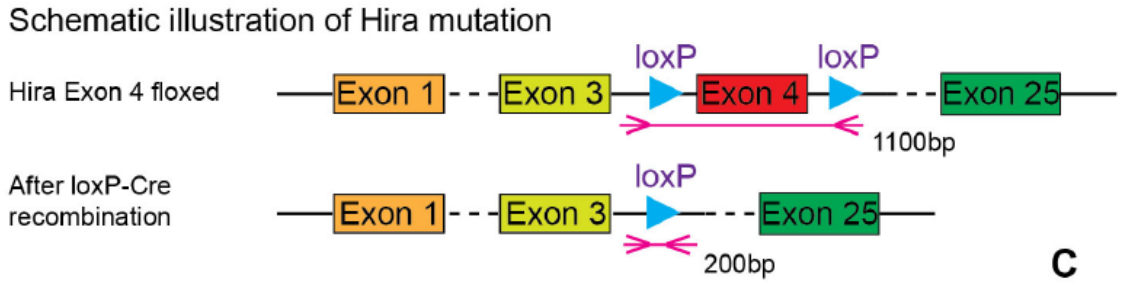

Fig 2.2. Schematic illustration of HIRA locus targeting. *This figure is adapted with permission from "Continuous histone replacement by HIRA is essential for normal transcriptional regulation and de novo DNA methylation during mouse oogenesis" Nashun, Hill et al., (Nashun et al., 2015b)*

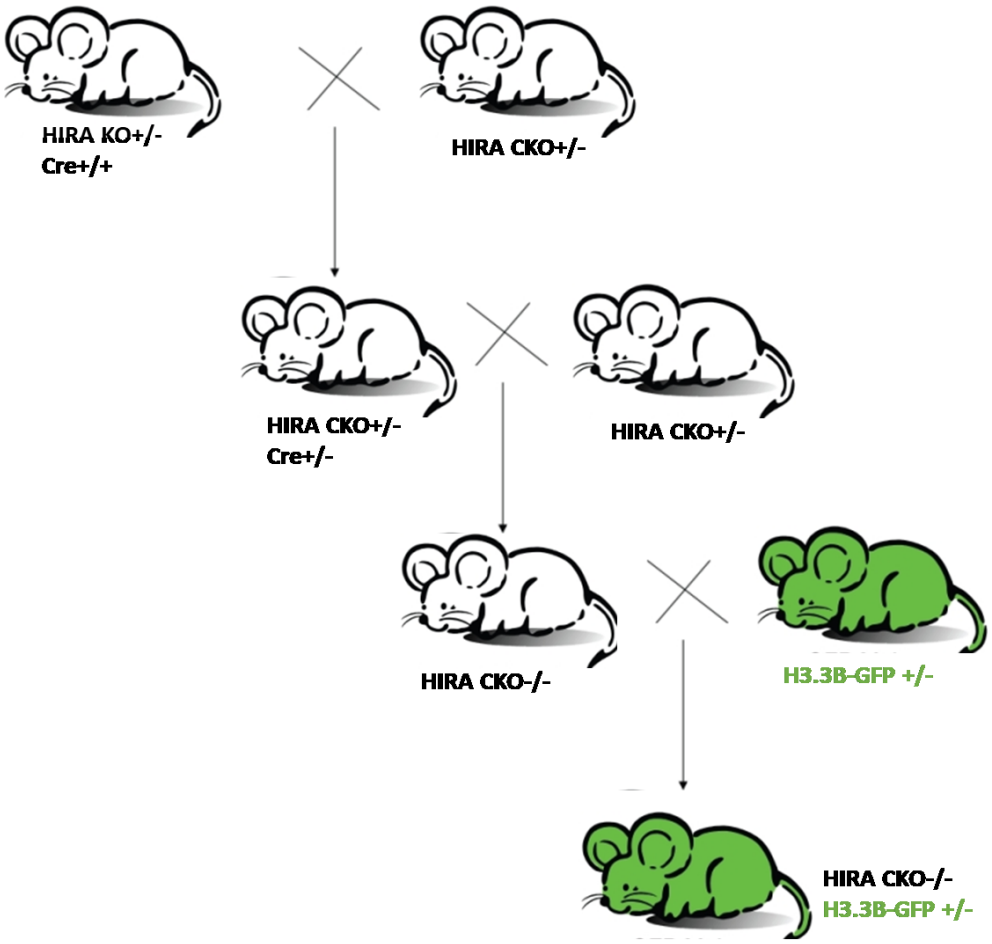

Fig 2.3. Schematic diagram demonstrating the mating scheme of the HIRA H3.3B-EGFP mice. *Mice with heterozygous conditional knockout of HIRA and heterozygous of Cre (HIRA CKO+/-, Cre+/-) were generated by mating the heterozygous knockout of HIRA with Cre (HIRA KO+/-, Cre+/+) mice with the heterozygous conditional knockout of HIRA (HIRA CKO+/-) mice. By interbreeding these mice, mice with homozygous conditional knock out of HIRA (HIRA CKO-/-) were generated. Mice with homozygous conditional knockout of HIRA and expressing H3.3B-EGFP (HIRA CKO-/-, H3.3B-EGFP +/-) were generated by mating the HIRA CKO-/- mice with the H3.3B-EGFP knock-in mice (H3.3B-EGFP +/-).*

2.1.2.3 HP1γ knockout (HP1γ-KO) mice

HP1γ KO mice were generated with a gene-trap method, in which, a single gene-trap retroviral vector (ROSAN β-geo) was inserted into intron 1 (998bp downstream of exon 1) of the *Cbx3* gene (encoding HP1γ) (Naruse *et al*., 2007) (Fig 2.4). With this insertion, a fusion transcript containing HP1γ exon 1 and β-geo of the gene-trap vector is generated, and transcription

stopped prematurely at the inserted polyadenylation site (poly A). Thus, functional HP1γ protein cannot be produced. HP1γ KO mice were originally on a C57BL/6 background which were then back-crossed at least ten times on to the CBA/ca background.

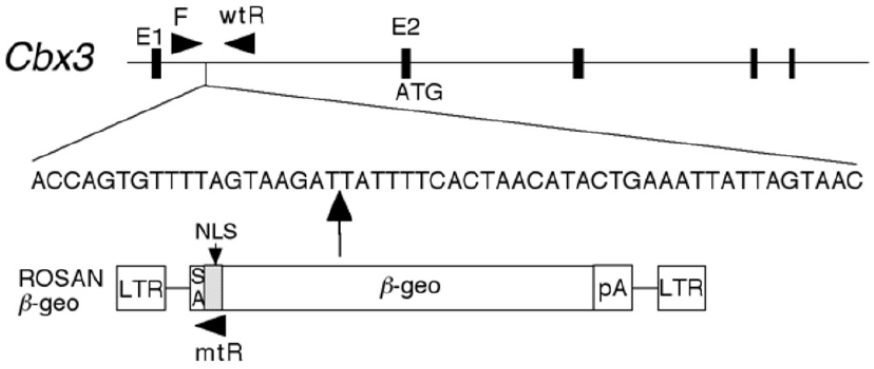

Fig 2.4. Schematic diagram illustrating the insertion site of the gene-trap vector in the Cbx3 gene in the HP1γ KO mice. *A single gene-trap retroviral vector (ROSANβ-geo) was inserted into intron 1 of the Cbx3 gene. Insertion leads to generation of non-functional HP1γ protein. PCR primers for genotyping are indicated by bold arrows on top: HP1γ common forward (F), HP1γ wild type reverse (wtR), HP1γ mutant reverse (mtR). This Figure is adapted with permission from "HP1gamma links histone methylation marks to meiotic synapsis in mice" Takada, Y et al. (Takada et al., 2011)*

2.1.2.4 HP1γ knockout H3.3B-EGFP (HP1γ KO H3.3B-EGFP) mice

HP1γ H3.3B-EGFP mice having heterozygous knock out of *HP1γ* (*HP1γ* +/-) and expressing H3.3B-EGFP fusion protein (H3.3B-EGFP +/-) were generated by mating the HP1γ KO mice (*HP1γ* +/-) with the H3.3B-EGFP mice (H3.3B-EGFP +/-). By interbreeding these mice, E13.5 embryos which express the H3.3B-EGFP fusion protein and are either wild type (*HP1γ* +/+, H3.3B-EGFP +/-) or homozygous knock out for HP1γ (*HP1γ* -/-, H3.3B-EGFP +/-) were generated. Mouse embryonic fibroblasts (MEFs) were subsequently derived from these embryos and used for experiments in this thesis. Fig 2.5 illustrates the mating scheme of this line.

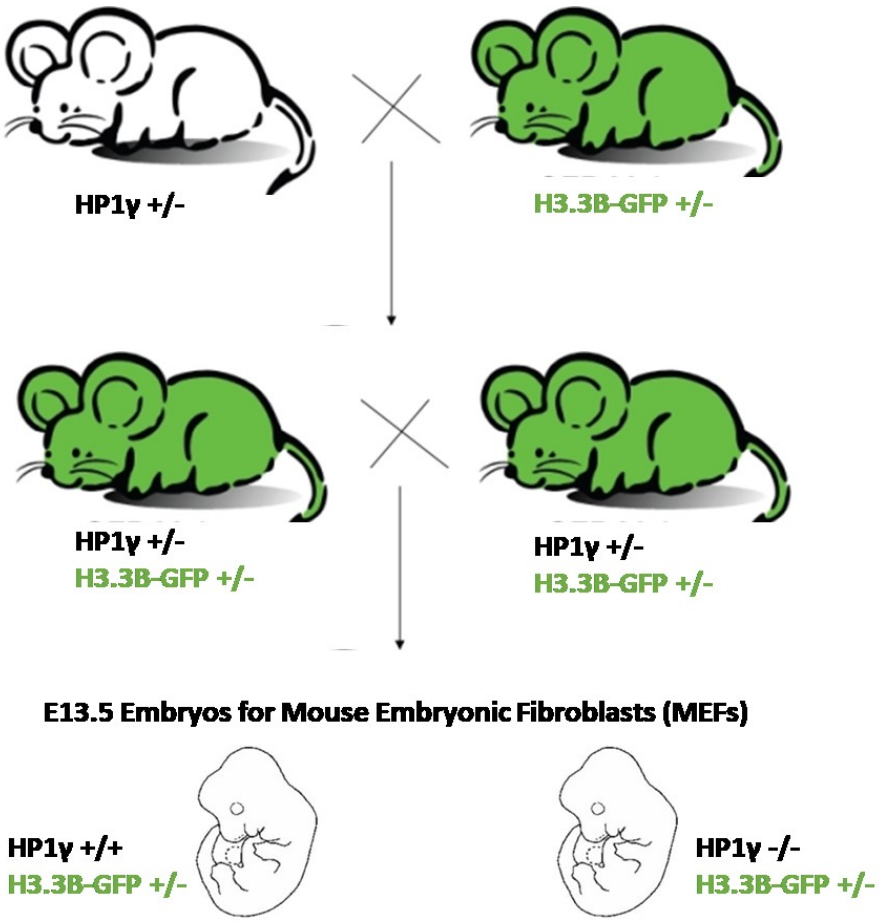

Fig 2.5. Schematic diagram demonstrating the mating scheme of the HP1γ/H3.3B-EGFP mice. *Mice with heterozygous knockout of HP1γ and expressing H3.3B-EGFP (HP1γ +/-, H3.3B-EGFP +/-) were generated by mating the HP1γ KO mice (HP1γ +/-) with the H3.3B-EGFP knock-in mice (H3.3B-EGFP +/-). By interbreeding these mice, E13.5 embryos with either WT or homozygous knock out HP1γ which express H3.3B-EGFP fusion protein were generated and MEFs were then derived from these embryos.*

2.2 Generation of Mouse Embryonic Fibroblasts (MEFs)

The uterus was obtained from pregnant female mice that were sacrificed at day 13.5 of gestation (E13.5) (considering the day of vaginal plug found as day 0) and placed in cold 1x PBS. Embryos were removed from the uterus and transferred to a fresh petri dish containing cold 1x PBS. Under the light microscope, placenta and yolk sack were separated from the embryo and internal organs were removed. The body of the embryo was transferred to 1ml of PBS and finely minced. 1.5 ml of 0.25% trypsin-EDTA (Sigma) was added to the suspended tissue and incubated at 37°C for 1.5min. To inactivate trypsin, 10ml of culture medium was added to the suspension and the sample was passed through a 0.7µm cell strainer. Then 10ml culture medium was used to rinse the cell strainer, giving a final cell suspension volume of 22.5ml. Cells in the suspension were then collected by centrifugation at 300g at 23°C for 5min. The supernatant was discarded, and the cell pellet was resuspended in 5ml culture medium and then transferred to a 6cm culture dish and incubated overnight (O/N) at 37°C, 5% CO2. Next day, culture medium was replaced with fresh culture medium. The cells were then cultured and expanded according to growth rate. Culturing conditions and details of genotyping can be found in later sections.

2.3 Cell culture

2.3.1 Culturing and passaging

2.3.1.1 Mouse embryonic fibroblasts (MEFs)

MEF cells were cultured until 95% confluent in 10cm dishes. Culture media were discarded, and the cells were washed once with 1x PBS at room temperature. Cells were detached by adding 1ml of 0.25% Trypsin-EDTA per dish followed by 3 min incubation at 37ºC for 5 min. Trypsin was inactivated by addition of 5ml culture media and the cells were transferred to Falcon tubes. The cells were collected by centrifugation at 300g at 23°C for 5 min. Supernatant was discarded and the cell pellet was re-suspended in fresh culture media. 1/3 of cells were seeded into each fresh 10cm dish with final culture media volume as 10ml and cultured at 37ºC, 5% CO2.

2.3.1.2 TX1072 female embryonic stem cell (ESC) line

This is a genetically polymorphic ESC line that was derived in Neil Brockdorff's lab (Oxford) from a mouse with one X-chromosome (X-chr) from the *Mus musculus castaneus* (Cast) origin and the other of *Mus musculus domesticus*, C57BL/6 (BL6) strain origin, containing an inducible promoter on the BL6 Xist allele; Differentiation and simultaneous induction of Xist for 4 days results in the inactivation of only the BL6-derived X-chromosome and coating by JARID2 (Jumonji And AT-Rich Interaction Domain Containing 2) protein. This generates cells with non-random X-inactivation on the BL6 allele which can then be identified by single nucleotide polymorphisms (SNP). Culturing and passaging conditions are the same as MEFs in section 2.3.1.1.

2.3.2 Culture medium

DMEM high glucose (GIBCO ®), Fetal bovine serum (Sigma) (15% v/v), Penicillin (GIBCO ®) (1% v/v), GlutaMAXTM-I 100x (GIBCO ®) (1% v/v).

2.4 MEF cell proliferation assay

To determine the effect of HP1γ knock out on MEF cell proliferation in both sexes, a cell proliferation assay was used to compare the cell proliferation rate in the different genotypes. The same number of cells (1 x 10^5) were seeded in 12-well plates in each passage when sub culturing MEFs. After 3 days incubation, the total cell number (Nx) in each well was counted by Muse® machine. 50µl MEFs were obtained and diluted in 450µl Guava ViaCount® solution (Guava Technologies®, USA) (10 times dilution). After 1 min incubation, samples were vigorously mixed and analysed with a Muse® Cell Analyzer. Then, the population doubling of MEFs was calculated by the following formula:

Population doubling in each passage = log2 (Nx/10^5)

Accumulative population doubling = Sum (P1: Px)

2.5 Propidium Iodide (PI) Staining for Cell-cycle Analysis

To investigate the effect of HP1γ KO on cell cycle, MEFs were stained by PI, a nucleic acid-binding fluorescent molecule. Firstly, 1x 10^6 MEFs were harvested and washed by 1x PBS at 1500rpm for 5min. Then, resuspend cells in 100µl 1x PBS followed by adding cell suspension to 1ml 70% ethanol (pre-stored at -20°C) drop by drop. After overnight incubation at -20°C, the samples were spun at 600g for 5min at 4°C and the supernatant was discarded. Subsequently, the cell pellet was washed by 1x PBS at 600g for 5 min at 4°C. Then, the pellet was resuspended in 250µl 1x PBS containing 5µl RNAse A (10mg/ml) and incubated at 37°C for 30min to remove the RNA in cells. After incubation, cells were washed with 1x PBS and centrifuged at 600g for 5min at 4°. 350µl PI solution (50 µg/ml, Calbiochem®, USA) was added to resuspend the cell pellet and the sample was incubated at room temperature for 10 min. The fluorescence of stained cells was detected by fluorescent activated cell sorter (FACS) BDTM LSR and gated according to viable single cell population. Cell cycle of the sample was further analyzed by FlowJo® using a Watson model. The stage of cell cycle can be distinguished according to DNA content.

2.6 Genotyping

For genotyping of transgenic mice, ear clips were lysed in 200µl of lysis buffer (0.1M Tris HCl pH8.0, 5mM EDTA pH8.0, 0.2M NaCl, 0.2% SDS) added freshly with proteinase K (200 µg/ml) (Roche). DNA from samples were extracted and purified with phenol/chloroform (see section 2.7) and precipitated with ethanol. Precipitated DNA was resuspended in sterile water and used for PCR genotyping with Biotaq DNA polymerase (Bioline). PCR products were analyzed by running in DNA agarose gel electrophoresis. List of primers used can be found in later section 2.21.

2.6.1 Genotyping PCR conditions

2.6.1.1 *HIRA* genotyping

This PCR was performed to determine whether the transgenic mice are WT or homozygous conditional knock out of *HIRA*. PCR on HIRA WT mice will give a single band of 417 bp. PCR on HIRA HOM CKO mice will give a single band at 291bp. PCR on HIRA heterozygous KO will give two bands at 417bp and 291bp. Examples of PCR results can be found in Fig S1 in Appendix.

PCR reaction mix:

Component (Qiagen)	
10x NH_4 reaction buffer	2µl
$MgCl_2$ (25mM)	0.6µl
dNTPs (10mM)	0.4µl
HIRA 44760 (F) (10mM)	0.2µl
HIRA 44760 (R) (10mM)	0.2µl
DNA template	(35ng)
Taq DNA polymerase	0.2µl
Water	Up to 25µl

PCR condition:

Cycles	Tempera	Time
1	94 ºC	5 min
34	94 ºC	30 sec
	56 ºC	30 sec
	72 ºC	30 sec
1	72 ºC	5 min
1	12 ºC	hold

2.6.1.2 *Cre* genotyping

This PCR was performed to determine whether the transgenic mice contain Cre recombinase expression on one allele under control of murine CD4 promoter in Thymus. PCR on DNA from mice with this knock in construct will give a single band of 148bp whilst DNA from WT mice show no band. Examples of PCR results can be found in Fig S1.

PCR reaction mix:

Component (Bioline)	
10x NH4 reaction buffer	2.5µl
MgCl2 (50mM)	1.25µl
BSA (10mg/ml)	0.75µl
dNTPs (10mM)	0.5µl
Cre617 (F) (10mM)	0.5µl
Cre765 (R) (10mM)	0.5µl
DNA template	(35ng)
Taq DNA polymerase	0.1µl
Water	Up to 25µl

PCR condition:

Cycles	Temperat	Time
1	94 ºC	2 min
20	94 ºC	30 sec
	65 ºC (-0.5°C)	1 min 30 sec
	70 ºC	2 min
23	94 ºC	30 sec
	55 ºC	1 min 30 sec
	70 ºC	2 min
1	70 ºC	7 min
1	10 ºC	hold

2.6.1.3 *EGFP* genotyping

This PCR was performed to determine whether the transgenic mice contain H3.3B-EGFP knock-in constructs. PCR on DNA from mice with this knock-in construct will give a single band of 272bp whilst DNA from WT mice will give no band. Examples of PCR results can be found in Fig S1. Confirmation of EGFP fusion protein in H3.3B-EGFP transgenic mouse thymocytes by flow cytometry (FACS) is showing in Fig S2.

PCR reaction mix:

Component (Bioline)	
10x NH4 reaction buffer	2.5µl
MgCl2 (50mM) BSA (10mg/ml)	1.25µl 0.75µl
dNTPs (10mM)	0.5µl
GFP (F) (10mM)	0.5µl
GFP (R) (10mM)	0.5µl
DNA template	(35ng)
Taq DNA polymerase	0.2µl
Water	Up to 25µl

PCR condition:

Cycles	Tempe	Time
1	96 ºC	5 min
35	96 ºC	30 sec
	65 ºC	30 sec
	72 ºC	30 sec
1	72 ºC	10 min
1	12 ºC	hold

2.6.1.4 *HP1γ* genotyping

This PCR was performed to determine whether the transgenic mice or embryos are WT, heterozygous or homozygous knock out of HP1γ. PCR on HP1γ WT mice will give a single band of 501bp in WT allele PCR and no band for the mutant allele PCR. PCR on HP1γ KO mice will give a single band of 525bp for the mutant allele PCR and no band for the WT allele PCR. PCR on heterozygous HP1γ KO mice will have both 501bp and 525bp bands. Examples of PCR results can be found in Fig S1.

PCR reaction mix:

Component (Bioline)	WT allele PCR	Mutant allele PCR
10x NH4 reaction buffer	2.5µl	2.5µl
MgCl2 (50mM)	1.25µl	1.25µl
BSA (10mg/ml)	0.75µl	0.75µl
dNTPs (10mM)	0.5µl	0.5µl
HP1γ common forward(10mM)	0.5µl	0.5µl
HP1γ wild-type reverse (10mM)	0.5µl	0µl
HP1γ mutant reverse (10mM)	0 µl	0.5µl
DNA template	(50ng)	(50ng)
Taq DNA polymerase	0.2µl	0.2µl
Water	Up to 25µl	Up to 25µl

PCR condition:

Cycles	Temperature	Time
1	96 ºC	3 min
5	96 ºC	15 sec
	70 ºC (-1 ºC/cycle)	15 sec
	72 ºC	40 sec
30	96 ºC	15 sec
	58 ºC	15 sec
	72 ºC	45 sec
1	72 ºC	10 min
1	12 ºC	hold

2.6.1.5 *Kdm5d* genotyping for sex determination of embryos

To determine the sex of the embryos harvested for generation of MEFs in this thesis, PCR on the Y chromosome gene *Kdm5d* was performed. PCR on DNA from male mice will give a single band of 597bp while DNA from female mice show no band. Examples of PCR results can be found in Fig S1.

PCR reaction mix:

Component (Bioline)	
10x NH4 reaction buffer	2.5µl
MgCl2 (50mM)	1.25µl
BSA (10mg/ml)	0.75µl
dNTPs (10mM)	0.5µl
Kdm5d (F) (10mM)	0.5µl
Kdm5d (R) (10mM)	0.5 µl
DNA template	(25ng)
Taq DNA polymerase	0.2µl
Water	Up to 25µl

PCR condition:

Cycles	Temperatur	Time
1	96 ºC	5 min
35	96 ºC	30 sec
	60 ºC	30 sec
	72 ºC	15 sec
1	72 ºC	10 min
1	12 ºC	hold

2.7 Phenol/Chloroform extraction and purification of DNA

DNA in aqueous solution was extracted and purified with equal volumes of phenol/chloroform solution (phenol: chloroform: isoamyl alcohol (25: 24: 1)). Samples were mixed vigorously and centrifuged at 12,000g, 4°C for 15min. Upper aqueous layer was obtained, and the DNA was precipitated by mixing with 1:10 volume of 3M of sodium acetate (NaOAc) at pH 5.2 and excess of absolute ethanol. The samples were then incubated at -20°C or -80°C for at least 1 hour and centrifuged at 12,000g 4°C for 30min. The precipitated DNA pellet was then washed with 500ul of 70% ethanol and centrifuged at 12,000g 4°C for 15min. The DNA pellet was air-dried and resuspended in DNAse-free water. DNA concentration was estimated by NanoDrop® Spectrophotometer ND-1000 with ND-1000 v3.3.1 software.

2.8 Total RNA Extraction

Total RNA from MEFs and mouse thymus were extracted using TRIZOL® Reagent (Invitrogen) following the protocol provided. 0.5 x 10^6 MEF cells or thymocytes were used per RNA extraction reaction. Cells were pelleted by centrifugation at 300g, room temperature for 5min and lysed with 1ml TRIZOL® Reagent. For mouse thymus, frozen tissue samples were homogenized using the IKA ultra-turret T25 homogenizer at highest power in 1ml TRIZOL® Reagent. Samples were then centrifuged at 12,000g, 4 ºC for 5min. After the fatty top layer was removed, the clear homogenate solution was transferred to a fresh tube. Both homogenized cell and tissue samples were incubated for 5min at room temperature. Afterwards, 200µl chloroform per 1ml TRIZOL® Reagent was added to each sample which was vigorously shaken for 15sec. Samples were incubated at room temperature for 5 min and centrifuged at 12,000g, 4 ºC for 15min. The aqueous phase was then transferred to a fresh tube and mixed with 500µl isopropanol per 1ml TRIZOL® Reagent. Samples were incubated at room temperature for 10min and centrifuged at 12,000g, 4 ºC for 25min. Supernatant was discarded and 1ml 70% ethanol per 1ml TRIZOL® Reagent was added to the precipitated RNA pellet. Samples were mixed by vortex and centrifuged at 7500g, 4 ºC for 15min. Supernatant was discarded, and the RNA pellets were air-dried followed by DNase treatment with Ambien® DNA free kit (Invitrogen), in which, the air-dried RNA pellet was resuspended in 40µl master mix containing 33µl RNase free water, 2µl Superjacent RNase inhibitor (Thermo Fisher Scientific), 4µl 10x DNase I buffer and 1µl DNase I followed by subsequent incubation at 37ºC for 30min. Reactions were then stopped by addition of 4µl of inactivation reagent to the samples and incubation at room temperature for 2min. Samples were centrifuged at 10,000g for 2min and 35µl supernatant containing the isolated RNA was retained for subsequent analysis or stored at -80°C.

2.9 Complementary DNA (cDNA) synthesis and amplification

ThermoScript® kit (Invitrogen) was used to reverse transcribe the total RNA extracted (with TRIOZOL® Reagent) into complementary DNA (cDNA) using a non-gradient cycler PCR machine (Peltier Thermal Cycler (PTC-200, BIORAD)). 1-2 mg of RNA was incubated at 65°C for 5min with 50ng of random hexamer and 2µl of 10mM dNTP. 4µl of cDNA synthesis buffer (5x), 1µl of DTT (0.1M) and 1µl of Thermo Script TM reverse transcriptase (15U/µl) was added to the reaction and incubated at 50°C for 60min and then at 85°C for 5 min. cDNAs generated were then analyzed using quantitative real time polymerase chain reaction (QRT-PCR) or stored at -20°C.

2.10 Chromatin Immunoprecipitation (ChIP)

2.10.1 Thymocytes

3x10^7 thymocytes/ChIP reaction were fixed by 1.42 % formaldehyde (Sigma, UK). Fixed cells were lysed by resuspension in 1ml IP buffer containing protease inhibitors (5 µl of protease inhibitor cocktail (Sigma, UK) and 50 µl PMSF added to 10 ml IP buffer). The nuclei were recovered by centrifugation at 12,000g, 4°C for 2 min and the pellet was washed with 1ml IP buffer (with protease inhibitors). To shear the chromatin, the washed pellet was re-suspended in 1 ml IP buffer (with protease inhibitors) and sonicated (sonicator model Bioruptor, Diagenode) for 45 min at a high power with alternating pulses. Sonicated material was then centrifuged at 16,000g, 4°C for 30min and the sheared chromatin in the supernatant was retained. 50µl chromatin sample was reverse crosslinked by adding 100µl water, 5µl proteinase K (10µg/µl) and 6µl 5M Nalco and incubated at 65°C for 4 hours. Sonication efficiency was checked on agarose gel (see Fig S3 for representative sonication gel picture). For immunoprecipitation, the antibody of choice was added at the recommended concentration and sonicated for 45 min at low power. Subsequently the chromatin was centrifuged at 12,000g, 4°C for 10 min. Top ~90% of cleared chromatin was added in the tubes with 50µl Dynabeads Protein G (Invitrogen, Norway cat. 100.04D) washed 3 times with IP buffer (with inhibitors) and incubated overnight on a rotating wheel at 4°C for binding.

2.10.2 MEFs

1.8x10^6 MEFs were seeded in each 10cm tissue culture dish and incubated at 37°C, 5% CO2 overnight to obtain about 2.5x10^6 cells per dish the following day. The culture medium per dish was adjusted to 10ml and the cells were fixed in 1% formaldehyde at room temperature for 10min. The formaldehyde fixation reaction was quenched by adding glycine for a final concentration of 125mM glycine for 5min at room temperature. The cells were washed three

times by ice-cold PBS and incubated in 4ml swelling buffer at 4°C for 10min. Cells were collected by scraping and the nuclei were isolated using a dunce homogenizer with tight pestle (40 strokes). Nuclei were then collected by centrifuging at 3,000g, 4°C for 5min. To generate chromatin, nuclei pellet generated from 10^7 cells was resuspended in 1ml sonication buffer and transferred to a 15ml polystyrene tube. The nuclei suspension was sonicated using a Disruptor® (Diagnose) for 20min at high energy with alternating pulses. Sonicated material was then centrifuged at 16,000g 4°C for 30min and the sheared chromatin in the supernatant was retained. 50µl chromatin sample was reverse crosslinked by adding 100µl water, 5µl proteinase K (10µg/µl) and 6µl 5M Nalco and incubated at 65°C for 4 hours. Sonication efficiency was checked on agarose gel (Fig S3). For immunoprecipitation, specific antibodies were added to 200µl chromatin aliquots (equivalent to 2x10^6 cells) and incubated in the Disruptor® for 45min, at low energy with alternating pulses. Samples were centrifuged at 12,000g, 4°C for 10min and the supernatant was added to 50µl Nanobeads® Protein G (Invitrogen) washed three times with sonication buffer and incubated overnight at 4°C.

For both thymocytes and MEFs, after the incubation with beads, the next day, beads with antibody-chromatin complex were washed once with each sonication buffer, wash buffer A, wash buffer B and twice with 1 x TE buffer for 5min, 4°C with rotation. Elution of immune complexes and purification of DNA were performed using IPure Kit (Diagenode). In brief, 100µl of elution buffer (composed of 96.2% buffer A and 3.8% buffer B from kit) was added to washed beads and incubated at 65°C for at least 4h with continuous shaking. For the input sample, 10µl of chromatin samples were mixed with 90µl elution buffer prepared as stated above and incubated at 65°C for at least 4h with continuous shaking. Supernatant was obtained and mixed with 2µl of 'carrier' provided by the kit and 100µl of 100% isopropanol. 15µl of DNA-binding magnetic beads was then added to each sample and incubated at room

temperature for 1h with rotation. The supernatant was discarded, and beads/DNA complexes were washed once with 100µl wash buffer 1 and then wash buffer 2 for 5min at room temperature with rotation. Captured DNA was eluted by incubating twice with 25µl buffer C from the kit at room temperature for 15min and giving sample with total volume of 50µl. Samples were then used for downstream applications (QRT-PCR or ChIP-sequencing library preparation) or stored at -20°C until further use. A list of antibodies used in ChIP can be found in section 2.22.

2.11 Quantitative real-time polymerase chain reaction (QRT-PCR)

Quantitative real-time polymerase chain reaction (QRT-PCR) was used to analyses samples from ChIP experiments and check the expression level of genes after RNA extraction and cDNA synthesis. QRT-PCR reactions were prepared using SYBR® Green Jumpstart^{TM} Taq ReadyMix^{TM} (Sigma-Aldrich®) and performed in Low 96-well White Multiplate® PCR plates^{TM} (BIORAD).

PCR reaction mix:

Component	
SYBR®	10µl
Forward primer (10mM)	0.5µl
Reverse primer (10mM)	0.5µl
DNA template	Δ
Water	Up to 20µl
Total	20µl

PCR condition:

Cycles	Temperature	Time
1	95 ºC	10 min
40	95 ºC	30 sec
	58 ºC	30 sec
	72 ºC	30 sec
1	80 ºC	1 sec (Plate read)

Full list of primers used for QRT-PCR can be found in section 2.21. The efficiency of all the primers used in this thesis were calculated by a standard curve generated by QRT-PCR on serial diluted DNA samples. Efficiency of primers in percentage were calculated by the formula:

$$\text{Primer efficiency (\%)} = (10^{(-1/\text{slope})}-1) * 100$$

where the slope is the slope of the standard curve generated. This value represents the increased amount of PCR product after each PCR cycle. All primers used in this thesis have primer efficiency of 90-110%.

2.12 ChIP sequencing (ChIP-seq) library preparation and sequencing

ChIP-seq libraries were prepared using the NEBNext® Ultra™ DNA Library Prep Kit for Illumina® (#E7370, New England BioLabs®). Input and ChIP DNA were estimated by Quant-iT™ PicoGreen® dsDNA Assay (#11496, Invitrogen™). 8ng of DNA was obtained per ChIP-seq library preparation reaction. End repair reaction was prepared as follow:

End repair reaction mix:

Component of end repair reaction	
End Prep Enzyme Mix	3µl
End Repair Reaction Buffer (10X)	6.5µl
Input/ChIP DNA	(8-10ng)
Water	Δ
Total	65µl

End repair reaction samples were incubated at 20°C for 30min, 65°C for 30min and held at 4°C. Sequencing adaptor ligation was then performed as follow: Adaptor ligation reaction mix:

Component of adaptor ligation	
End-repaired DNA sample	65µl
Blunt/TA Ligase Master Mix	15µl
NEBNext® Adaptor for Illumina® (1.5µM) *	2.5µl
Ligation Enhancer	1µl
Total	83.5µl

*NEBNext® Multiplex Oligos for Illumina® (#E7335, New England BioLabs®)

Samples were incubated at 20°C for 15min. 3µl of the USER™ Enzyme was added to each ligation reaction samples and incubated at 37°C for 15min.

To clean up adaptor-ligated DNA, 86.5µl of Agencourt AMPure®XP Beads (#A63881, Beckman Coulter) was added to each sample and incubated at room temperature for 5min. Supernatant was discarded, and the beads were washed twice with 200µl freshly prepared 80% ethanol. Beads were air-dried for 5min and the bound-fraction was eluted in 20µl 0.1 x TE.

Cleaned-up adaptor ligated DNA samples were enriched by PCR amplification as follows:

PCR amplification reaction mix:

Component	
Adaptor Ligated	20µl
NEBNext® High Fidelity 2X PCR	25µl
Master Mix	2.5µl
Index Primer*	2.5µl
Universal PCR Primer* Total	50µl

*NEBNext® Multiplex Oligos for Illumina® (#E7335, New England BioLabs®)

Cycles	Temperature	Time
1	98 ºC	5 min
12	98 ºC	10 sec
	65 ºC	30 sec
	72 ºC	30 sec
1	72 ºC	5 min
1	4 ºC	hold

Enriched DNA samples were resolved in 2% agarose gels (prepared with 0.5 X TAE). DNA fragments of 200-400bp were extracted and cleaned up by a QIAquick® Gel extraction kit (#28706 Qiagen) following manufacturer's protocol. Prior to sequencing, the purified DNA fragments were analyzed with the Agilent 2100 Bioanalyzer using High Sensitivity DNA Analysis Kits (#5067-4626, Agilent Technologies, Inc.) following the manufacturer's protocol (see Fig S7 for representative Bioanalyzer result). Samples of enough quality were sequenced with HiSeq 2500 (Illumina®).

2.13 ChIP sequencing analysis

ChIP-seq reads were aligned to the mouse genome version mm9 using bwa version 0.7.5a. Peak calling was performed using macs/1.4.1. Quality control plot and statistics were generated

using ChIP QC package from Bioconductor (Carroll *et al*., 2014). Feature visualization and normalizations were carried out with soGGi package from Bioconductor (Dharmalingam G, 2015).

2.14 Co-immunoprecipitation (Co-IP)

6 x 10^6 MEFs were used per Co-IP experiment. Cells were pelleted at 300g, room temperature for 5min and washed once with 500µl buffer A, followed by centrifugation at 300g, 4°C for 5 min. Supernatant was discarded and cell pellets were lysed with 500µl buffer A containing 0.2% Triton X-100 and incubated on ice for 10 min. Samples were then centrifuged at 600g, 4°C for 5 min and the nuclei pellets were obtained. Nuclei were resuspended in 250µl of buffer A containing 2mM CaCl2 and 1U of Micrococcal Nuclease (MNase) (Sigma) and incubated at 1400rpm, 4°C for 50 min. The reaction of MNase was stopped by addition of EGTA to a final concentration of 10mM. 5M NaCl was added to each sample to a final concentration of 340mM and the samples were incubated at 4°C for 60 min with gentle mixing. Samples were centrifuged at 8,000g, 4°C for 5min and the supernatants (nuclear extract) were obtained. Equilibration buffer was added to each sample to lower the salt concentration to 150mM NaCl. For immunoprecipitation, specific antibody was mixed with nuclear lysate and 50µl Protein G Dynabeads® (Invitrogen) washed three times with buffer A. Samples were then incubated overnight at 4°C. Beads were then washed three times in 200µl wash buffer by vortexing. Immunoprecipitated material was eluted in 30µl SDS sample buffer and boiled for 10min. Dithiothreitol (DTT) was then added to final concentration of 1mM and boiled again for 10min. Samples were then analyzed by western blotting. Details of antibodies used for immunoprecipitation can be found in section 2.22.

2.15 Protein extraction

Protein lysate used for experiments in this thesis was prepared using RIPA buffer (supplemented with protease inhibitors freshly before use) and the protein concentration was estimated using a bovine serum albumin (BSA) dilution standard curve with the Bradford Protein Assay (BIO-RAD). Prior to loading into the gel for western blotting, protein sample were mixed 1:1 with 2x Laemmlli buffer and denatured by heating at 100°C for 10min. Protein samples were stored at -20°C.

2.16 Western blotting

10-30μg of denatured protein samples were resolved in denaturing SDS-PAGE gels prepared as follow using the BIO-RAD Mini-PROTEAN® Tetra Systems (BIO-RAD) with 1mm plate separation.

	Resolving gel (12.5%)	Stacking gel (4%)
Water	3.125ml	6ml
30% Acrylamide	4.17ml	1.33ml
1.5M Tris pH8.8	2.5ml	0ml
10% SDS	100μl	100μl
10% ammonium persulphate (APS)	100μl	100μl
Total	10ml	10ml

Protein samples were resolved by running the SDS-PAGE gel at 150V for 70-90min. After electrophoresis was completed, the SDS-PAGE gel was then incubated in 1x transfer buffer. The transfer stack was prepared by sandwiching the SDS-PAGE gel and the Hybond-N+ PVDF membrane (GE Healthcare) (activated by incubating in 100% methanol for about 2min and subsequently rinsed with 1x transfer buffer) with 3 pieces of Whatman 3MM filter papers on either side and placed into the Mini Trans-Blot® system (BIO-RAD) with the PVDF membrane and the SDS-PAGE gel facing the negative and positive electrode respectively. Protein in the SDS-PAGE gel was transferred to the membrane at 100V, 4°C for 1h. After transfer, the membrane was blocked for 1 hour at room temperature with 5% milk (in PBST/TBST). Primary antibody diluted in 5% milk or 5% BSA (in PBST/TBST) was added to the membrane and incubated at room temperature for 2 hours or 4°C overnight. The membrane was then washed three times for 10min at room temperature with PBST or TBST and incubated with horseradish peroxidase (HRP) - conjugated secondary antibody diluted in 5% milk (in PBST/TBST) for 1 hour at room temperature. Next, the membrane was washed three times with PBST or TBST for 10min at room temperature and the blot

was developed using AMER sham ECL Prime Western Blotting Detection Reagent (GE Healthcare) following the manufacturer's protocol in the darkroom. A list of antibodies used in western blotting can be found in section 2.22.

2.17 Fluorescence activated cell sorting (FACS)

T cells expressing H3.3B-EGFP derived from thymus or mesenteric lymph nodes were washed in 1 x PBS and then centrifuged at 300rpm, 4°C for 7 min. Single cell suspensions obtained from lymphatic tissues were stained with 50 g/ml CD4-PE, CD8-APC, CD44-PECY5, CD62L-FITC, CD19-PE, TCRβ-FITC antibodies on ice for 30 min and analyzed using a flow cytometer (FACS Caliber; BD Biosciences, Mountain View, CA). For CD71 cell sorting process, CD4-PE, CD8-APC and CD71-BV42 antibodies were used to select the CD71- double positive (DP) cells. Two size gates were set for selecting the lymphocytes by forward - and side - scatter (FSC & SSC) on the total cell population and small DP cells by using FSC and SSC on CD4/8 DP CD71- gated cells. A list of antibodies used in FACS can be found in section 2.22.

2.18 K means clustering for analyzing protein network

K-means clustering uses the Hartigan–Wong algorithm which was performed in R following a schematic step to identify and confirm protein groups that clustered together with feature similarity (Dickinson *et al*., 2018). This method has been applied in the analysis of mass spectrometry data following the co-immunoprecipitation materials in this thesis (collaboration with Axel Imhof, Munich).

2.19 Multivariate analysis of transcript splicing (MATS)

MATS is a computational tool to detect differential alternative splicing events from RNA-Seq data. The statistical model of MATS calculates the P-value and false discovery rate (FDR) that the difference in the isoform ratio of a gene between two conditions exceeds a given user-defined threshold. From the RNA-Seq data, MATS can automatically detect and analyze alternative splicing events corresponding to all major types of alternative splicing patterns. MATS processes replicate RNA-Seq data from both paired and unpaired study design.

2.20 Mass spectrometry (MS)

To identify proteins binding to HP1γ, Co-IP followed by western blot were performed on MEFs (both sexes). Input, HP1γ IP, IgG IP and unbound fractions were obtained for western blot for the confirmation of HP1γ presence. Next the western blot materials were sent to our collaborator, Axel Imhof (LMU Munich) for further MS analysis. Protein network was analyzed according to the string database (http://string-db.org), network after K means clustering proteins into groups with feature similarities.

2.21 Lists of primers

2.21.1 List of primers used for genotyping

Primer name	Purpose	Primer sequences (5'-3')
HIRA forward	HIRA genotyping	CATGTCTCAGATTGG TGCTGTG
HIRA reverse	HIRA genotyping	GGATGTCTTTCCCAG AACTTTCC
Cre forward	Cre genotyping	CCGCAGGTGTAGAGA GAAGGC
Cre reverse	Cre genotyping	CTGGCTGGTGGCAGA TGG
HP1γ common forward	HP1γ genotyping	GAGTGATTACCGACACC
HP1γ wild-type reverse	HP1γ genotyping	TTTAATCGGAGACTTGA AGAGC
HP1γ mutant reverse	HP1γ genotyping	GTTCGCTTCTCGCTTCTG
GFP (F)	H3.3B-EGFP genotyping	GACCGCTTCCTCGTGCT
GFP (R)	H3.3B-EGFP genotyping	GAGCCACAGTGCTCACA
Kdm5d (F)	Sex determination	ACAAAGTGGGGGCAAA
Kdm5d (R)	Sex determination	AGTTATGACCCTCACCA

2.21.2 List of primers used for QRT-PCR for checking gene expression level and RNA splicing:

Primer name	Gene	Specie	Primer sequences (5'-3')
Mbeta-actin (F)	B-actin	Mouse	GCTACAGCTTCACCACCACA
Mbeta-actin (R)	B-actin	Mouse	ATGCCACAGGATTCCATACC
HIRA (F2)	HIRA	Mouse	CCACCGTTCGGGGGATAAG
HIRA (R2)	HIRA	Mouse	GGCAACACATACCACATCACAG
Srp19 (F)	Srp	Mouse	CAATAGGCTGAGCAAGTTCT
Srp19 (R)	Srp	Mouse	GGTGCTTGTGCTAAGAAAG
Rik (F)	Rik	Mouse	CAAATGTCTCTCTCCCAGA
Rik (R)	Rik	Mouse	ATGGTGGTTGTCTGTGTTG
Gdi (F)	Gdi	Mouse	CTGGATCAGCCCTCTCTT
Gdi (R)	Gdi	Mouse	ATGGTGGTTGTCTGTGTTG
Rnf167 (F)	Rnf	Mouse	CAGTCAGTTGTGAGCTGCTA
Rnf167 (R)	Rnf	Mouse	GGGAGTTCTAGGGGTTGTAG
Mtf2 (F)	Mtf	Mouse	CAGATCTGTCTGCACCTG
Mtf2 (R)	Mtf	Mouse	AGTTGCTGATGTGAACTCAA
Asf7 (F)	Asf	Mouse	CTTTTGGGCATTTTCG
Asf7 (R)	Asf	Mouse	TTTACTAGATTGAAATATAAGCAC
Ptdss2 (F)	Ptdss	Mouse	TCTGCAGTGAGACCAAC
Ptdss2 (R)	Ptdss	Mouse	AGTGCTGGGATTGCTTCT
Ap1m1 (F)	Ap1m1	Mouse	AGCTACCAGAACAGGTCCAG
Ap1m1 (R)	Ap1m1	Mouse	TCAAGGGACTAAGGAAAACG
Tbxa2r (F)	Tbxa2r	Mouse	CCAGCCTGGTCTACACAGAG
Tbxa2r (R)	Tbxa2r	Mouse	CCATCAGGTTCCACAGCTT

2.21.3 List of primers used for ChIP QRT-PCR

Primer name	Gene	Species	Primer sequences (5'-3')
Gapdh+4K(F)	Gapdh	Mouse	GAGCCCTCCCTACTCTCTTGAAT
Gapdh+4K(R)	Gapdh	Mouse	ACACCGCATTAAAACCAAGGA
Gapdh(F)	Gapdh	Mouse	AGTCCGTATTTATAGGAACCCGGATGGTGG
Gapdh(R)	Gapdh	Mouse	ATGAGAGAGGCCCAGCTACTCGCG
Mj-sat (F)	Major-Satellite	Mouse	GCTTTAGACGACTTGAAAAATGACGAAATC
Mj-sat (R)	Major-Satellite	Mouse	CATATTCCAGGTCCTTCAGTGTGC
Neurod6(F)	Neurod6	Mouse	TTTTTCCCTATCAGTCTAACCTCCTGTGTTGA
Neurod6(R)	Neurod6	Mouse	AAAAGTGACATTGATGCCAACTGCCAGAGC
Pdx(F)	Pdx	Mouse	GAAGTCCTCCGGACATCTCCCCATACGAAG
Pdx(R)	Pdx	Mouse	GGATTTCATCCACGGGAAAGGGAGCTGAC

2.22 Lists of antibodies

2.22.1 List of antibodies for chromatin immunoprecipitation (ChIP)

Antibody	Type/Isotype	Dilution	Company	Catalogue no.
Anti-GFP	Rabbit polyclonal, IgG	10µg/IP	Abcam	Ab290
Anti-H3	Rabbit polyclonal, IgG	6ug/IP	Abcam	Ab1791
Anti-H3.3	Rabbit polyclonal, IgG	10µg/IP	Millipore	09-838
Anti-HP1γ	Mouse monoclonal, IgG1	8µg/IP	Millipore	05-690
Anti-HP1γ	Mouse monoclonal, IgG	10µg/IP	Millipore	17-646

2.22.2 List of antibodies for co-immunoprecipitation (Co-IP)

Antibody	Type/Isotype	Dilutions	Company	Catalogue no.
Anti-GFP	Rabbit polyclonal, IgG	10µg/IP	Abcam	Ab290
Anti-H3	Mouse monoclonal, IgG1	5µg/IP	Abcam	Ab1218
Anti-HP1γ	Rabbit polyclonal, IgG	5µg/IP	Abcam	Ab10480
Mouse IgG	Normal mouse IgG	5µg/IP	Santa-cruz	sc-2025
Rabbit IgG	Normal rabbit IgG	5µg/IP	Millipore	PP64B

2.22.3 List of primary antibodies for western blot

Antibody	Type/Isotype	Dilutions	Compa	Catalogue no.
Anti-α-tubulin	Mouse IgG1	1:1000	Sigma	T5168
Anti-GFP	Rabbit polyclonal, IgG	1:1000	Abcam	Ab290
Anti-H3	Rabbit polyclonal, IgG	1:1500	Abcam	Ab1791
Anti-H3.3*	Rabbit polyclonal	1:500	Millipor	09-838
Anti-HP1γ	Mouse IgG1	1:5000	Millipor	MAB3450

*Antibodies that require the use of BSA

2.22.4 List of Secondary antibodies for western blot

Antibody	Dilutions	Company	Catalogue no.
Goat anti-Mouse IgG, HRP-conjugated	1:20000	Life Technologies	G21040
Goat anti-Rabbit IgG, HRP- conjugated	1:20000	Santa-cruz	sc-2004
Goat anti-Rabbit IgG, HRP-conjugated	1:20000	Pierce	1858415

2.22.5 List of antibodies for FACS

Antigen	Product name	Description
CD19	PE-CF594 Rat Anti-Mouse CD19	B lymphocyte marker
TCRbeta	FITC Hamster Anti-Mouse TCR β Chain	T lymphocyte marker
CD44	PE-Cy™5 Rat Anti-Mouse CD44	naïve T cell marker
CD62L	FITC Rat Anti-Mouse CD62L	naïve T cell marker
CD25	FITC anti-mouse CD25	Late T activation marker
CD4	PE Rat Anti-Mouse CD4	CD4 +
CD8	RAT anti-MOUSE CD8a	CD8 +
CD71	BV711 Streptavidin	CD71

2.23 Solutions

Phosphate buffered saline (PBS) -171mM NaCl, 3.3mM KCl, 10.1mM Na2PO4, 1.8 mM KH2PO4, pH7.4

HEPES buffered saline (HPS) - 137mM NaCl, 5.1mM KCl, 0.7mM Na2PO4, 21mM HEPES, 0.1% (w/v) glucose, pH7.05

Phenylmethylsulphonyl Fluoride (PMSF) (0.1M) - Prepared in isopropanol

10x TE - 100 mM Tris-HCl, 10 mM EDTA

5x TBE - 450 mM Trisborate, 10 mM EDTA

0.5x TAE - 20 mM Tris acetate, 0.5 mM EDTA

Phenol/chloroform solution - Prepared by mixing 25:24:1 Phenol:chloroform:isoamylalcohol and equilibrated with 10 mM Tris-HCl, pH 8.0

Lysis buffer (genotyping) **-** 0.1M Tris HCl pH8.0, 5mM EDTA pH8.0, 0.2M NaCl, 0.2% SDS

Buffer A (co-immunoprecipitation) - 20mM HEPES, pH 7.9, 10mM KCl, 1.5mM MgCl2, 0.34M sucrose, 10% glycerol supplemented with 1mM dithiothreitol (DTT), 1 mM PMSF and 0.5µl of protease inhibitor cocktail per 1ml buffer freshly

Equilibration buffer (co-immunoprecipitation) - 20mM HEPES, pH7.9, 1.5mM MgCl2, 0.2mM EGTA, 25% glycerol. Supplemented with 0.5 mM PMSF, 0.5µl of protease inhibitor cocktail per 1ml buffer freshly

Wash buffer (co-immunoprecipitation) - 20mM HEPES, pH7.9, 150mM NaCl, 1.5mM MgCl2, 0.2mM EGTA, 0,2% Triton X-100, 10% glycerol. Supplemented with 0.5 mM PMSF, 0.5µl of protease inhibitor cocktail per 1ml buffer freshly

SDS Sample buffer (co-immunoprecipitation) - 100 mM Tris, pH 6.8, 4% SDS, and 20% glycerol

Swelling buffer (chromatin immunoprecipitation) - 25 mM HEPES pH 7.9, 1.5

mM MgCl2, 10 mM KCl, 0.1% NP-40, pH 7.9. Supplemented with 0.5 mM PMSF, 0.5µl of protease inhibitor cocktail per 1ml buffer freshly

Sonication buffer (chromatin immunoprecipitation) - 50 mM HEPES pH 7.9, 140 mM NaCl, 1mM EDTA, 1% Triton X-100, 0.1% Sodium deoxycholate, 0.1% SDS, pH 7.9. Supplemented with 0.5 mM PMSF, 0.5µl of protease inhibitor cocktail per 1ml buffer freshly

Wash buffer A (chromatin immunoprecipitation) - 50 mM HEPES pH 7.9, 500 mM NaCl, 1mM EDTA, 1% Triton X-100, 0.1% Sodium-deoxycholate, 0.1% SDS, pH 7.9

Wash buffer B (chromatin immunoprecipitation) - 20 mM Tris pH 8.0, 1 mM EDTA, 250 mM LiCl, 0.5% NP-40, 0.5% Sodium-deoxycholate, pH8.0

RIPA (Radio Immunoprecipitation Assay buffer) buffer (protein extraction) - 150 mM NaCl, 1.0% NP-40 or Triton X-100, 0.5% sodium deoxycholate, 0.1% SDS, 50 mM Tris, pH 8.0. Supplemented with 0.5 mM PMSF, 0.5µl of protease inhibitor cocktail per 1ml buffer freshly

Running buffer (western blot) - 25 mM Tris base, 190 mM glycine, 0.1% SDS, pH 8.3.

Transfer buffer (western blot) - 25 mM Tris base, 190 mM glycine, 20% methanol, pH 8.3

TBST (western blot) - 50 mM Tris.HCl, pH 7.4 and 150 mM NaCl, 0.1% Tween-20, pH7.5

PBST (western blot) - 171mM NaCl, 3.3mM KCl, 10.1mM Na2PO4, 1.8 mM KH2PO4, 0.1% Tween-20, pH7.4

Laemmli buffer (2X) (western blot) - 4% SDS, 10% 2-mercaptoehtanol, 20% glycerol, 0.004% bromophenol blue, 0.125 M Tris HCl

Phenylmethylsulphonyl Fluoride (PMSF) (0.1M) - Prepared in isopropanol Phosphate buffered saline (PBS) -171mM NaCl, 3.3mM KCl, 10.1mM Na2PO4, 1.8 mM KH2PO4, pH7

Chapter 3 - Investigation into the role of histone H3.3 and its chaperone HIRA *in vivo*

3.1 Introduction and background

H3.3 incorporation has been associated with active transcription and is the only H3 variant present in non-replicating cells (Wu *et al*., 1982). It has been shown that H3.3 is enriched at promoter regions of both active and repressed genes, the body of active genes, and a subset of regulatory elements (Goldberg *et al*., 2010, Ray-Gallet *et al*., 2011a). HIRA is a known chaperone for H3.3 (Goldberg *et al*., 2010) and is thought to deposit it close to the transcriptional start site (TSS) forming an unstable nucleosome. However, to date there is a paucity of *in vivo* data which addresses the importance of HIRA in gene regulation, DNA recombination and T cell development. The published genome-wide H3.3 deposition data derived from chromatin immunoprecipitation followed by next generation sequencing (ChIP-seq) was done by tagging HA onto the endogenous H3.3 and only done in a mouse ES cell line.

In this chapter, the role of HIRA in H3.3 deposition was studied *in vivo*, in which, we can study multiple effects on DNA metabolic processes. Especially in T lymphocyte, which is a well described differentiation system and the cells are easy to obtain in large numbers. More importantly, resting T cells in thymus will only have H3.3 and little or no H3.1 or H3.2, which make it a good model for us to study H3.3. So far, we already have transcriptomic data obtained from thymocytes, which gave us an insight into the effect of HIRA/H3.3 on gene expression in T cells. We will not only look at developmental cellular stages but also the T cell receptors (TCR) undergoing recombination, which is known to happen in the context of chromatin. Therefore, in this chapter, we can study both the transcriptional effects of HIRA/H3.3, but also the effects on TCR recombination and cellular differentiation in T cells.

In this chapter, further investigation into the effect of HIRA deficiency on T cell development will be studied *in vivo*.

3.2 Aims

1. To investigate the effect of HIRA deficiency on H3.3 deposition and nucleosome density in resting T cells.

2. To investigate whether HIRA is required for the development of the T cell lineages, both thymocytes and peripheral T cells will be examined by flow cytometry.

3. To determine the role of HIRA/H3.3 in T cell receptor rearrangement, the V(D)J locus of TCR α chain will be examined for H3.3 deposition, re-arrangement and expression in the presence or absence of HIRA in both thymocytes.

This work promises to determine essential gene regulatory functions of histone H3.3 and HIRA during T cell development *in vivo*.

3.3 H3.3B-EGFP transgenic mice are a good model for studying genome-wide deposition of H3.3 protein *in vivo*

Initially, anti-H3.3 antibody was used to examine H3.3 deposition on gene regions that were identified in a previous publication (Harada *et al*., 2012). Fig 3.1.1 showed that H3.3 antibody gave a very low signal (0.01, 0.06 and 0.3 respectively) and the variation between biological samples was large (SEM was 0.03, 0.06 and 0.15 respectively), which indicates the H3.3 antibody is not very reliable for picking up H3.3 binding in our system. In the absence of a good specific antibody for H3.3, we employed transgenic mice in which the EGFP gene had been knocked into exon 6 on one allele of the H3.3B gene at the 3' prime end (Fig 2.1 in section 2.1.2.1). This transgenic H3.3B-EGFP mouse model was created by Dr. Vineet Sharma (Imperial College London, London, U.K.) and Dr. Buhe Nashun (MRC Clinical Science Centre, London, U.K.). Hence, animals containing this targeted knock-in will produce H3.3B-EGFP fusion proteins.

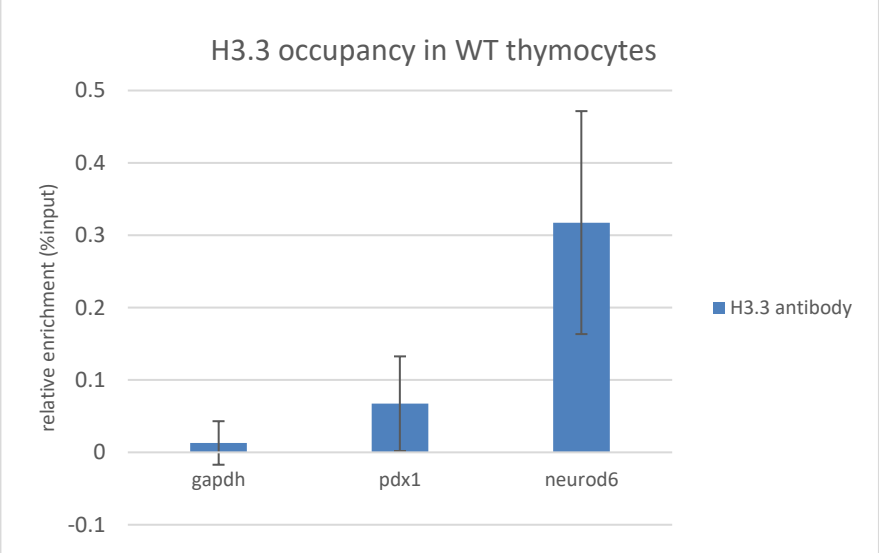

Fig 3.1.1. Relative enrichment of H3.3 on various genomic regions in WT thymocytes as revealed by ChIP. *H3.3 signal was obtained from Gapdh, Pdx1 and Neurod6 genes in thymocytes. Very low signal and big error bars on these regions was obtained in the WT thymocytes indicating the efficiency and specificity of the anti-H3.3 antibody used in this ChIP experiment. n=5 (Biological replicates). Error bars: standard error of the mean (SEM). Primers for targeting the genes used here are taking form Akihito Harada et al., paper (Harada et al., 2012).*

The presence of H3.3B-EGFP fusion protein was checked by flow cytometry, western blot and QRT-PCR respectively. The fluorescence signal of the EGFP tag was shown in Fig 3.1.2. EGFP signal in H3.3B-EGFP mouse T cells was present at high level (Right) and absent in wildtype T cells (Left). Western blot developed with an antibody against H3 also showed the H3.3B-EGFP fusion protein at a bigger size (45kDa) compared to the endogenous H3 band (17kDa) (Fig 3.1.3). Next, Chromatin immunoprecipitation (ChIP) was also performed by using anti-GFP antibody (Ab290, Abcam). In this experiment, we selected the highly expressed gene *Gapdh* in mouse thymocytes to investigate the specificity of this antibody on the immunoprecipitated DNA. The PCR primer targets the promoter region on this selected gene (Fig 3.1.5). As shown in Fig 3.1.4, H3.3B-EGFP was enriched on the promoter of *Gapdh* gene, consistent with a previously published study (Harada *et al*., 2012) (Fig 3.1.4). In contrast, the signal for H3.3B-EGFP was virtually absent in H3.3 wildtype (WT) thymocytes on this region indicating the specificity of this antibody and the presence of H3.3B-EGFP (Fig 3.1.4).

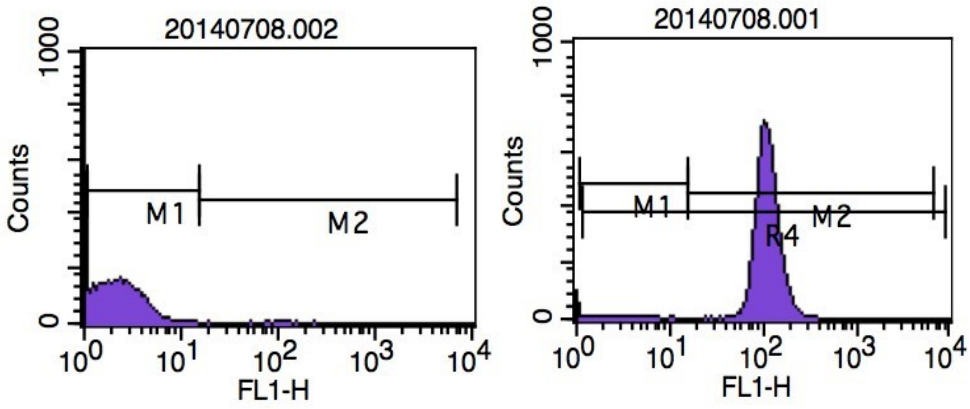

Fig 3.1.2. FACS analysis of EGFP expression in WT and GFP mouse T cells. *3x10^5 T cells were used for analysis. The y axis shows the relative cell number and the x axis shows the fluorescence intensity of EGFP in the green channel (FL1). Left shows WT has no EGFP expression. (Background signal in Gate M1). On the right, it shows the results for EGFP + T cells, which have an EGFP expression peak at 10^2 (shown in purple in Gate M2).*

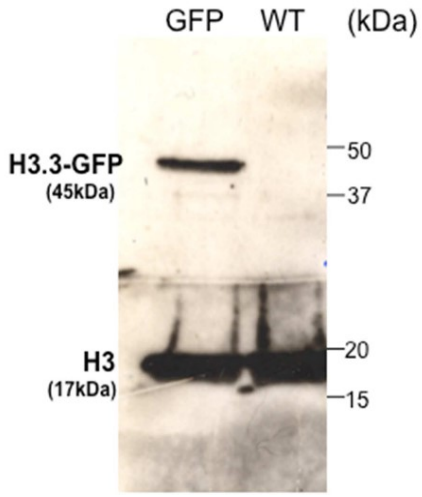

Fig 3.1.3. Western blot of H3.3-EGFP fusion protein isolated from H3.3-EGFP mouse thymocytes. *H3.3-EGFP fusion protein is 45kDa. Histone H3 was used as control, which is 17kDa. Anti-EGFP antibody (ab290, Abcam) and anti-H3 antibody (ab1791, Abcam) are used here with dilutions of (1:1000) and (1:1500) respectively. This anti-H3 antibody recognizes H3.1, H3.2 and H3.3 encoded by H3.3a gene. Anti-rabbit (sc2004) (1:20,000) and Anti-rabbit (PIERCE 1858415) (1:20,000) were used as secondary antibody against anti-EGFP and anti-H3 respectively. Sizes on the right were obtained by rainbow marker run in the same gel.*

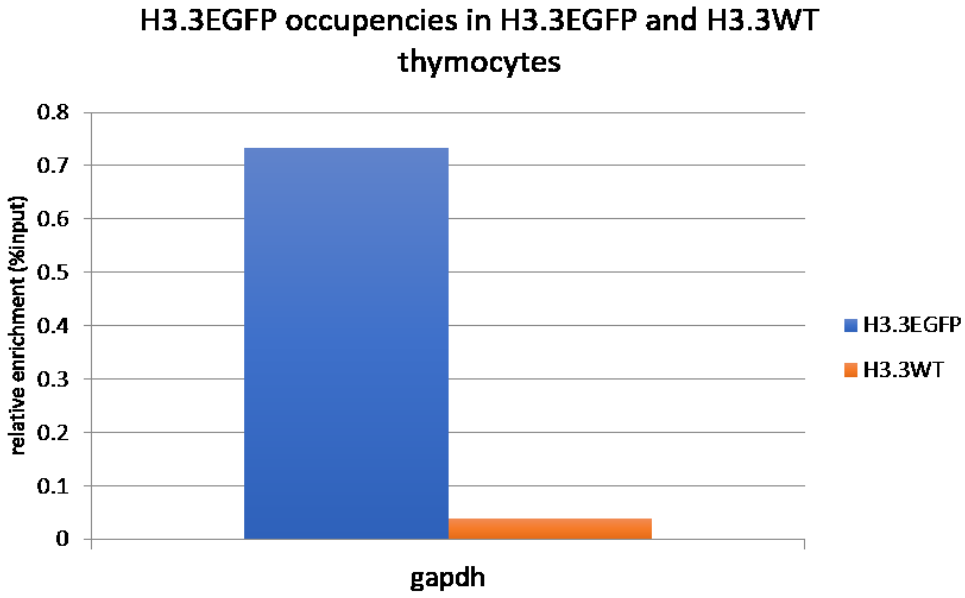

Fig 3.1.4. Relative enrichment of H3.3B-EGFP on house-keeping gene Gapdh in HIRA WT and H3.3B-EGFP thymocytes as revealed by ChIP. *H3.3B-EGFP signal was obtained from the transcriptionally active housekeeping gene Gapdh in H3.3B-EGFP thymocytes which express the H3.3B-EGFP fusion protein. Low signal on this region was obtained in the WT thymocytes indicating the specificity of the anti-GFP antibody used in this ChIP experiment. n=3 (PCR replicates). Error bars: SEM.*

To conclude, the presence of H3.3B-EGFP in the transgenic H3.3B-EGFP mouse and not in the WT suggests that this is a good model for studying the genome-wide H3.3 distribution by employing anti-EGFP antibody.

3.4 Chromatin Immunoprecipitation (ChIP) for localizing H3.3B-EGFP in the mouse genome

H3.3 incorporation has been revealed previously in a myoblast cell line (C2C12), in which *Neurod6* and *Pdx1* are completely silent (Harada *et al*., 2012). They showed that H3.3 was incorporated at a region upstream of the transcriptional start site (TSS) of a housekeeping gene (*Gapdh*), but not at the promoters of silent genes (*Pdx1* and *Neurod6*) in myoblasts (Harada *et al*., 2012). Although, *Pdx1* and *Neurod6* are thought to be tissue specific and they are said to be completely silenced in myoblast cells (Akihito paper), according to the Affymetrix microarray data (Wijchers and Festenstein personal communication) obtained from mouse thymus (Fig 3.1.6), *Pdx1* and *Neurod6* expressed at a relatively lower level compared to *Gapdh* in thymocytes. In addition, we mapped the primers taken from Akihito paper onto the mouse genome and we found that instead of targeting the promoters of *Pdx1* and *Neurod6* genes as described in the paper, both sets of primers target the gene bodies. (Fig 3.1.5) Whereas, the *Gapdh* primer is indeed targeting the promoter region of this gene, which is located 120bp upstream of the transcription start site (TSS) (Fig 3.1.5).

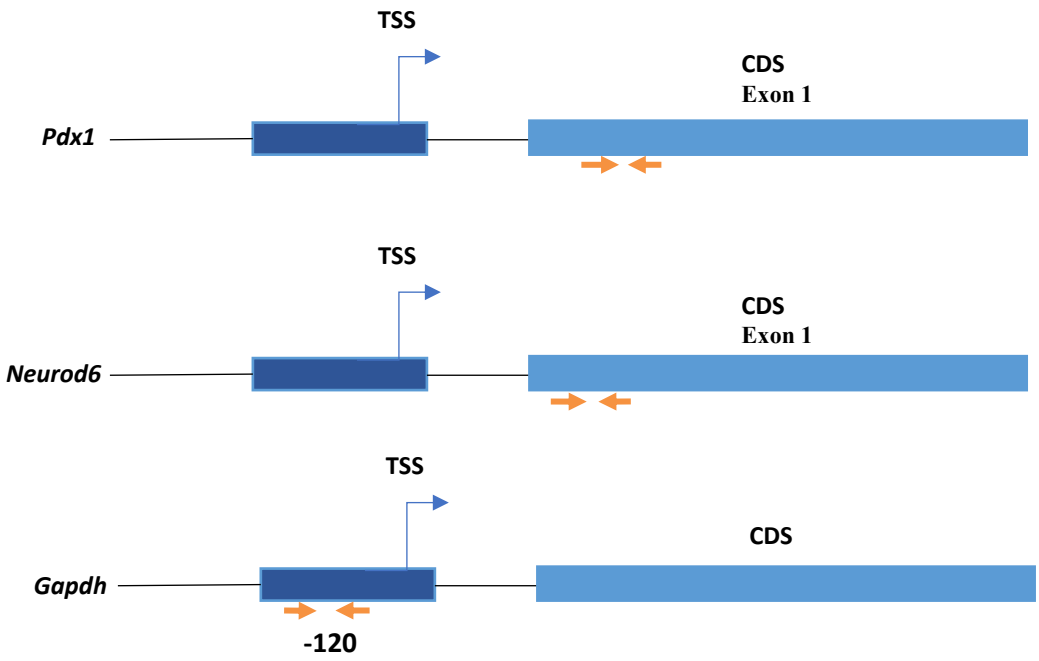

TSS – Transcription start site
CDS – Coding sequence (or) gene

Fig 3.1.5. Schematic diagram showing primers targeting regions on Pdx1, Neurod6 and Gapdh genes. *Primer sets are indicated in yellow arrows. A/B. Both primer sets target gene bodies of Pdx1 and Neurod6 genes respectively. C. Gapdh primer targets 120bp upstream of TSS at promoter.*

sym.mf	chrom.mf	AveExpr	ranking of total 45100 genes
Gapdh	6	12.17057	99
Pdx1	5	3.109373	29196
Neurod6	6	2.120253	44403

Fig 3.1.6. Table illustrating the expression level of selected genes in thymuses from mice by Affymetrix microarray. *This figure is modified from microarray data (Patrick J. Wijchers et al., 2010)*

They also showed that the level of H3.3 on the gene body correlated with gene expression at the transcriptional level. To confirm that our cells are a good model to study H3.3 occupancy genome-wide *in vivo,* we selected these three genes (*Gapdh*, *Pdx1* and *Neurod6*) in mouse thymocytes to investigate the H3.3 occupancy. The experiment shown here revealed a higher

level of H3.3B-EGFP when normalized to input (Fig 3.1.7), within the first exon of the *Pdx1*and *Neurod6* genes (Fig 3.1.5). The signal on the *Gapdh* gene was lower (Fig 3.1.7), however, the region examined was not within the gene body but about 120bp upstream of the TSS (Fig 3.1.5).

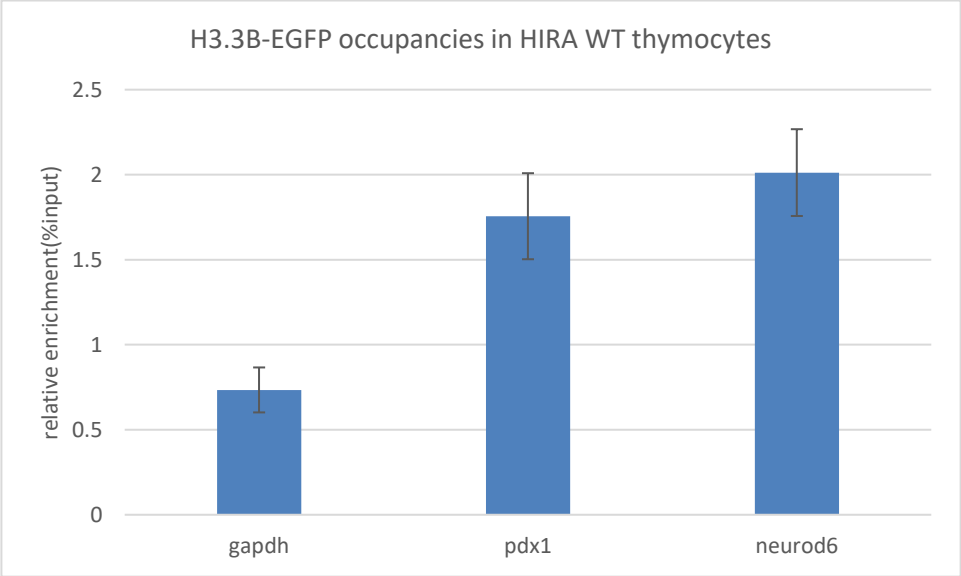

Fig 3.1.7. Relative enrichment of H3.3B-EGFP on Gapdh, Pdx1 and Neurod6 genes in H3.3B-EGFP thymocytes as revealed by ChIP. *H3.3B-EGFP was enriched on silent genes Neurod6 and Pdx1 and diminished on the active gene Gapdh relative to total input. Error bars: SEM. n=4 (biological replicates). Error bars: SEM.*

Importantly, as histone H3.3 is a component of the nucleosome, normalizing H3.3B-EGFP signal to total input may not reflect the proportion of nucleosomes containing H3.3B-EGFP in these regions. To estimate the proportion of H3.3B-EGFP containing nucleosomes on these regions, ChIP using anti-H3 antibody (which recognizes all histone H3) on the same chromatin samples was performed and used as normalization control. The level of histone H3, which represents the nucleosome density, was found to have the same pattern as H3.3B-EGFP ChIP (Fig 3.1.7 and Fig 3.1.8). Levels of H3.3B-EGFP (when normalized to H3) on *Gapdh, Pdx1* and *Neurod6* genes was similar (Fig 3.1.9). This indicates that there is a higher proportion of H3.3 on the promoter of *Gapdh* and less on gene bodies of *Pdx1* and Neurod6.

In summary, the H3.3B-EGFP deposition was revealed to be similar on the promoter region of *Gapdh* and gene bodies of *Pdx1* and *Neurod6* when relative to total histone H3 (Fig 3.1.9) regardless of different expression levels of these three genes in thymocytes.

Several DNA hypersensitive site (DHS) studies showed that DHS signals were high in regions proximal to TSS (He *et al*., 2014), which implies that there could be nucleosome free regions (NFRs) at this region. The explanation for this may be the fact that the promoters at transcriptionally active genes have nucleosomes that continuously replace H3.3 to keep the nucleosomes unstable at the TSS (Jin and Felsenfeld, 2007, Deal *et al*., 2010), which might explain the lower level of H3.3B-EGFP enrichment on promoters of the highly expressed gene *Gapdh* compared to low expressing genes *PdX1* and *Neurod6* (Fig 3.1.7). This would assume that even though a gene may be expressing at a lower level, a proportion of the H3 at the promoter is H3.3. Therefore, H3.3 level is determined not only by gene expression but also the location looked at within the target gene. As we know, there are different nucleosome partners on promoters including H3.3/H2A.Z, H3.3/H2A, H3/H2A and H3/H2A.Z, in the order from the least stable to the most stable (Jin and Felsenfeld, 2007). The nucleosomes that occupied the promoters of genes are different according to gene activity. The least stable nucleosomes such as those containing H3.3, are more likely enriched on the promoters of highly expressed genes than lower expressed genes, as disruption of the nucleosome is thought to be important for facilitating loading of RNA Pol II. To summarize, promoters at transcriptionally active genes have nucleosomes that simultaneously carry H3.3 and the proportion of H3.3 of the total H3 correlates with gene expression level. Future work can be found in section 3.6.1.

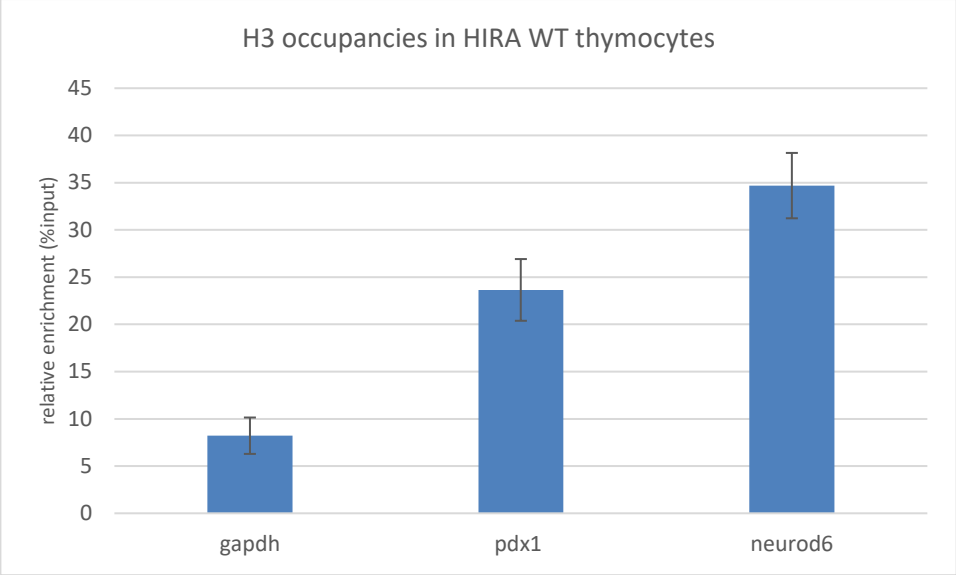

Fig 3.1.8. Relative enrichment of H3 on Gapdh, Pdx1 and Neurod6 genes in H3.3B-EGFP thymocytes as revealed by ChIP. *Level of histone H3 which represents the nucleosome occupancy was higher in Neurod6 and Pdx1 loci than Gapdh. Error bars: SEM. n=4 (biological replicates). Error bars: SEM.*

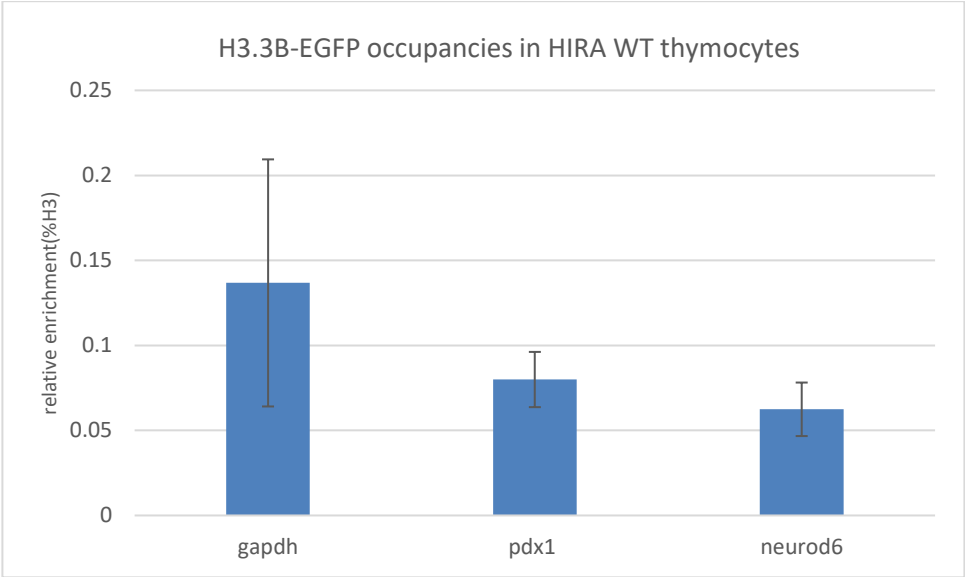

Fig 3.1.9. Relative enrichment of H3 on Gapdh, Pdx1 and Neurod6 genes in H3.3B-EGFP thymocytes as revealed by ChIP*. Similar level of H3.3B-EGFP was revealed on Gapdh, Pdx1 and Neurod6 relative to total histone H3. n=3* (biological replicates). Error bars: SEM.

3.5 HIRA homozygous conditional knockout (HIRA HOM CKO) mice are a good model for studying the role of HIRA in regulating genome-wide H3.3 distribution *in vivo*

The HIRA complex is an evolutionarily conserved H3-H4 histone chaperone that is implicated in a range of processes including embryonic development, angiogenesis, cellular senescence and aging (Gal *et al*., 2015). This complex is composed of HIRA in association with ubinuclein-1 (UBN1) and calcineurin-binding protein 1 (CABIN1) (Rai *et al*., 2011). In mammals, HIRA is associated with the histone variant H3.3, which is deposited into chromatin independently of DNA synthesis (Tagami *et al*., 2004). There is no genome-wide H3.3 deposition data published in a HIRA deficiency mouse *in vivo*, so we wanted to see the impact of HIRA knockout (KO) on genome-wide H3.3 deposition in our mouse system. In our mouse model, it was expected that the floxed *HIRA* exon 4 would be deleted in T cells upon exposure to Cre-recombinase (Cre), which would result in deletion of exon 4 and non-sense mediated decay of the mRNA, leading to the conditional KO (CKO) phenotype in specific tissues that expressing Cre such as in thymus, lymph node and spleen (Fig 2.2). Firstly, 500ng RNA was used to make cDNA, which was followed by Q-RTPCR using HIRA exon-exon junction primers (HIRA exon 4-5) to confirm the HIRA was completely knocked out in thymus. Fig 3.2.1 shows that the expression level of *HIRA* exon 4 is 5-fold less than WT with some background signal (Fig 3.2.1). Diminished level of HIRA mRNA in HIRA HOM CKO suggested it was a good model for studying the loss of function of HIRA.

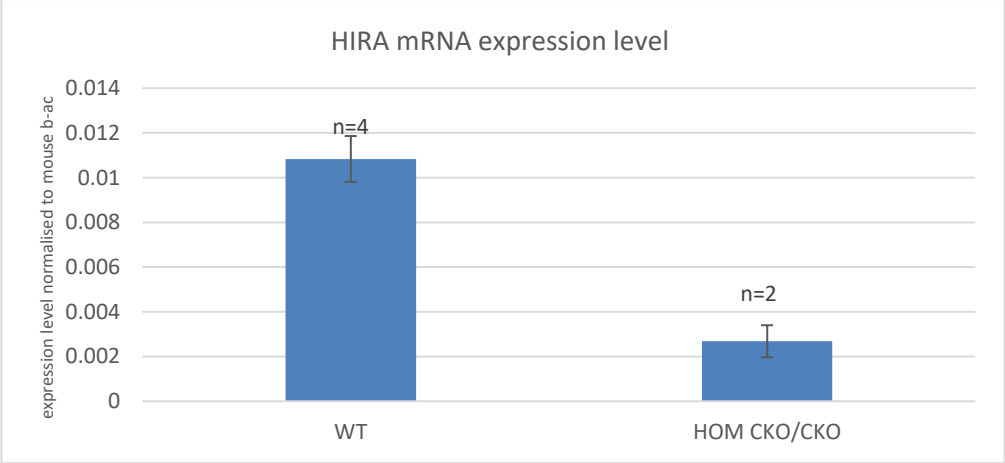

Fig 3.2.1. Q-RTPCR showing HIRA mRNA expression level in both WT and HOM CKO mouse thymocytes. *Primers used here target the LoxP/Cre excised HIRA exon 4. HIRA WT, n=4 and HIRA HOM CKO, n=2. Error bars: SEM.*

3.6 Deficiency of HIRA leads to altered H3.3 deposition on selected gene regions

Having got an indication of H3.3 distribution in WT thymocytes, next we asked if H3.3B-EGFP occupancies on the regions tested previously in section 3.4 were changed upon HIRA KO. Here we showed that in thymocytes, HIRA deficiency appears to result in decreased H3.3B-EGFP enrichment at the promoter region i.e.120bp upstream of the TSS of the *Gapdh* gene but an increase in H3.3B-EGFP enrichment at gene bodies of *Pdx1* and *Neurod6* genes (Fig 3.2.2). As HIRA is thought to be responsible for incorporating H3.3 at promoters and on gene bodies of transcriptionally active genes (Zhang *et al*., 2017b, Goldberg *et al*., 2010),its deficiency would therefore be expected to result in a decrease in H3.3 occupancy at promoter of *Gapdh* gene examined here. Same experiment by using anti-H3.3 antibody revealed that the enrichment of H3.3 was reduced by HIRA deficiency in thymocytes although the anti-H3.3 antibody has been shown to give a very low H3.3 signal and the variation is big (Fig S16). As mentioned above, *Pdx1* and *Neurod6* are expressing at very low level in thymus (Fig 3.1.5), HIRA may not be the main chaperone for loading H3.3 on these genes, in which case, other chaperones may come in and load H3.3 onto these regions. The relative fold change of H3.3B-EGFP enrichment was smaller at the promoter of *Gapdh* while bigger effects were observed in *Neurod6* and *Pdx1*, which are expressing at a lower level in thymus (Fig 3.2.3). Although none of these detected changes were individually statistically significant, taken together, deficiency in HIRA appears to have different effects on H3.3 deposition on different gene regions. Notably, as shown in previous western blot, H3.3-EGFP fusion protein is 45kDa whereas H3 is only 17kDa. The EGFP tag is much bigger than H3.3 protein itself, which in a way, one could speculate that this EGFP tag could interfere with H3.3 binding to chromatin.

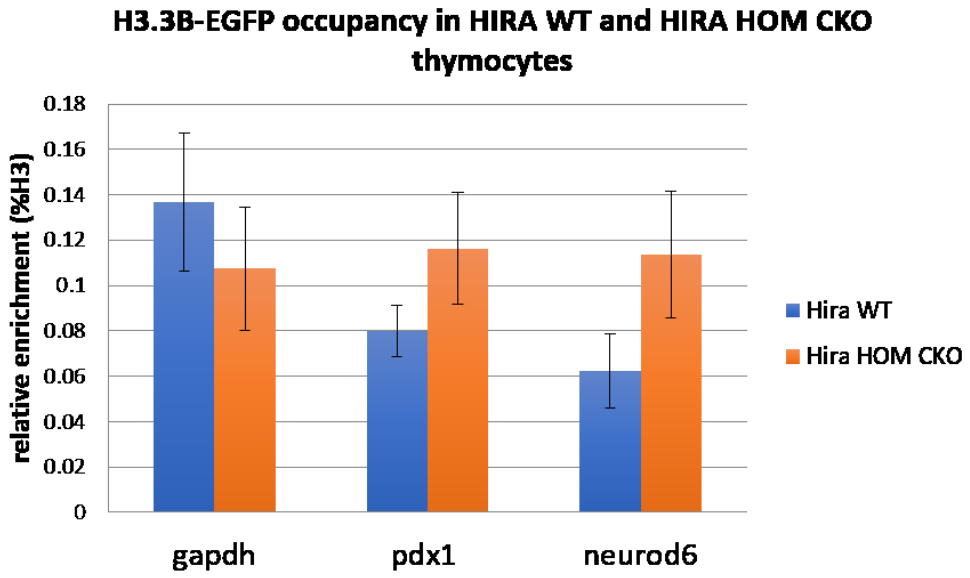

Fig 3.2.2. Relative enrichment of H3.3B-EGFP on various genomic regions in HIRA WT and CKO thymocytes. (Relative to H3) *Promoter region of Gapdh gene showed decrease level of H3.3B-EGFP upon HIRA HOM CKO, whereas both Pdx1 and Neurod6 genes showed increased level of H3.3B-EGFP on gene bodies upon HIRA HOM CKO. However, none of these changes were statistically significant (p values for Gapdh, Pdx1 and Neurod6 genes are 0.74, 0.29 and 0.1 respectively). HIRA WT n=4 (biological replicates). HIRA HOM CKO n=3 (biological replicates). Error bars: SEM.*

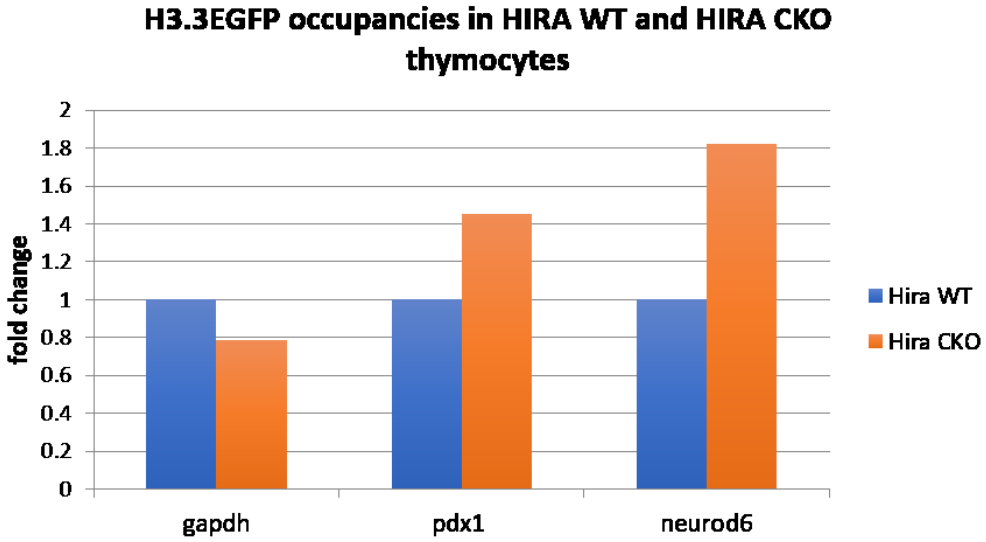

Fig 3.2.3. Relative fold change of H3.3B-EGFP signal relative to H3 detected by ChIP. *Fold change of H3.3B-EGFP signal on silent gene loci (Pdx1 and Neurod6) is bigger than that on active gene Gapdh in response to HIRA KO relative to WT.*

3.6.1 Future work

Future experiments to explain the observation seen in section 3.4 and 3.6 regarding: 1. The H3.3 enrichment on different regions on different genes expressing at different levels 2. The role of HIRA in incorporating H3.3 onto these regions would include:

1. To get a more general idea of genome-wide distribution of H3.3B-EGFP, H3.3B-EGFP ChIP-seq could be performed in HIRA WT mouse thymus. By data mining with the transcriptomic data we already have in T cells, we can conclude if there is any correlation between H3.3 enrichment and gene expression level in T cells. Moreover, we can also look into other tissues to compare if the deposition pattern of H3.3 is the same across different cell types in different tissues.

2. To investigate the effect of HIRA deficiency on H3.3 deposition, by comparing the genome-wide distribution pattern of H3.3 in HIRA WT and HIRA KO, we can get an idea of how HIRA deficiency exerts an effect on genome-wide H3.3 distribution and how this change correlates with gene expression.

Due to the difficulty in obtaining validation of the EGFP-ChIP result with primary antibody ChIP and the limited resources available it was decided to rather focus on the *in vivo* role of HIRA deficiency in T cell development.

3.7 Investigation into the role of HIRA in Immune system

3.7.1 Upregulation of CD44 upon HIRA KO was observed in lymphatic tissue in mouse

T cells originate in the bone marrow and populate the thymus and then migrate from cortex to medulla – a diagram showing the acquisition of key cell surface markers is shown in Fig 1.8.1.

To investigate if HIRA KO affects T cell development, cells collected from thymus, lymph node and spleen from both HIRA WT and HIRA KO mice were stained with CD4, CD8, CD62L (lymph node homing receptor), CD44 (memory marker), CD19 (B-lymphocyte antigen), TCRβ (T-cell receptor) antibody. FACS was performed and the different cell populations identified are shown in Fig 3.3.1. CD44 expression happens early in T cell development in the thymus. Just before the rearrangement of the TCRβ locus happens at stage DN3, these DN cells express the CD44 adhesion molecule but at a low level. Upon T cell activation by antigens in the periphery, CD44 expression is up-regulated. In our experiment, CD44 expression (memory marker) was upregulated in CD4 SP T cells in HIRA KO thymus, lymph node and spleen with the most obvious upregulation seen in lymph node compared to HIRA WT (Fig 3.3.1 A/B/E). And we also found this increase in CD8 SP T cell upon HIRA KO (Fig S4 C/D). Previously, a similar observation has been shown in transcriptomic data whereby, CD44 protein level was increased upon HIRA KO in the thymus (Vineet Sharma PhD thesis, 2014). However, CD44 was not upregulated in CD4/CD8 DP cells in the thymus upon HIRA KO (Fig S4 B). This suggests that HIRA might be involved in the repression pathway of the *CD44* gene. Additionally, T cell/B cell ratio was decreased according to the TCRβ/CD19 ratio in lymph node, which suggested that the total T cell output from the thymus decreased (Fig 3.3.1 D). The predominantly B cell population (DN staining), on the other hand, showed no obvious upregulation of CD44 in both HIRA KO lymph node and spleen compared to HIRA WT (Fig 3.3.1 F). The memory subpopulation is commonly found in the lymph nodes

and in the peripheral circulation like the spleen, but it is not common in thymus where the majority are naïve T cells. This indicates an increased CD4 SP memory T cell phenotype upon HIRA KO in the thymus, lymph node and spleen and an increased CD8 SP memory T cell phenotype upon HIRA KO in thymus, lymph node and spleen only. In addition, CD62L (lymph node homing receptor) expression remained similar in HIRA KO and WT (Fig 3.3.1 A/B/E), which indicates HIRA does not affect memory T cell migration into periphery tissue.

To summarize, we found by flow cytometry that HIRA deficiency results in premature expression of the 'memory' T cell marker CD44 in the naïve single positive T cells in the thymus and periphery. This aberrant upregulation might be due to: 1) decreased output from the thymus during T cell development leading to aberrant proliferation in the periphery; 2) premature activation of the commitment to the memory T cell lineage that circumvents exposure to antigen in the periphery or 3) a CD44 locus-specific effect of HIRA deficiency in de-repressing this gene which is normally transiently expressed during early development and then subsequently silenced.

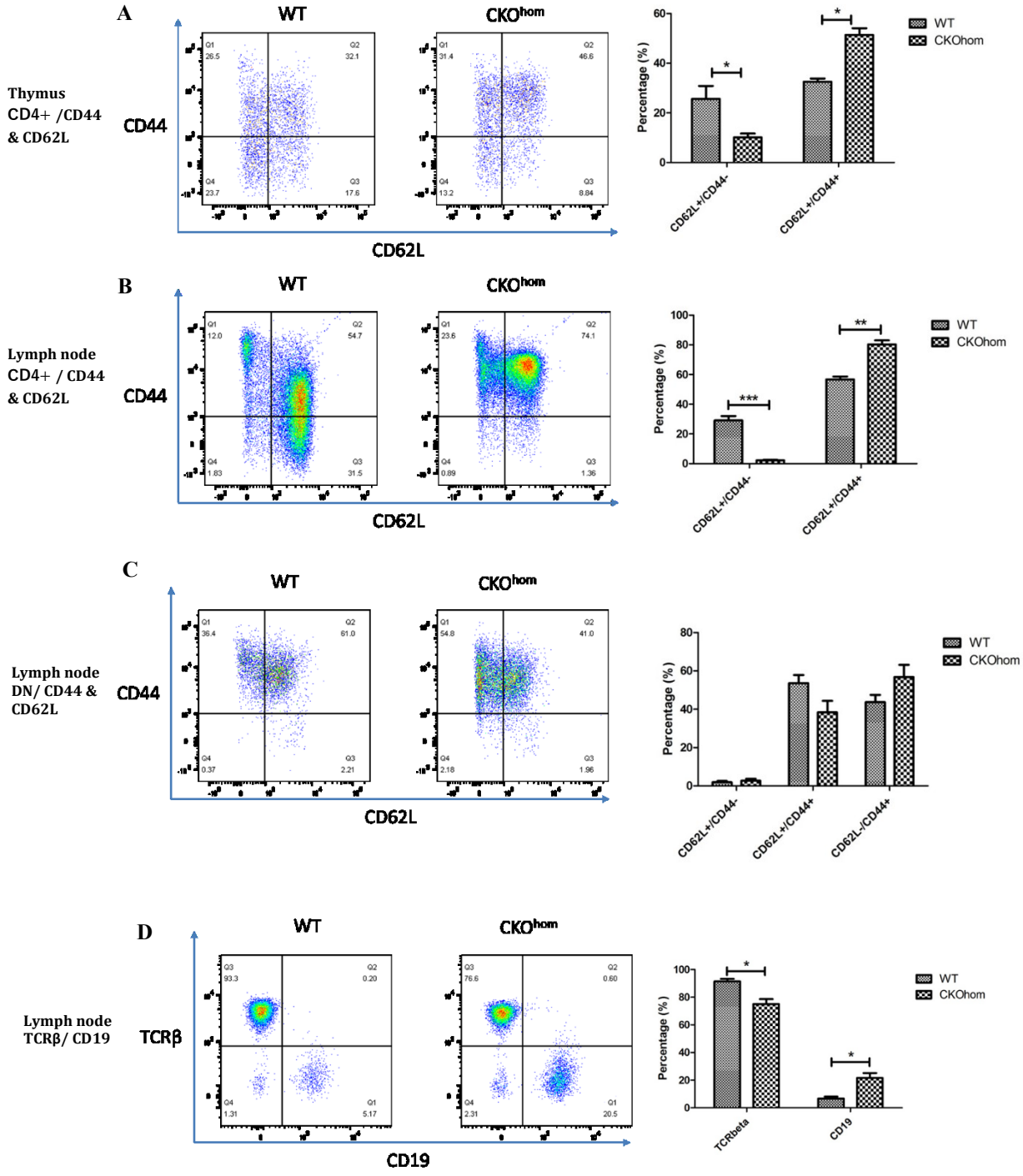
A
WT
CKOhom
CD44
CD62L
Thymus
CD4+ /CD44
& CD62L
Percentage (%)
CD62L+/CD44-
CD62L+/CD44+
WT
CKOhom
B
Lymph node
CD4+ / CD44
& CD62L
C
Lymph node
DN/ CD44 &
CD62L
CD62L-/CD44+
D
TCRβ
CD19
Lymph node
TCRβ/ CD19
TCRbeta

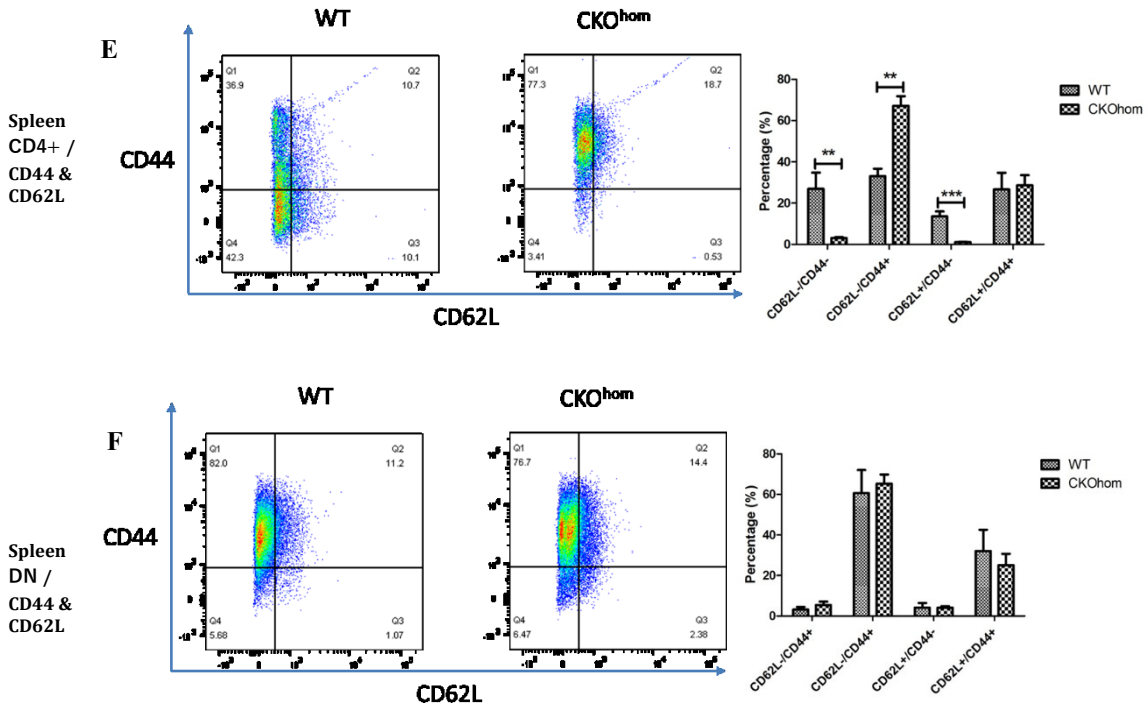

Fig 3.3.1. FACS plot showing the expression of different cell surface markers on different cell population in Thymus, Lymph node and Spleen. *A, B, E) CD44 was up-regulated on CD4+ T cells in Thymus, Lymph node and Spleen. C, F) No CD44 upregulation was detected on B cells in Lymph node and Spleen. D) T cell/B cell ratio in Lymph node decreased according to the TCRβ/CD19 ratio. This experiment was done together with Dr Jackson Chan, a postdoc in the lab. (n=3 for all FACS experiment in this Fig) (*-Statistically significant, *p value<0.05)*

3.7.2 TCRα V(D)J recombination in CD71- T cell population upon HIRA KO

In our system, HIRA conditional knockout (CKO) is under the control of the Cre/CD4 promoter (Abi-Ghanem *et al.*, 2015). Shortly after acquisition of CD4 and CD8, DP thymocytes lose the expression of CD71 and become non-proliferating CD71- DP cells in which H3.3 will be the only available H3 histone proteins that can be incorporated into chromatin. Therefore, it is well worth assessing whether the CD71- DP cell population was a clean model to study HIRA deficiency effects on T-cell development and T-cell receptor V(D)J recombination events possibly driven by incorporating H3.3 into chromatin. The expression of

CD4, CD8, CD71 and EGFP during CD71 cell sorting was confirmed by FACS (Fig S9). T cell development stages with CD71 expression is illustrated in Fig 3.3.2.

Following the scheme developed by Setian *et al* (Seitan *et al*., 2011) to confirm HIRA deficiency in the CD71- DP cell population, we set out to purify the CD71- DP cells from thymus by FACS cell sorting (Fig 3.3.3) and to verify the efficiency of HIRA KO, either by examining deletion of exon 4 of *HIRA* or by measuring HIRA protein levels by western blot (Fig 3.3.4 and 3.3.5). Firstly, we set the forward scatter (FSC) and side scatter (SSC) on the total cell population to obtain lymphocytes followed by single cell selection. Within the single cell population, cells with CD4+CD8+ (DP) signal were selected for by CD71 gating. In the CD71+ population, cells are heterogeneous with different cell sizes. For CD71- cells, we set another size gate to collect a pure population with a smaller cell size. *HIRA* deletion at the DNA level was checked by QPCR (Fig 3.3.4). This result suggested that exon 4 of the *HIRA* gene had been removed by Cre-recombination very efficiently in almost all the cells in the CD71- selected population. Western blot determined HIRA protein level in both HIRA WT and HIRA KO thymus before CD71 cell sorting (Fig 3.3.5). LaminB, with a protein band at 66kDa was used as a loading control and is shown in the lower panel (Fig 3.3.5). In the upper panel the blot is probed with a HIRA specific antibody revealing a protein band of the correct size of 112kDa (Fig 3.3.5).

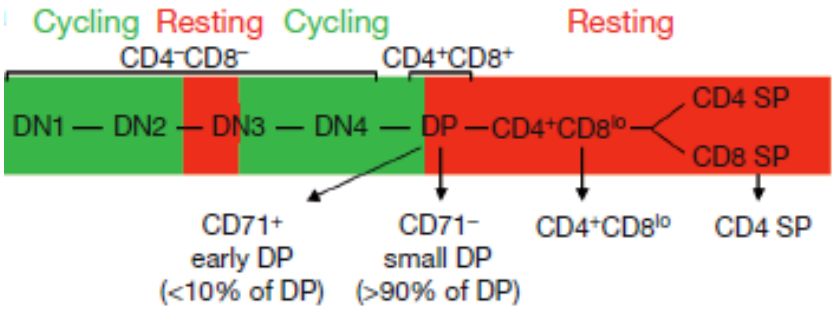

Fig 3.3.2. Illustration of T cell development with indicated transferrin receptor CD71 expression in mouse thymus. *Proliferating cells are showing in green box whereas non-proliferating cells are in red. During the transition from DN to DP, the transferrin receptor CD71 was lost. This figure is adapted with permission from Brekelmans et al. (Brekelmans et al., 1994).*

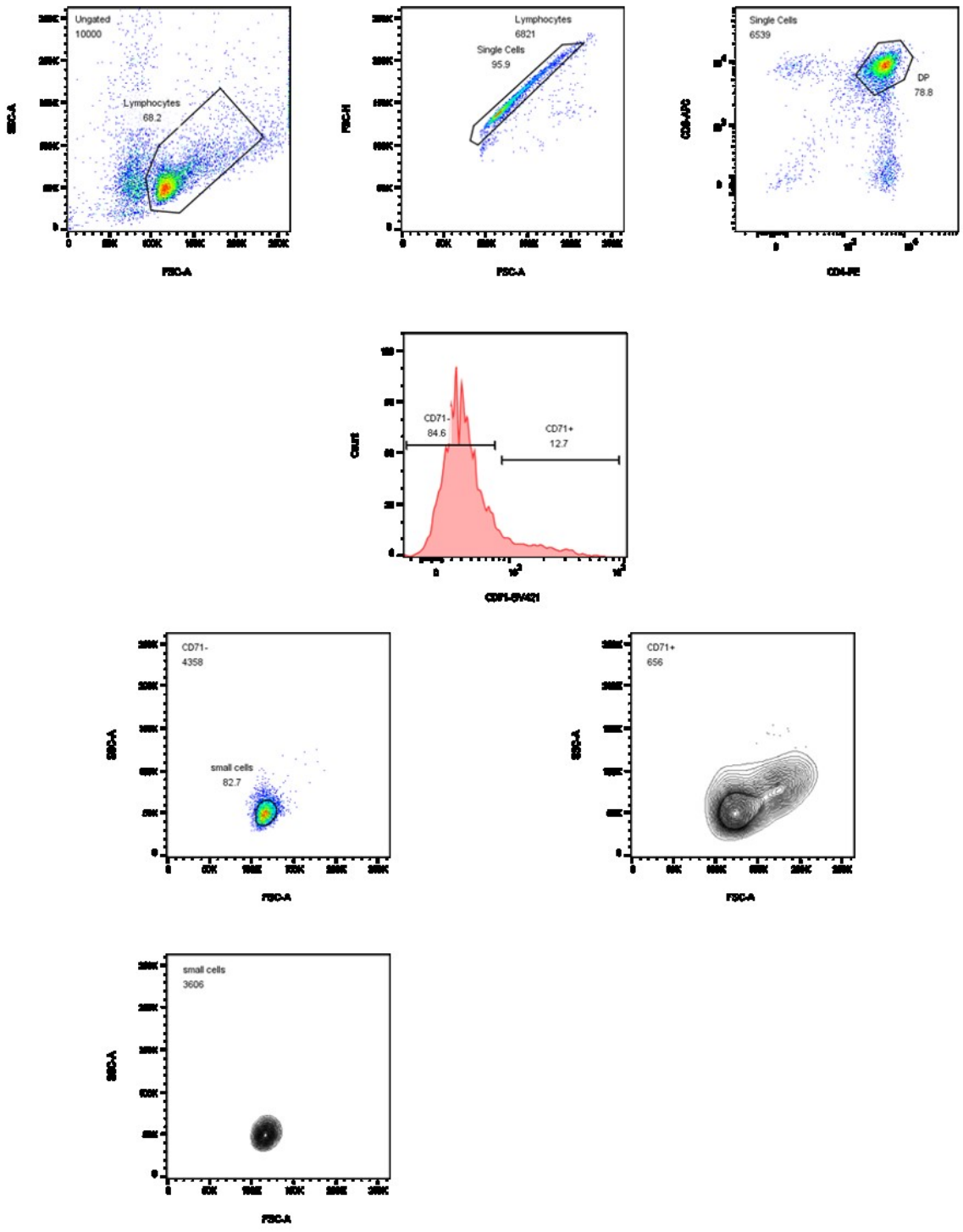

Fig 3.3.3. CD71 cell sorting process by using FACS. *2 size gates were set up in order to get the singlet small CD71- DP thymocytes. This cell sorting scheme is followed as stated in Setian et al., paper (Seitan et al., 2011).*

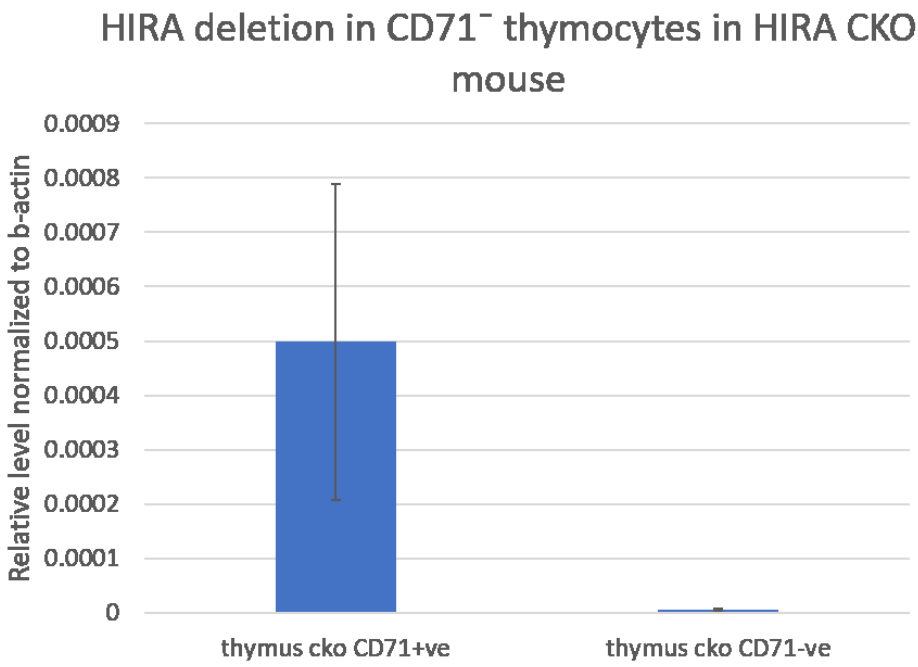

Fig 3.3.4. QRT-PCR showing the expression level of HIRA in CD71+ and CD71- thymocytes in mice. *HIRA mRNA copy number in HIRA CKO CD71- population was negligible compared to CD71+ population in HIRA CKO（n=4).*

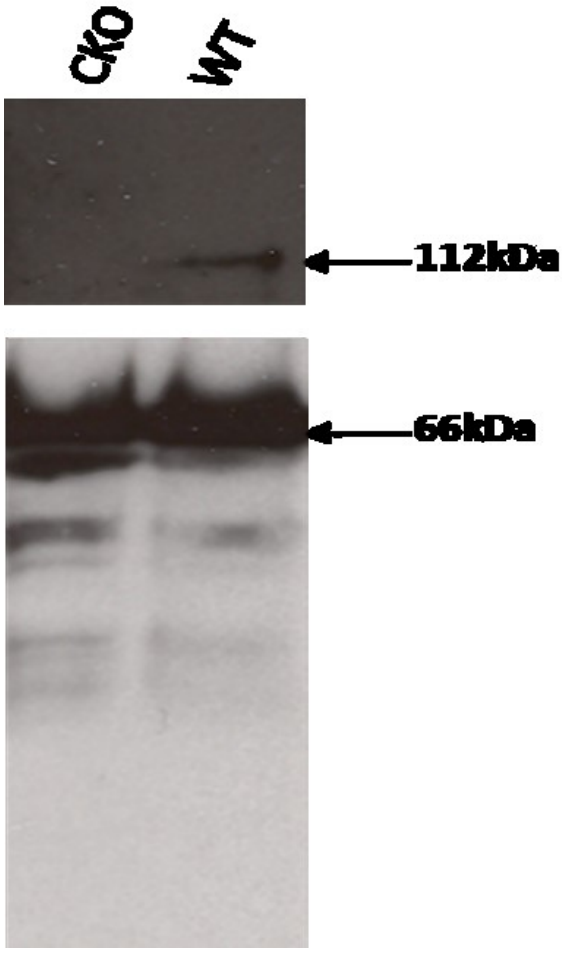

Fig 3.3.5. Western blot showing the detection of HIRA in mouse thymocytes. *HIRA protein band was undetectable in HIRA CKO mouse Thymus compared to the HIRA band （112kDa） in WT mouse Thymus. LaminB with a protein band at 66kDa was used as a loading control in this experiment.*

As shown in Fig 3.3.6, TCRα locus rearrangement happens later in CD4/CD8 DP stage and as mentioned before, there is a CD71- population at this stage that allows us to study the TCRα V(D)J recombination event in the absence of HIRA. Next, we examined the T cell receptor α chain (TCRα) V(D)J recombination in CD71- cell population in both HIRA WT and HIRA CKO mouse thymus by PCR with forward primers specific to Vα region and reverse primers specific to Jα region respectively and followed by visualization on the gel. Rearrangements of the TCRα loci are known to precede TCRα gene rearrangements at a later stage following TCRβ gene rearrangements during pro-T cell development. As shown in Fig 3.3.6, DN4 population that upregulates expression of CD4 and CD8 to yield double-positive (DP) cells,

which usually progress through an immature cycling of the CD8+ intermediate SP population, and initiates TCRα gene rearrangements.

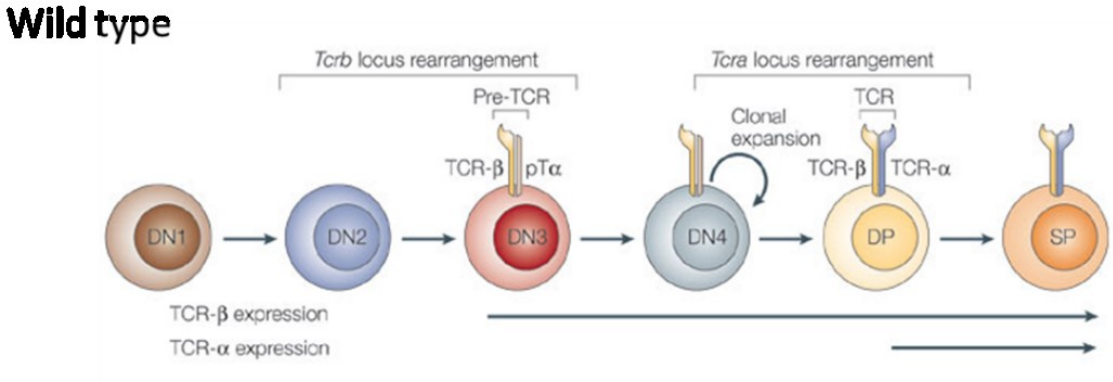

Fig 3.3.6. **An illustration of TCR rearrangement during T cell development with CD44 expression.** *This figure is adapted with permission from "Bcl-2 transgene expression promotes survival and reduces proliferation of CD3-CD4-CD8-T cell progenitors" Lorraine A O'Reilly et al. (O'Reilly et al., 1997).*

We performed PCR to amplify serial dilutions of genomic DNA from both CD71- and CD71+ DP T cells with forward primers specific to the Vα region and reverse primers specific to the Jα region respectively. PCR products could be separated by agarose gel electrophoresis and stained with ethidium bromide. This method shows the usage of each fragment during V(D)J rearrangement depending on the density of the band. Threefold serial dilutions of the DNA were analyzed for the presence of the indicated Vα-Jα rearrangements. Input DNA was normalized by amplification of a PCR fragment from the CD14 locus. The gene segments of the TCR locus are numbered according to Hayday *et al*. (Höflinger *et al*., 2004, Hayday *et al*., 1985). By semi-quantitative PCR analysis, we detected that Vα8-Jα61, Vα8-Jα50 and Vα8-Jα42 rearrangement were strongly affected within HIRA deficient CD71- thymocytes (Fig 3.3.7). However, there was no effect of HIRA deficiency on V(D)J recombination of Vα8-Jα50 and Vα8-Jα42 in the CD71+ cell population (Fig 3.3.7). This is as expected because these cells are at an earlier stage in the recombination program which proceeds from Vα8-Jα61 to Vα8-

Jα50 and finally Vα8-Jα42 (Fig 3.3.8). Because TCRα locus rearrangement happens later, at the CD4/CD8 DP stage, the CD71+ cells which showed no effect, were used as a control (Fig 3.3.7).

To conclude, HIRA deficiency seems to impair TCRα V(D)J rearrangement in CD71- DP cell population in thymus *in vivo.* For V(D)J genes, it is not known precisely what nucleosome density favors successful recombination.

6554 CKO^{hom} vs 6556 WT
CD71 -ve sorted thymocytes

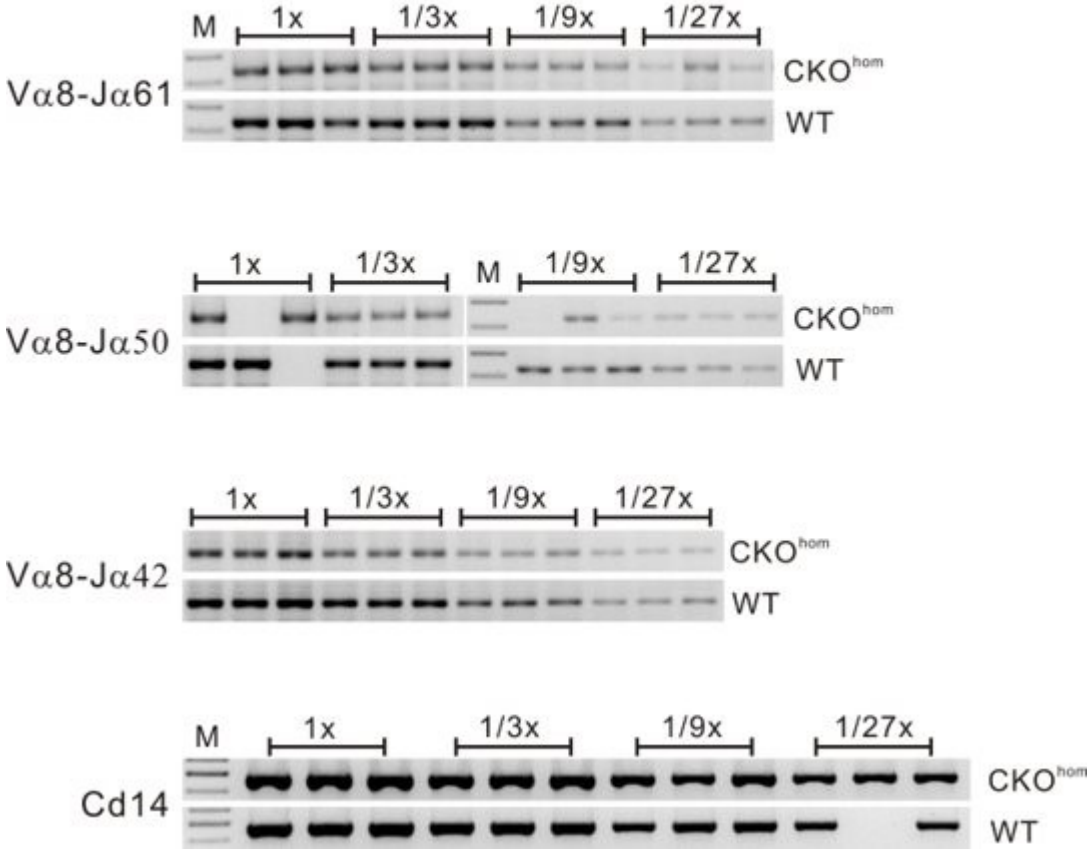

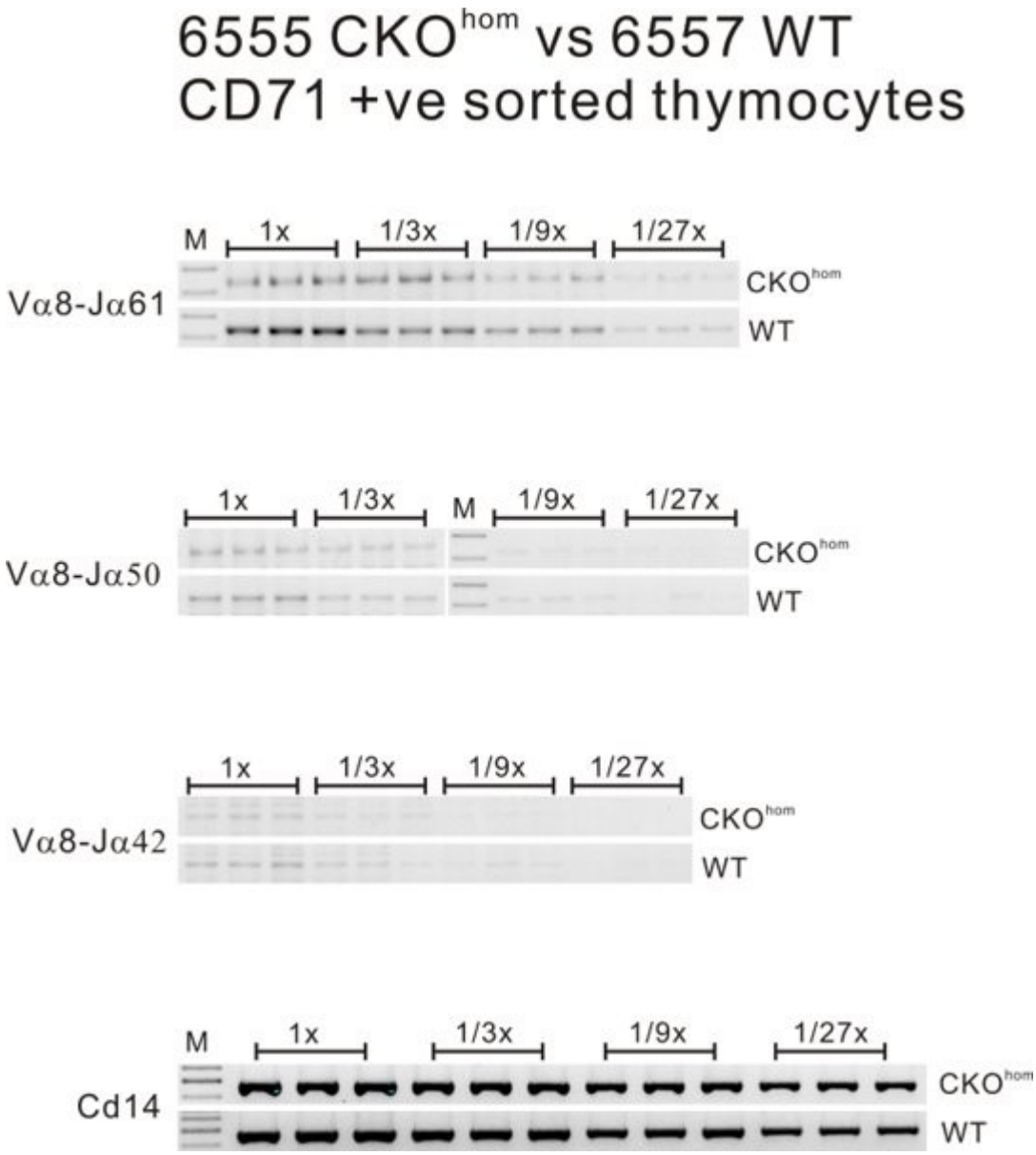

Fig 3.3.7. V(D)J recombination of the TCRα loci in CD71- DP T cells (upper) and CD71+ DP T cells (lower). *CD71+ cells are used as a control because TCRα locus rearrangement has not yet happened in these cells. Threefold serial dilutions of the DNA were analyzed by PCR for the presence of the indicated Vα-Jα rearrangements. Input DNA was normalized by amplification of a PCR fragment from the CD14 locus. The gene segments of the TCRα locus are numbered according to Hayday et al.(Hayday et al., 1985).*

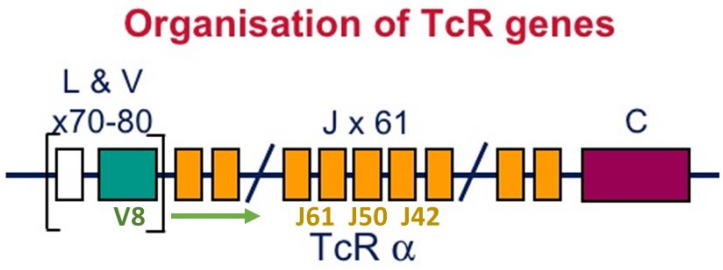

Fig 3.3.8. Schematic diagram showing the organization of mouse TCRα genes. *TCR genes segmented into variable (V), diversity (D) and joining (J) elements. In our particular case showing here, the recombination program proceeds from Vα8-Jα61 to Vα8-Jα50 and finally Vα8-Jα42 indicated by green arrow. This figure is modified from https://www.slideshare.net/rajud521/t-cell-antigen-receptor/17.*

3.7.3 Future work

3.7.3.1 To investigate the possibilities for CD44 upregulation

To determine whether the *CD44* gene is simply inappropriately switched on or the whole T cell developmental program for generating memory cells has been reprogrammed, we can take naïve T cells (from WT and CKO) and activate them artificially to see if they secrete cytokines, such as IL3 and IFNγ, which are normally produced in large quantities by memory T cells upon secondary encounter with antigen (Mirabella *et al*., 2010). If we can detect such memory-cell specific cytokines in the medium, then it suggests that the memory cell developmental pathway has been triggered earlier than normal in the absence of the physiological signal, i.e. encounter with antigen in the periphery. If we cannot detect abnormal cytokine production, then it indicates that a repressive pathway for keeping the *CD44* gene silenced might be affected or that CD44 has been upregulated as part of a compensatory expansion of the T cell population due to decreased output from the thymus.

Another way for checking memory programming is to isolate these cells with upregulated CD44 expression and perform RNA sequencing and compare the transcriptomic data with that obtained from naïve T cells – to identify transcriptomic 'fingerprints' for the different developmental stages. In addition, we can also check the cell apoptosis rate in thymus and periphery in order to see if this accounts for the decreased output (T cell/B cell ratio).

Thymic development and output will also be assessed using Bromodeoxyuridine (BrdU) labelling *in vivo* to identify proliferating T cells and tracking T cell development by incorporating into replicating DNA. BrdU can label proliferating (CD71+) DP cells but not resting CD4+CD8+, CD4+ or CD8+ SP cells. In the following chase period, BrdU labelling should be detectable in resting CD4+CD8+, CD4+ or CD8+ SP cells as DP cells differentiate (Seitan *et al*., 2011). By chasing BrdU labelling during T cell differentiation in HIRA KO thymus, we will calculate the proportion of DP cells that become CD4+ or CD8+ SP cells over time. Comparing WT and HIRA deficient animals will determine whether HIRA deficiency alters the dynamics of T cell development *in vivo*.

3.7.3.2 To investigate the consequences of gene expression and V(D)J recombination due to loss of H3.3 deposition

RAG1 V(D)J recombinase has been showed to target the acetylated and phosphorylated form of H3.3 (acetyl-H3.3 S31p) for ubiquitylation via its RING finger domain (Jones *et al*., 2011). Together with previous evidence reporting that V(D)J recombination loci are enriched with H3.3 (Johnson *et al*., 2004), we could speculate that a potential role of H3.3 in V(D)J recombination might be in forming a chromatin structure that favors V(D)J recombination. Further investigation into the changes of H3.3 deposition (over H3) on these V(D)J genes upon HIRA KO in CD71- DP T cells would give us a better understanding of how HIRA functions

in this recombination process. In the CD71^{-} T cell system, it would also be interesting to obtain transcriptomic (by RNA-seq) data and the genome-wide H3.3 deposition profile in both HIRA WT and CKO mouse. By comparing the H3.3-EGFP ChIP-Seq and RNA-Seq result, we can investigate whether changes in gene expression are likely to be due to the loss of H3.3 deposition by HIRA on these genes and whether the process of V(D)J recombination is also affected. The transcriptomic data would also allow us to determine whether the dynamic range of transcription in T cells is affected as was the case in developing oocytes (Nashun et al., 2015b).

Chapter 4 - Investigation into the sexual dimorphism regulation by HP1γ *in vivo*

4.1 Hypothesis and Aims

This chapter is based on the recent observation in the lab that HP1γ knockout (HP1γ KO) may slow down male mouse embryonic fibroblast (MEF) proliferation, while female MEF proliferation was not significantly affected. Meanwhile, transcriptomic analysis was carried out to study the effect of HP1γ on gene regulation genome-wide in male and female MEFs (Law *et al*., 2019). RNA-sequencing (RNA-seq) revealed that the effect of HP1γ KO is much greater in males than that in females (Fig 4.1.1), which indicates that males have a higher dependency on HP1γ to maintain a normal gene expression profile. Moreover, gene ontology (GO) analysis on the differentially expressed genes (comparing wild type and knockout cells) implicated HP1γ in various biological processes, including cell cycle regulation, cell proliferation, RNA processing and chromosome segregation.

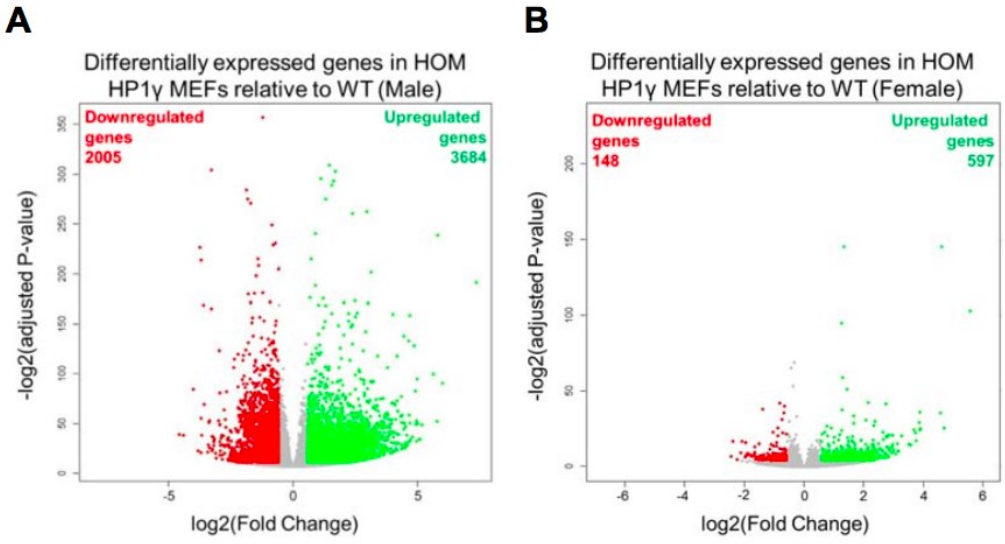

Fig 4.1.1. Volcano plot showing the differentially expressed genes in HP1γ wild-type MEFs compared to HOM MEFs. *Green and red dots represent genes that are up-regulated and down-regulated after HP1γ knockout respectively. Grey dots are genes not significantly affected.* ***A.*** *In male MEFs, 3684 genes were up-regulated and 2005 were down-regulated.* ***B.*** *In female MEFs, 597 genes were up-regulated and 148 were down-regulated. This figure is adapted with permission from Dr Pui-Pik Law (Law, 2015).*

To study the different response to HP1γ KO between males and females, 176 sexual dimorphic genes were firstly identified, which have different expression levels in HP1γ wildtype males (WTM) compared with wildtype females (WTF) (Fig 4.1.2 A), including 114 female higher genes, where their expression level was higher in females and 62 male higher genes, where their expression level was higher in males. Interestingly, after HP1γ KO in males, the expression level of most female-higher genes was significantly increased (Fig 4.1.2 B/C), and the expression level of male higher genes was significantly reduced (Fig 4.1.2 E/F). However, the effect of HP1γ KO in females was less obvious (Fig 4.1.2 D/G).

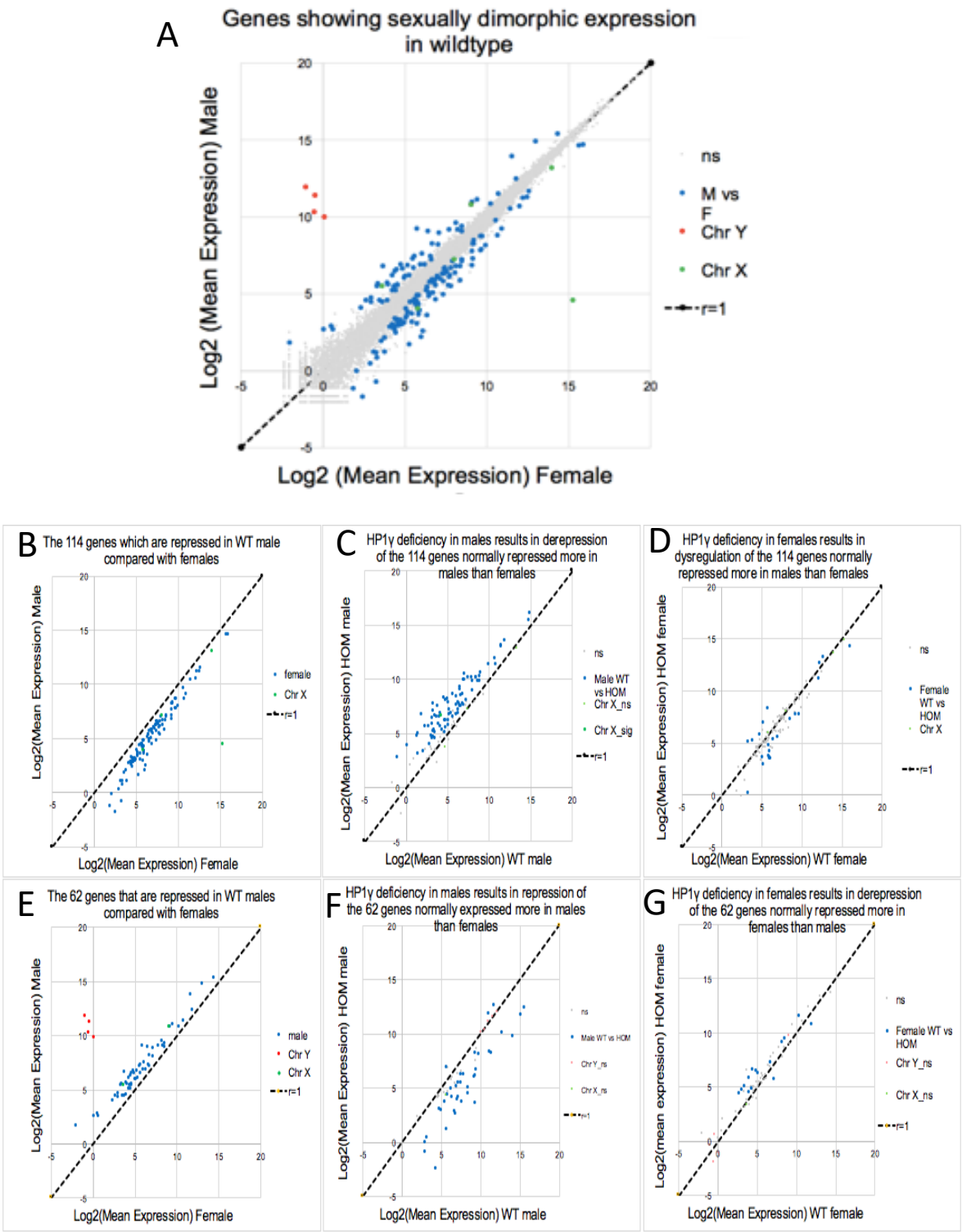
A
Genes showing sexually dimorphic expression in wildtype
Log2 (Mean Expression) Male
Log2 (Mean Expression) Female
ns
M vs F
Chr Y
Chr X
r=1
B
The 114 genes which are repressed in WT male compared with females
Log2(Mean Expression) Male
Log2(Mean Expression) Female
female
Chr X
r=1
C
HP1γ deficiency in males results in derepression of the 114 genes normally repressed more in males than females
Log2(Mean Expression) HOM male
Log2(Mean Expression) WT male
ns
Male WT vs HOM
Chr X_ns
Chr X_sig
r=1
D
HP1γ deficiency in females results in dysregulation of the 114 genes normally repressed more in males than females
Log2(Mean Expression) HOM female
Log2(Mean Expression) WT female
ns
Female WT vs HOM
Chr X
r=1
E
The 62 genes that are repressed in WT males compared with females
Log2(Mean Expression) Male
Log2(Mean Expression) Female
male
Chr Y
Chr X
r=1
F
HP1γ deficiency in males results in repression of the 62 genes normally expressed more in males than females
Log2(Mean Expression) HOM male
Log2(Mean Expression) WT male
ns
Male WT vs HOM
Chr Y_ns
Chr X_ns
r=1
G
HP1γ deficiency in females results in derepression of the 62 genes normally repressed more in females than males
Log2(mean expression) HOM female
Log2(Mean Expression) WT female
ns
Female WT vs HOM
Chr Y_ns
Chr X_ns
r=1

Fig 4.1.2. Sexual dimorphic gene expression in WT MEFs and their sexual dimorphic response to HP1γ KO. A. *Density plot of differentially expressed genes in HP1γ WTM and WTF MEFs. Dots above the black line are 62 genes with higher expression level in male (Male-higher genes); and dots below the black line are 114 genes with higher expression level in female (Female-higher genes).* ***B.*** *Expression level of female-higher genes in HP1γ WTM compared with WTF MEFs.* ***C.*** *Expression level of female-higher genes in HP1γ WTM compared with KOM MEFs.* ***D.*** *Expression level of female-higher genes in HP1γ WTF compared with KOF MEFs.* ***E.*** *Expression level of male-higher genes in HP1γ WTM compared with WTF MEFs.* ***F.*** *Expression level of male-higher genes in HP1γ WTM compared with KOM MEFs.* ***G.*** *Expression level of male-higher genes in HP1γ WTF compared with KOF MEFs. This figure is adapted with permission from Dr Pui-Pik Law (Law et al., 2019).*

As HP1γ was strongly implicated in regulating sexually dimorphic gene expression, a hypothesis was proposed that HP1γ participates with factors encoded by sex chromosomes to regulate autosomal gene expression and regulate different cell proliferation rates according to sex. Whether the effect of HP1γ in regulating the sexually dimorphic genes is direct or indirect is currently being investigated by ChIP-seq.

Therefore, the present study was aimed at:

1) Identifying the role of HP1γ in cell proliferation by comparing cell proliferation rate of HP1γ WT MEFs with HOM MEFs in both genders.
2) Identifying the role of HP1γ on cell cycle progression by Propidium Iodide (PI) staining.
3) Investigation on inactive X chromosome to see if inactive X chromosome could act as the "sink" for HP1γ.

4.2 Sex difference in proliferation rate and cell cycle upon HP1γ KO in MEFs

Males and females possess sexual inequality in the number and type of sex chromosomes, which has been recognized as playing an important role in the determination of sex differences in physiology, behavior and susceptibility to many diseases (Arnold, 2012). A number of previous studies have shown the sex dimorphism in growth rate of mammalian embryos before differentiation of gonads in which, males were found to be developmentally more advanced relative to females (Burgoyne *et al*., 1995, Burgoyne, 1993, Thornhill and Burgoyne, 1993). However, the molecular mechanisms for these observations are not clear. Using gene ontology (GO) analysis of *ex vivo* primary MEFs, we found that cell cycle-related biological processes are affected in males but not in females upon HP1γ KO (Law, 2019). It has been shown previously that males were found to be developmentally more advanced in growth relative to females (Burgoyne *et al*., 1995, Thornhill and Burgoyne, 1993, Burgoyne, 1993). In line with these studies, we observed that male mouse embryonic fibroblasts (MEFs) (derived from embryonic day 13.5 (E13.5)) proliferate at a higher rate than female MEFs (Fig 4.2.1). To further investigate this sex difference, the genome-wide transcriptional profile of these cells by RNA-sequencing (RNA-seq) followed by Gene Set Enrichment Analysis (GSEA) recently done in our lab showed a significant sex difference in expressing a set of cell-cycle related genes between males and females (data not shown) (Law *et al*., 2019). This finding was consistent with the cell proliferation rate difference seen in this thesis (Fig 4.2.1). When we knocked out HP1γ in these cells, the proliferation rate of male MEFs reduced to a comparable level to that observed in WT females while the proliferation rate of female MEFs was unaffected (Fig 4.2.1). Moreover, another experiment done previously in our lab (Lakshmi Cadavieco, MSc student 2015) also showed that the proliferation rate of female MEFs appears not to be affected by HP1γ KO by comparing the change in cell number in females (data not shown). A proliferative defect was also detected in embryonic stem cells (ESCs) where HP1γ

knockdown slowed down the cell cycle of ESCs (Caillier *et al*., 2010). In most studies to date, the gender of the cells investigated was not specified, so the sex bias might be obscured.

To summarize, depletion of HP1γ specifically slowed down male MEFs proliferation and hence equalized the different proliferation rate between the two sexes in HP1γ WT. Therefore, these data together suggest that HP1γ might be required for maintaining the sex difference in growth rate in mice (Burgoyne, 1995). It should be noted, that as the fetal Leydig cells have only started to produce androgen (male sex hormone) at E13.5, therefore, the sexual difference in proliferation rate seen here is likely to be largely regulated by sex chromosome complement rather than gonadal hormones (Wijchers and Festenstein, 2011).

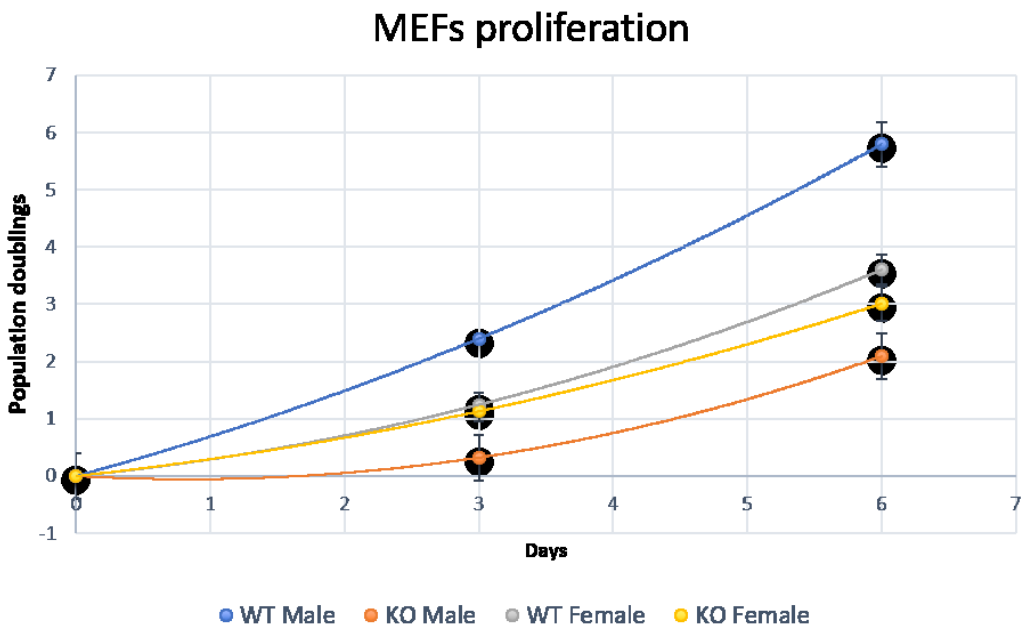

Fig 4.2.1. Growth curve of male and female HP1γ WT and HP1γ KO MEFs. *This graph is plotted by calculating the cell population doublings from day 0 to day 6. n≥3 (biological replicates) for each group. Error bars: SEM.*

Next, Propidium iodide (PI) staining followed by Florescence-activated cell costing (FACS) analysis was employed to investigate the cell-cycle changes between different genotypes in males. The result showed that in male MEFs, the proportion of cells at G1/0 stage of the cell

cycle was increased from 63.6% to 69.1% upon HP1γ KO; and the proportion of cells at S and G2/M stages was decreased from 21.6% and 19.8% to 11.6% and 10% respectively (Fig 4.2.2). A similar trend of cell population shift was seen in female MEFs, where the cell population in G1 phase was increased by approximately 10% (60.9%-70.1%) and decreased in S and G2/M phase by 6.77% and 3.02% respectively (Fig 4.2.2). Moreover, the same cell population shift was observed in female MEFs in Lakshimi Cadavieco's result (MSc student, 2015) (Fig S8), which indicates that a higher proportion of MEFs were arrested at G1 phase in both HP1γ deficient male and female cells compared with WT. This suggests that this cell-cycle phenotype is not sexual dimorphic but occurs in both males and females following HP1γ KO.

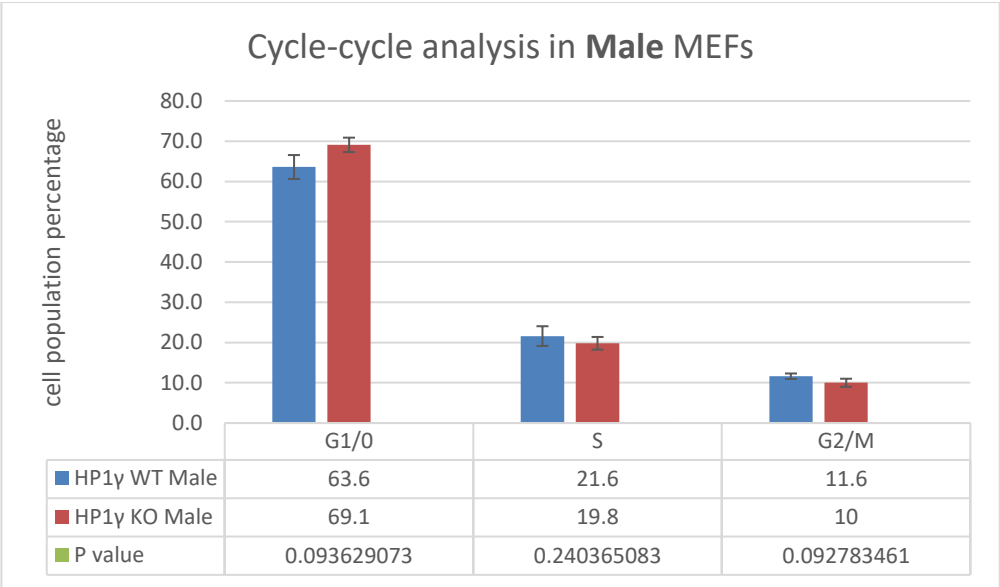

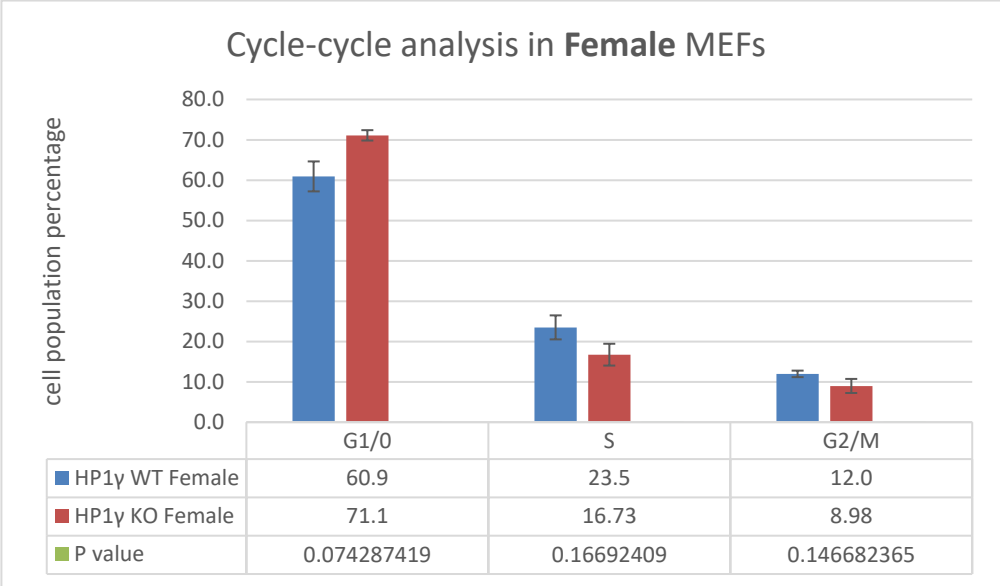

Fig 4.2.2. Bar chart showing the cell-cycle analysis in MEFs in Males and Females. *It showed the proportion of cells in each stage of cell cycle for HP1γ WT Male(n=3), Female(n=4) and HP1γ KO Male(n=3), Female(n=3). Three or four biological replicates gave the SEM, which is represented by the error bar. P values were calculated using student T test and showing at the bottom in green in each table. This data was produced together with Cristina Zhi (MSc thesis, 2016).*

Interestingly, the Gene Set Enrichment Analysis (GSEA) mentioned above also suggested that there were many more genes found to be dysregulated in male MEFs than in female MEFs in response to the HP1γ KO (Law *et al*., 2019). Among the 176 genes with sexually dimorphic expression identified by RNA-seq in WT cells, a key cell cycle inhibitor, *Cdkn2a*, was

identified, the expression of which was upregulated in HP1γ deficient male MEFs, but not in female MEFs. This gene might be implicated in the sexually dimorphic cell-cycle and cell-proliferation response to HP1γ deficiency. Therefore, the mechanism underlying the sex-difference in proliferation is amenable to further investigation given that *Cdkn2a* was found to be differentially expressed between the sexes in a HP1-dependent manner.

4.3 Different proteins bind to HP1γ in male and female MEFs as revealed by proteomic analysis

Recently, we have obtained HP1γ immunoprecipitated (IP) protein samples in both sexes for mass spectrometry (MS) analysis (collaboration with Axel Imhof, Munich) to search for sex-specific HP1γ binding proteins. Such proteins might be expected to target HP1γ to different regions of the genome in males and females leading to the sex-dimorphic effect of HP1γ in regulating autosomal gene expression. A list of the proteins found in each sex group is shown in Fig 4.3.1. The presence of CBX3 (HP1γ) in both sexes (red) indicates that the co-immunoprecipitation of HP1γ worked (Fig 4.3.1). There is another important well-known protein identified in both sexes, Transcription intermediary factor 1-beta (also called KAP1 (KRAB-associated protein-1); encoded by Tripartite motif-containing 28 (TRIM28) gene)), which interacts with KRAB-zinc finger proteins (KRAB-ZFPs) and targets HP1 to the inactive chromatin to repress gene transcription (Imbeault *et al*., 2017). Therefore, its presence in both sexes also indicated that the HP1γ Co-IP was effective (Fig 4.3.1 green). Additional approaches for checking the protein enrichment following IP are shown in Fig S5 and S6. Clearly, the HP1γ Co-IP in male appeared to work better and gave us higher protein enrichment (more proteins) (75 male only proteins) than female (23 female only proteins), although this might reflect a biological difference. By comparing male-only and female-only proteins, the binding of HP1γ to different groups of proteins found in male and female seems not differ much in terms of cellular functions. This could be solely due to the limitation of this experiment in this case i.e. quantity and quality of starting material.

Male only Proteins

Protein names
Sodium/potassium-transporting ATPase subunit alpha-2
40S ribosomal protein SA
Surfeit locus protein 4
Cytochrome c oxidase subunit 5A, mitochondrial
Catenin beta-1; Catenin beta; Armadillo segment polarity protein
60S ribosomal protein L36a
Translational activator GCN1
FERM, RhoGEF and pleckstrin domain-containing protein 1
Nucleolar protein 56
Heterogeneous nuclear ribonucleoprotein K
Coatomer subunit beta
Stress-70 protein, mitochondrial
Dolichyl-diphosphooligosaccharide--protein glycosyltransferase 48 kDa subunit
Barrier-to-autointegration factor; Barrier-to-autointegration factor, N-terminally processed
Allograft inflammatory factor 1
Serine/arginine-rich splicing factor 10
Ig kappa chain V-I region Ka
Glyceraldehyde-3-phosphate dehydrogenase
Sodium/potassium-transporting ATPase subunit alpha-1; Sodium/potassium-transporting ATPase subunit alpha-3
Protein S100-A10
Integrin beta-1; Integrin beta-1-A
60S ribosomal protein L5
40S ribosomal protein S30
Histone H2B type 1-F/J/Histone H2B type 1-L; Histone H2B type 1-P; Histone H2B type 1-K; Histone H2B; Histone H2B type 3-A; Histone H2B type 3-B; Histone H2B type 1-A
40S ribosomal protein S14
Hematopoietic lineage cell-specific protein
60S ribosomal protein L9
60S ribosomal protein L35
60S ribosomal protein L17
60S ribosomal protein L13a; Putative 60S ribosomal protein L13a protein RPL13AP3
rRNA 2-O-methyltransferase fibrillarin
Coatomer subunit beta
Talin-1
Dynamin
V-type proton ATPase catalytic subunit A
60S ribosomal protein L22
60S ribosomal protein L36

Ran GTPase-activating protein 1
40S ribosomal protein S5;40S ribosomal protein S5, N-terminally processed;40S ribosomal protein S5-1;40S ribosomal protein S5-2;40S ribosomal protein S5;40S ribosomal protein S5a
60S ribosomal protein L29
Translocon-associated protein subunit delta
Coatomer subunit gamma-1
Coatomer subunit alpha; Xenin; Proxenin
40S ribosomal protein S29
40S ribosomal protein S25
40S ribosomal protein S28;40S ribosomal protein S28-2
60S ribosomal protein L11
Transformer-2 protein homolog beta
Mitochondrial fission 1 protein
DNA topoisomerase 2-beta; DNA topoisomerase 2
FACT complex subunit SSRP1
KH domain-containing, RNA-binding, signal transduction-associated protein 1
Calponin-1
Calponin-2
Neuroblast differentiation-associated protein AHNAK
Inverted formin-2
Serine/arginine-rich splicing factor 7
Nucleolar RNA helicase 2
Coiled-coil domain-containing protein 102A
Nucleolar protein 58
Malectin; Malectin-B; Malectin-A
Probable ATP-dependent RNA helicase DDX5
Protein phosphatase 1 regulatory subunit 12A
NADH dehydrogenase [ubiquinone] 1 alpha subcomplex subunit 12
60S ribosomal protein L10a
EH domain-containing protein 2
Sphingosine-1-phosphate lyase 1
Leucine zipper protein 1
Keratin, type II cuticular Hb2
Reticulon-4
NADH-cytochrome b5 reductase 3; NADH-cytochrome b5 reductase 3 membrane-bound form; NADH-cytochrome b5 reductase 3 soluble form
Activity-dependent neuroprotector homeobox protein
Core histone macro-H2A.1

Female only Proteins

Protein names
Putative elongation factor 1-alpha-like 3; Elongation factor 1-alpha 1; Elongation factor 1-alpha, somatic form; Elongation factor 1-alpha 2
Heat shock cognate 71 kDa protein
ATP synthase subunit alpha, mitochondrial
40S ribosomal protein S9
Polymerase I and transcript release factor
Prelamin-A/C; Lamin-A/C
Fibronectin; Anastellin
Clathrin heavy chain 1
60S ribosomal protein L7a
60S ribosomal protein L7
Histone H1.2
Histone H2A type 1-D
60S ribosomal protein L13
Histone H1.1
Histone H1.3
60S ribosomal protein L6
High mobility group protein HMGI-C
14-3-3 protein gamma;14-3-3 protein gamma, N-terminally processed;14-3-3 protein gamma-A;14-3-3 protein gamma-1;14-3-3 protein gamma-B
Ubiquitin-40S ribosomal protein S27a; Ubiquitin;40S ribosomal protein S27a; Ubiquitin-60S ribosomal protein L40; Ubiquitin;60S ribosomal protein L40; Polyubiquitin;Ubiquitin;Polyubiquitin-B;Ubiquitin;Polyubiquitin-C;Ubiquitin;Polyubiquitin-C;Ubiquitin;Ubiquitin-related 1;Ubiquitin-related 2;Polyubiquitin-C;Ubiquitin;Ubiquitin-related
Guanine nucleotide-binding protein subunit beta-2-like 1; Guanine nucleotide-binding protein subunit beta-2-like 1, N-terminally processed
Enhancer of rudimentary homolog
Elongation factor 1-gamma
Tropomyosin alpha-4 chain
Cytoskeleton-associated protein 4
Actin-related protein 2/3 complex subunit 1B

Proteins in **both** sexes

Proteins names
60S ribosomal protein L19
60S ribosomal protein L15
Transcription intermediary factor 1-beta
Histone H2A.V; Histone H2A.Z; Histone H2A.v
40S ribosomal protein S4;40S ribosomal protein S4, X isoform;40S ribosomal protein S4, Y isoform 1
Histone H2A type 2-A; Histone H2A type 2-C; Histone H2A type 2-B
Chromobox protein homolog 3
ADP/ATP translocase 1; ADP/ATP translocase 3; ADP/ATP translocase 3, N-terminally processed
60S ribosomal protein L18a
40S ribosomal protein S6

Fig 4.3.1. Tables illustrating a list of proteins found associated with HP1γ by Mass Spectrometry (MS) in each group. *There are 3 groups of proteins: Male only proteins, Female only proteins and proteins in both sexes. CBX3 protein in red in both sexes indicates the co-immunoprecipitation (Co-IP) of HP1γ worked. Proteins highlighted in green are splicing factors identified only in male HP1γ pull-down samples.*

The comparison on HP1γ protein binding profile between female and male by mass spectrometry is shown in Fig 4.3.2. Proteins only identified in males (male only) are identified indicated by blue dots and they are lying on the X-axis as the normalization was done to male itself (Fig 4.3.2 blue). Whereas proteins only identified in females (female only) are shown as pink dots and they are spread along Y-axis with higher enrichment on the top (Fig 4.3.2 pink). Proteins identified in both sexes are showing as green dots with different enrichment following HP1γ IP (Fig 4.3.2 green). The numbers on each axis were calculated by the intensity ratio between the HP1γ IP and the control (IgG) IP (Log2 transformed and subtracted). As the male IP worked better compared to females, we normalized the signal of female only proteins and proteins in both sexes to males, which gave us an idea of the different proteins associated with HP1γ in each sex.

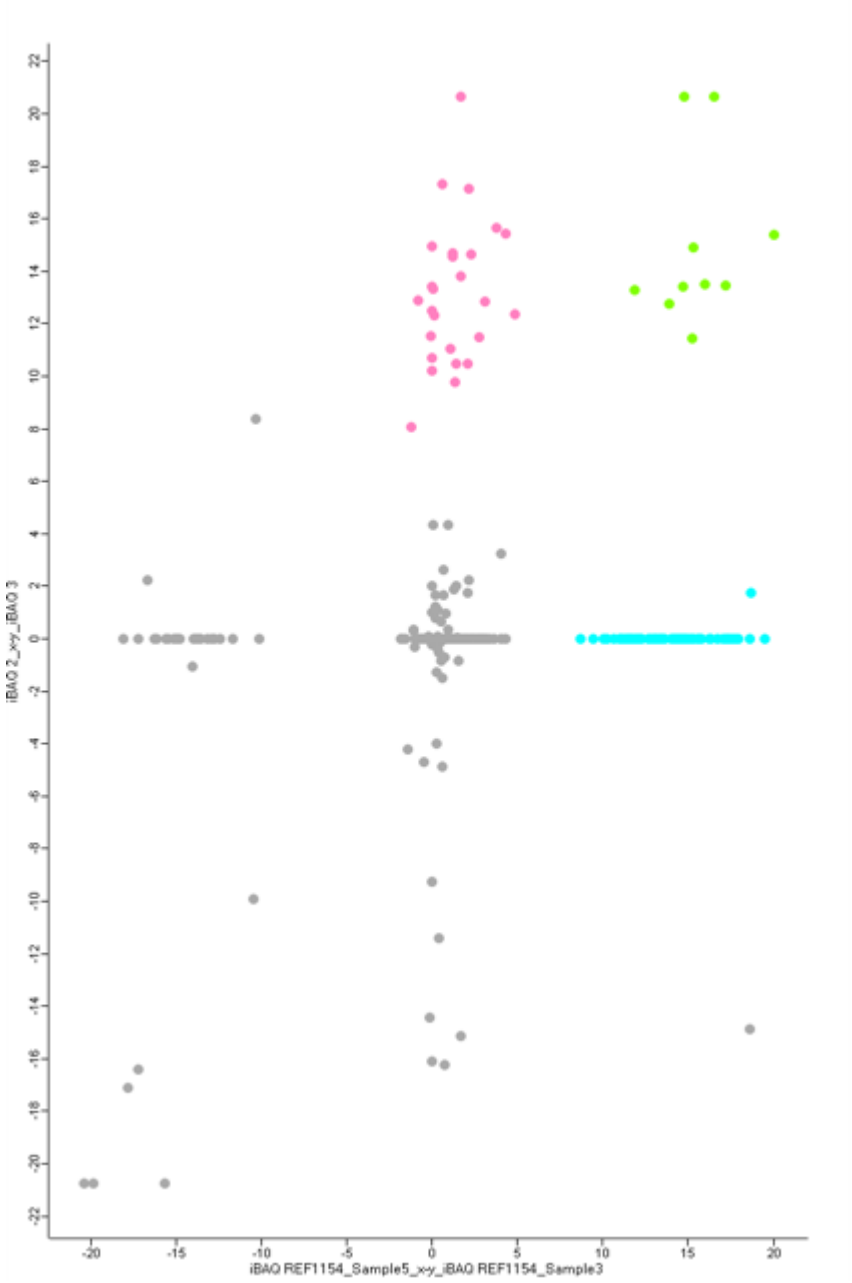

Fig 4.3.2. Scatter Plot of comparison on HP1γ protein binding profiles between female and male by MS. The intensity ratio between the HP1γ IP and the control IP (Log2 transformed and subtracted) from male and female samples is illustrated on X-axis and Y-axis respectively. *Pink – female only proteins. Blue – male only proteins. Green – proteins in both sexes. Software for analyzing is adapted with permission from "Andromeda: A Peptide Search Engine Integrated into the Max Quant Environment" Jurgen Cox et al., (Cox et al., 2011) (Axel Imhof, Munich).*

4.4 HP1γ is involved in different protein networks

Protein networks identified by clustering proteins into groups with feature similarities indicated that HP1γ might play a role in the context of chromatin, RNA splicing, coatomer and ribosomes (Fig 4.3.3). According to the string database (**http://string-db.org),** every node equals a protein and the lines between the nodes (edges) reflect known interactions from the literature (can be physical interactions or genetic interactions or simply based on text co-occurrence, hence the different colours of the edges).

HP1γ is a well-known pericentric heterochromatin (PCH) structural protein that regulates gene silencing and to date, there is growing evidence suggesting that the role for HP1 proteins in epigenome stability goes beyond heterochromatin structure as they have been found in euchromatin (Minc *et al*., 2000) and play a role in gene expression, DNA replication, DNA repair, cell cycle, cell differentiation, and development (Maison and Almouzni, 2004). Therefore, it is not surprising to see the association between HP1γ and a number of proteins identified here functioning in the context of chromatin such as histone proteins, Signal Recognition Particle protein and Signal Sequence Receptor protein, which are involved in recognising and targeting nascent proteins to their proper membrane localization (Akopian *et al*., 2013) (Fig 4.3.3).

4.4.1 HP1γ interacts with Coatomer proteins

There is another group of proteins that belong to the Coatomer family which also showed interaction with HP1γ. Coatomer is the coat protein of a soluble macromolecular Coat Protein Complex (COPs) that is involved in membrane traffic through the Golgi complex (Draper *et*

al., 2001). It contains seven non-identical subunits (α, β, β′, γ, δ, ε, and ζ) (Waters *et al*., 1991, Malhotra *et al*., 1989). Coatomer coats Golgi-derived vesicles moving in bi-directions, either toward the plasma membrane or returning to the endoplasmic reticulum (ER) (Draper *et al*., 2001). The association between HP1γ and Coatomer therefore might indicate, either that HP1γ exerts a real functioning role in these cytoplasmic processes (e.g. translation, membrane transport) or might just be due to the fact that HP1γ was pulled down during the co-immunoprecipitation (Co-IP) process while being processed in the cytoplasm. Validation experiments to solve this problem could be that either we purify the nucleus separately from cytoplasm and perform HP1γ IP followed by mass spectrometry analysis or we could do western blot and immunofluorescence (IF) to validate. Recently, an HP1 isoform localization study in *Drosophila* reported that HP1b and HP1c, but not HP1a, are targeted to both the nucleus and cytoplasm via the C-terminal extension region (CTE) (Lee *et al*., 2019). This finding suggests that that HP1γ in our case might play a role in the cytoplasm. Of note, mass spectrometry is not strictly quantitative in this case but can be used to identify HP1γ partner proteins in males and females. To date, there appears to be no evidence in the literature showing sex differences in coatomer or the link between HP1 and coatomer.

4.4.2 HP1γ interacts with ribosomal proteins

The observations here showed that different ribosomal proteins were pulled down together with HP1γ following HP1γ Co-IP (Fig 4.3.3). Male MEFs have more ribosome proteins (18) identified than females (5) (Fig 4.3.1). To date, the sexually dimorphic expression of genes encoding ribosomal proteins L17 and L37 (RPL 17 and RPL37) in male and female zebras finches has been reported related to the sex difference in zebra finch song system (Tang and Wade, 2010). In their study, they showed more telecenphalon cell nuclei expressing RPL 17

and RPL37 in males compared to females, and the sex differences increased as animals matured. However, the mechanism that underlies this differential expression in male and female was not fully explored. Interestingly, this is consistent with our observation that we only found ribosomal protein RPL17 in the male samples as well (Fig 4.3.1 highlighted in yellow), which indicates that the sexual dimorphic regulation by HP1γ might involve the direct HP1γ and ribosomal protein interaction although the mechanism is unclear.

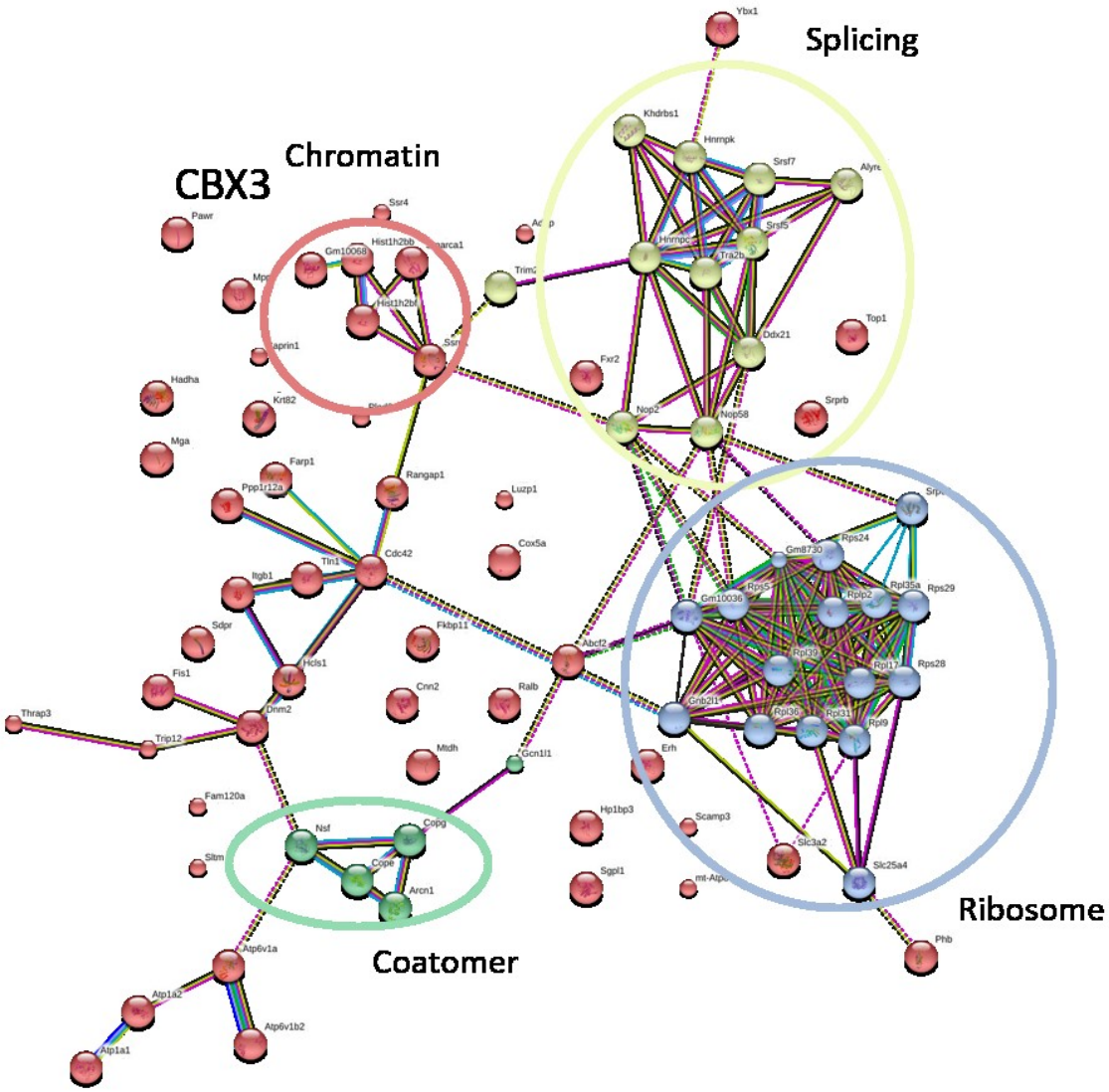

Fig 4.3.3. String network of proteins that were only identified in HP1γ IP but not in IgG IP (http://string-db.org). *Lines that connect adjacent nodes (proteins) indicate different interaction between them. According to the String database (http://version10.string-db.org/help/getting_started/#a-note-on-the-network-drawing-algorithm), Red line - indicates the presence of fusion evidence; Green line - neighbourhood evidence; Blue line - cooccurrence evidence; Purple line - experimental evidence; Yellow line – text mining evidence; Light blue line - database evidence; Black line – co-expression evidence. Network after K means clustering into 4 clusters (Chromatin, Splicing, Coatomer and Ribosome) (Axel Imhof, Munich).*

4.4.3 HP1γ interacts with proteins involved in RNA splicing

There are multi-level splicing cascades that regulate sex determination and sex-specific development in *Drosophila melanogaster* (Telonis-Scott *et al*., 2009, Schutt and Nothiger, 2000, Baker *et al*., 1989, Forch and Valcarcel, 2003). The sex-determination gene, *Sex-lethal* (*Sxl*) is functionally expressed only in female flies and its expression is regulated by alternative RNA splicing which results in either the inclusion or exclusion of the third exon containing the translation stop codon (Sakamoto *et al*., 1992). In a more recent study, 417 multi-transcript genes that have been shown to be sex-specific in *Drosophila melanogaster* were examined by using exon-specific microarrays (Telonis-Scott *et al*., 2009). In this study, they showed that most of these loci possessed sex-biased splicing with 135 genes showing different alternative transcript usage in males compared to females (Telonis-Scott *et al*., 2009). This sex-biased splicing was seen in both gonadal tissue as well as somatic tissue, head. One underlying mechanism for HP1γ in regulating RNA splicing in *Drosophila* suggested that H3K9me3 and HP1 proteins appeared to recruit Heterogeneous Nuclear Ribonucleoproteins (hnRNPs) to form a chromatin-splicing adaptor system (Piacentini *et al*., 2009).

To date, there has been strong evidence showing sex difference in RNA splicing in adult human brain and during sex determination in mice (Planells *et al*., 2019, Trabzuni *et al*., 2013). In

mammalian systems, HP1γ has also been implicated in regulating alternative RNA splicing in a way that facilitates the inclusion of the alternative exons by slowing down RNA polymerase II elongation (Saint-Andre *et al*., 2011). In their study, it was suggested that HP1γ controls the rate of transcriptional elongation which favours different alternative splicing events. Although we have shown sex-dimorphic effects of HP1γ in transcriptional regulation (Law *et al*., 2019), nothing was known about any sex-dimorphic effect of HP1γ in RNA splicing yet. In this section, I examined whether the sex-dimorphic transcription difference previously identified resulted in an alternative splicing difference between the sexes or *vice versa*.

Previous mass spectrometry analysis done in a Hela cell line identified some alternative splicing factors, as the interaction-partners of methylated H3 peptides which also pulled-down HP1 proteins (Loomis *et al*., 2009). My mass spectrometry results also revealed proteins that are involved in RNA processing (SRp20, hnRNPs and Helicases etc.) in HP1γ pull-down fractions (Fig 4.3.1 and 4.3.3). Taken together, it is reasonable to speculate that HP1γ might promote optimal co-transcriptional RNA processing through recruitment of the splicing machinery and further investigations on HP1γ in regulating RNA splicing will be discussed below. Importantly, the splicing factors were only pulled-down in the IP performed on male cells (Fig 4.3.1 highlighted in green) and were not pulled-down in the protein samples from the female cells.

In this thesis, I investigated individual alternative splicing (AS) events (Fig 4.3.4) rather than transcript abundance, as the accurate quantification of the expression of individual transcripts is challenging with short or low abundance transcripts and genes with complex structures (Zhang *et al*., 2017a, Kanitz *et al*., 2015). This work, which was done with the help of the bioinformatician at MRC LMS (Sanjay Khadayate), identified groups of genes that were

alternatively spliced in a sexually dimorphic manner in E13.5 MEFs. Moreover, we also investigated the effect of HP1γ deficiency on both sexually dimorphically spliced genes and on all genes in male and female. This would address the hypothesis that HP1γ is important for sexually dimorphic alternative splicing.

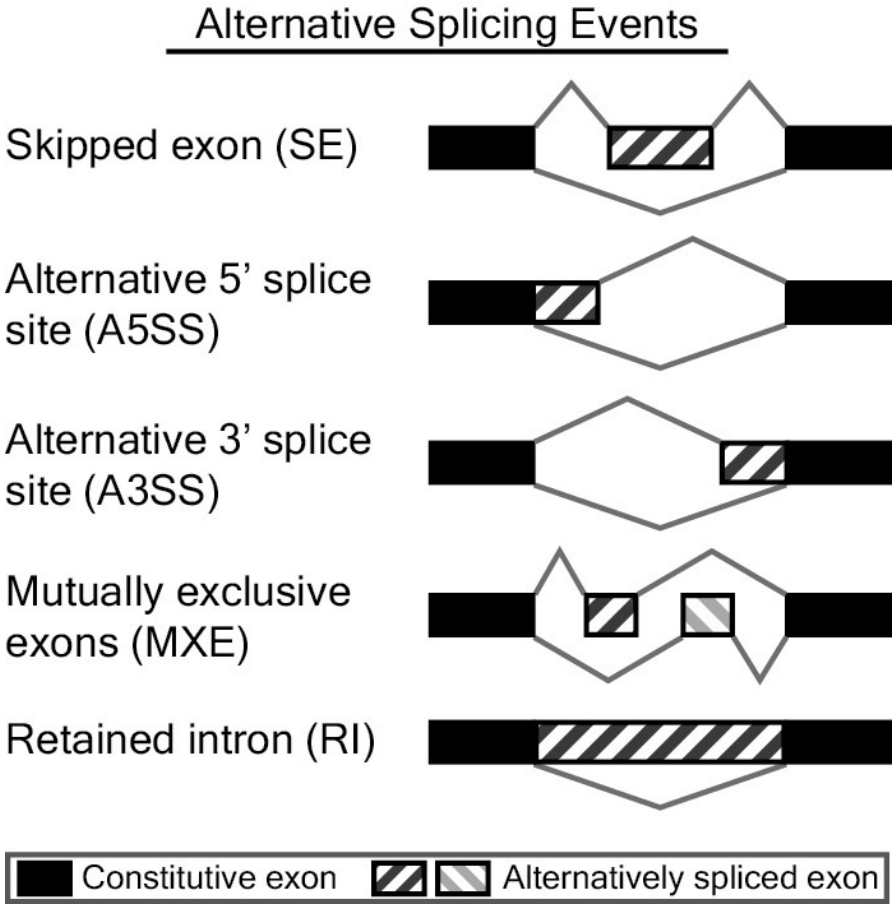

Fig 4.3.4. Schematic diagram of the exclusion and inclusion isoforms for the five models of Alternatve Splicing events that were examined in this thesis. *SE: skipped exon/exon inclusion; A3SS/A5SS: alternative 3'/5' splice site; MEX: mutually exclusive exons; RI: retained intron. White boxes, flanking constitutive exons; black boxes, alternative spliced exons/regions; solid lines, splice junctions supporting the inclusion isoform; This figure is adpted with permission from "Transcriptome analysis of alternative splicing events regulated by SRSF10 reveals position-dependent splicing modulation" Zhou X et al., (Zhou et al., 2014)*

To investigate if there is any correlation between sex dimorphic gene expression and sex dimorphic splicing, I made a comparison between sex dimorphic gene expression and sex dimorphic splicing in males and females (Fig 4.3.5). In terms of gene expression, there is very little/no overlap between sex dimorphic splicing with the sex dimorphic gene expression result previously obtained (Law, 2019), which indicates that the sex difference in gene expression is not a result of difference in splicing and *vice versa*. Also, it has been suggested that HP1γ is regulating RNA splicing by facilitating the inclusion of the alternative exons by slowing down RNA polymerase II elongation (Saint-André *et al*., 2011). As previous RNA-seq. data revealed that HP1γ was essential for sexually dimorphic gene expression (Law *et al*., 2019), we wanted to find out if HP1γ is also regulating RNA splicing differently in males and females. In order to further investigate the role of HP1γ in regulating RNA splicing in our models, the overlap between differentially spliced genes upon HP1γ KO in each sex were compared with the sex dimorphically spliced genes in HP1γ WT (Fig 4.3.6). For Skipped Exon (SE) and Retained Intron (RI) events, there are much more genes that are affected by HP1γ KO in males compared with that in females (Fig 4.3.6). A table containing a list of genes of which, the SE and RI events are sensitive to HP1γ KO in males and females are in Fig S14. Therefore, it would suggest that in general, males are more sensitive to HP1γ KO than females with respect to alternative splicing. More interestingly, we see a reduction in the number of sex dimorphically spliced genes when comparing male HP1γ KO to female HP1γ WT and an increase in the number of sex dimorphically spliced genes when comparing female HP1γ KO to male HP1γ WT in SE and RI events (Fig 4.3.6, 4.3.7 and 4.3.8). A table containing the genes whose sex dimorphic splicing was equalized by HP1γ KO in males and genes that acquired difference between the sexes in females with respect to SE and RI events upon HP1γ KO are shown in Fig S15. This indicates that HP1γ exerts opposite effects in regulating alternative splicing in males and females. This also suggests a potential role of HP1γ KO in ameliorating the sex

difference in alternative splicing. This result is consistent with the mass spec data following HP1γ pull-down which identified the splicing factors in the male samples but not the female (Fig 4.3.1 – splicing factors highlighted in green).

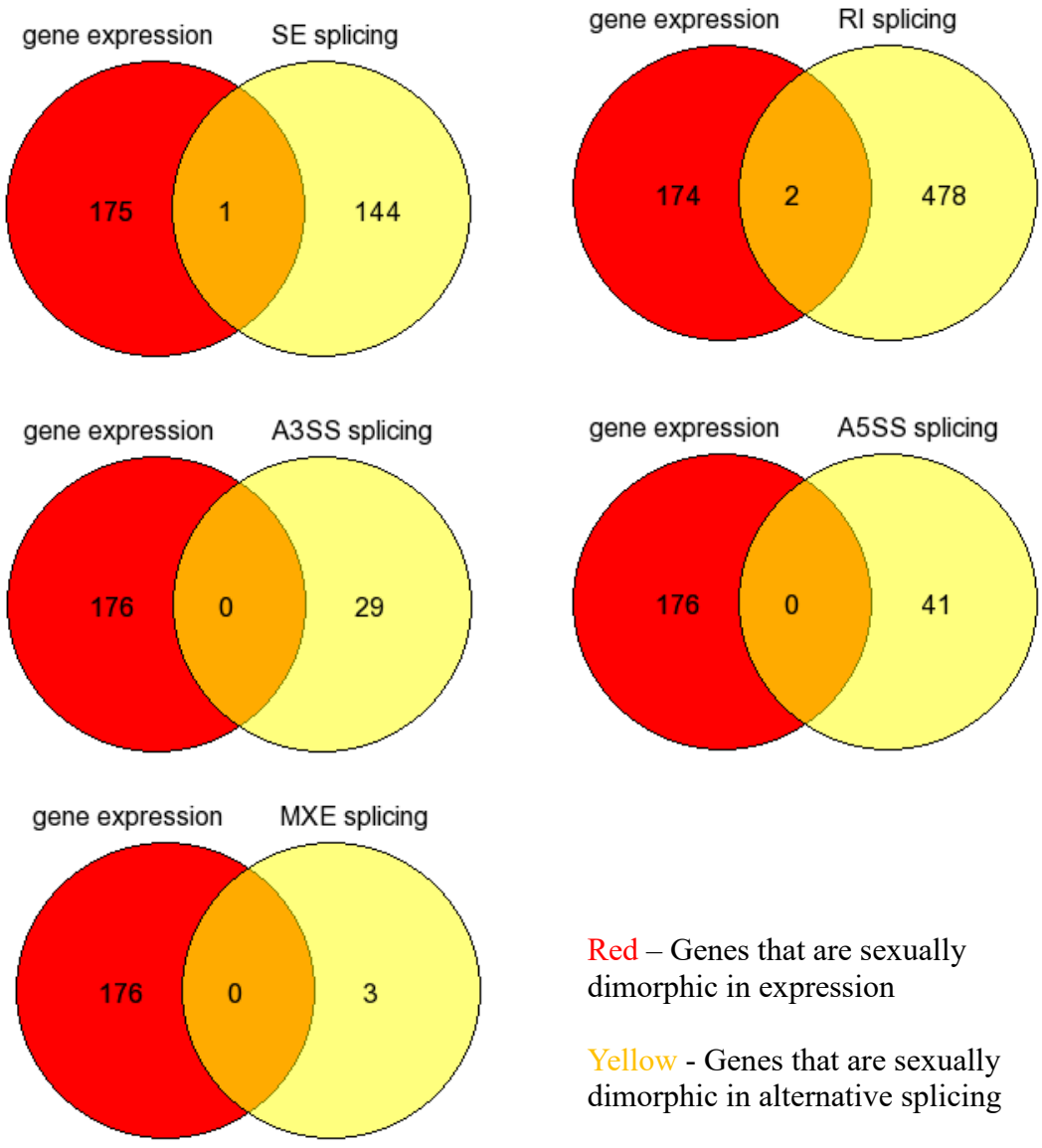

Fig 4.3.5. Schematic diagram showing little overlap between genes that are sexually dimorphic in expression and genes that are sexually dimorphic in alternative splicing in male and female MEFs for the five models of AS events that were investigated in this thesis. *The analysis was done with help of Sanjay Khadayate (MRC London Institute of Medical Sciences, Imperial College London) using the statistical method multivariate analysis of transcript splicing (MATS) for detecting differential AS events from RNA-Seq data. Genes with significantly differential splicing were detected at a false-discovery rate (FDR) cut-off of 0.05. Sex dimorphic in gene expression (yellow) on the right-hand side in each event include female higher genes and male higher genes identified by RNA-seq (Fig S11) (Shen et al., 2012, Law et al., 2019).*

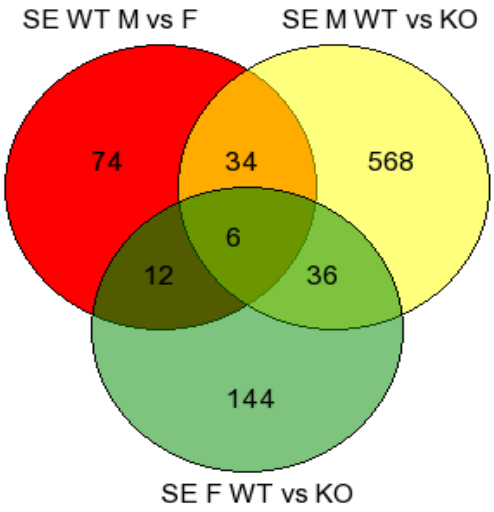

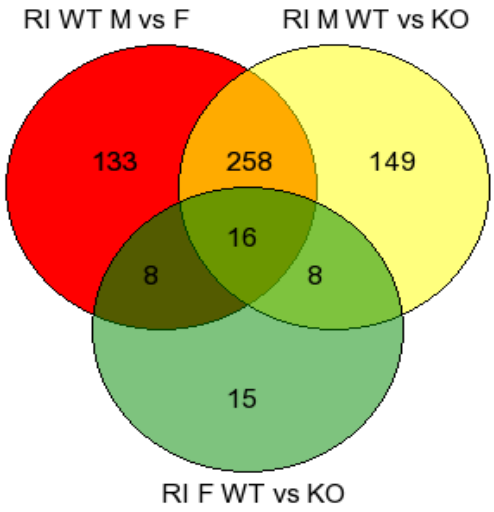

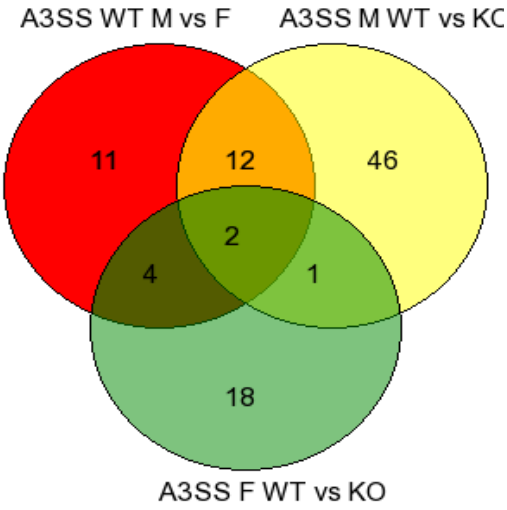

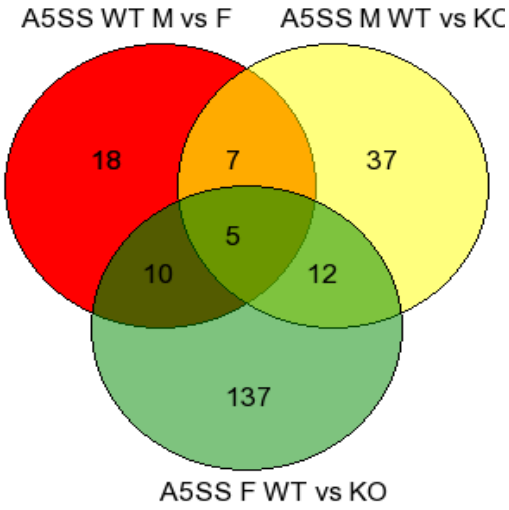

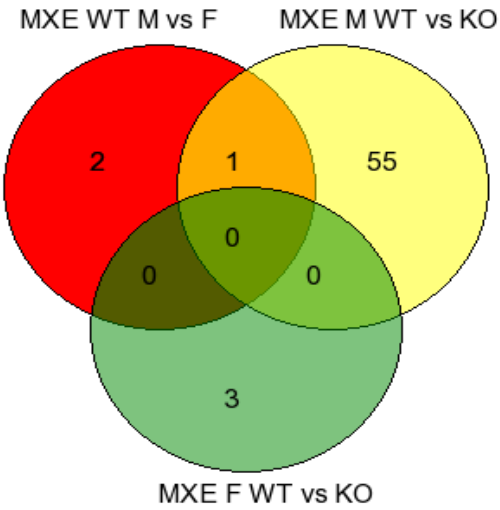

Red – Genes that are sexually dimorphic in alternative splicing

Yellow - Genes that are differentially spliced upon HP1γ KO in Males

Green - Genes that are differentially spliced upon HP1γ KO in Females

Fig 4.3.6. Schematic diagram showing the overlap between genes that are sexually dimorphic in alternative splicing, genes that are differentially spliced upon HP1γ KO in males and genes that are differentially spliced upon HP1γ KO in females.

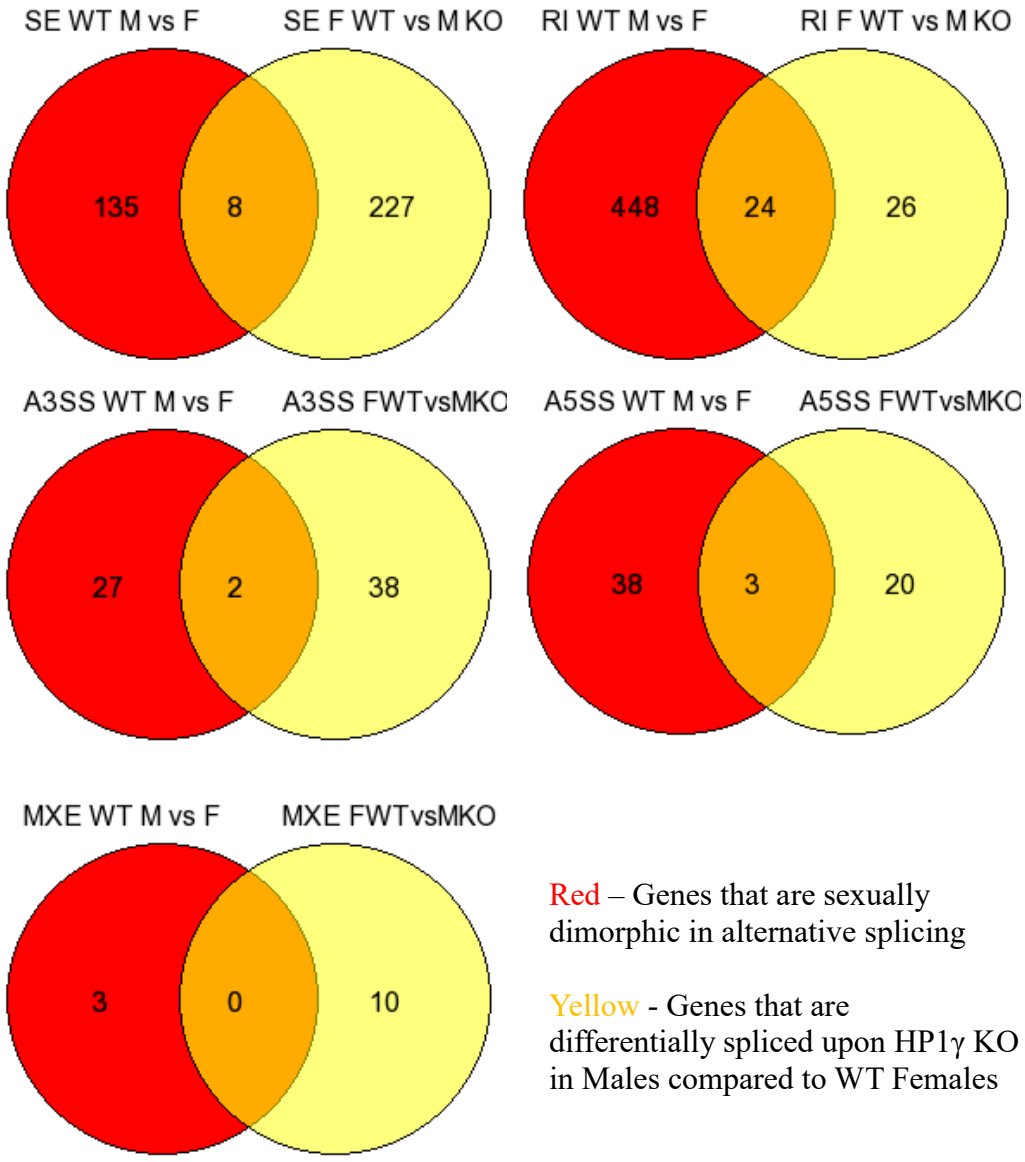

Fig 4.3.7. Schematic diagram showing the overlap between genes that are sexually dimorphic in alternative splicing and genes that are differentially spliced upon HP1γ KO in males compared to WT females.

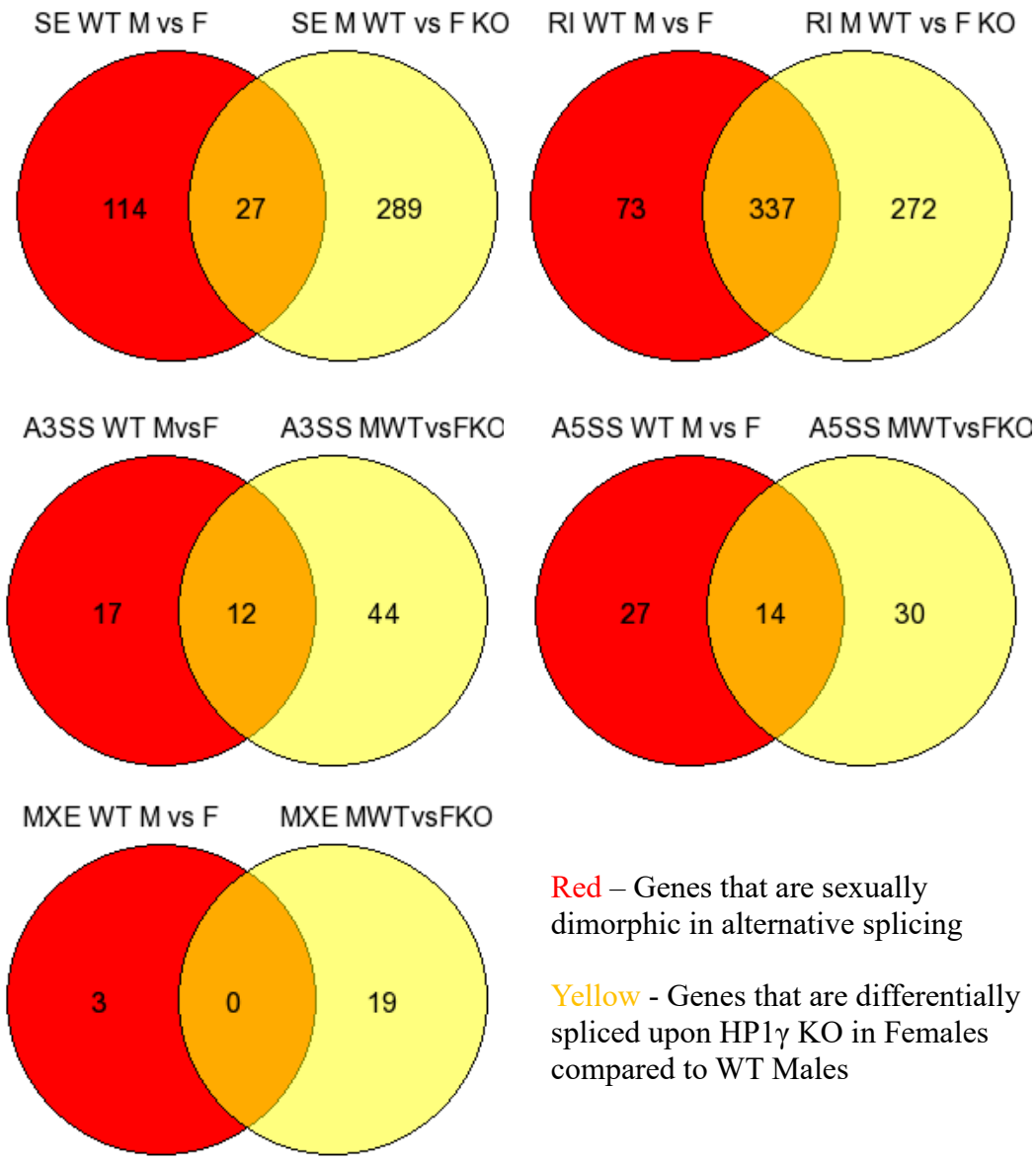

Fig 4.3.8. Schematic diagram showing the overlap between genes that are sexually dimorphic in alternative splicing and genes that are differentially spliced upon HP1γ KO in females compared to WT males.

In conclusion, HP1γ seems to play an important role in regulating sex dimorphic alternative splicing in males although the underlying mechanism is not yet known, the effect seems to be direct given that HP1γ appears to associate with the splicing factors in males but not females (see above). See section 4.7 for future work.

4.5 Inactive X chromosome – a 'sink' for HP1γ?

4.5.1 Background

Recently the importance of HP1γ in regulating sex differences has been demonstrated in our lab. How HP1γ contributes to the sexually dimorphic regulation of these genes remains unclear, however, there are several possibilities that can be tested relating to the X-chromosome 'sink' hypothesis and how HP1γ might be specifically targeted in a sex-specific manner to autosomal genes.

The inequality in genomic dose of X genes leads to sex differences in traits via at least three possible mechanisms: escape from X-inactivation, X imprinting and epigenetic sinks (Arnold, 2012). Recently, a growing body of studies, by employing the selected mouse models with the same type of gonad but with one versus two copies of the X chromosome, showed that mice with one X chromosome were strikingly different from those with two X chromosomes without the effect of gonadal hormones (Arnold *et al*., 2016). Mammalian X chromosome inactivation is a process that effectively reduces sex difference in expression of the X chromosome genes to compensate for having two X chromosomes in females compared to the one X chromosome in males (Itoh *et al*., 2007). However, X inactivation is not 100% complete, it has been reported that the number of genes that escape inactivation, 'X escapees', is about 15% of the X chromosome genes in humans, and 3% in mice (Carrel *et al*., 1999, Berletch *et al*., 2010). An 'epigenetic sink' represents the presence of a large inactive and heterochromatic X chromosome in XX cells that may attract heterochromatin modifiers or factors away from other chromosomes (Wijchers and Festenstein, 2011). Such a sink might explain the sex dimorphic effects of HP1γ on autosomal gene expression. In a way, it provides a reservoir for those factors, which might result in a shift in the epigenetic status of the genome and gene expression (Arnold, 2012, Wijchers and Festenstein, 2011, Silkaitis and Lemos, 2014).

4.5.2 Results

The aim in this section was to investigate if the inactive X chromosome in females is acting as a heterochromatic 'sink' which sequesters HP1γ to H3K9me3 sites on the inactive X chromosome. Here, we employed immortalized MEFs derived from F1 mice in which there is non-random X-chromosome inactivation (collaboration with Neil Brockdorff) to see the difference in HP1γ enrichment on the inactive X chromosome by performing HP1γ ChIP-seq. In these immortalized MEFs, the inactive X chromosome can be identified by single nucleotide polymorphisms (see Methods 2.3.1.2). The HP1γ enrichment in MEFs (with known inactive X chromosome) is shown in Fig 4.4.1, where the red track on the top represents the RNA-sequencing data from the inactive chromosome X, followed by the published CBX3 (HP1γ) ChIP-sequencing data (Smallwood *et al*., 2012) (CBX3 IP – dark green; input – light green). The dark red and pink tracks at the bottom represents the HP1γ ChIP-sequencing results for HP1γ IP and input in immortalized MEFs respectively. By comparison, the overall pattern of HP1γ enrichment on the X chromosome is similar between the published CBX3 data in human (dark green) and HP1γ data in MEFs (dark red) if the background signal is subtracted (input lane – pink) (Fig 4.4.1). As mentioned in Smallwood *et al*.'s study, the genome-wide localization of CBX3 was enriched at genic regions, which is in strong correlation with gene activity across multiple cell types in human (Smallwood *et al*., 2012), the positive correlation between gene activity on the X chromosome and HP1γ enrichment has also been seen here (red – gene activity; dark red - HP1γ enrichment) (Fig 4.4.1). Next, we discriminated the active (Xa) and inactive X chromosomes (Xi) and compared the HP1γ enrichment on these 2 chromosomes. We found that HP1γ enrichment on the Xi chromosome (green track at bottom) was diminished compared to the Xa chromosome (blue track above) (Fig 4.4.2), which suggests that the Xi chromosome might not serve as a sink for the HP1γ protein. The known inactive X escapee gene, *Eif2s3x*, which expressed on both Xa and Xi chromosomes showed high level of

expression on both alleles (blue and green peaks) compared to X chromosome gene, *Zfx*, of which, the expressed was only available on the Xa chromosome (Fig 4.4.3). The inactive X escapee gene, *Eif2s3x* also has HP1γ enrichment on Xi chromosome as well and it also correlates to the expression level. Therefore, the Xi chromosome seems to sequester HP1γ to genes that express on Xi chromosome, in other words, genes that escaped the X chromosome inactivation.

To summarize, the HP1γ ChIP-seq result showed that HP1γ was enriched on the genic region of the *Msn* gene that is located on Xa chromosome and the level of enrichment correlated with its gene activity (Fig 4.4.1). However, when we looked at the Xi chromosome, where there is no *Msn* gene activity, the enrichment of HP1γ was diminished (Fig 4.4.2). Moreover, the inactive X-escapee gene, *Eif2s3x* (express on Xi chromosome) showed HP1γ enrichment on the Xi chromosome, which also correlated with its expression level (Fig 4.4.3). Therefore, the Xi chromosome seems not be the 'sink' for HP1γ but only to sequester HP1γ to genes that express on Xi chromosome, in other words, genes that escaped the X chromosome inactivation.

However, it is important to note that during this analysis repetitive DNA sequences have largely been excluded as they cannot be uniquely mapped. As these repeats might be acting to sequester HP1γ, the sink effect might therefore not be visible. Further work should repeat the analysis using paired-end sequencing which is more likely to lead to mappable reads as well as an analysis of X-chromosome specific repetitive sequences.

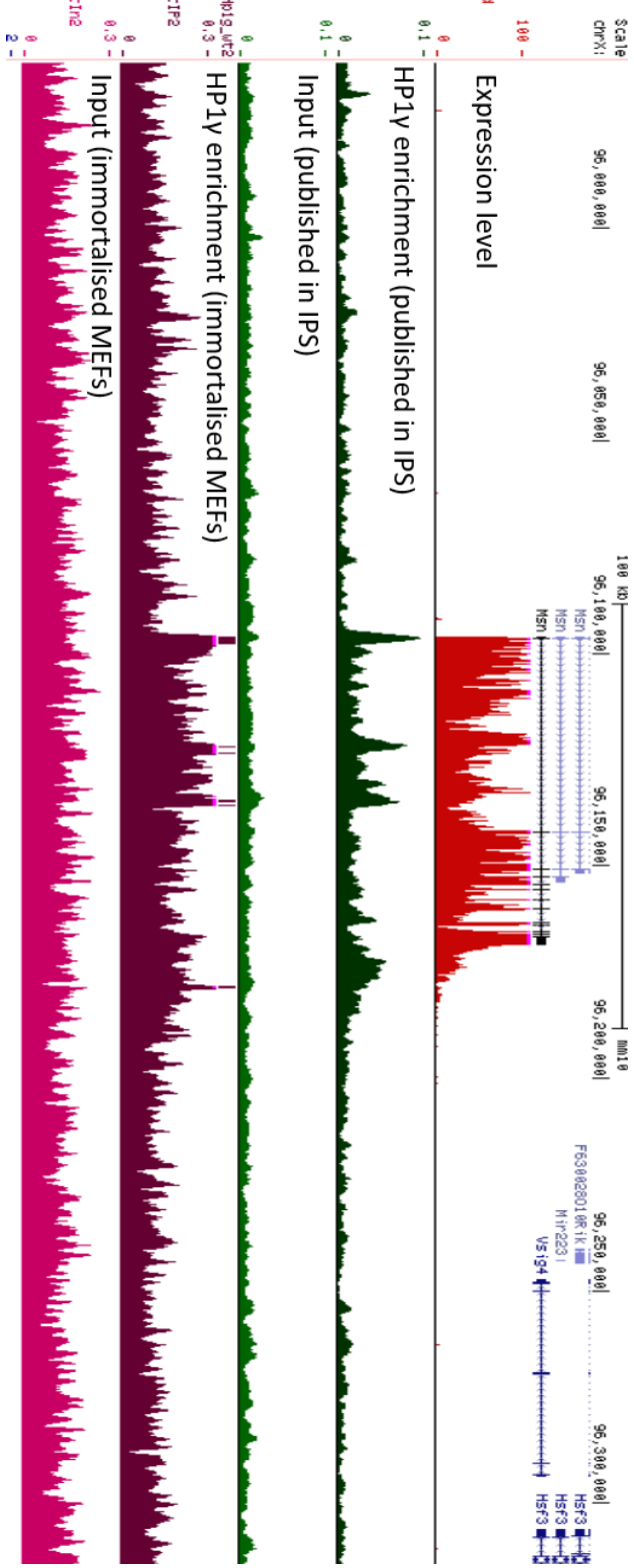

Fig 4.4.1. ChIP-seq profiles of HP1γ enrichment on Msn gene on Xa chromosome in IPS cells and immortalized MEFs. *Top track is showing the gene expression profile for Msn gene RNA-seq in WT MEFs. The following track in dark green is representing the CBX3 enrichment calculated as log2(IP/input) in IPS cells (Smallwood et al., 2012). Dark red track is the HP1γ enrichment calculated as log2(IP/input) in immortalized MEFs. Pink track is input.*

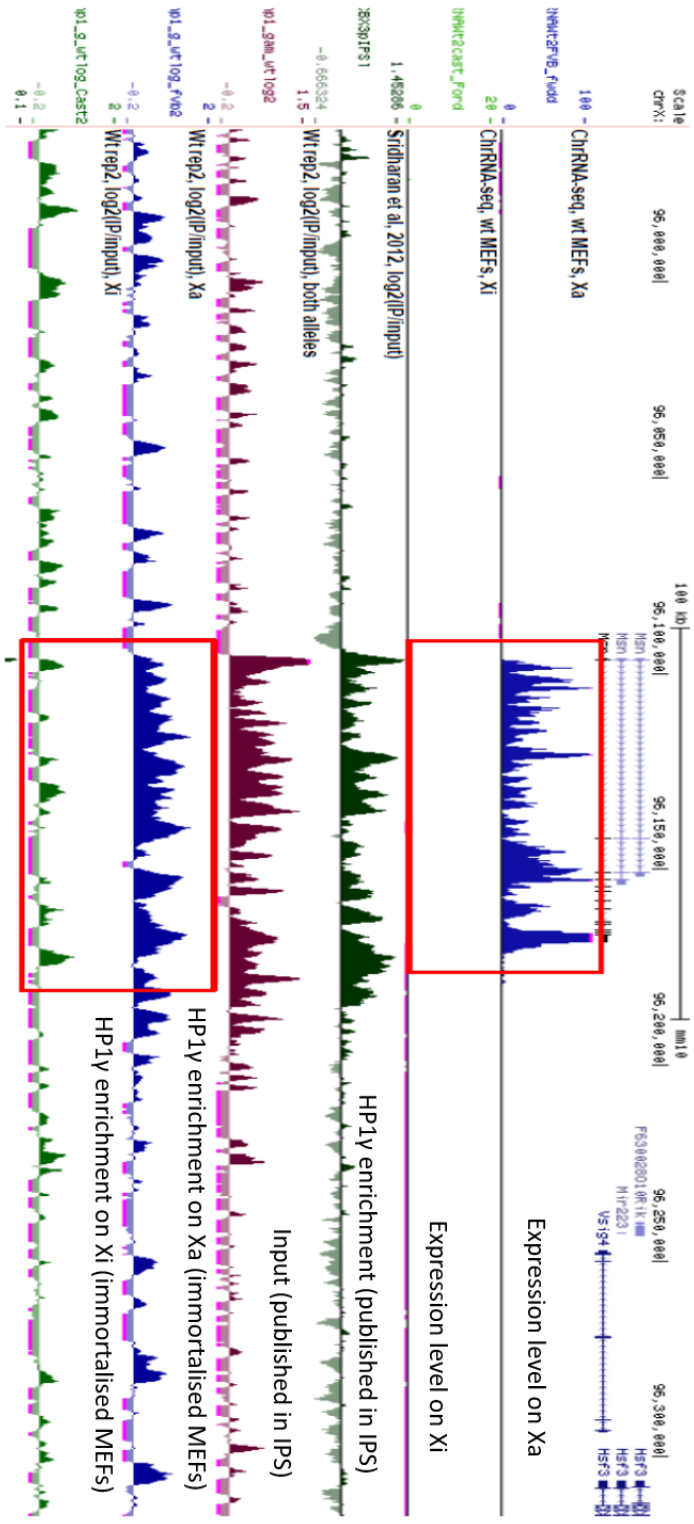

Fig 4.4.2. ChIP-seq profiles of HP1γ enrichment on Msn gene on both Xa and Xi chromosomes in IPS cells and immortalized MEFs. *Top 2 blue tracks are showing the gene expression profile for Msn gene on both Xa and Xi chromosome by RNA-seq in WT MEFs respectively. The following track in dark green is representing the CBX3 enrichment calculated as log2(IP/input) in iPS cells (Smallwood et al., 2012) and dark red track below is the HP1γ enrichment calculated as log2(IP/input) on both alleles in immortalized MEFs. Two separated HP1γ enrichment on active and inactive X chromosome are showing in the consecutive tracks down at the bottom.*

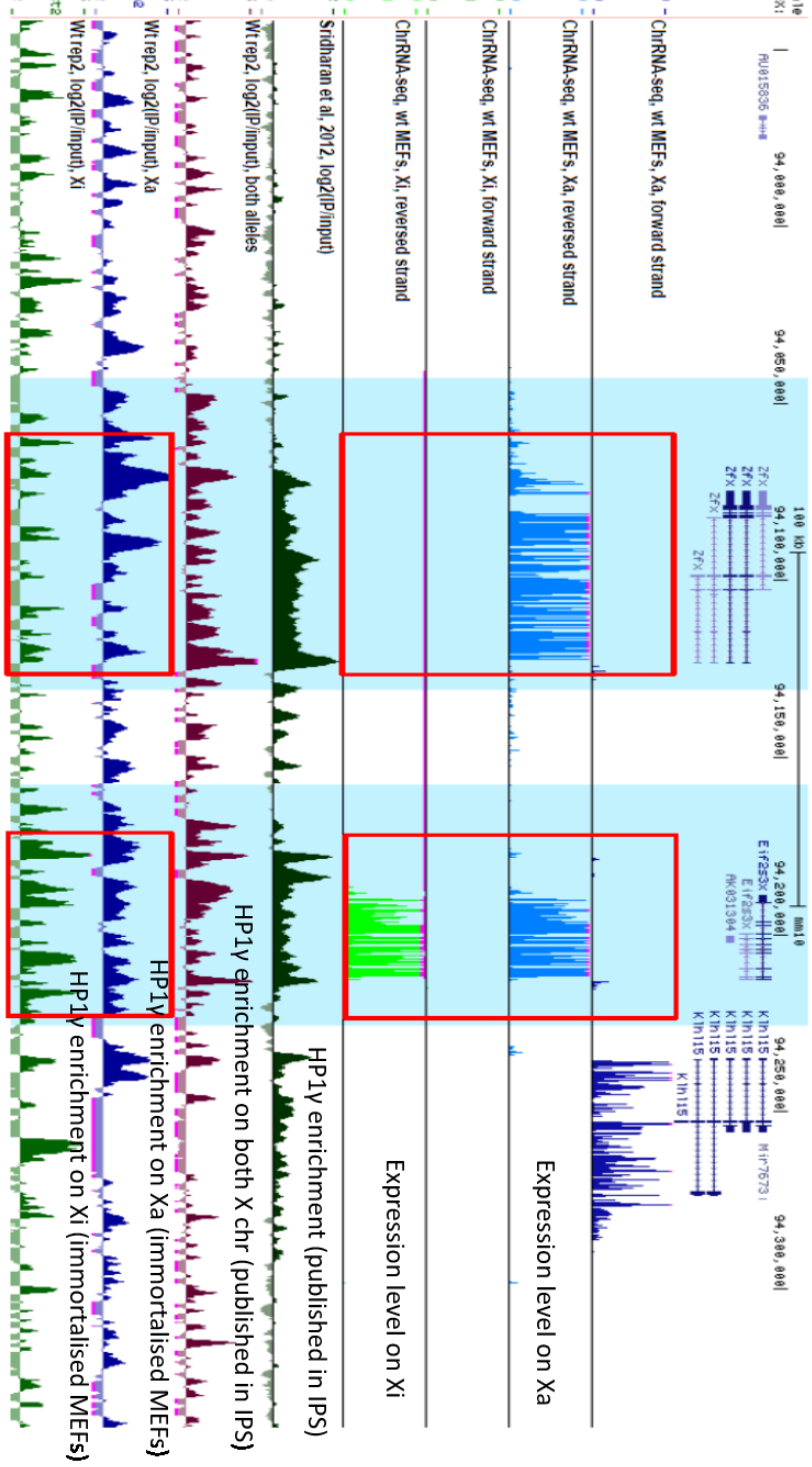

Fig 4.4.3. ChIP-seq profiles of HP1γ enrichment on Zfx and Eif2s3x genes in IPS cells and immortalized MEFs. *Top 2 red squares showing Zfx expresses on active X chromosome only but Eif2s3x expresses on both alleles. CBX3 and HP1γ enrichment calculated as log2(IP/input) in IPS cells (Smallwood et al., 2012) and immortalized MEFs are followed. Dark red lane represents CBX3 enrichment on both alleles while, HP1γ enrichment is illustrated in 2 constitutive lanes representing active and inactive X chromosome at the bottom.*

4.6 *Cdkn2a* is implicated in sexual dimorphic cell-cycle response to HP1γ KO

Among 176 sexual dimorphic genes, there is a key cell cycle regulator gene identified through RNA-seq analysis, *Cdkn2a* (cyclin dependent kinase inhibitor 2A), which may be implicated in the sexually dimorphic response to HP1γ deficiency shown here to affect cell cycle and cell proliferation. *Cdkn2a* is also known as the *INK4A/ARF* locus and is located on chromosome 4 in mice (Zhang *et al*., 1998). It encodes two alternatively spliced transcripts, p16(INK4A) and p14(ARF), which differ in their first exon (Al-Kaabi *et al*., 2014) (Fig 4.5). p16(INK4A) acts at the G1/S checkpoint by binding to two cyclin-dependent kinases, CDK4 and CDK6 (cell cycle regulator), thus preventing phosphorylation of the retinoblastoma protein Rb. This further inhibits the release of transcription factors (TFs) that induce S phase progression. Rb is capable of inducing an irreversible state of cellular senescence via repression of E2F target genes and alterations in chromatin structure (Baker *et al*., 2008). Deficiency in p16(INK4) protein leads to improper progression from the G1 to the S phase, allowing continuous uncontrolled cell proliferation (Goldstein *et al*., 2006) (Fig 4.5). In contrast, p14(ARF) stabilizes and activates the tumor suppressor gene p53 from ubiquitin-mediated degradation by MDM2. Active p53 induces the expression of p21, a negative cell cycle regulator which is an inhibitor of the CDK1-cyclin A/B complexes, thereby preventing G2/M progression (Fig 4.5). Activation of p53 triggers cell death by inducing expression of a number of downstream target genes implicated in apoptosis (e.g., Bim, Puma, Noxa, Bid, Bax and Apaf1) (Baker *et al*., 2008). The human papillomavirus oncoproteins E6 and E7 interfere in the Rb pathway and in the p53 pathway respectively, in order to bypass the cell cycle checkpoints (Al-Kaabi *et al*., 2014) Therefore, both p16(INK4) and p14(ARF) are negative regulators of cell proliferation and hence tumor suppressor genes (Li *et al*., 2011).

Cdkn2a has been found expressed higher in HP1γ WT females than WT male according to the RNA-seq data (Fig S11 highlighted in yellow) and this has been validated by QRT-PCR (Cristina, MSc thesis, 2016) (Fig S10). However, the number of *Cdkn2a* transcripts was increased in male in response to HP1γ KO but there was no significant change in female by QRT-PCR (Cristina, MSc thesis, 2016) (Fig S10). The elevated expression of *Cdkn2a* may arrest the cell cycle and slow down cell proliferation (Krishnamurthy *et al*., 2006). Interestingly, overexpression using a vector encoding *Cdkn2a* can lead to G1 phase arrest in NIH3T3 mouse embryonic fibroblasts (Quelle *et al*., 1995). In a recent study, the neural subtype of human glioblastoma (GBM) with *Cdkn2a* deletion has been found to exhibit sex differences (Sun *et al*., 2015).

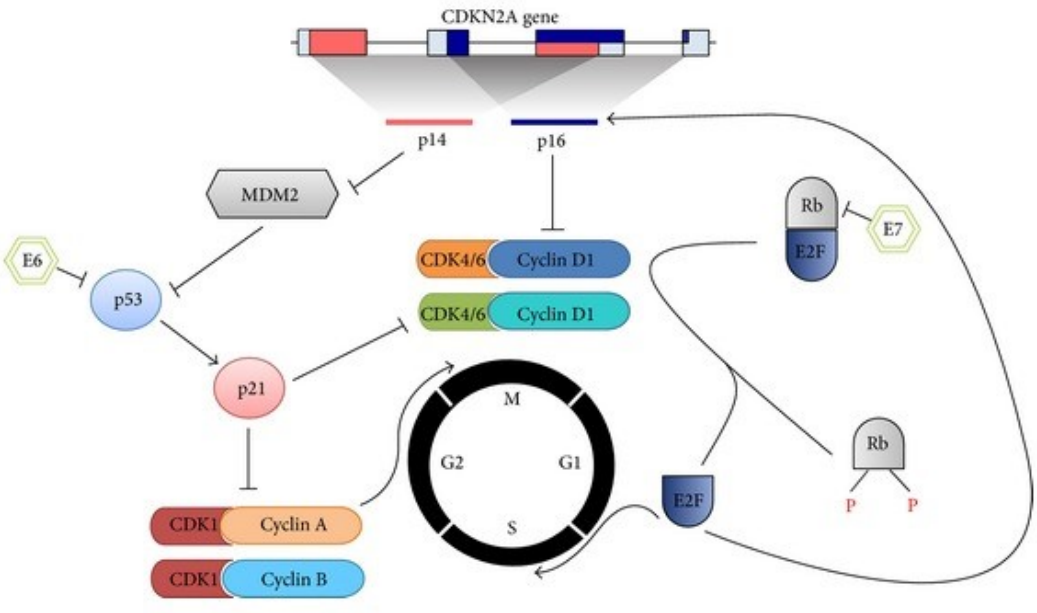

Fig 4.5. Cell cycle arrest by Cdkn2a. *The Cdkn2a gene encodes two proteins, p16(INK4A) and p14(ARF), which differ in their first exon. The p16(INK4A) protein inhibits the CDK4/6-cyclin D1 complexes, keeping the retinoblastoma (Rb) proteins in a dephosphorylated state, and enables binding and inactivating the E2F transcription factors. p16(INK4A) is also upregulated by E2F. In contrast, p14(ARF) stabilizes and activates the tumor suppressor gene p53 by inhibiting MDM2, which inactivates p53 by ubiquitin-mediated degradation. Active p53 induces the expression of p21, a negative cell cycle regulator which is an inhibitor of the CDK1-cyclin A/B complexes, thereby preventing G2/M progression. The human papillomavirus oncoproteins E6 and E7 interfere in the Rb pathway and in the p53 pathway, to bypass the cell cycle checkpoints. This figure is adapted with permission from "p16INK4A and p14ARF Gene Promoter Hypermethylation as Prognostic Biomarker in Oral and Oropharyngeal Squamous Cell Carcinoma: A Review" Ai-Kaabi et al., (Al-Kaabi et al., 2014).*

4.7 Future work

Future experiments to explain the observations seen in Chapter 4 regarding:

1. Role of HP1γ in regulating sexually dimorphic gene expression.
2. Proliferation advantage in males is completely dependent upon HP1γ.
3. Differential protein binding to HP1γ in male and female MEFs.
4. Sex dimorphic regulation of RNA alternative splicing by HP1γ.

Role of HP1γ in regulating sexually dimorphic gene expression

Together with previous transcriptomic data that showed the effect of HP1γ in regulating sexually dimorphic gene expression, where HP1γ KO exerted a bigger effect in male MEFs than females. This suggests that HP1γ may play an essential role in regulating the differential autosomal gene expression in male and female.

To date, little is known about the molecular mechanisms underlying these sexual differences. Further investigation on the genome-wide HP1γ distribution on sexual dimorphic genes will determine whether the sex-specific regulation might be due to different genomic distributions of HP1γ. This will be done by HP1γ Chromatin immunoprecipitation followed by high throughout sequencing (ChIP-seq).

Proliferation advantage in males is completely dependent upon HP1γ

Cdkn2a may be an interesting target for investigating the sex-difference in proliferation regulated by HP1γ, given that *Cdkn2a is* differentially expressed between the sexes in an HP1γ -dependent manner. Since *Cdkn2a* is a master regulator of cell-cycle arrest and cellular senescence as discussed above, further studies will focus on whether the increased expression of *Cdkn2a* in HP1γ KO male MEFs is the main cause of their senescence. Firstly, Senescence-

associated-β-galactosidase (SA-β-gal) cytochemical method will be used to measure the proportion of senescent cells in each passage and in the meantime, the expression level of *Cdkn2a* will be detected by QRT-PCR in each passage. A rescue experiment that knocks-down or knocks-out *Cdkn2a* in HP1γ KO male MEFs would help determine whether the potentially increased cellular senescence in HP1γ KO male MEFs is due to the overexpression of *Cdkn2a*.

Differential protein binding to HP1γ in male and female MEFs.

The Mass Spec. experiments reported here suggest sex dimorphic binding of proteins to HP1γ. This result needs to be reproduced and validated by Co-IP and western blot. The underlying mechanism of sex-specific binding needs to be addressed (see Section 4.5.1 and 1.9). It is possible that HP1 or its binding partners are post-translationally modified to facilitate sex-specific binding or that a sex specific protein is responsible for the sex dimorphism detected here.

Sex dimorphic regulation of RNA alternative splicing by HP1γ

HP1γ has been implicated in regulating alternative RNA splicing by slowing down RNA polymerase II elongation to facilitate the inclusion of the alternative exons (Saint-Andre *et al*., 2011). Here we show, for the first time, that sex-dimorphic alternative splicing is regulated in a subset of mammalian genes by HP1γ. This group of sexually dimorphically spliced genes did not overlap with those genes previously identified from the same data as differentially expressed between the sexes. This makes it unlikely that the differences in splicing were directly due to expression levels. ChIP sequencing data (currently being pursued in the lab by Manos Stylianakis) will determine whether there is any sex difference in the binding to the splice sites of the genes identified here as differentially spliced.

Chapter 5 – Concluding Remarks

This thesis has focused on two distinct but potentially related chromatin proteins, HIRA and HP1γ to investigate their roles *in vivo* in mice. This final section discusses potential similarities and differences in their possible roles and further experiments to investigate how they might co-operate *in vivo*.

5.1 Conclusions - Chapter 3

HIRA deficiency results in premature expression of the 'memory' T cell marker CD44 in naïve single positive T cells in the thymus. Moreover, the CD44 population in the periphery (lymph node and spleen) was also increased. These effects might be due to: 1) pre-mature activation of the commitment to the memory T cell lineage that circumvents exposure to antigen in the thymus; 2) a CD44 locus-specific effect of HIRA deficiency in de-repressing this specific gene which is normally transiently expressed during early development (Fig 1.8.1) and then subsequently silenced and 3) decreased output of total number of T cells from the thymus during T cell development leading to aberrant proliferation in the periphery. Further investigations on how to dissect these possibilities were discussed in section 3.7.3.1.

HIRA deficiency inhibits TCRα V(D)J rearrangement in the CD71- double positive cell population in mouse thymus *in vivo*. We considered that this might be due to: 1) direct regulation by altered H3.3 incorporation. A previous study found that H3.3 was enriched at the V(D)J region of Ig loci (Aida *et al*., 2013), which implies that H3.3 might also participate in TCRα V(D)J recombination as these regions which are subjected to frequent histone exchange in terms of both the recycling and turnover of histones. Further looking into what nucleosome density favors successful recombination will provide an indication as to whether the impaired

VDJ recombination upon HIRA KO is directly regulated via H3.3 or not (also see section 3.7.3.2), 2) an indirect regulation - in this case dysregulation of the components of the TCR recombination machinery upon HIRA KO leads to downstream impairment of V(D)J recombination (see section 1.8.5), 3) HIRA deficiency may also affect other cellular pathways (e.g. CD44 upregulation), which results in cells that cannot respond efficiently to the recombination signal or progress through differentiation. Finally, it is unclear if HIRA KO influences a subset of cells or whether all cells are affected equally, further studies might include high-throughput single-cell analysis by ATAC-seq (Chen *et al*., 2018) and RNA-seq.

5.2 Conclusions - Chapter 4

5.2.1 Depletion of HP1γ specifically affects male MEFs' proliferation and hence equalized the difference in cellular proliferation rate between the two sexes.

This indicates that HP1γ is required for maintaining the sex difference in cellular proliferation in MEFs. As there is a documented sex difference in embryonic growth rate (Burgoyne *et al*., 1995), it is possible that the proliferation difference seen here underpins this embryonic phenomenon, further experiments in the lab are currently assessing growth rate of embryos with and without HP1γ. As mentioned previously (see section 4.2), GSEA showed a large set of cell-cycle genes that are differentially expressed between the sexes and these genes are affected *enbloc* by HP1γ deficiency in males but not females. The underlying mechanism of regulation of these genes is unclear. However, *Cdkn2a* is a good candidate as target for the HP1γ effect and this effect could be direct or indirect. Ways to dissect this would involve: a rescue experiment, in which we can overexpress *Cdkn2a* gene in HP1γ KO male MEFs to see if male MEFs proliferate to a similar rate as female MEFs as HP1γ appears to act as a repressor of the *Cdkn2a* gene in males. Meanwhile ChIP would reveal whether HP1γ binds to the *Cdkn2a* gene in a sex-biased manner which would favor a direct effect.

Cell-cycle arrest at G1/0 after HP1γ KO was minor and is not a sexually dimorphic phenotype as it occurred in both sexes (Fig 4.2.2). So, this is unlikely, therefore to account for the cellular proliferation difference seen between the sexes.

5.2.2 HP1γ is implicated in the regulation of sex dimorphism in alternative RNA splicing in males

During transcription, RNA Pol II passage requires the disruption of chromatin structure, which is known to be dynamically regulated by chromatin modifiers, post translational modifications

on histones and histone variants (Kulaeva *et al*., 2007). HP1γ has been shown to regulate splicing (Saint-Andre *et al*., 2011, Smallwood *et al*., 2012, Rachez *et al*., 2019) (Fig S13), where they showed that accumulation of HP1γ on *CD44* pre-mRNA slows down the RNA Pol II, which in turn facilitates recruitment of splicing factors leading to inclusion of CD44 variant exons (Saint-Andre *et al*., 2011). Although the alternative splicing events we investigated here (SE and RI mainly) are different from those in that paper, where they examine exon inclusion, our analysis suggests that HP1γ regulates alternative RNA splicing in a sex-biased way, where males are more sensitive to HP1γ KO (Fig 4.3.6). Our analysis by comparing the sex dimorphic effect of HP1γ KO on alternative splicing and gene expression suggests that the sex difference in gene expression is not a result of the difference in splicing and *vice versa* (Fig 4.3.5).

The data shown here strongly implicate HP1γ in regulating sex differences in alternative splicing. This is because: 1) splicing factors were identified by mass spec as associating with HP1γ only in males (Fig 4.3.1) and 2) the difference in alternative splicing between the sexes, identified in wildtype MEFs, was strongly ameliorated by HP1γ KO in males but not in females (Figure 4.3.7, 4.3.8 and 4.3.9).

5.2.3 Why are both HP1γ and H3.3 localized to highly expressing genes?

There are some intriguing similarities in the distribution of both HP1γ and H3.3 in relation to gene expression. To date there is no clear explanation for why HP1γ is present at higher levels on expressing genes. Interestingly, H3.3 also has this property. Several experiments previously published have shown an association between HP1γ and H3.3 (Law, 2015, Kim *et al*., 2011). In the study by Kim *et al* both HP1γ and H3.3 were shown to cooperate in the expression of the *HSP70* gene (Kim *et al*., 2011). Pui Pik Law, a PhD in the lab, co-immunoprecipitated both

HP1γ and H3.3 showing that indeed in our system they are interacting (data not shown). Several hypotheses have been suggested to explain the presence of HP1γ on highly expressed genes; one suggestion is that HP1γ stabilizes the primary transcript which further facilitates RNA splicing and RNA processing (Smallwood *et al*., 2012, Piacentini and Pimpinelli, 2010). The reason put forward to explain why H3.3 is found in a similar distribution on highly expressed genes has been attributed to the less stable nucleosomal properties, when they contain H3.3, thereby facilitating progress of RNAPII through the highly active genes. It is possible that there are, as yet unknown functionally important interactions between HP1γ and H3.3 in this context and further work would be necessary to define any precise functional interaction. For example, *in vitro* mutagenesis studies could elucidate the precise interacting domains which could be mutated in cells or animals to investigate the effect on transcriptional regulation.

To further investigate the potential functional interaction between H3.3, HIRA and HP1γ *in vivo*, the following experiments could be done:

1. Biochemical approaches include IP and mass spectrometry on HIRA and HP1γ. The HP1γ mass spectrometry experiment presented in this thesis did not pull-down HIRA but this may be due to the absence of a direct association between them or alternatively HIRA may be difficult to be picked up with mass spectrometry. Alternatively, immunoprecipitation followed by western blot would enable checking whether HIRA is enriched in the HP1γ pull-down.

2. *In vivo* genetic approaches include looking for effects on H3.3 or HP1γ genome-wide enrichment in HIRA KO and HP1γ KO cells. This could be done by ChIP-seq for these proteins comparing WT with KO. An analysis of the genome-wide distribution of H3.3B-EGFP in both HP1γ WT and HP1γ KO MEFs has been done in the lab (Law,

2015), which showed that the HP1γ deficiency leads to a disproportionate increase in H3.3B-EGFP enrichment around the TSS compared with the gene body and with the biggest change seen on highly expressed genes (Fig S12). Of course, at present the function of HP1γ on the gene bodies and promoters of active genes is unknown. Thus, there appears to be an interaction between HP1γ and H3.3 genomic localization, however the mechanism whereby HP1γ deficiency changes H3.3 localization and the potential functional significance is unknown. It would be important to verify the change in H3.3 distribution by a different method using the H3.3 antibody for ChIP rather than relying on the EGFP tag. If this result was verified it is possible therefore that HP1γ and H3.3 interact to regulate gene transcription with different effects at the TSS and the gene body. The result as it stands suggests that HP1γ prevents the incorporation of H3.3 to a greater extent at the TSS compared with the gene body on highly expressed genes (Fig S12). This suggests that HP1γ might be involved in the regulation of DNA accessibility (see section 1.5.5.1) at the promoter and perhaps affect RNA splicing (see section 1.7.2) on the gene body via affecting H3.3 turnover. Further experiments in the lab are currently investigating this by using CAGE (Cap analysis gene expression).

5.2.4 HIRA and HP1γ regulate senescence in a possible pathway involving *cdkn2a*

Two cell-cycle inhibitors p16/INK4 and p19/ARF were found to be expressed at high levels in cultured senescing cells, which are believed to play an important role in the establishment of the senescent state (Kamijo *et al*., 1997, Sherr, 2001). They are both encoded by *Cdkn2a* genes. In our study of HP1γ, *Cdkn2a* was found to be differentially expressed between the sexes in an HP1γ-dependent manner (Fig S11), which may implicate a possible mechanism/pathway that involves both HP1γ and *Cdkn2a* in regulating sex difference in cell proliferation in MEFs. As

discussed before, p16INK4/pRB pathway is a key effector of cellular senescence (Mirzayans *et al*., 2012), senescence regulation by *Cdkn2a* therefore might involve HP1γ because HP1γ appears to repress *Cdkn2a* expression in males (as HP1γ KO leads to *Cdkn2a* upregulation in male MEFs) (See section 4.6 and Fig S11). Given that HP1γ and H3K9Me2/3 are components of senescence-associated heterochromatin foci (SAHF) formed in many senescent cells (Mirzayans *et al*., 2012) it is also possible that HP1 may play a role in their formation although the function of these foci is unclear and they have not been clearly observed in mice (Aird and Zhang, 2013). Interestingly, HIRA has also been shown to play a key role in the formation of SAHF (Zhang *et al*., 2007). During the formation of SAHF, physical interactions between anti-silencing function 1a (ASF1a) with H3 and HIRA is essential and only HP1γ but not HP1α/β becomes phosphorylated in order to be incorporated into SAHF (Zhang *et al*., 2007). It is interesting that both HIRA and HP1γ as well as HIRA's binding partners (UBN1, CABIN1, and ASF1a) have been implicated in chromatin regulation in senescent cells (Banumathy *et al*., 2009, Zhang *et al*., 2005b)

Non-proliferating senescent cells express a subset of replication-dependent histone genes (Marzluff *et al*., 2008) in which HIRA is responsible for the trafficking of histones (mainly histone H3.3 and H4) into chromatin at PML bodies (Delbarre *et al*., 2013, Chang *et al*., 2013). This process is accompanied by DAXX targeting histone H3.3 to pericentromeric heterochromatin in senescent cells (Corpet *et al*., 2014). Moreover, HIRA deficient mice also showed both impaired differentiation and senescence that led to epidermal hyperplasia in mice, indicating that HIRA plays a key role in regulating the chromatin landscape of senescent cells (Rai *et al*., 2014).

5.2.5 HP1γ, HIRA and Immunology

The gene ontology term for immune function was highly enriched upon HP1γ KO in males on analysis of the transcriptomic data from MEFs (Law, 2015). Moreover, analysis of transcriptomic data from HIRA deficient thymocytes also identified enrichment for GO terms related to T cell biology, in which, most biological processes that were affected significantly were those related to T-cell biology (Vineet Sharma PhD thesis 2014). Interestingly, proteomic analysis also suggested that HIRA deficiency led to altered protein levels of enzymes for catalyzing histone PTMs such as SUV39H1 (-26%), HAT1(-24%) HDAC2 (-28%) HDAC1 (-10%) DNMT1 (-29%), SETD7 (+18%) as well as HP1 proteins of which all three isoforms showed altered protein levels, HP1γ (-44%), HPα (-42%) and HP1β (-47%) in HIRA KO thymus (Vineet Sharma PhD thesis 2014). Both HIRA and HP1γ are implicated in the immune system which led us to consider whether these two proteins participate in the same axis for regulating genes in the immune pathway. The coordination between H3.3 and HP1γ has been reported previously on the *HSP70* gene, in which, H3.3 and HP1γ have been found co-enriched at the promoter of *HSP70* gene by immunoprecipitation (Kim *et al*., 2011). Studies on T cell turnover suggested that typical naïve T cells are long-lived resting cells that can remain in the resting state for years in humans and even some memory T cells appear to return to a resting state eventually (Tough and Sprent, 1995). Therefore, histone H3.3 would be the only H3 that are being synthesized in these resting T cells as it is thought to be expressed throughout the whole cell cycle (Wu *et al*., 1982). Also, in the lab, we have shown by co-immunopreciptation and western blot that H3.3 and HP1γ interact in MEFs (Law, 2015) (data now shown). Additionally, there are many examples of autoimmune disorders that are sex biased and hence, it is possible that the interaction between HP1γ and HIRA/H3.3 is important for the sexually dimorphic gene expression.

5.3 Summary

In Chapter 3, we demonstrated that HIRA deficiency results in premature expression of the 'memory' T cell marker CD44 in naïve single positive T cells in the thymus and periphery as well as impaired TCRα V(D)J rearrangement in CD71- double positive cell population in mouse thymus *in vivo.* Moreover, HIRA deficiency identified Gene Ontology (GO) terms including the immune system (Vineet Sharma PhD thesis 2014).

Taken together, these observations suggest a potential role of HIRA in regulating T cell development and TCRα V(D)J recombination. Future investigations could be done in two directions: firstly, to determine if the whole T cell developmental program for generating memory cells has been reprogrammed, we can either look for the memory type cytokine secretion by artificially activating naïve T cells (from HIRA WT and CKO) or compare the transcriptomic data obtained from these upregulated CD44 expressing cells with normal naïve T cells. Secondly, if abnormal T cell development is not the cause of premature CD44 expression, HIRA may play a role in a repressive pathway for keeping the *CD44* gene silenced. This could be further studied by examining genome-wide H3.3 deposition in these abnormal CD44 expressing T cells. Similarly, looking further into what nucleosome density favors successful V(D)J recombination is desired and will indicate whether this downregulation effect upon HIRA KO is directly via H3.3 or not.

The results listed in Chapter 4 suggest a male-specific role for HP1γ in regulating sexually dimorphic gene expression and alternative splicing which in turn contributes to sexual differences. Interestingly, HP1γ pull-downs suggested a sex dimorphism in the binding of other proteins to HP1γ. However, the molecular mechanism underlying sexual dimorphism mediated by HP1γ remains to be further studied. To explain the male-specific regulation, there are

several possibilities including the ‘sink hypothesis’, inactive-X chromosome escapees, and Y chromosome genes. In this chapter, we raised the hypothesis that the inactive X chromosome in females might be acting as a heterochromatic ‘sink’ that sequesters HP1γ away from the euchromatic regions. However, the ChIP-seq result obtained in immortalized MEFs with non-random X inactivation suggests that the inactive X chromosome might not be a ‘sink’ for HP1γ but instead sequesters HP1γ to genes that express on the Xi chromosome, in other words, genes that escaped X chromosome inactivation. However, as discussed before (section 4.5.2), the ‘sink’ effect might not be visible due to the exclusion of the repetitive DNA sequences that cannot be uniquely mapped in this study. Further work should repeat the analysis using paired-end sequencing which is more likely to lead to mappable reads as well as an analysis of X-chromosome specific repetitive sequences. Further studies on the Y chromosome genes that are uniquely present in males could be another direction to explore the underlying the mechanisms that contribute to HP1γ’s largely male-specific regulation of gene expression.

References

ABE, K., NARUSE, C., KATO, T., NISHIUCHI, T., SAITOU, M. & ASANO, M. 2011. Loss of heterochromatin protein 1 gamma reduces the number of primordial germ cells via impaired cell cycle progression in mice. *Biol Reprod,* 85**,** 1013-24.

ABI-GHANEM, J., SAMSONOV, S. A. & PISABARRO, M. T. 2015. Insights into the preferential order of strand exchange in the Cre/loxP recombinase system: impact of the DNA spacer flanking sequence and flexibility. *J Comput Aided Mol Des,* 29**,** 271-82.

ADAM, S., POLO, S. E. & ALMOUZNI, G. 2013. Transcription recovery after DNA damage requires chromatin priming by the H3.3 histone chaperone HIRA. *Cell,* 155**,** 94-106.

ADKINS, M. W., CARSON, J. J., ENGLISH, C. M., RAMEY, C. J. & TYLER, J. K. 2007. The histone chaperone anti-silencing function 1 stimulates the acetylation of newly synthesized histone H3 in S-phase. *J Biol Chem,* 282**,** 1334-40.

ADUSUMALLI, S., NGIAN, Z. K., LIN, W. Q., BENOUKRAF, T. & ONG, C. T. 2019. Increased intron retention is a post-transcriptional signature associated with progressive aging and Alzheimer's disease. *Aging Cell,* 18**,** e12928.

AHMAD, K. & HENIKOFF, S. 2002. The histone variant H3.3 marks active chromatin by replication-independent nucleosome assembly. *Molecular Cell,* 9**,** 1191-1200.

AIDA, M., HAMAD, N., STANLIE, A., BEGUM, N. A. & HONJO, T. 2013. Accumulation of the FACT complex, as well as histone H3.3, serves as a target marker for somatic hypermutation. *Proc Natl Acad Sci U S A,* 110**,** 7784-9.

AIRD, K. M. & ZHANG, R. 2013. Detection of senescence-associated heterochromatin foci (SAHF). *Methods Mol Biol,* 965**,** 185-96.

AKIYAMA, T., SUZUKI, O., MATSUDA, J. & AOKI, F. 2011. Dynamic replacement of histone H3 variants reprograms epigenetic marks in early mouse embryos. *PLoS Genet,* 7**,** e1002279.

AKONDY, R. S., FITCH, M., EDUPUGANTI, S., YANG, S., KISSICK, H. T., LI, K. W., YOUNGBLOOD, B. A., ABDELSAMED, H. A., MCGUIRE, D. J., COHEN, K. W., ALEXE, G., NAGAR, S., MCCAUSLAND, M. M., GUPTA, S., TATA, P., HAINING, W. N., MCELRATH, M. J., ZHANG, D., HU, B., GREENLEAF, W. J., GORONZY, J. J., MULLIGAN, M. J., HELLERSTEIN, M. & AHMED, R. 2017. Origin and differentiation of human memory CD8 T cells after vaccination. *Nature,* 552**,** 362.

AKOPIAN, D., SHEN, K., ZHANG, X. & SHAN, S. O. 2013. Signal recognition particle: an essential protein-targeting machine. *Annu Rev Biochem,* 82**,** 693-721.

AL-KAABI, A., VAN BOCKEL, L. W., POTHEN, A. & WILLEMS, S. 2014. *p16INK4A and p14ARF Gene Promoter Hypermethylation as Prognostic Biomarker in Oral and Oropharyngeal Squamous Cell Carcinoma: A Review*.

ALBERTS B, J. A., LEWIS J, ET AL. 2002a. *Molecular Biology of the Cell.*, New York: Garland Science.

ALBERTS B, J. A., LEWIS J, ET AL. 2002b. *Molecular Biology of the Cell.* , New York: Garland Science.

ALLSHIRE, R. C., JAVERZAT, J. P., REDHEAD, N. J. & CRANSTON, G. 1994. Position effect variegation at fission yeast centromeres. *Cell,* 76**,** 157-69.

ALLSHIRE, R. C. & KARPEN, G. H. 2008. Epigenetic regulation of centromeric chromatin: old dogs, new tricks? *Nat Rev Genet,* 9**,** 923-37.

ANDREWS, A. J., CHEN, X., ZEVIN, A., STARGELL, L. A. & LUGER, K. 2010. The histone chaperone Nap1 promotes nucleosome assembly by eliminating nonnucleosomal histone DNA interactions. *Mol Cell,* 37**,** 834-42.

ANGELOPOULOU, R., LAVRANOS, G. & MANOLAKOU, P. 2006. Establishing sexual dimorphism in humans. *Coll Antropol,* 30**,** 653-8.

ARNOLD, A. P. 2004. Sex chromosomes and brain gender. *Nat Rev Neurosci,* 5**,** 701-8.

ARNOLD, A. P. 2012. The end of gonad-centric sex determination in mammals. *Trends Genet,* 28**,** 55-61.

ARNOLD, A. P. 2014. Conceptual frameworks and mouse models for studying sex differences in physiology and disease: why compensation changes the game. *Exp Neurol,* 259**,** 2-9.

ARNOLD, A. P. & CHEN, X. 2009. What does the "four core genotypes" mouse model tell us about sex differences in the brain and other tissues? *Front Neuroendocrinol,* 30**,** 1-9.

ARNOLD, A. P., CHEN, X., LINK, J. C., ITOH, Y. & REUE, K. 2013. Cell-autonomous sex determination outside of the gonad. *Dev Dyn,* 242**,** 371-9.

ARNOLD, A. P., REUE, K., EGHBALI, M., VILAIN, E., CHEN, X., GHAHRAMANI, N., ITOH, Y., LI, J., LINK, J. C., NGUN, T. & WILLIAMS-BURRIS, S. M. 2016. The importance of having two X chromosomes. *Philos Trans R Soc Lond B Biol Sci,* 371**,** 20150113.

AUCOTT, R., BULLWINKEL, J., YU, Y., SHI, W., BILLUR, M., BROWN, J. P., MENZEL, U., KIOUSSIS, D., WANG, G., REISERT, I., WEIMER, J., PANDITA, R. K., SHARMA, G. G., PANDITA, T. K.,

FUNDELE, R. & SINGH, P. B. 2008. HP1-beta is required for development of the cerebral neocortex and neuromuscular junctions. *J Cell Biol,* 183**,** 597-606.
AUSIO, J. 2006. Histone variants--the structure behind the function. *Brief Funct Genomic Proteomic,* 5**,** 228-43.
AUSIO, J., ABBOTT, D. W., WANG, X. & MOORE, S. C. 2001. Histone variants and histone modifications: a structural perspective. *Biochem Cell Biol,* 79**,** 693-708.
AVVAKUMOV, N., NOURANI, A. & COTE, J. 2011. Histone Chaperones: Modulators of Chromatin Marks. *Molecular Cell,* 41**,** 502-514.
BACHU, M., TAMURA, T., CHEN, C., NARAIN, A., NEHRU, V., SARAI, N., GHOSH, S. B., GHOSH, A., KAVARTHAPU, R., DUFAU, M. L. & OZATO, K. 2019. A versatile mouse model of epitope-tagged histone H3.3 to study epigenome dynamics. *J Biol Chem,* 294**,** 1904-1914.
BAKER, B. S., BURTIS, K., GORALSKI, T., MATTOX, W. & NAGOSHI, R. 1989. Molecular genetic aspects of sex determination in Drosophila melanogaster. *Genome,* 31**,** 638-45.
BAKER, D. J., JIN, F. & VAN DEURSEN, J. M. 2008. The yin and yang of the Cdkn2a locus in senescence and aging. *Cell Cycle,* 7**,** 2795-802.
BALAJI, S., IYER, L. M. & ARAVIND, L. 2009. HPC2 and ubinuclein define a novel family of histone chaperones conserved throughout eukaryotes. *Molecular Biosystems,* 5**,** 269-275.
BANASZYNSKI, L. A., ALLIS, C. D. & LEWIS, P. W. 2010. Histone variants in metazoan development. *Dev Cell,* 19**,** 662-74.
BANASZYNSKI, L. A., WEN, D., DEWELL, S., WHITCOMB, S. J., LIN, M., DIAZ, N., ELSASSER, S. J., CHAPGIER, A., GOLDBERG, A. D., CANAANI, E., RAFII, S., ZHENG, D. & ALLIS, C. D. 2013. Hira-dependent histone H3.3 deposition facilitates PRC2 recruitment at developmental loci in ES cells. *Cell,* 155**,** 107-20.
BANNISTER, A. J. & KOUZARIDES, T. 2011. Regulation of chromatin by histone modifications. *Cell Res,* 21**,** 381-95.
BANNISTER, A. J., ZEGERMAN, P., PARTRIDGE, J. F., MISKA, E. A., THOMAS, J. O., ALLSHIRE, R. C. & KOUZARIDES, T. 2001. Selective recognition of methylated lysine 9 on histone H3 by the HP1 chromo domain. *Nature,* 410**,** 120-4.
BANUMATHY, G., SOMAIAH, N., ZHANG, R., TANG, Y., HOFFMANN, J., ANDRAKE, M., CEULEMANS, H., SCHULTZ, D., MARMORSTEIN, R. & ADAMS, P. D. 2009. Human UBN1 is an ortholog of yeast Hpc2p and has an essential role in the HIRA/ASF1a chromatin-remodeling pathway in senescent cells. *Mol Cell Biol,* 29**,** 758-70.
BARSKI, A., CUDDAPAH, S., CUI, K., ROH, T. Y., SCHONES, D. E., WANG, Z., WEI, G., CHEPELEV, I. & ZHAO, K. 2007. High-resolution profiling of histone methylations in the human genome. *Cell,* 129**,** 823-37.
BARTOVA, E., PACHERNIK, J., HARNICAROVA, A., KOVARIK, A., KOVARIKOVA, M., HOFMANOVA, J., SKALNIKOVA, M., KOZUBEK, M. & KOZUBEK, S. 2005. Nuclear levels and patterns of histone H3 modification and HP1 proteins after inhibition of histone deacetylases. *J Cell Sci,* 118**,** 5035-46.
BASSING, C. H., ALT, F. W., HUGHES, M. M., D'AUTEUIL, M., WEHRLY, T. D., WOODMAN, B. B., GÄRTNER, F., WHITE, J. M., DAVIDSON, L. & SLECKMAN, B. P. 2000. Recombination signal sequences restrict chromosomal V(D)J recombination beyond the 12/23 rule. *Nature,* 405**,** 583.
BATSCHE, E., YANIV, M. & MUCHARDT, C. 2006. The human SWI/SNF subunit Brm is a regulator of alternative splicing. *Nat Struct Mol Biol,* 13**,** 22-9.
BEDFORD, M. T. & CLARKE, S. G. 2009. Protein arginine methylation in mammals: who, what, and why. *Mol Cell,* 33**,** 1-13.
BELMONT, A. S. & BRUCE, K. 1994. Visualization of G1 chromosomes: a folded, twisted, supercoiled chromonema model of interphase chromatid structure. *J Cell Biol,* 127**,** 287-302.
BERARD, M. & TOUGH, D. F. 2002. Qualitative differences between naive and memory T cells. *Immunology,* 106**,** 127-38.
BERLETCH, J. B., YANG, F. & DISTECHE, C. M. 2010. Escape from X inactivation in mice and humans. *Genome Biol,* 11**,** 213.
BERNSTEIN, B. E., HUMPHREY, E. L., ERLICH, R. L., SCHNEIDER, R., BOUMAN, P., LIU, J. S., KOUZARIDES, T. & SCHREIBER, S. L. 2002. Methylation of histone H3 Lys 4 in coding regions of active genes. *Proc Natl Acad Sci U S A,* 99**,** 8695-700.
BERNSTEIN, E., DUNCAN, E. M., MASUI, O., GIL, J., HEARD, E. & ALLIS, C. D. 2006. Mouse polycomb proteins bind differentially to methylated histone H3 and RNA and are enriched in facultative heterochromatin. *Mol Cell Biol,* 26**,** 2560-9.
BEYER, A. L. & OSHEIM, Y. N. 1988. Splice site selection, rate of splicing, and alternative splicing on nascent transcripts. *Genes Dev,* 2**,** 754-65.
BOSCH-PRESEGUE, L., RAURELL-VILA, H., THACKRAY, J. K., GONZALEZ, J., CASAL, C., KANE-GOLDSMITH, N., VIZOSO, M., BROWN, J. P., GOMEZ, A., AUSIO, J., ZIMMERMANN, T.,

ESTELLER, M., SCHOTTA, G., SINGH, P. B., SERRANO, L. & VAQUERO, A. 2017. Mammalian HP1 Isoforms Have Specific Roles in Heterochromatin Structure and Organization. *Cell Rep,* 21**,** 2048-2057.

BRASHER, S. V., SMITH, B. O., FOGH, R. H., NIETLISPACH, D., THIRU, A., NIELSEN, P. R., BROADHURST, R. W., BALL, L. J., MURZINA, N. V. & LAUE, E. D. 2000. The structure of mouse HP1 suggests a unique mode of single peptide recognition by the shadow chromo domain dimer. *EMBO J,* 19**,** 1587-97.

BREKELMANS, P., VAN SOEST, P., VOERMAN, J., PLATENBURG, P. P., LEENEN, P. J. & VAN EWIJK, W. 1994. Transferrin receptor expression as a marker of immature cycling thymocytes in the mouse. *Cell Immunol,* 159**,** 331-9.

BRODSKY, A. S., MEYER, C. A., SWINBURNE, I. A., HALL, G., KEENAN, B. J., LIU, X. S., FOX, E. A. & SILVER, P. A. 2005. Genomic mapping of RNA polymerase II reveals sites of co-transcriptional regulation in human cells. *Genome Biol,* 6**,** R64.

BURGESS, R. J. & ZHANG, Z. 2013. Histone chaperones in nucleosome assembly and human disease. *Nature Structural &Amp; Molecular Biology,* 20**,** 14.

BURGOYNE, P. S. 1993. A Y-chromosomal effect on blastocyst cell number in mice. *Development,* 117**,** 341-5.

BURGOYNE, P. S., THORNHILL, A. R., BOUDREAN, S. K., DARLING, S. M., BISHOP, C. E. & EVANS, E. P. 1995. The genetic basis of XX-XY differences present before gonadal sex differentiation in the mouse. *Philos Trans R Soc Lond B Biol Sci,* 350**,** 253-60 discussion 260-1.

BUSH, K. M., YUEN, B. T., BARRILLEAUX, B. L., RIGGS, J. W., O'GEEN, H., COTTERMAN, R. F. & KNOEPFLER, P. S. 2013. Endogenous mammalian histone H3.3 exhibits chromatin-related functions during development. *Epigenetics & Chromatin,* 6.

BUTTERFIELD, K., FATHMAN, C. G. & BUDD, R. C. 1989. A subset of memory CD4+ helper T lymphocytes identified by expression of Pgp-1. *J Exp Med,* 169**,** 1461-6.

CACERES, J. F. & KORNBLIHTT, A. R. 2002. Alternative splicing: multiple control mechanisms and involvement in human disease. *Trends Genet,* 18**,** 186-93.

CAILLIER, M., THENOT, S., TRIBOLLET, V., BIROT, A. M., SAMARUT, J. & MEY, A. 2010. Role of the epigenetic regulator HP1gamma in the control of embryonic stem cell properties. *PLoS One,* 5**,** e15507.

CARREL, L., COTTLE, A. A., GOGLIN, K. C. & WILLARD, H. F. 1999. A first-generation X-inactivation profile of the human X chromosome. *Proc Natl Acad Sci U S A,* 96**,** 14440-4.

CARROLL, T. S., LIANG, Z. W., SALAMA, R., STARK, R. & DE SANTIAGO, I. 2014. Impact of artifact removal on ChIP quality metrics in ChIP-seq and ChIP-exo data. *Frontiers in Genetics,* 5.

CHANG, F. T., MCGHIE, J. D., CHAN, F. L., TANG, M. C., ANDERSON, M. A., MANN, J. R., ANDY CHOO, K. H. & WONG, L. H. 2013. PML bodies provide an important platform for the maintenance of telomeric chromatin integrity in embryonic stem cells. *Nucleic Acids Res,* 41**,** 4447-58.

CHASIN, L. A. 2007. Searching for splicing motifs. *Adv Exp Med Biol,* 623**,** 85-106.

CHEN, P., ZHAO, J., WANG, Y., WANG, M., LONG, H., LIANG, D., HUANG, L., WEN, Z., LI, W., LI, X., FENG, H., ZHAO, H., ZHU, P., LI, M., WANG, Q. F. & LI, G. 2013. H3.3 actively marks enhancers and primes gene transcription via opening higher-ordered chromatin. *Genes Dev,* 27**,** 2109-24.

CHEN, T. & DENT, S. Y. 2014. Chromatin modifiers and remodellers: regulators of cellular differentiation. *Nat Rev Genet,* 15**,** 93-106.

CHEN, X., MIRAGAIA, R. J., NATARAJAN, K. N. & TEICHMANN, S. A. 2018. A rapid and robust method for single cell chromatin accessibility profiling. *Nat Commun,* 9**,** 5345.

CHEN, X., XU, H., YUAN, P., FANG, F., HUSS, M., VEGA, V. B., WONG, E., ORLOV, Y. L., ZHANG, W., JIANG, J., LOH, Y. H., YEO, H. C., YEO, Z. X., NARANG, V., GOVINDARAJAN, K. R., LEONG, B., SHAHAB, A., RUAN, Y., BOURQUE, G., SUNG, W. K., CLARKE, N. D., WEI, C. L. & NG, H. H. 2008. Integration of external signaling pathways with the core transcriptional network in embryonic stem cells. *Cell,* 133**,** 1106-17.

CHODAVARAPU, R. K., FENG, S., BERNATAVICHUTE, Y. V., CHEN, P.-Y., STROUD, H., YU, Y., HETZEL, J. A., KUO, F., KIM, J., COKUS, S. J., CASERO, D., BERNAL, M., HUIJSER, P., CLARK, A. T., KRÄMER, U., MERCHANT, S. S., ZHANG, X., JACOBSEN, S. E. & PELLEGRINI, M. 2010. Relationship between nucleosome positioning and DNA methylation. *Nature,* 466**,** 388.

COLLINS, S. R., MILLER, K. M., MAAS, N. L., ROGUEV, A., FILLINGHAM, J., CHU, C. S., SCHULDINER, M., GEBBIA, M., RECHT, J., SHALES, M., DING, H. M., XU, H., HAN, J. H., INGVARSDOTTIR, K., CHENG, B., ANDREWS, B., BOONE, C., BERGER, S. L., HIETER, P., ZHANG, Z. G., BROWN, G. W., INGLES, C. J., EMILI, A., ALLIS, C. D., TOCZYSKI, D. P., WEISSMAN, J. S., GREENBLATT, J. F. & KROGAN, N. J. 2007. Functional dissection of protein complexes involved in yeast chromosome biology using a genetic interaction map. *Nature,* 446**,** 806-810.

COOPER, T. A., WAN, L. & DREYFUSS, G. 2009. RNA and disease. *Cell,* 136**,** 777-93.

CORPET, A. & ALMOUZNI, G. 2009. Making copies of chromatin: the challenge of nucleosomal organization and epigenetic information. *Trends Cell Biol,* 19**,** 29-41.
CORPET, A., OLBRICH, T., GWERDER, M., FINK, D. & STUCKI, M. 2014. Dynamics of histone H3.3 deposition in proliferating and senescent cells reveals a DAXX-dependent targeting to PML-NBs important for pericentromeric heterochromatin organization. *Cell Cycle,* 13**,** 249-67.
COULDREY, C., CARLTON, M. B., NOLAN, P. M., COLLEDGE, W. H. & EVANS, M. J. 1999. A retroviral gene trap insertion into the histone 3.3A gene causes partial neonatal lethality, stunted growth, neuromuscular deficits and male sub-fertility in transgenic mice. *Hum Mol Genet,* 8**,** 2489-95.
COX, J., NEUHAUSER, N., MICHALSKI, A., SCHELTEMA, R. A., OLSEN, J. V. & MANN, M. 2011. Andromeda: a peptide search engine integrated into the MaxQuant environment. *J Proteome Res,* 10**,** 1794-805.
DAVIES, E. G. 2013. Immunodeficiency in DiGeorge Syndrome and Options for Treating Cases with Complete Athymia. *Front Immunol,* 4**,** 322.
DE LA CHAPELLE, A., HERVA, R., KOIVISTO, M. & AULA, P. 1981. A deletion in chromosome 22 can cause DiGeorge syndrome. *Hum Genet,* 57**,** 253-6.
DE LA MATA, M., ALONSO, C. R., KADENER, S., FEDEDA, J. P., BLAUSTEIN, M., PELISCH, F., CRAMER, P., BENTLEY, D. & KORNBLIHTT, A. R. 2003. A slow RNA polymerase II affects alternative splicing in vivo. *Mol Cell,* 12**,** 525-32.
DEAL, R. B., HENIKOFF, J. G. & HENIKOFF, S. 2010. Genome-wide kinetics of nucleosome turnover determined by metabolic labeling of histones. *Science,* 328**,** 1161-4.
DELANEY, K., MAILLER, J., WENDA, J. M., GABUS, C. & STEINER, F. A. 2018. Differential Expression of Histone H3.3 Genes and Their Role in Modulating Temperature Stress Response in Caenorhabditis elegans. *Genetics,* 209**,** 551-565.
DELBARRE, E., IVANAUSKIENE, K., KUNTZIGER, T. & COLLAS, P. 2013. DAXX-dependent supply of soluble (H3.3-H4) dimers to PML bodies pending deposition into chromatin. *Genome Res,* 23**,** 440-51.
DHAMI, P., SAFFREY, P., BRUCE, A. W., DILLON, S. C., CHIANG, K., BONHOURE, N., KOCH, C. M., BYE, J., JAMES, K., FOAD, N. S., ELLIS, P., WATKINS, N. A., OUWEHAND, W. H., LANGFORD, C., ANDREWS, R. M., DUNHAM, I. & VETRIE, D. 2010. Complex exon-intron marking by histone modifications is not determined solely by nucleosome distribution. *PLoS One,* 5**,** e12339.
DHARMALINGAM G, C. T. 2015. soggi: visualise ChIP-seq, MNase-seq and motif occurrence as aggregate plots summarised over grouped genomic intervals.
DIALYNAS, G. K., TERJUNG, S., BROWN, J. P., AUCOTT, R. L., BARON-LUHR, B., SINGH, P. B. & GEORGATOS, S. D. 2007. Plasticity of HP1 proteins in mammalian cells. *J Cell Sci,* 120**,** 3415-24.
DICKINSON, E., RUSILOWICZ, M. J., DICKINSON, M., CHARLTON, A. J., BECHTOLD, U., MULLINEAUX, P. M. & WILSON, J. 2018. Integrating transcriptomic techniques and k-means clustering in metabolomics to identify markers of abiotic and biotic stress in Medicago truncatula. *Metabolomics,* 14**,** 126.
DION, M. F., KAPLAN, T., KIM, M., BURATOWSKI, S., FRIEDMAN, N. & RANDO, O. J. 2007. Dynamics of replication-independent histone turnover in budding yeast. *Science,* 315**,** 1405-8.
DIPAK AMIN, A., VISHNOI, N. & PROCHASSON, P. 2011. *A global requirement for the HIR complex in the assembly of chromatin*.
DRANE, P., OUARARHNI, K., DEPAUX, A., SHUAIB, M. & HAMICHE, A. 2010. The death-associated protein DAXX is a novel histone chaperone involved in the replication-independent deposition of H3.3. *Genes Dev,* 24**,** 1253-65.
DRAPER, R. K., HUDSON, R. T. & HU, T. 2001. Use of aminoglycoside antibiotics and related compounds to study ADP-ribosylation factor (ARF)/coatomer function in Golgi traffic. *Methods Enzymol,* 329**,** 372-9.
DRISCOLL, R., HUDSON, A. & JACKSON, S. P. 2007. Yeast Rtt109 promotes genome stability by acetylating histone H3 on lysine 56. *Science,* 315**,** 649-652.
DUNN, J., MCCUAIG, R., TU, W. J., HARDY, K. & RAO, S. 2015. Multi-layered epigenetic mechanisms contribute to transcriptional memory in T lymphocytes. *BMC Immunol,* 16**,** 27.
EGGER, G., LIANG, G., APARICIO, A. & JONES, P. A. 2004. Epigenetics in human disease and prospects for epigenetic therapy. *Nature,* 429**,** 457-63.
EISSENBERG, J. C., JAMES, T. C., FOSTER-HARTNETT, D. M., HARTNETT, T., NGAN, V. & ELGIN, S. C. 1990. Mutation in a heterochromatin-specific chromosomal protein is associated with suppression of position-effect variegation in Drosophila melanogaster. *Proc Natl Acad Sci U S A,* 87**,** 9923-7.
EISSENBERG, J. C. A. E., SARAH CR 2014. Heterochromatin and Euchromatin. *In: eLS. John Wiley & Sons, Ltd: Chichester.*
ELGIN, S. C. & REUTER, G. 2013. Position-effect variegation, heterochromatin formation, and gene silencing in Drosophila. *Cold Spring Harb Perspect Biol,* 5**,** a017780.

ELSASSER, S. J., HUANG, H., LEWIS, P. W., CHIN, J. W., ALLIS, C. D. & PATEL, D. J. 2012. DAXX envelops a histone H3.3-H4 dimer for H3.3-specific recognition. *Nature,* 491**,** 560-5.
FARRELL, M. J., STADT, H., WALLIS, K. T., SCAMBLER, P., HIXON, R. L., WOLFE, R., LEATHERBURY, L. & KIRBY, M. L. 1999. HIRA, a DiGeorge syndrome candidate gene, is required for cardiac outflow tract septation. *Circ Res,* 84**,** 127-35.
FELSENFELD, G. & GROUDINE, M. 2003. Controlling the double helix. *Nature,* 421**,** 448-53.
FESTENSTEIN, R., SHARGHI-NAMINI, S., FOX, M., RODERICK, K., TOLAINI, M., NORTON, T., SAVELIEV, A., KIOUSSIS, D. & SINGH, P. 1999. Heterochromatin protein 1 modifies mammalian PEV in a dose- and chromosomal-context-dependent manner. *Nat Genet,* 23**,** 457-61.
FESTENSTEIN, R., TOLAINI, M., CORBELLA, P., MAMALAKI, C., PARRINGTON, J., FOX, M., MILIOU, A., JONES, M. & KIOUSSIS, D. 1996. Locus control region function and heterochromatin-induced position effect variegation. *Science,* 271**,** 1123-5.
FILIPESCU, D., SZENKER, E. & ALMOUZNI, G. 2013a. Developmental roles of histone H3 variants and their chaperones. *Trends Genet,* 29**,** 630-40.
FILIPESCU, D., SZENKER, E. & ALMOUZNI, G. 2013b. Developmental roles of histone H3 variants and their chaperones. *Trends in Genetics,* 29**,** 630-640.
FILLINGHAM, J., RECHT, J., SILVA, A. C., SUTER, B., EMILI, A., STAGLJAR, I., KROGAN, N. J., ALLIS, C. D., KEOGH, M. C. & GREENBLATT, J. F. 2008. Chaperone control of the activity and specificity of the histone H3 acetyltransferase Rtt109. *Mol Cell Biol,* 28**,** 4342-53.
FISCHLE, W., TSENG, B. S., DORMANN, H. L., UEBERHEIDE, B. M., GARCIA, B. A., SHABANOWITZ, J., HUNT, D. F., FUNABIKI, H. & ALLIS, C. D. 2005. Regulation of HP1-chromatin binding by histone H3 methylation and phosphorylation. *Nature,* 438**,** 1116-22.
FISCHLE, W., WANG, Y., JACOBS, S. A., KIM, Y., ALLIS, C. D. & KHORASANIZADEH, S. 2003. Molecular basis for the discrimination of repressive methyl-lysine marks in histone H3 by Polycomb and HP1 chromodomains. *Genes Dev,* 17**,** 1870-81.
FONT-BURGADA, J., ROSSELL, D., AUER, H. & AZORIN, F. 2008. Drosophila HP1c isoform interacts with the zinc-finger proteins WOC and Relative-of-WOC to regulate gene expression. *Genes Dev,* 22**,** 3007-23.
FORCH, P. & VALCARCEL, J. 2003. Splicing regulation in Drosophila sex determination. *Prog Mol Subcell Biol,* 31**,** 127-51.
FORMOSA, T. 2012. The role of FACT in making and breaking nucleosomes. *Biochim Biophys Acta,* 1819**,** 247-55.
FRANK, D., DOENECKE, D. & ALBIG, W. 2003. Differential expression of human replacement and cell cycle dependent H3 histone genes. *Gene,* 312**,** 135-43.
FREY, A., LISTOVSKY, T., GUILBAUD, G., SARKIES, P. & SALE, J. E. 2014. Histone H3.3 is required to maintain replication fork progression after UV damage. *Curr Biol,* 24**,** 2195-2201.
GAL, C., MOORE, K. M., PASZKIEWICZ, K., KENT, N. A. & WHITEHALL, S. K. 2015. The impact of the HIRA histone chaperone upon global nucleosome architecture. *Cell Cycle,* 14**,** 123-34.
GERBERICK, G. F., CRUSE, L. W., MILLER, C. M., SIKORSKI, E. E. & RIDDER, G. M. 1997. Selective modulation of T cell memory markers CD62L and CD44 on murine draining lymph node cells following allergen and irritant treatment. *Toxicol Appl Pharmacol,* 146**,** 1-10.
GIRTON, J. R. & JOHANSEN, K. M. 2008. Chromatin structure and the regulation of gene expression: the lessons of PEV in Drosophila. *Adv Genet,* 61**,** 1-43.
GODFREY, D. I., KENNEDY, J., SUDA, T. & ZLOTNIK, A. 1993. A developmental pathway involving four phenotypically and functionally distinct subsets of CD3-CD4-CD8- triple-negative adult mouse thymocytes defined by CD44 and CD25 expression. *J Immunol,* 150**,** 4244-52.
GOLDBERG, A. D., BANASZYNSKI, L. A., NOH, K. M., LEWIS, P. W., ELSAESSER, S. J., STADLER, S., DEWELL, S., LAW, M., GUO, X., LI, X., WEN, D., CHAPGIER, A., DEKELVER, R. C., MILLER, J. C., LEE, Y. L., BOYDSTON, E. A., HOLMES, M. C., GREGORY, P. D., GREALLY, J. M., RAFII, S., YANG, C., SCAMBLER, P. J., GARRICK, D., GIBBONS, R. J., HIGGS, D. R., CRISTEA, I. M., URNOV, F. D., ZHENG, D. & ALLIS, C. D. 2010. Distinct factors control histone variant H3.3 localization at specific genomic regions. *Cell,* 140**,** 678-91.
GOLDSTEIN, A. M., CHAN, M., HARLAND, M., GILLANDERS, E. M., HAYWARD, N. K., AVRIL, M. F., AZIZI, E., BIANCHI-SCARRA, G., BISHOP, D. T., BRESSAC-DE PAILLERETS, B., BRUNO, W., CALISTA, D., CANNON ALBRIGHT, L. A., DEMENAIS, F., ELDER, D. E., GHIORZO, P., GRUIS, N. A., HANSSON, J., HOGG, D., HOLLAND, E. A., KANETSKY, P. A., KEFFORD, R. F., LANDI, M. T., LANG, J., LEACHMAN, S. A., MACKIE, R. M., MAGNUSSON, V., MANN, G. J., NIENDORF, K., NEWTON BISHOP, J., PALMER, J. M., PUIG, S., PUIG-BUTILLE, J. A., DE SNOO, F. A., STARK, M., TSAO, H., TUCKER, M. A., WHITAKER, L., YAKOBSON, E. & MELANOMA

GENETICS, C. 2006. High-risk melanoma susceptibility genes and pancreatic cancer, neural system tumors, and uveal melanoma across GenoMEL. *Cancer Res,* 66**,** 9818-28.
GROTH, A., ROCHA, W., VERREAULT, A. & ALMOUZNI, G. 2007. Chromatin challenges during DNA replication and repair. *Cell,* 128**,** 721-33.
HA, M., KRAUSHAAR, D. C. & ZHAO, K. 2014. Genome-wide analysis of H3.3 dissociation reveals high nucleosome turnover at distal regulatory regions of embryonic stem cells. *Epigenetics Chromatin,* 7**,** 38.
HAKE, S. B. & ALLIS, C. D. 2006. Histone H3 variants and their potential role in indexing mammalian genomes: the "H3 barcode hypothesis". *Proc Natl Acad Sci U S A,* 103**,** 6428-35.
HAKE, S. B., GARCIA, B. A., KAUER, M., BAKER, S. P., SHABANOWITZ, J., HUNT, D. F. & ALLIS, C. D. 2005. Serine 31 phosphorylation of histone variant H3.3 is specific to regions bordering centromeres in metaphase chromosomes. *Proc Natl Acad Sci U S A,* 102**,** 6344-9.
HAMMARLUND, E., LEWIS, M. W., HANSEN, S. G., STRELOW, L. I., NELSON, J. A., SEXTON, G. J., HANIFIN, J. M. & SLIFKA, M. K. 2003. Duration of antiviral immunity after smallpox vaccination. *Nat Med,* 9**,** 1131-7.
HAN, J. H., ZHOU, H., HORAZDOVSKY, B., ZHANG, K. L., XU, R. M. & ZHANG, Z. G. 2007. Rtt109 acetylates histone H3 lysine 56 and functions in DNA replication. *Science,* 315**,** 653-655.
HARADA, A., OKADA, S., KONNO, D., ODAWARA, J., YOSHIMI, T., YOSHIMURA, S., KUMAMARU, H., SAIWAI, H., TSUBOTA, T., KURUMIZAKA, H., AKASHI, K., TACHIBANA, T., IMBALZANO, A. N. & OHKAWA, Y. 2012. Chd2 interacts with H3.3 to determine myogenic cell fate. *EMBO J,* 31**,** 2994-3007.
HAYAKAWA, T., HARAGUCHI, T., MASUMOTO, H. & HIRAOKA, Y. 2003. Cell cycle behavior of human HP1 subtypes: distinct molecular domains of HP1 are required for their centromeric localization during interphase and metaphase. *J Cell Sci,* 116**,** 3327-38.
HAYDAY, A. C., SAITO, H., GILLIES, S. D., KRANZ, D. M., TANIGAWA, G., EISEN, H. N. & TONEGAWA, S. 1985. Structure, organization, and somatic rearrangement of T cell gamma genes. *Cell,* 40**,** 259-69.
HE, Y., CARRILLO, J. A., LUO, J., DING, Y., TIAN, F., DAVIDSON, I. & SONG, J. 2014. Genome-wide mapping of DNase I hypersensitive sites and association analysis with gene expression in MSB1 cells. *Front Genet,* 5**,** 308.
HENIKOFF, S. & SMITH, M. M. 2015. Histone variants and epigenetics. *Cold Spring Harb Perspect Biol,* 7**,** a019364.
HODGES, E., SMITH, A. D., KENDALL, J., XUAN, Z., RAVI, K., ROOKS, M., ZHANG, M. Q., YE, K., BHATTACHARJEE, A., BRIZUELA, L., MCCOMBIE, W. R., WIGLER, M., HANNON, G. J. & HICKS, J. B. 2009. High definition profiling of mammalian DNA methylation by array capture and single molecule bisulfite sequencing. *Genome Res,* 19**,** 1593-605.
HÖFLINGER, S., KESAVAN, K., FUXA, M., HUTTER, C., HEAVEY, B., RADTKE, F. & BUSSLINGER, M. 2004. *Analysis of Notch1 Function by In Vitro T Cell Differentiation of Pax5 Mutant Lymphoid Progenitors*.
HORSLEY, D., HUTCHINGS, A., BUTCHER, G. W. & SINGH, P. B. 1996. M32, a murine homologue of Drosophila heterochromatin protein 1 (HP1), localises to euchromatin within interphase nuclei and is largely excluded from constitutive heterochromatin. *Cytogenet Cell Genet,* 73**,** 308-11.
HUBNER, M. R., ECKERSLEY-MASLIN, M. A. & SPECTOR, D. L. 2013. Chromatin organization and transcriptional regulation. *Curr Opin Genet Dev,* 23**,** 89-95.
HUISINGA, K. L., BROWER-TOLAND, B. & ELGIN, S. C. 2006. The contradictory definitions of heterochromatin: transcription and silencing. *Chromosoma,* 115**,** 110-22.
IMBEAULT, M., HELLEBOID, P.-Y. & TRONO, D. 2017. KRAB zinc-finger proteins contribute to the evolution of gene regulatory networks. *Nature,* 543**,** 550.
INGOUFF, M., RADEMACHER, S., HOLEC, S., SOLJIC, L., XIN, N., READSHAW, A., FOO, S. H., LAHOUZE, B., SPRUNCK, S. & BERGER, F. 2010. Zygotic resetting of the HISTONE 3 variant repertoire participates in epigenetic reprogramming in Arabidopsis. *Curr Biol,* 20**,** 2137-43.
ITOH, Y., MELAMED, E., YANG, X., KAMPF, K., WANG, S., YEHYA, N., VAN NAS, A., REPLOGLE, K., BAND, M. R., CLAYTON, D. F., SCHADT, E. E., LUSIS, A. J. & ARNOLD, A. P. 2007. Dosage compensation is less effective in birds than in mammals. *J Biol,* 6**,** 2.
J. MOTICKA, E. 2016. Chapter 2. Hallmarks of the Adaptive Immune Responses.
JACOB, Y., BERGAMIN, E., DONOGHUE, M. T., MONGEON, V., LEBLANC, C., VOIGT, P., UNDERWOOD, C. J., BRUNZELLE, J. S., MICHAELS, S. D., REINBERG, D., COUTURE, J. F. & MARTIENSSEN, R. A. 2014. Selective methylation of histone H3 variant H3.1 regulates heterochromatin replication. *Science,* 343**,** 1249-53.
JACOBS, S. A. & KHORASANIZADEH, S. 2002. Structure of HP1 chromodomain bound to a lysine 9-methylated histone H3 tail. *Science,* 295**,** 2080-3.

JANG, C. W., SHIBATA, Y., STARMER, J., YEE, D. & MAGNUSON, T. 2015a. Histone H3.3 maintains genome integrity during mammalian development. *Genes & Development,* 29**,** 1377-1392.
JANG, C. W., SHIBATA, Y., STARMER, J., YEE, D. & MAGNUSON, T. 2015b. Histone H3.3 maintains genome integrity during mammalian development. *Genes Dev,* 29**,** 1377-92.
JENUWEIN, T. & ALLIS, C. D. 2001. Translating the histone code. *Science,* 293**,** 1074-80.
JIANG, C. & PUGH, B. F. 2009. Nucleosome positioning and gene regulation: advances through genomics. *Nat Rev Genet,* 10**,** 161-72.
JIANG, W. Q., NGUYEN, A., CAO, Y., CHANG, A. C. & REDDEL, R. R. 2011. HP1-mediated formation of alternative lengthening of telomeres-associated PML bodies requires HIRA but not ASF1a. *PLoS One,* 6**,** e17036.
JIAO, Y., SHI, C., EDIL, B. H., DE WILDE, R. F., KLIMSTRA, D. S., MAITRA, A., SCHULICK, R. D., TANG, L. H., WOLFGANG, C. L., CHOTI, M. A., VELCULESCU, V. E., DIAZ, L. A., JR., VOGELSTEIN, B., KINZLER, K. W., HRUBAN, R. H. & PAPADOPOULOS, N. 2011. DAXX/ATRX, MEN1, and mTOR pathway genes are frequently altered in pancreatic neuroendocrine tumors. *Science,* 331**,** 1199-203.
JIN, C. & FELSENFELD, G. 2006. Distribution of histone H3.3 in hematopoietic cell lineages. *Proc Natl Acad Sci U S A,* 103**,** 574-9.
JIN, C. & FELSENFELD, G. 2007. Nucleosome stability mediated by histone variants H3.3 and H2A.Z. *Genes Dev,* 21**,** 1519-29.
JIN, C., ZANG, C., WEI, G., CUI, K., PENG, W., ZHAO, K. & FELSENFELD, G. 2009. H3.3/H2A.Z double variant-containing nucleosomes mark 'nucleosome-free regions' of active promoters and other regulatory regions. *Nat Genet,* 41**,** 941-5.
JOHNSON, K., PFLUGH, D. L., YU, D., HESSLEIN, D. G., LIN, K. I., BOTHWELL, A. L., THOMAS-TIKHONENKO, A., SCHATZ, D. G. & CALAME, K. 2004. B cell-specific loss of histone 3 lysine 9 methylation in the V(H) locus depends on Pax5. *Nat Immunol,* 5**,** 853-61.
JONES, D. O., COWELL, I. G. & SINGH, P. B. 2000. Mammalian chromodomain proteins: their role in genome organisation and expression. *Bioessays,* 22**,** 124-37.
JONES, D. O., MATTEI, M. G., HORSLEY, D., COWELL, I. G. & SINGH, P. B. 2001. The gene and pseudogenes of Cbx3/mHP1 gamma. *DNA Seq,* 12**,** 147-60.
JONES, J. M., BHATTACHARYYA, A., SIMKUS, C., VALLIERES, B., VEENSTRA, T. D. & ZHOU, M. 2011. The RAG1 V(D)J recombinase/ubiquitin ligase promotes ubiquitylation of acetylated, phosphorylated histone 3.3. *Immunol Lett,* 136**,** 156-62.
JONES, M. E. & ZHUANG, Y. 2007. Acquisition of a functional T cell receptor during T lymphocyte development is enforced by HEB and E2A transcription factors. *Immunity,* 27**,** 860-70.
KAECH, S. M. & CUI, W. 2012. Transcriptional control of effector and memory CD8+ T cell differentiation. *Nat Rev Immunol,* 12**,** 749-61.
KAMADA, R., YANG, W., ZHANG, Y., PATEL, M. C., YANG, Y., OUDA, R., DEY, A., WAKABAYASHI, Y., SAKAGUCHI, K., FUJITA, T., TAMURA, T., ZHU, J. & OZATO, K. 2018. Interferon stimulation creates chromatin marks and establishes transcriptional memory. *Proc Natl Acad Sci U S A,* 115**,** E9162-E9171.
KAMAKAKA, R. T. & BIGGINS, S. 2005. Histone variants: deviants? *Genes Dev,* 19**,** 295-310.
KAMIJO, T., ZINDY, F., ROUSSEL, M. F., QUELLE, D. E., DOWNING, J. R., ASHMUN, R. A., GROSVELD, G. & SHERR, C. J. 1997. Tumor suppression at the mouse INK4a locus mediated by the alternative reading frame product p19ARF. *Cell,* 91**,** 649-59.
KANITZ, A., GYPAS, F., GRUBER, A. J., GRUBER, A. R., MARTIN, G. & ZAVOLAN, M. 2015. Comparative assessment of methods for the computational inference of transcript isoform abundance from RNA-seq data. *Genome Biol,* 16**,** 150.
KASSIS, J. A., KENNISON, J. A. & TAMKUN, J. W. 2017. Polycomb and Trithorax Group Genes in Drosophila. *Genetics,* 206**,** 1699-1725.
KAUFMAN, P. D., KOBAYASHI, R., KESSLER, N. & STILLMAN, B. 1995. The p150 and p60 subunits of chromatin assembly factor I: a molecular link between newly synthesized histones and DNA replication. *Cell,* 81**,** 1105-14.
KELLEY, R. I., ZACKAI, E. H., EMANUEL, B. S., KISTENMACHER, M., GREENBERG, F. & PUNNETT, H. H. 1982. The association of the DiGeorge anomalad with partial monosomy of chromosome 22. *J Pediatr,* 101**,** 197-200.
KHAN, D. H., JAHAN, S. & DAVIE, J. R. 2012. Pre-mRNA splicing: role of epigenetics and implications in disease. *Adv Biol Regul,* 52**,** 377-88.
KIM, H., HEO, K., CHOI, J., KIM, K. & AN, W. 2011. Histone variant H3.3 stimulates HSP70 transcription through cooperation with HP1gamma. *Nucleic Acids Res,* 39**,** 8329-41.

KNEZETIC, J. A. & LUSE, D. S. 1986. The presence of nucleosomes on a DNA template prevents initiation by RNA polymerase II in vitro. *Cell,* 45**,** 95-104.
KOLASINSKA-ZWIERZ, P., DOWN, T., LATORRE, I., LIU, T., LIU, X. S. & AHRINGER, J. 2009. Differential chromatin marking of introns and expressed exons by H3K36me3. *Nat Genet,* 41**,** 376-81.
KORNBLIHTT, A. R., DE LA MATA, M., FEDEDA, J. P., MUNOZ, M. J. & NOGUES, G. 2004. Multiple links between transcription and splicing. *RNA,* 10**,** 1489-98.
KORNBLIHTT, A. R., SCHOR, I. E., ALLO, M. & BLENCOWE, B. J. 2009. When chromatin meets splicing. *Nat Struct Mol Biol,* 16**,** 902-3.
KORNBLIHTT, A. R., SCHOR, I. E., ALLO, M., DUJARDIN, G., PETRILLO, E. & MUNOZ, M. J. 2013a. Alternative splicing: a pivotal step between eukaryotic transcription and translation (vol 14, pg 153, 2013). *Nature Reviews Molecular Cell Biology,* 14.
KORNBLIHTT, A. R., SCHOR, I. E., ALLÓ, M., DUJARDIN, G., PETRILLO, E. & MUÑOZ, M. J. 2013b. Alternative splicing: a pivotal step between eukaryotic transcription and translation. *Nature Reviews Molecular Cell Biology,* 14**,** 153.
KOUZARIDES, T. 2007. Chromatin modifications and their function. *Cell,* 128**,** 693-705.
KRISHNAMURTHY, J., RAMSEY, M. R., LIGON, K. L., TORRICE, C., KOH, A., BONNER-WEIR, S. & SHARPLESS, N. E. 2006. p16INK4a induces an age-dependent decline in islet regenerative potential. *Nature,* 443**,** 453-7.
KULAEVA, O. I., GAYKALOVA, D. A. & STUDITSKY, V. M. 2007. Transcription through chromatin by RNA polymerase II: histone displacement and exchange. *Mutat Res,* 618**,** 116-29.
KUO, T. C. & SCHLISSEL, M. S. 2009. Mechanisms controlling expression of the RAG locus during lymphocyte development. *Curr Opin Immunol,* 21**,** 173-8.
L DORMANN, H., TSENG, B. S., ALLIS, C., FUNABIKI, H. & FISCHLE, W. 2007. *Dynamic Regulation of Effector Protein Binding to Histone Modifications: The Biology of HP1 Switching*.
LACHNER, M., O'CARROLL, D., REA, S., MECHTLER, K. & JENUWEIN, T. 2001. Methylation of histone H3 lysine 9 creates a binding site for HP1 proteins. *Nature,* 410**,** 116-20.
LAKY, K., FLEISCHACKER, C. & FOWLKES, B. 2006. *TCR and notch signaling in CD4 and CD8 T-cell development*.
LAKY, K. & FOWLKES, B. J. 2008. Notch signaling in CD4 and CD8 T cell development. *Curr Opin Immunol,* 20**,** 197-202.
LAN, F. & SHI, Y. 2009. Epigenetic regulation: methylation of histone and non-histone proteins. *Sci China C Life Sci,* 52**,** 311-22.
LAU, C. M., ADAMS, N. M., GEARY, C. D., WEIZMAN, O. E., RAPP, M., PRITYKIN, Y., LESLIE, C. S. & SUN, J. C. 2018. Epigenetic control of innate and adaptive immune memory. *Nat Immunol,* 19**,** 963-972.
LAW, P.-P., CHAN, P.-K., MCEWEN, K., ZHI, H., LIANG, B., NARUSE, C., ASANO, M., TAN-UN, K.-C., CHAN, G. C.-F. & FESTENSTEIN, R. 2019. Sex differences in gene expression and proliferation are dependent on the epigenetic modifier HP1γ. *bioRxiv***,** 563940.
LAW, P. P. 2015. *Investigation into the role of heterochromatin protein 1 gamma (HP1γ) in gene regulation in mammals*
Authors: *Law, Pui Pik.* PhD PhD, Imperial College London.
LEE, D. H., RYU, H. W., KIM, G. W. & KWON, S. H. 2019. Comparison of three heterochromatin protein 1 homologs in Drosophila. *J Cell Sci,* 132.
LEMOS, B., BRANCO, A. T. & HARTL, D. L. 2010. Epigenetic effects of polymorphic Y chromosomes modulate chromatin components, immune response, and sexual conflict. *Proc Natl Acad Sci U S A,* 107**,** 15826-31.
LEROY, G., WESTON, J. T., ZEE, B. M., YOUNG, N. L., PLAZAS-MAYORCA, M. D. & GARCIA, B. A. 2009. Heterochromatin protein 1 is extensively decorated with histone code-like post-translational modifications. *Mol Cell Proteomics,* 8**,** 2432-42.
LEWIS, P. W., ELSAESSER, S. J., NOH, K. M., STADLER, S. C. & ALLIS, C. D. 2010. Daxx is an H3.3-specific histone chaperone and cooperates with ATRX in replication-independent chromatin assembly at telomeres. *Proc Natl Acad Sci U S A,* 107**,** 14075-80.
LI, J., POI, M. J. & TSAI, M. D. 2011. Regulatory mechanisms of tumor suppressor P16(INK4A) and their relevance to cancer. *Biochemistry,* 50**,** 5566-82.
LISTERMAN, I., SAPRA, A. K. & NEUGEBAUER, K. M. 2006. Cotranscriptional coupling of splicing factor recruitment and precursor messenger RNA splicing in mammalian cells. *Nat Struct Mol Biol,* 13**,** 815-22.
LIU, L. P., NI, J. Q., SHI, Y. D., OAKELEY, E. J. & SUN, F. L. 2005. Sex-specific role of Drosophila melanogaster HP1 in regulating chromatin structure and gene transcription. *Nat Genet,* 37**,** 1361-6.
LOMBERK, G., BENSI, D., FERNANDEZ-ZAPICO, M. E. & URRUTIA, R. 2006a. Evidence for the existence of an HP1-mediated subcode within the histone code. *Nat Cell Biol,* 8**,** 407-15.

LOMBERK, G., WALLRATH, L. & URRUTIA, R. 2006b. The Heterochromatin Protein 1 family. *Genome Biol,* 7**,** 228.
LOOMIS, R. J., NAOE, Y., PARKER, J. B., SAVIC, V., BOZOVSKY, M. R., MACFARLAN, T., MANLEY, J. L. & CHAKRAVARTI, D. 2009. Chromatin binding of SRp20 and ASF/SF2 and dissociation from mitotic chromosomes is modulated by histone H3 serine 10 phosphorylation. *Mol Cell,* 33**,** 450-61.
LOPPIN, B., BONNEFOY, E., ANSELME, C., LAURENCON, A., KARR, T. L. & COUBLE, P. 2005. The histone H3.3 chaperone HIRA is essential for chromatin assembly in the male pronucleus. *Nature,* 437**,** 1386-90.
LORAIN, S., DEMCZUK, S., LAMOUR, V., TOTH, S., AURIAS, A., ROE, B. A. & LIPINSKI, M. 1996. Structural Organization of the WD repeat protein-encoding gene HIRA in the DiGeorge syndrome critical region of human chromosome 22. *Genome Res,* 6**,** 43-50.
LOYOLA, A. & ALMOUZNI, G. 2007. Marking histone H3 variants: how, when and why? *Trends Biochem Sci,* 32**,** 425-33.
LOYOLA, A., BONALDI, T., ROCHE, D., IMHOF, A. & ALMOUZNI, G. 2006. PTMs on H3 variants before chromatin assembly potentiate their final epigenetic state. *Mol Cell,* 24**,** 309-16.
LUCO, R. F., ALLO, M., SCHOR, I. E., KORNBLIHTT, A. R. & MISTELI, T. 2011. Epigenetics in alternative pre-mRNA splicing. *Cell,* 144**,** 16-26.
LUCO, R. F., PAN, Q., TOMINAGA, K., BLENCOWE, B. J., PEREIRA-SMITH, O. M. & MISTELI, T. 2010. Regulation of alternative splicing by histone modifications. *Science,* 327**,** 996-1000.
LUND, E. G., COLLAS, P. & DELBARRE, E. 2015a. Transcription outcome of promoters enriched in histone variant H3.3 defined by positioning of H3.3 and local chromatin marks. *Biochemical and Biophysical Research Communications,* 460**,** 348-353.
LUND, E. G., COLLAS, P. & DELBARRE, E. 2015b. Transcription outcome of promoters enriched in histone variant H3.3 defined by positioning of H3.3 and local chromatin marks. *Biochem Biophys Res Commun,* 460**,** 348-53.
MACALPINE, D. M. & ALMOUZNI, G. 2013. Chromatin and DNA replication. *Cold Spring Harb Perspect Biol,* 5**,** a010207.
MAISON, C. & ALMOUZNI, G. 2004. HP1 and the dynamics of heterochromatin maintenance. *Nat Rev Mol Cell Biol,* 5**,** 296-304.
MALHOTRA, V., SERAFINI, T., ORCI, L., SHEPHERD, J. C. & ROTHMAN, J. E. 1989. Purification of a novel class of coated vesicles mediating biosynthetic protein transport through the Golgi stack. *Cell,* 58**,** 329-36.
MARINO-RAMIREZ, L., KANN, M. G., SHOEMAKER, B. A. & LANDSMAN, D. 2005. Histone structure and nucleosome stability. *Expert Rev Proteomics,* 2**,** 719-29.
MARZLUFF, W. F., WAGNER, E. J. & DURONIO, R. J. 2008. Metabolism and regulation of canonical histone mRNAs: life without a poly(A) tail. *Nat Rev Genet,* 9**,** 843-54.
MATEESCU, B., BOURACHOT, B., RACHEZ, C., OGRYZKO, V. & MUCHARDT, C. 2008. Regulation of an inducible promoter by an HP1beta-HP1gamma switch. *EMBO Rep,* 9**,** 267-72.
MAZE, I., WENDERSKI, W., NOH, K. M., BAGOT, R. C., TZAVARAS, N., PURUSHOTHAMAN, I., ELSASSER, S. J., GUO, Y., IONETE, C., HURD, Y. L., TAMMINGA, C. A., HALENE, T., FARRELLY, L., SOSHNEV, A. A., WEN, D., RAFII, S., BIRTWISTLE, M. R., AKBARIAN, S., BUCHHOLZ, B. A., BLITZER, R. D., NESTLER, E. J., YUAN, Z. F., GARCIA, B. A., SHEN, L., MOLINA, H. & ALLIS, C. D. 2015. Critical Role of Histone Turnover in Neuronal Transcription and Plasticity. *Neuron,* 87**,** 77-94.
MCELREAVEY, K. D., VILAIN, E., BOUCEKKINE, C., VIDAUD, M., JAUBERT, F., RICHAUD, F. & FELLOUS, M. 1992. XY sex reversal associated with a nonsense mutation in SRY. *Genomics,* 13**,** 838-40.
MEHTA, S. & JEFFREY, K. L. 2015. Beyond receptors and signaling: epigenetic factors in the regulation of innate immunity. *Immunol Cell Biol,* 93**,** 233-44.
MELLO, J. A. & ALMOUZNI, G. 2001. The ins and outs of nucleosome assembly. *Curr Opin Genet Dev,* 11**,** 136-41.
MERSCHER, S., FUNKE, B., EPSTEIN, J. A., HEYER, J., PUECH, A., LU, M. M., XAVIER, R. J., DEMAY, M. B., RUSSELL, R. G., FACTOR, S., TOKOOYA, K., JORE, B. S., LOPEZ, M., PANDITA, R. K., LIA, M., CARRION, D., XU, H., SCHORLE, H., KOBLER, J. B., SCAMBLER, P., WYNSHAW-BORIS, A., SKOULTCHI, A. I., MORROW, B. E. & KUCHERLAPATI, R. 2001. TBX1 is responsible for cardiovascular defects in velo-cardio-facial/DiGeorge syndrome. *Cell,* 104**,** 619-29.
MINC, E., ALLORY, Y., WORMAN, H. J., COURVALIN, J. C. & BUENDIA, B. 1999. Localization and phosphorylation of HP1 proteins during the cell cycle in mammalian cells. *Chromosoma,* 108**,** 220-34.
MINC, E., COURVALIN, J. C. & BUENDIA, B. 2000. HP1gamma associates with euchromatin and heterochromatin in mammalian nuclei and chromosomes. *Cytogenet Cell Genet,* 90**,** 279-84.

MIRABELLA, F., BAXTER, E. W., BOISSINOT, M., JAMES, S. R. & COCKERILL, P. N. 2010. The human IL-3/granulocyte-macrophage colony-stimulating factor locus is epigenetically silent in immature thymocytes and is progressively activated during T cell development. *J Immunol,* 184**,** 3043-54.

MIRZAYANS, R., ANDRAIS, B., HANSEN, G. & MURRAY, D. 2012. Role of p16(INK4A) in Replicative Senescence and DNA Damage-Induced Premature Senescence in p53-Deficient Human Cells. *Biochem Res Int,* 2012**,** 951574.

MITO, Y., HENIKOFF, J. G. & HENIKOFF, S. 2005a. Genome-scale profiling of histone H3.3 replacement patterns. *Nat Genet,* 37**,** 1090-7.

MITO, Y., HENIKOFF, J. G. & HENIKOFF, S. 2005b. Genome-scale profiling of histone H3.3 replacement patterns. *Nature Genetics,* 37**,** 1090-1097.

MOOSAVI, A. & MOTEVALIZADEH ARDEKANI, A. 2016. Role of Epigenetics in Biology and Human Diseases. *Iran Biomed J,* 20**,** 246-58.

NAEIM, F. 2013. *Atlas of hematopathology : morphology, immunophenotype, cytogenetics, and molecular approaches,* London, Academic Press.

NAHKURI, S., TAFT, R. J. & MATTICK, J. S. 2009. Nucleosomes are preferentially positioned at exons in somatic and sperm cells. *Cell Cycle,* 8**,** 3420-4.

NAKAYAMA, M. 2014. Antigen Presentation by MHC-Dressed Cells. *Front Immunol,* 5**,** 672.

NARUSE, C., FUKUSUMI, Y., KAKIUCHI, D. & ASANO, M. 2007. A novel gene trapping for identifying genes expressed under the control of specific transcription factors. *Biochem Biophys Res Commun,* 361**,** 109-15.

NASHUN, B., HILL, P. W., SMALLWOOD, S. A., DHARMALINGAM, G., AMOUROUX, R., CLARK, S. J., SHARMA, V., NDJETEHE, E., PELCZAR, P., FESTENSTEIN, R. J., KELSEY, G. & HAJKOVA, P. 2015a. Continuous Histone Replacement by Hira Is Essential for Normal Transcriptional Regulation and De Novo DNA Methylation during Mouse Oogenesis. *Mol Cell,* 60**,** 611-25.

NASHUN, B., HILL, P. W., SMALLWOOD, S. A., DHARMALINGAM, G., AMOUROUX, R., CLARK, S. J., SHARMA, V., NDJETEHE, E., PELCZAR, P., FESTENSTEIN, R. J., KELSEY, G. & HAJKOVA, P. 2015b. Continuous Histone Replacement by Hira Is Essential for Normal Transcriptional Regulation and De Novo DNA Methylation during Mouse Oogenesis. *Mol Cell*.

NG, R. K. & GURDON, J. B. 2008. Epigenetic memory of an active gene state depends on histone H3.3 incorporation into chromatin in the absence of transcription. *Nat Cell Biol,* 10**,** 102-9.

NG, S. S., YUE, W. W., OPPERMANN, U. & KLOSE, R. J. 2009. Dynamic protein methylation in chromatin biology. *Cell Mol Life Sci,* 66**,** 407-22.

NIE, X., WANG, H., LI, J., HOLEC, S. & BERGER, F. 2014. The HIRA complex that deposits the histone H3.3 is conserved in Arabidopsis and facilitates transcriptional dynamics. *Biol Open,* 3**,** 794-802.

NIELSEN, A. L., ORTIZ, J. A., YOU, J., OULAD-ABDELGHANI, M., KHECHUMIAN, R., GANSMULLER, A., CHAMBON, P. & LOSSON, R. 1999. Interaction with members of the heterochromatin protein 1 (HP1) family and histone deacetylation are differentially involved in transcriptional silencing by members of the TIF1 family. *EMBO J,* 18**,** 6385-95.

NIELSEN, A. L., OULAD-ABDELGHANI, M., ORTIZ, J. A., REMBOUTSIKA, E., CHAMBON, P. & LOSSON, R. 2001. Heterochromatin formation in mammalian cells: interaction between histones and HP1 proteins. *Mol Cell,* 7**,** 729-39.

NORWOOD, L. E., GRADE, S. K., CRYDERMAN, D. E., HINES, K. A., FURIASSE, N., TORO, R., LI, Y., DHASARATHY, A., KLADDE, M. P., HENDRIX, M. J., KIRSCHMANN, D. A. & WALLRATH, L. L. 2004. Conserved properties of HP1(Hsalpha). *Gene,* 336**,** 37-46.

O'REILLY, L., HARRIS, A. W. & STRASSER, A. 1997. *Bcl-2 transgene expression promotes survival and reduces proliferation of CD3-CD4-CD8-T cell progenitors*.

OETTINGER, M. A., SCHATZ, D. G., GORKA, C. & BALTIMORE, D. 1990. RAG-1 and RAG-2, adjacent genes that synergistically activate V(D)J recombination. *Science,* 248**,** 1517-23.

OHSUGI, T. 2013. A transgenic mouse model of human T cell leukemia virus type 1-associated diseases. *Front Microbiol,* 4**,** 49.

OKI, M., AIHARA, H. & ITO, T. 2007. Role of histone phosphorylation in chromatin dynamics and its implications in diseases. *Subcell Biochem,* 41**,** 319-36.

OMILUSIK, K. D. & GOLDRATH, A. W. 2017. The origins of memory T cells. *Nature,* 552**,** 337-339.

OSLEY, M. A. 1991. The regulation of histone synthesis in the cell cycle. *Annu Rev Biochem,* 60**,** 827-61.

PALMER, E. 2003. Negative selection--clearing out the bad apples from the T-cell repertoire. *Nat Rev Immunol,* 3**,** 383-91.

PAPAIOANNOU, V. E. & SILVER, L. M. 1998. The T-box gene family. *Bioessays,* 20**,** 9-19.

PENNOCK, N. D., WHITE, J. T., CROSS, E. W., CHENEY, E. E., TAMBURINI, B. A. & KEDL, R. M. 2013. T cell responses: naive to memory and everything in between. *Adv Physiol Educ,* 37**,** 273-83.

PHOENIX, C. H., GOY, R. W., GERALL, A. A. & YOUNG, W. C. 1959. Organizing action of prenatally administered testosterone propionate on the tissues mediating mating behavior in the female guinea pig. *Endocrinology,* 65**,** 369-82.

PIACENTINI, L., FANTI, L., NEGRI, R., DEL VESCOVO, V., FATICA, A., ALTIERI, F. & PIMPINELLI, S. 2009. Heterochromatin protein 1 (HP1a) positively regulates euchromatic gene expression through RNA transcript association and interaction with hnRNPs in Drosophila. *PLoS Genet,* 5**,** e1000670.

PIACENTINI, L. & PIMPINELLI, S. 2010. Positive regulation of euchromatic gene expression by HP1. *Fly (Austin),* 4**,** 299-301.

PLANELLS, B., GÓMEZ-REDONDO, I., PERICUESTA, E., LONERGAN, P. & GUTIÉRREZ-ADÁN, A. 2019. Differential isoform expression and alternative splicing in sex determination in mice. *BMC Genomics,* 20**,** 202.

POLO, S. E. 2015. Reshaping chromatin after DNA damage: the choreography of histone proteins. *J Mol Biol,* 427**,** 626-36.

POLO, S. E. & JACKSON, S. P. 2011. Dynamics of DNA damage response proteins at DNA breaks: a focus on protein modifications. *Genes & Development,* 25**,** 409-433.

PRIYADHARSCINI, R. A. & SABARINATH, T. 2013. Barr bodies in sex determination. *J Forensic Dent Sci,* 5**,** 64-7.

QUELLE, D. E., ASHMUN, R. A., HANNON, G. J., REHBERGER, P. A., TRONO, D., RICHTER, K. H., WALKER, C., BEACH, D., SHERR, C. J. & SERRANO, M. 1995. Cloning and characterization of murine p16INK4a and p15INK4b genes. *Oncogene,* 11**,** 635-45.

RACHEZ, C., LEGENDRE, R., COSTALLAT, M., VARET, H., YI, J., KORNOBIS, E., PROUX, C. & MUCHARDT, C. 2019. An impact of HP1γ on the fidelity of pre-mRNA splicing arises from its ability to bind RNA via intronic repeated sequences. *bioRxiv***,** 686790.

RAI, T. S., COLE, J. J., NELSON, D. M., DIKOVSKAYA, D., FALLER, W. J., VIZIOLI, M. G., HEWITT, R. N., ANANNYA, O., MCBRYAN, T., MANOHARAN, I., VAN TUYN, J., MORRICE, N., PCHELINTSEV, N. A., IVANOV, A., BROCK, C., DROTAR, M. E., NIXON, C., CLARK, W., SANSOM, O. J., ANDERSON, K. I., KING, A., BLYTH, K. & ADAMS, P. D. 2014. HIRA orchestrates a dynamic chromatin landscape in senescence and is required for suppression of neoplasia. *Genes Dev,* 28**,** 2712-25.

RAI, T. S., PURI, A., MCBRYAN, T., HOFFMAN, J., TANG, Y., PCHELINTSEV, N. A., VAN TUYN, J., MARMORSTEIN, R., SCHULTZ, D. C. & ADAMS, P. D. 2011. Human CABIN1 is a functional member of the human HIRA/UBN1/ASF1a histone H3.3 chaperone complex. *Mol Cell Biol,* 31**,** 4107-18.

RATTNER, J. B. & LIN, C. C. 1985. Radial loops and helical coils coexist in metaphase chromosomes. *Cell,* 42**,** 291-6.

RAY-GALLET, D., WOOLFE, A., VASSIAS, I., PELLENTZ, C., LACOSTE, N., PURI, A., SCHULTZ, D. C., PCHELINTSEV, N. A., ADAMS, P. D., JANSEN, L. E. & ALMOUZNI, G. 2011a. Dynamics of histone H3 deposition in vivo reveal a nucleosome gap-filling mechanism for H3.3 to maintain chromatin integrity. *Mol Cell,* 44**,** 928-41.

RAY-GALLET, D., WOOLFE, A., VASSIAS, I., PELLENTZ, C., LACOSTE, N., PURI, A., SCHULTZ, D. C., PCHELINTSEV, N. L. A., ADAMS, P. D., JANSEN, L. E. T. & ALMOUZNI, G. 2011b. Dynamics of Histone H3 Deposition In Vivo Reveal a Nucleosome Gap-Filling Mechanism for H3.3 to Maintain Chromatin Integrity. *Molecular Cell,* 44**,** 928-941.

RICKETTS, M. D. & MARMORSTEIN, R. 2017. A Molecular Prospective for HIRA Complex Assembly and H3.3-Specific Histone Chaperone Function. *J Mol Biol,* 429**,** 1924-1933.

RIGBY, N. & KULATHINAL, R. J. 2015. Genetic Architecture of Sexual Dimorphism in Humans. *J Cell Physiol,* 230**,** 2304-10.

RINN, J. L. & SNYDER, M. 2005. Sexual dimorphism in mammalian gene expression. *Trends Genet,* 21**,** 298-305.

ROBERTS, C., SUTHERLAND, H. F., FARMER, H., KIMBER, W., HALFORD, S., CAREY, A., BRICKMAN, J. M., WYNSHAW-BORIS, A. & SCAMBLER, P. J. 2002. Targeted mutagenesis of the Hira gene results in gastrulation defects and patterning abnormalities of mesoendodermal derivatives prior to early embryonic lethality. *Mol Cell Biol,* 22**,** 2318-28.

ROTH, D. B. 2014. V(D)J Recombination: Mechanism, Errors, and Fidelity. *Microbiol Spectr,* 2.

ROTHENBERG, E. V. & ZHANG, J. A. 2012. T-cell identity and epigenetic memory. *Curr Top Microbiol Immunol,* 356**,** 117-43.

RUFIANGE, A., JACQUES, P. E., BHAT, W., ROBERT, F. & NOURANI, A. 2007. Genome-wide replication-independent histone H3 exchange occurs predominantly at promoters and implicates H3 K56 acetylation and Asf1. *Mol Cell,* 27**,** 393-405.

RYU, H. W., LEE, D. H., FLORENS, L., SWANSON, S. K., WASHBURN, M. P. & KWON, S. H. 2014. Analysis of the heterochromatin protein 1 (HP1) interactome in Drosophila. *J Proteomics,* 102**,** 137-47.
SAINT-ANDRE, V., BATSCHE, E., RACHEZ, C. & MUCHARDT, C. 2011. Histone H3 lysine 9 trimethylation and HP1gamma favor inclusion of alternative exons. *Nat Struct Mol Biol,* 18**,** 337-44.
SAINT-ANDRÉ, V., BATSCHÉ, E., RACHEZ, C. & MUCHARDT, C. 2011. Histone H3 lysine 9 trimethylation and HP1γ favor inclusion of alternative exons. *Nature Structural &Amp; Molecular Biology,* 18**,** 337.
SAKAI, A., SCHWARTZ, B. E., GOLDSTEIN, S. & AHMAD, K. 2009. Transcriptional and developmental functions of the H3.3 histone variant in Drosophila. *Curr Biol,* 19**,** 1816-20.
SAKAMOTO, H., INOUE, K., HIGUCHI, I., ONO, Y. & SHIMURA, Y. 1992. Control of Drosophila Sex-lethal pre-mRNA splicing by its own female-specific product. *Nucleic Acids Res,* 20**,** 5533-40.
SAMBANDAM, A., MAILLARD, I., ZEDIAK, V. P., XU, L., GERSTEIN, R. M., ASTER, J. C., PEAR, W. S. & BHANDOOLA, A. 2005. Notch signaling controls the generation and differentiation of early T lineage progenitors. *Nat Immunol,* 6**,** 663-70.
SANTENARD, A. & TORRES-PADILLA, M. E. 2009. Epigenetic reprogramming in mammalian reproduction: contribution from histone variants. *Epigenetics,* 4**,** 80-4.
SARAI, N., NIMURA, K., TAMURA, T., KANNO, T., PATEL, M. C., HEIGHTMAN, T. D., URA, K. & OZATO, K. 2013. WHSC1 links transcription elongation to HIRA-mediated histone H3.3 deposition. *EMBO J,* 32**,** 2392-406.
SCHMITT, T. M., CIOFANI, M., PETRIE, H. T. & ZUNIGA-PFLUCKER, J. C. 2004. Maintenance of T cell specification and differentiation requires recurrent notch receptor-ligand interactions. *J Exp Med,* 200**,** 469-79.
SCHNEIDERMAN, J. I., ORSI, G. A., HUGHES, K. T., LOPPIN, B. & AHMAD, K. 2012. Nucleosome-depleted chromatin gaps recruit assembly factors for the H3.3 histone variant. *Proceedings of the National Academy of Sciences of the United States of America,* 109**,** 19721-19726.
SCHUTT, C. & NOTHIGER, R. 2000. Structure, function and evolution of sex-determining systems in Dipteran insects. *Development,* 127**,** 667-77.
SCHWARTZENTRUBER, J., KORSHUNOV, A., LIU, X. Y., JONES, D. T., PFAFF, E., JACOB, K., STURM, D., FONTEBASSO, A. M., QUANG, D. A., TONJES, M., HOVESTADT, V., ALBRECHT, S., KOOL, M., NANTEL, A., KONERMANN, C., LINDROTH, A., JAGER, N., RAUSCH, T., RYZHOVA, M., KORBEL, J. O., HIELSCHER, T., HAUSER, P., GARAMI, M., KLEKNER, A., BOGNAR, L., EBINGER, M., SCHUHMANN, M. U., SCHEURLEN, W., PEKRUN, A., FRUHWALD, M. C., ROGGENDORF, W., KRAMM, C., DURKEN, M., ATKINSON, J., LEPAGE, P., MONTPETIT, A., ZAKRZEWSKA, M., ZAKRZEWSKI, K., LIBERSKI, P. P., DONG, Z., SIEGEL, P., KULOZIK, A. E., ZAPATKA, M., GUHA, A., MALKIN, D., FELSBERG, J., REIFENBERGER, G., VON DEIMLING, A., ICHIMURA, K., COLLINS, V. P., WITT, H., MILDE, T., WITT, O., ZHANG, C., CASTELO-BRANCO, P., LICHTER, P., FAURY, D., TABORI, U., PLASS, C., MAJEWSKI, J., PFISTER, S. M. & JABADO, N. 2012. Driver mutations in histone H3.3 and chromatin remodelling genes in paediatric glioblastoma. *Nature,* 482**,** 226-31.
SEITAN, V. C., HAO, B., TACHIBANA-KONWALSKI, K., LAVAGNOLLI, T., MIRA-BONTENBAL, H., BROWN, K. E., TENG, G., CARROLL, T., TERRY, A., HORAN, K., MARKS, H., ADAMS, D. J., SCHATZ, D. G., ARAGON, L., FISHER, A. G., KRANGEL, M. S., NASMYTH, K. & MERKENSCHLAGER, M. 2011. A role for cohesin in T-cell-receptor rearrangement and thymocyte differentiation. *Nature,* 476**,** 467-71.
SHEN, S., PARK, J. W., HUANG, J., DITTMAR, K. A., LU, Z. X., ZHOU, Q., CARSTENS, R. P. & XING, Y. 2012. MATS: a Bayesian framework for flexible detection of differential alternative splicing from RNA-Seq data. *Nucleic Acids Res,* 40**,** e61.
SHERR, C. J. 2001. The INK4a/ARF network in tumour suppression. *Nat Rev Mol Cell Biol,* 2**,** 731-7.
SHI, L., WEN, H. & SHI, X. 2017. The Histone Variant H3.3 in Transcriptional Regulation and Human Disease. *J Mol Biol,* 429**,** 1934-1945.
SHIH, H. Y. & KRANGEL, M. S. 2013. Chromatin architecture, CCCTC-binding factor, and V(D)J recombination: managing long-distance relationships at antigen receptor loci. *J Immunol,* 190**,** 4915-21.
SHIMAZAKI, N. & LIEBER, M. R. 2014. Histone methylation and V(D)J recombination. *Int J Hematol,* 100**,** 230-7.
SHIMAZAKI, N. & R LIEBER, M. 2014. *Histone methylation and V(D)J recombination*.
SHUKLA, S. & OBERDOERFFER, S. 2012. Co-transcriptional regulation of alternative pre-mRNA splicing. *Biochim Biophys Acta,* 1819**,** 673-83.
SILKAITIS, K. & LEMOS, B. 2014. Sex-biased chromatin and regulatory cross-talk between sex chromosomes, autosomes, and mitochondria. *Biol Sex Differ,* 5**,** 2.

SIMS, R. J., 3RD, MILLHOUSE, S., CHEN, C. F., LEWIS, B. A., ERDJUMENT-BROMAGE, H., TEMPST, P., MANLEY, J. L. & REINBERG, D. 2007. Recognition of trimethylated histone H3 lysine 4 facilitates the recruitment of transcription postinitiation factors and pre-mRNA splicing. *Mol Cell,* 28**,** 665-76.
SINGH, P. B., MILLER, J. R., PEARCE, J., KOTHARY, R., BURTON, R. D., PARO, R., JAMES, T. C. & GAUNT, S. J. 1991. A sequence motif found in a Drosophila heterochromatin protein is conserved in animals and plants. *Nucleic Acids Res,* 19**,** 789-94.
SKENE, P. J. & HENIKOFF, S. 2013. Histone variants in pluripotency and disease. *Development,* 140**,** 2513-24.
SMALLWOOD, A., HON, G. C., JIN, F., HENRY, R. E., ESPINOSA, J. M. & REN, B. 2012. CBX3 regulates efficient RNA processing genome-wide. *Genome Res,* 22**,** 1426-36.
SMOTHERS, J. F. & HENIKOFF, S. 2001. The hinge and chromo shadow domain impart distinct targeting of HP1-like proteins. *Mol Cell Biol,* 21**,** 2555-69.
SNELL, D. M. & TURNER, J. M. A. 2018. Sex Chromosome Effects on Male-Female Differences in Mammals. *Curr Biol,* 28**,** R1313-R1324.
SPIES, N., NIELSEN, C. B., PADGETT, R. A. & BURGE, C. B. 2009. Biased chromatin signatures around polyadenylation sites and exons. *Mol Cell,* 36**,** 245-54.
STILLMAN, B. 1986. Chromatin assembly during SV40 DNA replication in vitro. *Cell,* 45**,** 555-65.
STRAUB, T. 2003. Heterochromatin dynamics. *PLoS Biol,* 1**,** E14.
SUBRAHMANYAM, R. & SEN, R. 2010. RAGs' eye view of the immunoglobulin heavy chain gene locus. *Semin Immunol,* 22**,** 337-45.
SUN, T., PLUTYNSKI, A., WARD, S. & RUBIN, J. B. 2015. An integrative view on sex differences in brain tumors. *Cell Mol Life Sci,* 72**,** 3323-42.
SURH, C. D. & SPRENT, J. 2000. Homeostatic T cell proliferation: how far can T cells be activated to self-ligands? *J Exp Med,* 192**,** F9-F14.
SZENKER, E., RAY-GALLET, D. & ALMOUZNI, G. 2011. The double face of the histone variant H3.3. *Cell Res,* 21**,** 421-34.
TAGAMI, H., RAY-GALLET, D., ALMOUZNI, G. & NAKATANI, Y. 2004. Histone H3.1 and H3.3 complexes mediate nucleosome assembly pathways dependent or independent of DNA synthesis. *Cell,* 116**,** 51-61.
TAKADA, Y., NARUSE, C., COSTA, Y., SHIRAKAWA, T., TACHIBANA, M., SHARIF, J., KEZUKA-SHIOTANI, F., KAKIUCHI, D., MASUMOTO, H., SHINKAI, Y., OHBO, K., PETERS, A. H., TURNER, J. M., ASANO, M. & KOSEKI, H. 2011. HP1gamma links histone methylation marks to meiotic synapsis in mice. *Development,* 138**,** 4207-17.
TALBERT, P. B. & HENIKOFF, S. 2010. Histone variants--ancient wrap artists of the epigenome. *Nat Rev Mol Cell Biol,* 11**,** 264-75.
TAMURA, T., SMITH, M., KANNO, T., DASENBROCK, H., NISHIYAMA, A. & OZATO, K. 2009. Inducible deposition of the histone variant H3.3 in interferon-stimulated genes. *J Biol Chem,* 284**,** 12217-25.
TAN, J. B., VISAN, I., YUAN, J. S. & GUIDOS, C. J. 2005. Requirement for Notch1 signals at sequential early stages of intrathymic T cell development. *Nat Immunol,* 6**,** 671-9.
TANG, M. C., JACOBS, S. A., MATTISKE, D. M., SOH, Y. M., GRAHAM, A. N., TRAN, A., LIM, S. L., HUDSON, D. F., KALITSIS, P., O'BRYAN, M. K., WONG, L. H. & MANN, J. R. 2015. Contribution of the two genes encoding histone variant h3.3 to viability and fertility in mice. *PLoS Genet,* 11**,** e1004964.
TANG, Y. P. & WADE, J. 2010. Sex- and age-related differences in ribosomal proteins L17 and L37, as well as androgen receptor protein, in the song control system of zebra finches. *Neuroscience,* 171**,** 1131-40.
TELONIS-SCOTT, M., KOPP, A., WAYNE, M. L., NUZHDIN, S. V. & MCINTYRE, L. M. 2009. Sex-specific splicing in Drosophila: widespread occurrence, tissue specificity and evolutionary conservation. *Genetics,* 181**,** 421-34.
TEVES, S. S., WEBER, C. M. & HENIKOFF, S. 2014. Transcribing through the nucleosome. *Trends Biochem Sci,* 39**,** 577-86.
THORNHILL, A. R. & BURGOYNE, P. S. 1993. A paternally imprinted X chromosome retards the development of the early mouse embryo. *Development,* 118**,** 171-4.
TILGNER, H., NIKOLAOU, C., ALTHAMMER, S., SAMMETH, M., BEATO, M., VALCÁRCEL, J. & GUIGÓ, R. 2009. *Nucleosome positioning as a determinant of exon recognition*.
TORRES-PADILLA, M. E., BANNISTER, A. J., HURD, P. J., KOUZARIDES, T. & ZERNICKA-GOETZ, M. 2006. Dynamic distribution of the replacement histone variant H3.3 in the mouse oocyte and preimplantation embryos. *Int J Dev Biol,* 50**,** 455-61.
TOUGH, D. F. & SPRENT, J. 1995. Life span of naive and memory T cells. *Stem Cells,* 13**,** 242-9.
TRABZUNI, D., RAMASAMY, A., IMRAN, S., WALKER, R., SMITH, C., WEALE, M. E., HARDY, J., RYTEN, M. & NORTH AMERICAN BRAIN EXPRESSION, C. 2013. Widespread sex differences in gene expression and splicing in the adult human brain. *Nat Commun,* 4**,** 2771.

TROJER, P. & REINBERG, D. 2007. Facultative heterochromatin: is there a distinctive molecular signature? *Mol Cell,* 28**,** 1-13.
TURNER, B. M. 2002. Cellular memory and the histone code. *Cell,* 111**,** 285-291.
VAKOC, C. R., MANDAT, S. A., OLENCHOCK, B. A. & BLOBEL, G. A. 2005. Histone H3 lysine 9 methylation and HP1gamma are associated with transcription elongation through mammalian chromatin. *Mol Cell,* 19**,** 381-91.
VAN GENT, D. C., HIOM, K., PAULL, T. T. & GELLERT, M. 1997. Stimulation of V(D)J cleavage by high mobility group proteins. *EMBO J,* 16**,** 2665-70.
VAN KAER, L. 2015. Innate and virtual memory T cells in man. *Eur J Immunol,* 45**,** 1916-20.
VARGA-WEISZ, P. D. & BECKER, P. B. 2006. Regulation of higher-order chromatin structures by nucleosome-remodelling factors. *Curr Opin Genet Dev,* 16**,** 151-6.
VENKATESH, S. & WORKMAN, J. L. 2015. Histone exchange, chromatin structure and the regulation of transcription. *Nat Rev Mol Cell Biol,* 16**,** 178-89.
VERREAULT, A. 2000. De novo nucleosome assembly: new pieces in an old puzzle. *Genes Dev,* 14**,** 1430-8.
VILLA, R. 2009. *Role of epigenetic modifications in acute promyelocytic leukemia*.
VOO, K. S., CARLONE, D. L., JACOBSEN, B. M., FLODIN, A. & SKALNIK, D. G. 2000. Cloning of a mammalian transcriptional activator that binds unmethylated CpG motifs and shares a CXXC domain with DNA methyltransferase, human trithorax, and methyl-CpG binding domain protein 1. *Mol Cell Biol,* 20**,** 2108-21.
WADDINGTON, C. H. 1940. *Organisers and genes.*, Cambridge Biological Studies. University Press, Cambridge.
WANG, G., MA, A., CHOW, C. M., HORSLEY, D., BROWN, N. R., COWELL, I. G. & SINGH, P. B. 2000. Conservation of heterochromatin protein 1 function. *Mol Cell Biol,* 20**,** 6970-83.
WATERS, M. G., SERAFINI, T. & ROTHMAN, J. E. 1991. 'Coatomer': a cytosolic protein complex containing subunits of non-clathrin-coated Golgi transport vesicles. *Nature,* 349**,** 248-251.
WEBER, C. M. & HENIKOFF, S. 2014. Histone variants: dynamic punctuation in transcription. *Genes Dev,* 28**,** 672-82.
WEST, M. H. & BONNER, W. M. 1980. Histone 2A, a heteromorphous family of eight protein species. *Biochemistry,* 19**,** 3238-45.
WIDOM, J. & KLUG, A. 1985. Structure of the 300A chromatin filament: X-ray diffraction from oriented samples. *Cell,* 43**,** 207-13.
WIEDEMANN, S. M., MILDNER, S. N., BONISCH, C., ISRAEL, L., MAISER, A., MATHEISL, S., STRAUB, T., MERKL, R., LEONHARDT, H., KREMMER, E., SCHERMELLEH, L. & HAKE, S. B. 2010. Identification and characterization of two novel primate-specific histone H3 variants, H3.X and H3.Y. *J Cell Biol,* 190**,** 777-91.
WIJCHERS, P. J. & FESTENSTEIN, R. J. 2011. Epigenetic regulation of autosomal gene expression by sex chromosomes. *Trends Genet,* 27**,** 132-40.
WILMING, L. G., SNOEREN, C. A., VAN RIJSWIJK, A., GROSVELD, F. & MEIJERS, C. 1997. The murine homologue of HIRA, a DiGeorge syndrome candidate gene, is expressed in embryonic structures affected in human CATCH22 patients. *Hum Mol Genet,* 6**,** 247-58.
WIRBELAUER, C., BELL, O. & SCHUBELER, D. 2005. Variant histone H3.3 is deposited at sites of nucleosomal displacement throughout transcribed genes while active histone modifications show a promoter-proximal bias. *Genes Dev,* 19**,** 1761-6.
WITT, O., ALBIG, W. & DOENECKE, D. 1996. Testis-specific expression of a novel human H3 histone gene. *Exp Cell Res,* 229**,** 301-6.
WORKMAN, J. L. & KINGSTON, R. E. 1998. Alteration of nucleosome structure as a mechanism of transcriptional regulation. *Annu Rev Biochem,* 67**,** 545-79.
WU, C. & MORRIS, J. R. 2001. Genes, genetics, and epigenetics: a correspondence. *Science,* 293**,** 1103-5.
WU, R. S., TSAI, S. & BONNER, W. M. 1982. Patterns of histone variant synthesis can distinguish G0 from G1 cells. *Cell,* 31**,** 367-74.
XIAO, T., HALL, H., KIZER, K. O., SHIBATA, Y., HALL, M. C., BORCHERS, C. H. & STRAHL, B. D. 2003. Phosphorylation of RNA polymerase II CTD regulates H3 methylation in yeast. *Genes Dev,* 17**,** 654-63.
XU, C. R. & FEENEY, A. J. 2009. The epigenetic profile of Ig genes is dynamically regulated during B cell differentiation and is modulated by pre-B cell receptor signaling. *J Immunol,* 182**,** 1362-9.
YAGI, H., FURUTANI, Y., HAMADA, H., SASAKI, T., ASAKAWA, S., MINOSHIMA, S., ICHIDA, F., JOO, K., KIMURA, M., IMAMURA, S., KAMATANI, N., MOMMA, K., TAKAO, A., NAKAZAWA, M., SHIMIZU, N. & MATSUOKA, R. 2003. Role of TBX1 in human del22q11.2 syndrome. *Lancet,* 362**,** 1366-73.
YANG, X. J. & SETO, E. 2008. Lysine acetylation: codified crosstalk with other posttranslational modifications. *Mol Cell,* 31**,** 449-61.

YOUNGBLOOD, B., HALE, J. S., KISSICK, H. T., AHN, E., XU, X., WIELAND, A., ARAKI, K., WEST, E. E., GHONEIM, H. E., FAN, Y., DOGRA, P., DAVIS, C. W., KONIECZNY, B. T., ANTIA, R., CHENG, X. & AHMED, R. 2017. Effector CD8 T cells dedifferentiate into long-lived memory cells. *Nature,* 552**,** 404.

YUN, M., WU, J., WORKMAN, J. L. & LI, B. 2011. Readers of histone modifications. *Cell Res,* 21**,** 564-78.

ZHANG, C., ZHANG, B., LIN, L. L. & ZHAO, S. 2017a. Evaluation and comparison of computational tools for RNA-seq isoform quantification. *BMC Genomics,* 18**,** 583.

ZHANG, H., GAN, H., WANG, Z., LEE, J. H., ZHOU, H., ORDOG, T., WOLD, M. S., LJUNGMAN, M. & ZHANG, Z. 2017b. RPA Interacts with HIRA and Regulates H3.3 Deposition at Gene Regulatory Elements in Mammalian Cells. *Mol Cell,* 65**,** 272-284.

ZHANG, H., ROBERTS, D. N. & CAIRNS, B. R. 2005a. Genome-wide dynamics of Htz1, a histone H2A variant that poises repressed/basal promoters for activation through histone loss. *Cell,* 123**,** 219-31.

ZHANG, H. L., GAN, H. Y., WANG, Z. Q., LEE, J. H., ZHOU, H., ORDOG, T., WOLD, M. S., LJUNGMAN, M. & ZHANG, Z. G. 2017c. RPA Interacts with HIRA and Regulates H3.3 Deposition at Gene Regulatory Elements in Mammalian Cells. *Molecular Cell,* 65**,** 272-284.

ZHANG, J. A., MORTAZAVI, A., WILLIAMS, B. A., WOLD, B. J. & ROTHENBERG, E. V. 2012. Dynamic transformations of genome-wide epigenetic marking and transcriptional control establish T cell identity. *Cell,* 149**,** 467-82.

ZHANG, R., CHEN, W. & ADAMS, P. D. 2007. Molecular dissection of formation of senescence-associated heterochromatin foci. *Mol Cell Biol,* 27**,** 2343-58.

ZHANG, R., POUSTOVOITOV, M. V., YE, X., SANTOS, H. A., CHEN, W., DAGANZO, S. M., ERZBERGER, J. P., SEREBRIISKII, I. G., CANUTESCU, A. A., DUNBRACK, R. L., PEHRSON, J. R., BERGER, J. M., KAUFMAN, P. D. & ADAMS, P. D. 2005b. Formation of MacroH2A-containing senescence-associated heterochromatin foci and senescence driven by ASF1a and HIRA. *Dev Cell,* 8**,** 19-30.

ZHANG, S., RAMSAY, E. S. & MOCK, B. A. 1998. Cdkn2a, the cyclin-dependent kinase inhibitor encoding p16INK4a and p19ARF, is a candidate for the plasmacytoma susceptibility locus, Pctr1. *Proc Natl Acad Sci U S A,* 95**,** 2429-34.

ZHANG, T., COOPER, S. & BROCKDORFF, N. 2015. The interplay of histone modifications - writers that read. *EMBO Rep,* 16**,** 1467-81.

ZHAO, T., HEYDUK, T., ALLIS, C. D. & EISSENBERG, J. C. 2000. Heterochromatin protein 1 binds to nucleosomes and DNA in vitro. *J Biol Chem,* 275**,** 28332-8.

ZHOU, X., WU, W., LI, H., CHENG, Y., WEI, N., ZONG, J., FENG, X., XIE, Z., CHEN, D., MANLEY, J. L., WANG, H. & FENG, Y. 2014. Transcriptome analysis of alternative splicing events regulated by SRSF10 reveals position-dependent splicing modulation. *Nucleic Acids Res,* 42**,** 4019-30.

ZLOTOFF, D. A. & BHANDOOLA, A. 2011. Hematopoietic progenitor migration to the adult thymus. *Ann N Y Acad Sci,* 1217**,** 122-38.

ZUNIGA-PFLUCKER, J. C. 2012. When three negatives made a positive influence in defining four early steps in T cell development. *J Immunol,* 189**,** 4201-2.

ZWEIDLER, A. 1984. Core histone variants of the mouse: primary structure and differential expression. *Organization Structure, G.S Regulation, J.L Stein, Stein, W.F Marzluff (Eds.), Histone Genes, John Wiley & Sons, New York*.

ZWEIER, C., STICHT, H., AYDIN-YAYLAGUL, I., CAMPBELL, C. E. & RAUCH, A. 2007. Human TBX1 missense mutations cause gain of function resulting in the same phenotype as 22q11.2 deletions. *Am J Hum Genet,* 80**,** 510-7.

Appendix

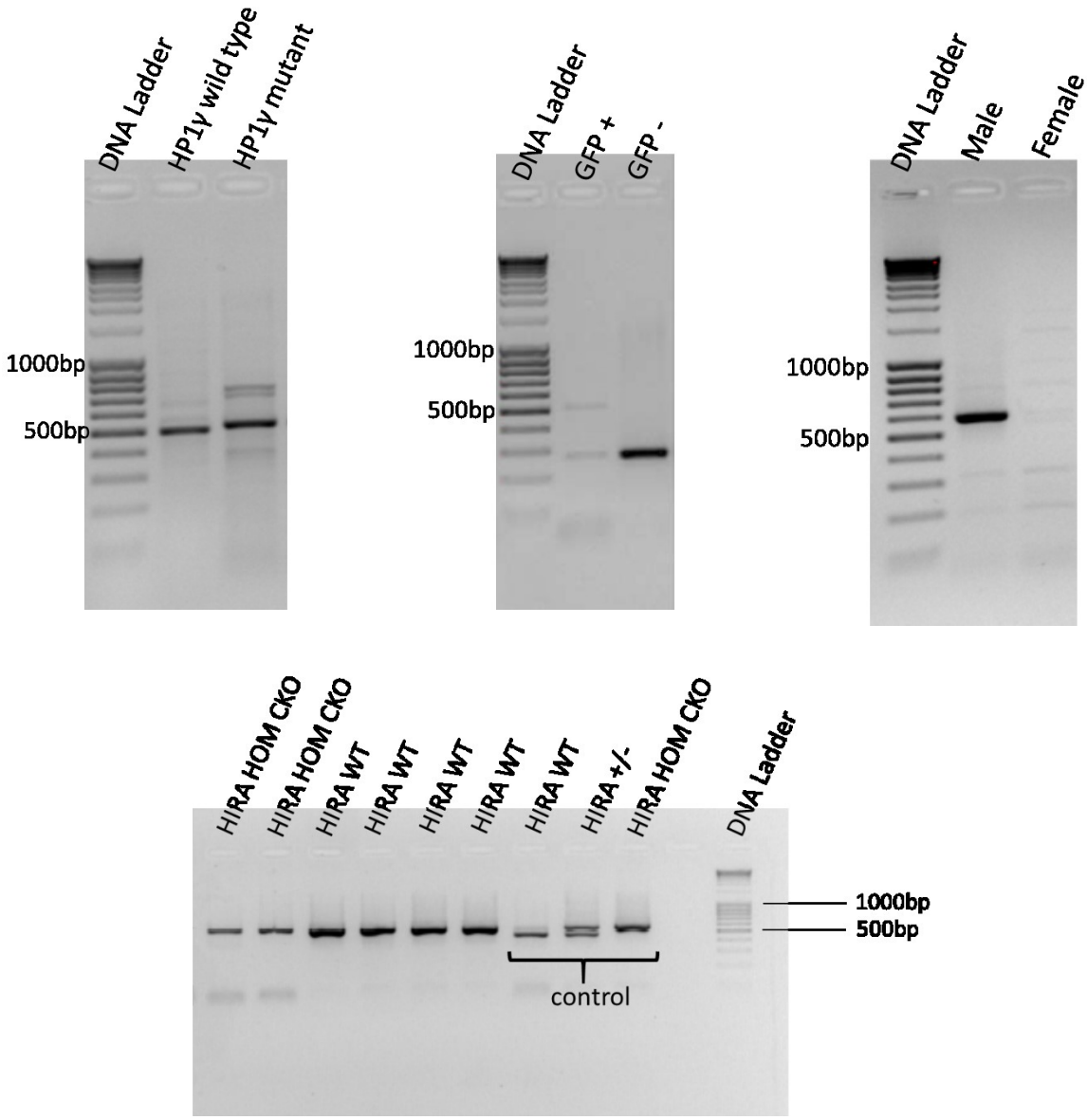
DNA Ladder
HP1γ wild type
HP1γ mutant
1000bp
500bp
DNA Ladder
GFP +
GFP -
1000bp
500bp
DNA Ladder
Male
Female
1000bp
500bp
HIRA HOM CKO
HIRA HOM CKO
HIRA WT
HIRA WT
HIRA WT
HIRA WT
HIRA WT
HIRA +/-
HIRA HOM CKO
DNA Ladder
1000bp
500bp
control

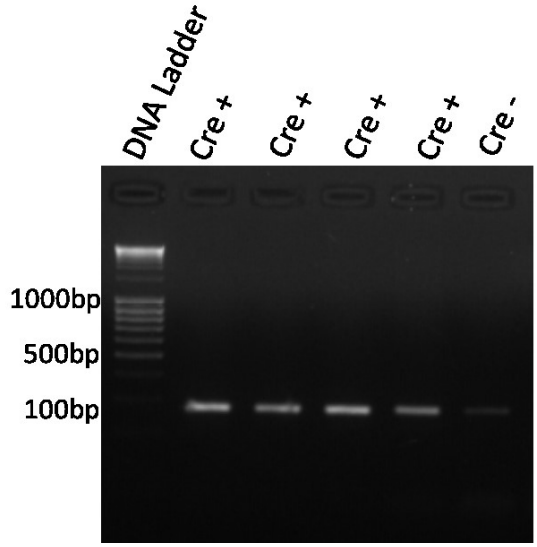

Fig S1. Representative genotyping results. *Genotype of transgenic animals or E13.5 embryos were determined by PCR followed by visualisation of PCR products on DNA agarose gel. (A) PCR result for HP1γ genotyping. PCR for HP1γ genotyping showed a 501bp band for wild type allele and a 525bp band for mutant allele. (B) PCR result for H3.3B-EGFP genotyping. Animals which express H3.3B-EGFP fusion protein showed a 272bp band while wild type animals show no band on gel. (C) PCR result for Kdm5d genotyping for sex determination of embryos. Male animals showed a 597bp band while female animal showed no band. (D) PCR result for HIRA genotyping. Heterozygous animal (HIRA +/-) which expresses both wild type and mutant allele showed 2 bands at bp and bp respectively. HIRA WT animal only showed upper band 417at bp and HIRA HOM CKO animal only showed lower band at 291bp. (E) PCR result for Cre genotyping. Animals which express Cre showed a band at 148bp while Cre negative animal showed no band.*

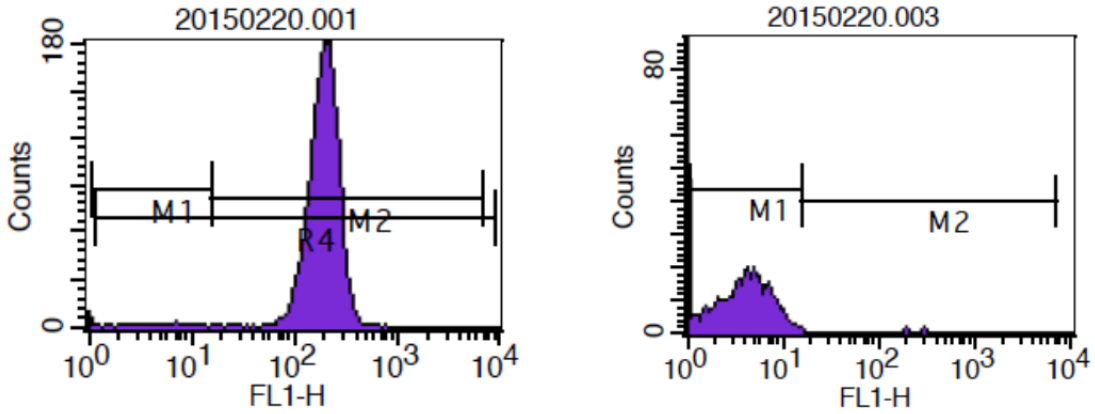

Fig S2. EGFP expression as measured by Flow cytometry. *The histogram on the left is showing the thymocytes taken from transgenic (H3.3B-EGFP) mouse, which has an EGFP gene knocked in to H3.3B gene. It showed a specific high signal of EGFP compared to that in WT mouse thymocytes which didn't show any signal in Gate M2.*

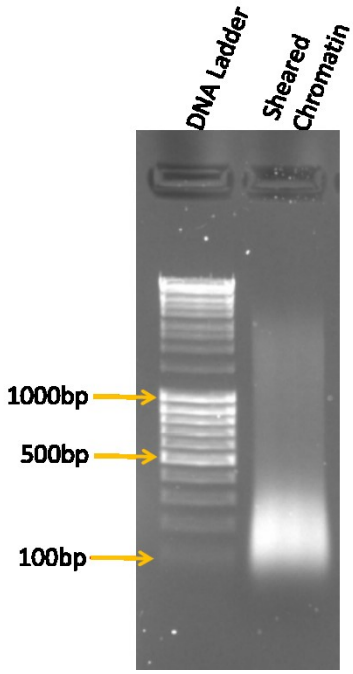

Fig S3. Representative gel for sheared chromatin. *Chromatin from MEFs and thymocytes was prepared using Bioruptor® (Diagenode) to obtain sample enriched in chromatin fragments with size of about 150-300bp.*

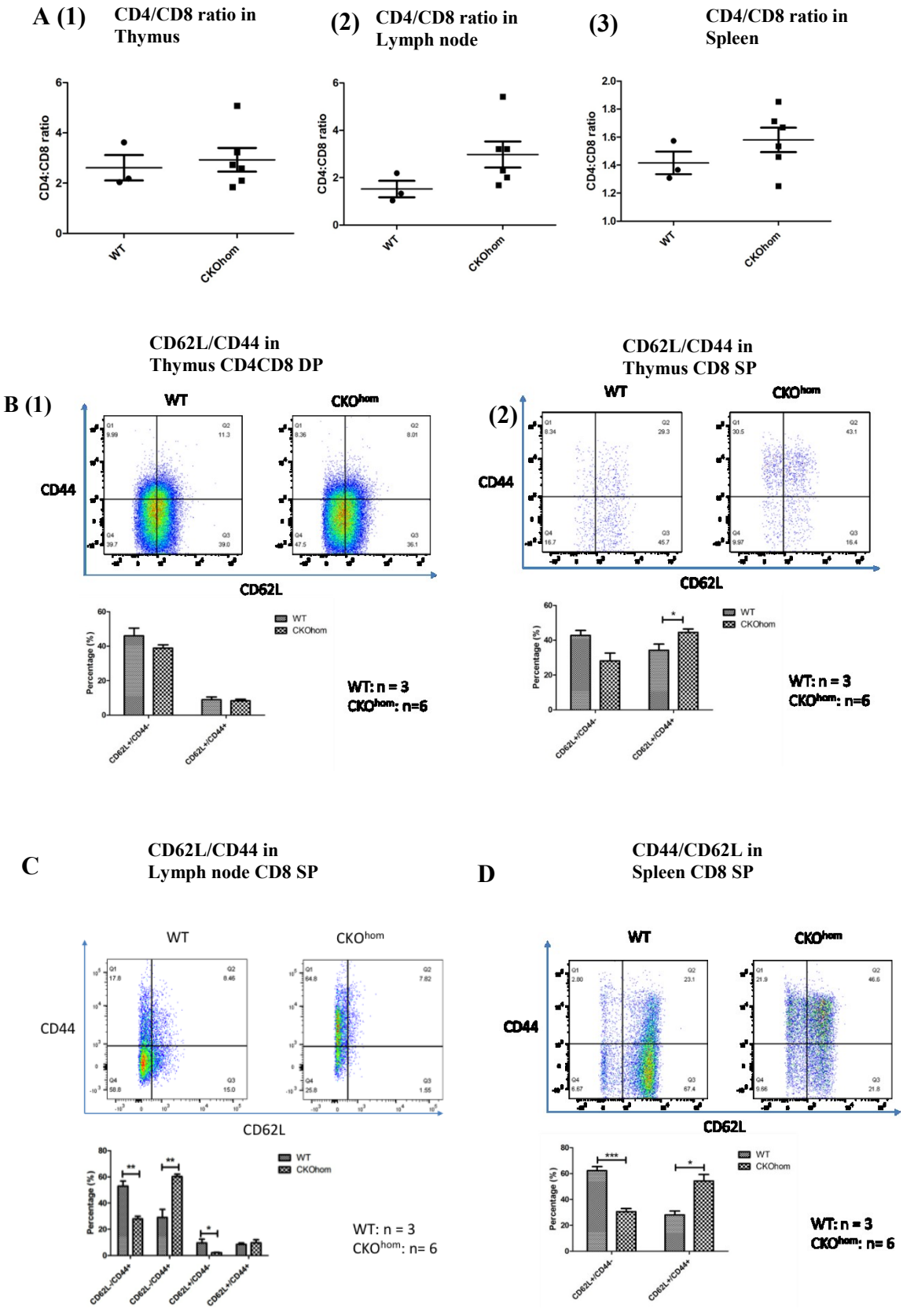
A (1)
CD4/CD8 ratio in Thymus
(2)
CD4/CD8 ratio in Lymph node
(3)
CD4/CD8 ratio in Spleen
CD4:CD8 ratio
WT
CKOhom
B (1)
CD62L/CD44 in Thymus CD4CD8 DP
(2)
CD62L/CD44 in Thymus CD8 SP
CD44
CD62L
Percentage (%)
WT: n = 3
CKOhom: n=6
C
CD62L/CD44 in Lymph node CD8 SP
D
CD44/CD62L in Spleen CD8 SP
WT: n = 3
CKOhom: n= 6

Fig S4. FACS plots showing different T cell marker expression in different cell population in mouse thymus, lymph node and spleen. *A. CD4 T cell/CD8 T cell ratio didn't change much in thymus, lymph node and spleen. B/C/D. FACS plots showing CD44 upregulation in different cell populations in lymph node and spleen. But CD44 expression didn't change in DP cells in thymus.*

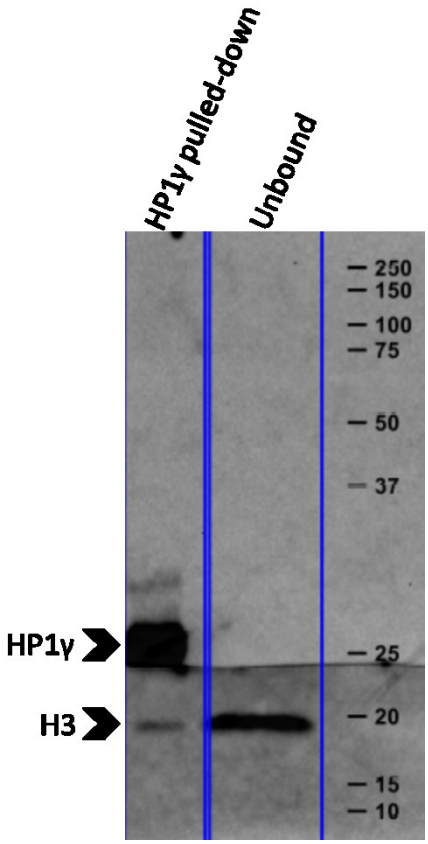

Fig S5. Validation of co-immunoprecipitation experiment. *HP1γ protein was enriched in the pulled-down fraction prepared using anti-HP1γ antibody and diminished in the unbound fraction. This result indicates the high efficiency of pull-down. Co-immunoprecipitation experiment in WT MEFs using anti-H3 antibody revealed H3 in both HP1γ pulled-down and unbound fractions acts as an internal control.*

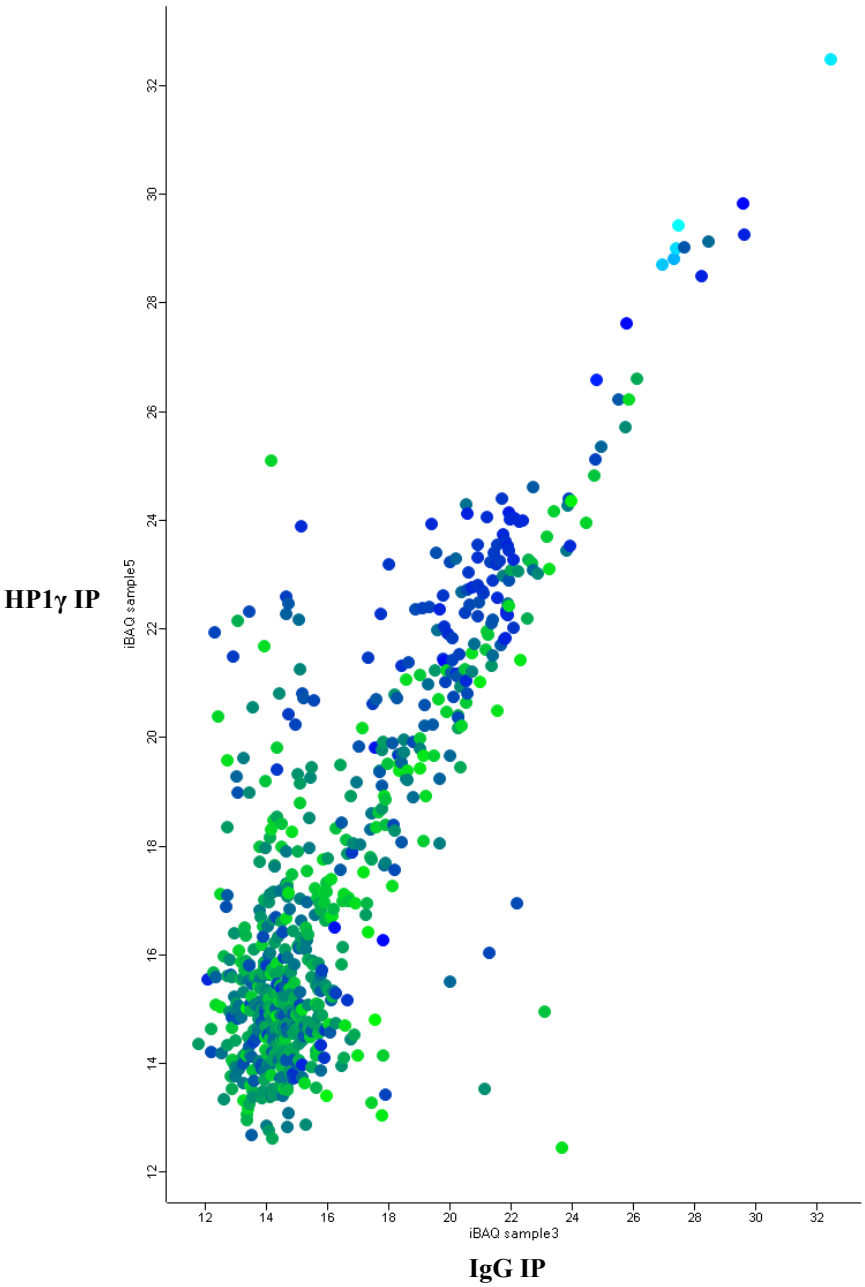

Fig S6. Scatter Plot of comparison between HP1γ IP vs IgG IP in female sample. *This comparison was used to check protein enrichment following IP. iBAQ values (intensity based absolute values) of HP1γ _IP (y-axis) versus IgG IP (x-axis). Green color: low abundance in input. Blue color: high abundance in input. Dots located close to Y-axis have a higher enrichment. "Andromeda: A Peptide Search Engine Integrated into the MaxQuant Environment" Jurgen Cox et al. (Cox et al. 2011).*

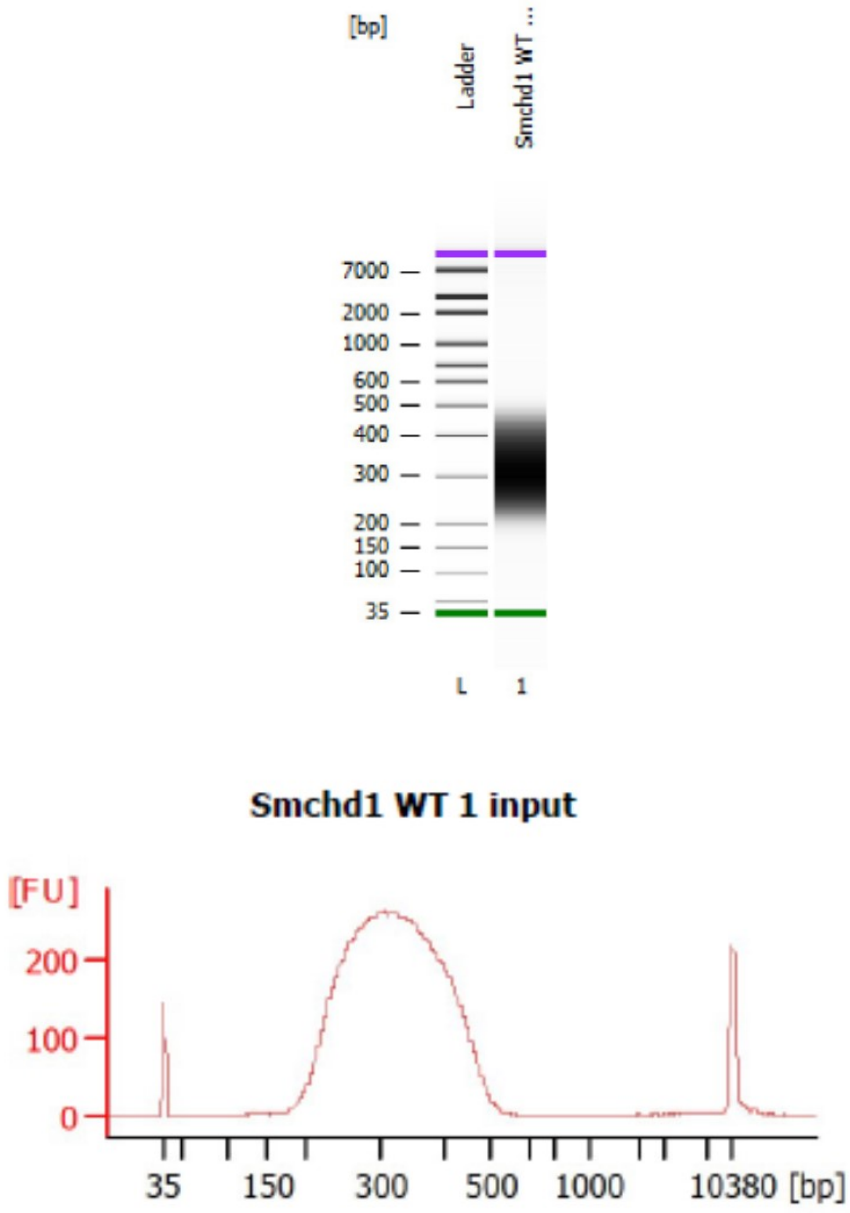

Fig S7. Representative result obtained from Bioanalyzer High Sensitivity DNA Analysis for checking size and quality of ChIP sequencing library. *(A) Gel image and (B) electropherograms of the prepared ChIP sequencing library showing enrichment of DNA fragment of about 200-400bp which indicate the size of DNA to be sequenced are of about 150-350bp (without ligated adaptors).*

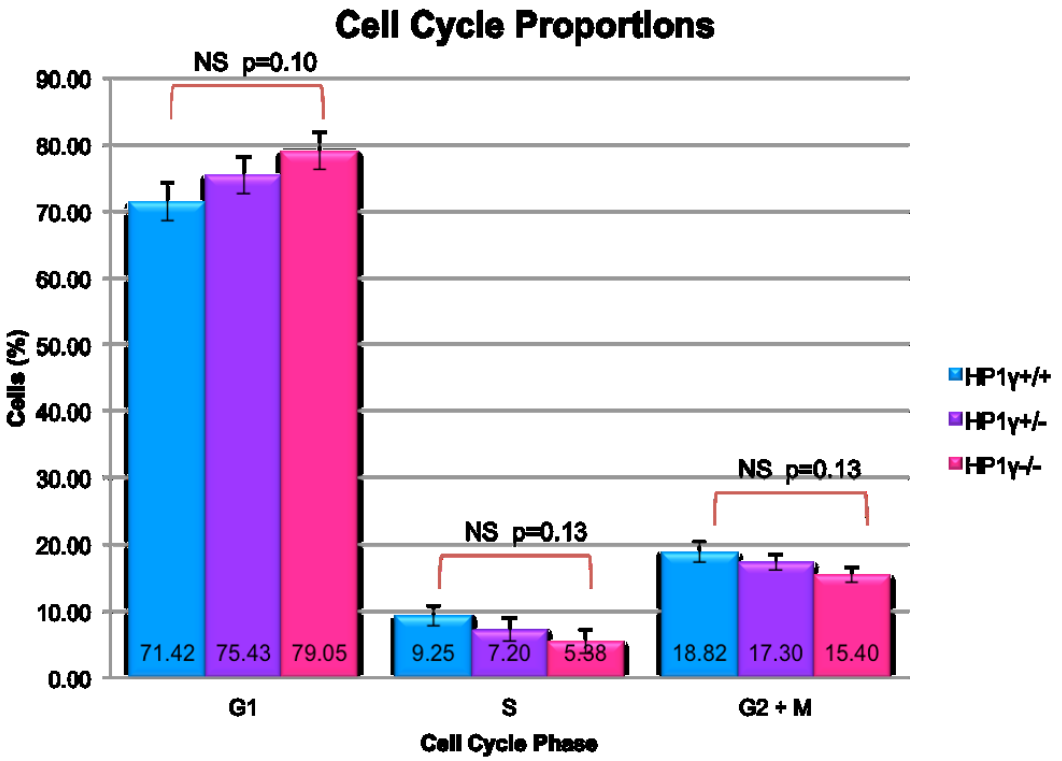

***Fig S8. Cell-cycle analysis as assessed by PI staining using flow cytometry (FACS) (work done by* Lakshmi Cadavieco, MSc student, 2015).** *Chart displaying the mean proportion of cells in each cycle phase for the genotypes HP1γ KO (n=4), HP1γ Heterozygous (n=3) and HP1γ WT (n=6) of female MEFs. The error bar corresponds to the SEM. Student's T test indicated as p value comparing HP1γ WT and HP1γ KO.*

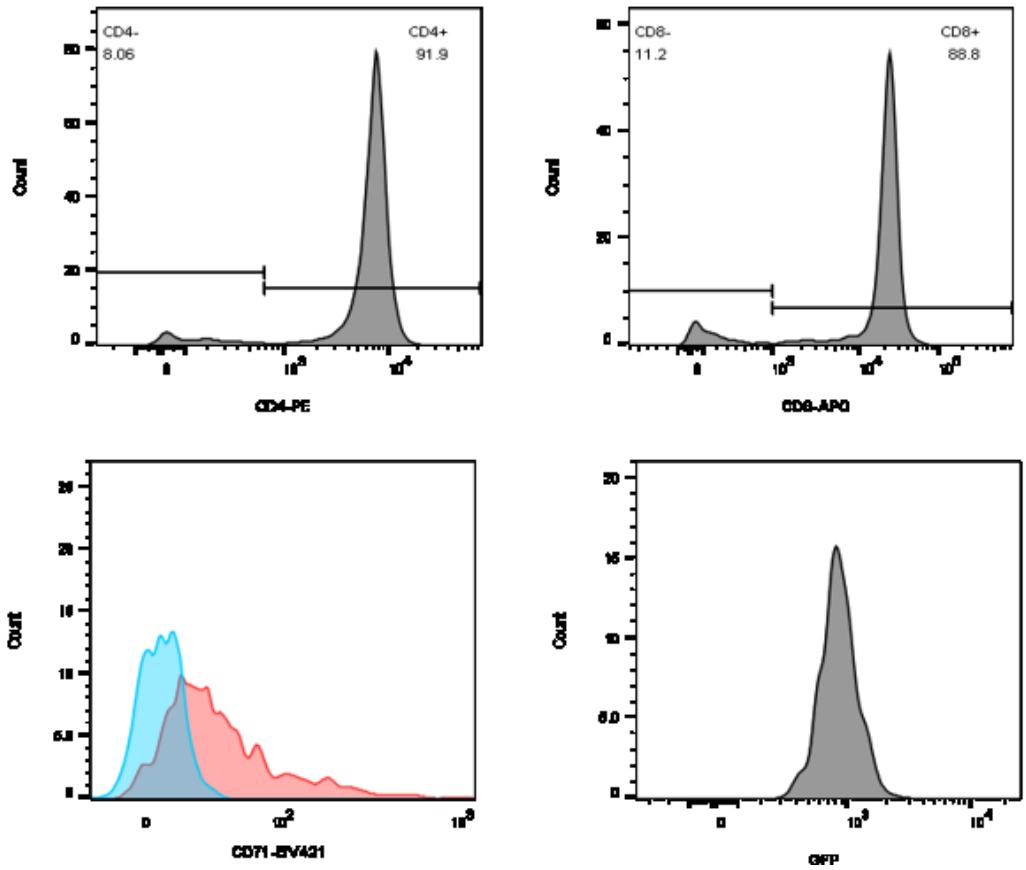

Fig S9. FACS plots showing CD4, CD8, CD71 and EGFP expression during CD71 cell sorting.

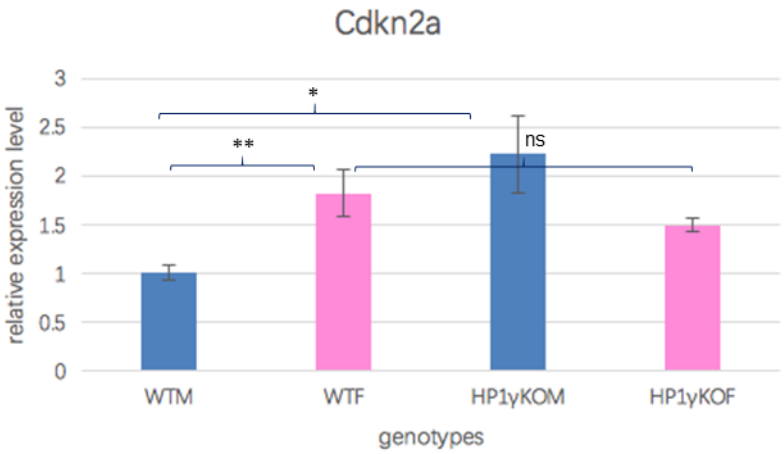

RNA-seq	WTM_log2(avg)	WTF_log2(avg)	KOM_log2(avg)	KOF_log2(avg)
Cdkn2a	10.57313584	11.35945317	12.09354846	11.37460995

Fig S10. Gene expression level of Cdkn2a in original RNA-seq samples. This figure shows the relative expression level of *Cdkn2a* in original RNA-seq samples detected by QRT-PCR. *Cdkn2a* expression level didn't change much in response to HP1γ KO in female according to the student's two-tailed t-test. However, in male, the level of *Cdkn2a* expression went up by 50%. (18s rRNA expression was used to normalize the data. The error bars stand for SEM of three biological replicates.) * represents $0.001<P<0.05$, ** represents $P<0.001$, "ns" represents non-significant ($P\geq0.05$) The table below shows the expression level of different genotypes obtained by RNA-seq. This figure is adapted with permission from Cristina MSc thesis, 2015.

Sex dimorphic genes identified in WT MEFs by RNA-seq

higher expression in male	higher expression in female
Eif2s3y	Xist
Ddx3y	Eif2s3x
Kdm5d	5530601H04Rik
Uty	Ppef1
Erdr1	Gda
Gpr165	Malat1
Lrrc10b	Neat1
Dkk1	4933411K16Rik
Tslp	Pcdha10
Pi16	9430076G02Rik
Chodl	Mc2r
Col2a1	Gm4013
Krt75	Pcdha9
Fgf9	Abcg1
Gjb6	Rgs11
Thbs4	Xdh
Hapln1	Pisd-ps2
Adcy2	C2
Dlk1	Rhbdl1
Syndig1l	Stap2
Klhl29	H2-DMb1
2810032G03Rik	1700071M16Rik
Ramp2	Liph
Ace	4930565N06Rik
Krt13	Nlrc3
Krt14	Kcnj15
S100b	Kng2
Susd2	Slc7a4
Bmp5	Kifc2
Stac	Parp10
1700048O20Rik	Cma2
Gsta4	Ptger2
Gramd2	Gzmd
1700102P08Rik	Gzmc
Cdh8	Mcpt8
Clgn	Hist1h3d
Lpl	Fam228b
Acan	4930447C04Rik
Scube2	F730043M19Rik
Hif3a	Ccl8

Ntrk3	Doc2b
Gpr27	Pisd-ps1
Klf14	Rasl10b
Tril	Fbxw10
Eln	Sfi1
Col8a2	Bzrap1
Frem1	Cntnap1
Col9a2	Havcr2
Ptx3	Slc16a11
Agtr1b	Arg1
Sfrp2	Hal
Snord73a	Gstt2
Fam83c	Gm5134
Mylk2	Acp5
Pcsk2	Fxyd2
Adamtsl2	Cxcr6
Wnt6	Mmp3
Pappa2	Cck
Col9a1	Cmtm8
Gsta3	Pstpip1
Angptl1	Mmp13
Darc	Mmp10
	Hapln4
	Chst5
	Mboat4
	Insl3
	Snord68
	Acta1
	Lrp2bp
	Slc27a1
	Slc5a5
	Nlrc5
	Gpr123
	Syt17
	2810047C21Rik1
	Apoc2
	Tnfrsf26
	Crym
	0610005C13Rik
	Calcb
	Fam19a1
	Clec2e

		Vwf
		B230378P21Rik
		Alox5
		Spp1
		Plac8
		Fbxo24
		Ppbp
		Tfr2
		Bmp8b
		Cdkn2a
		Rex2
		Tas1r1
		Angptl7
		1300002K09Rik
		Tnfrsf18
		Rnf207
		Car9
		LOC100038947
		Tgm2
		Angpt4
		Slc52a3
		Gm996
		1700020A23Rik
		Rhov
		Siglec1
		Olfr1316
		Htr2b
		Otos
		Nphs2
		Kcnh1
		Fam5c
		Creg2

Fig S11. List of genes with either higher expression in WT male compared to WT female or vice versa in MEFs (for at least 1.5 folds, adjusted P-value < 0.05). *Cdkn2a (highlighted in yellow), which may be implicated in the sexually dimorphic response to HP1γ deficiency shown here to affect cell cycle and cell proliferation. This figure is adapted with permission from Vineet Sharma PhD thesis 2014.*

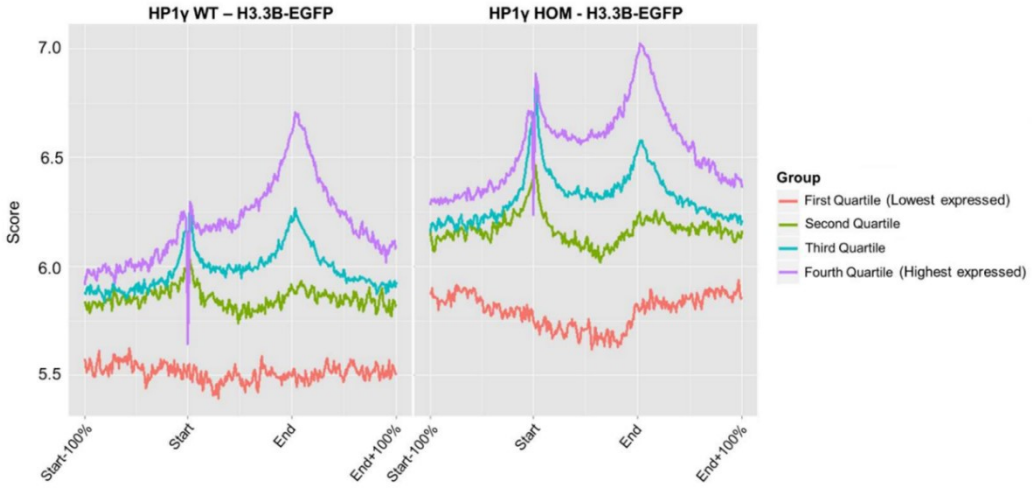

Fig S12. Average profile plot for H3.3B-EGFP enrichment of genes grouped into four tiers by expression level in HP1γ WT and HOM MEFs. *X-axis shows the normalized length where 'Start' indicates TSS and 'End' indicates TES. Y-axis shows the coverage in windows. 'First Quartile' represents genes with lowest expression level while "Fourth Quartile' represents genes with highest expression level. Data is shown as a proportion of input. In both HP1γ WT and KO MEFs, high level of H3.3B-EGFP enrichment was observed on highly expressed genes. High level of binding of H3.3B-EGFP was observed in both HP1γ WT and KO MEFs on highly expressed genes while lowest expressed genes have relatively low level of H3.3B-EGFP. The central dip at TSS was preserved on the highest expressed genes but lost on the lowest expressed genes. In HP1γ KO MEFs, enrichment of H3.3B-EGFP at the region around the TSS was increased on the top quartile of highly expressed genes. n=1(P. P. Law PhD thesis, 2016).*

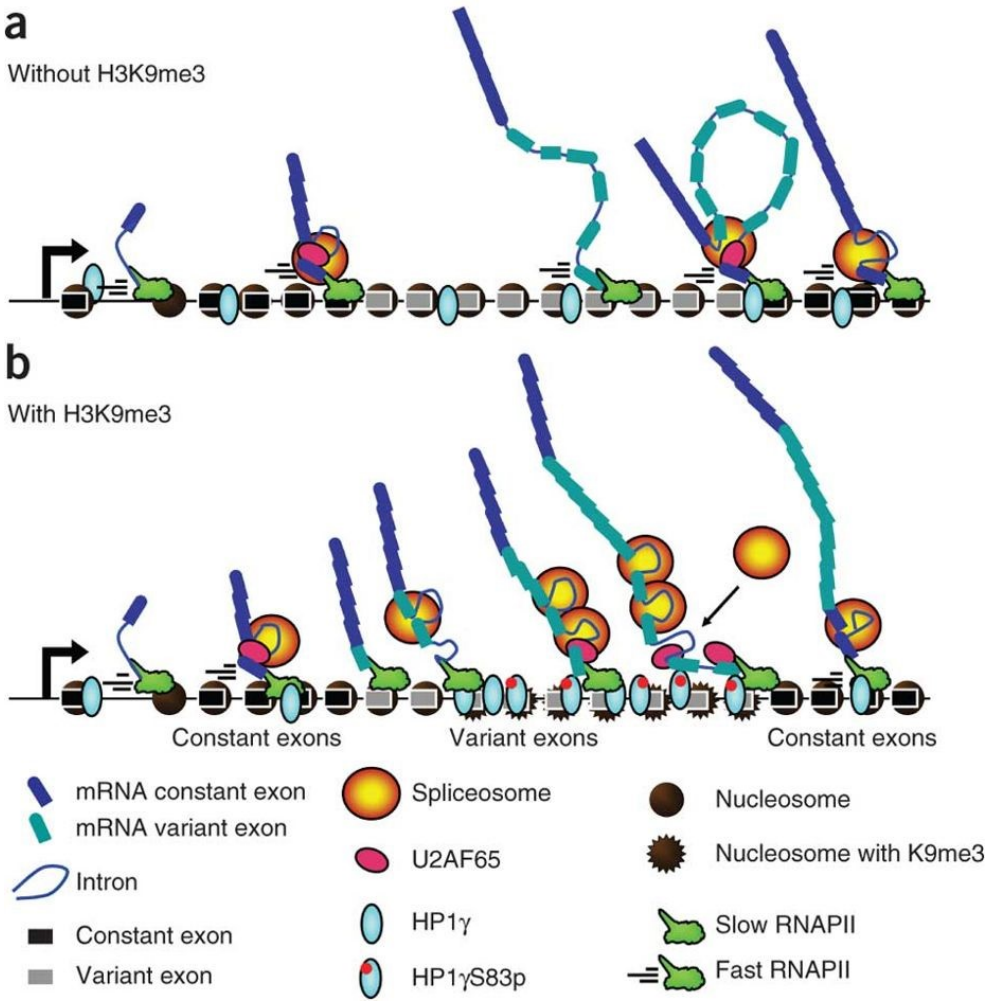

Fig S13. Schematic diagram showing the model of the regulation of CD44 splicing by H3K9me3 and HP1γ. *In the absence of the H3K9me3 mark, HP1γ is present at low levels on the chromatin, possibly via its interactions with the RNA Pol II or the globular domain of histone H3. Under these conditions the RNA Pol II moves fast along the variant region of the gene, and the spliceosome recognizes only the splice sites of constant exons. These constant exons remain in contact with the chromatin via the spliceosome and the RNA Pol II, whereas the variant exons not bound by spliceosomes keep contact with the chromatin only via the RNA Pol II. Altogether, this results in inclusion of only the constant exons in the mature mRNA. (b) When levels of H3K9me3 increase inside the CD44 gene and/or when HP1γ becomes more available (possibly released from the heterochromatin by phosphorylation), HP1γ forms an additional link with chromatin via its chromodomain. It accumulates on the coding region where it associates with the pre-mRNA and favors its transient retention on the chromatin. The generated chromatin structures slow down the RNA Pol II, which in turn facilitates recruitment of splicing factors such as U2AF65 and PRP8 on the pre-mRNA. This leads to increased inclusion of CD44 variant exons. This figure is adapted with permission from "Histone H3 lysine 9 trimethylation and HP1gamma favor inclusion of alternative exons" (Saint-André et al., 2011)*

SE sensitive to HP1γ KO in Males gene symbols (34 genes)	**RI sensitive to HP1γ KO in Males** gene symbols (258 genes)
Rbm39	Snapc4
0610011L14Rik	Cdk4
Mprip	Srrm1
Fam73b	Nfatc4
Srsf6	2400003C14Rik
4933431E20Rik	Nagk
Whrn	Nfx1
Zfp277	Celf1
Pcyox1	Hmgn3
Pde7a	Gpn3
Armcx1	Gba2
Pif1	Adamts10
St7	Gnb2
Cpa6	Ppp5c
Srsf3	Psrc1
Slc29a3	Mms19
Apbb2	Mtx1
Mrps10	Alad
2210015D19Rik	Sugp2
Sdcbp	Baz2b
Zcrb1	Rfx5
Slco4a1	Atp6v0a1
Ccdc46	Hdac3
Tcf3	Qars
Tsc2	Pqlc2
Srsf11	Nrbp1
Inca1	Brd8
Hsf1	1110038D17Rik
Usf2	Pnpt1
Abi3bp	Sharpin
2700081O15Rik	Ufd1l
Pkm2	1810074P20Rik
Vmn1r90	Surf2
Pan2	Idh3g
	Pick1
	Actr5
	Stab1
	Npr2
	Ing4
	Wdr54
	Spag9
	Acaa1a

		Armcx2
		Bcas2
		Orc3
		Skiv2l
		Atp13a2
		Cep110
		Smox
		Polr2i
		H2-Q4
		Cnot3
		Fam53a
		Vill
		Ipo8
		Npepl1
		Tnfaip2
		Nat10
		Anapc2
		Sirt7
		Cpsf4
		Fastk
		Ddx39
		Tfe3
		Tial1
		Wdr11
		Dvl1
		Golga1
		Dgkz
		Stx4a
		Slc35b4
		4930471M23Rik
		Lrdd
		Ddx5
		Chd8
		Ampd2
		Ciz1
		H2-T23
		Tbrg1
		Top3b
		Trp53
		Sh3glb2
		Arfrp1
		ORF61
		Hps1
		Rab4b

		Hnrnph1
		Mthfsd
		Hdac10
		Cpsf3l
		Tecpr1
		Ttc12
		9430008C03Rik
		Tmem87b
		Ctdsp1
		Zfp384
		Rpl30
		Mapk7
		Ppox
		Zfp326
		Wdr77
		Arrb2
		Tbxas1
		Rtel1
		Dmap1
		Rpl10a
		Slc30a9
		Cdk16
		Ppid
		Nek8
		Sgsm3
		Ppp1cc
		Nr1h2
		Sdccag3
		Rasal3
		Irf3
		Parp3
		Adam15
		Mars
		Lig3
		Stx5a
		Stk25
		Sec11c
		Dmxl2
		Msh3
		Ncf1
		Mettl17
		Ccdc59
		Dom3z
		Mrps17

		Zbtb17
		Polr2e
		Prpf40b
		Ints2
		Timm44
		Trafd1
		Edc4
		Klhdc4
		Rabep2
		Cdc25b
		Gtpbp2
		U2af1l4
		Rcbtb2
		Fbxl20
		Ctsa
		Kdelc1
		Scnm1
		Gpc2
		Rbmx
		F630028O10Rik
		Snx5
		Mrps26
		Rrp9
		1110034B05Rik
		1600027N09Rik
		Wdr8
		Neu1
		Mrps10
		Utp11l
		Gdi1
		Cope
		Ccnl2
		Prkcd
		Acad9
		Psmc5
		Sfrs18
		Cep250
		Uros
		Wipi2
		Pdlim7
		Eif4a1
		Zfp523
		Pddc1
		Mus81

		Saal1
		Rabl2
		Atg4b
		Ddx55
		Srp19
		Thoc2
		Tctex1d2
		Arhgap4
		Hps5
		Samhd1
		Emg1
		Gmppb
		Tnip2
		Tia1
		Fxc1
		Mum1
		S100pbp
		Wbp1
		Zranb2
		Snf8
		Phb2
		0610037L13Rik
		Becn1
		Map4k5
		Adsl
		Srsf5
		Ankzf1
		Wdr83
		Psmd4
		M6pr
		Nob1
		Slc50a1
		Haus5
		Farsa
		Dus1l
		Clk2
		Sec63
		Copg
		Smpd4
		Arhgef2
		Arhgef1
		Map4k2
		Bcl6
		Ppp2r4

	Cnbp
	Pnkp
	Tubgcp3
	Slc25a22
	Cenpa
	Trim28
	Skp2
	Aifm1
	Chkb
	Lrrc56
	Jtb
	Use1
	Tcirg1
	Maged1
	Htra2
	Mllt3
	Alkbh6
	Pcyt2
	Arrdc1
	Ino80e
	Mib2
	Adrbk1
	Phkg2
	Plk3
	Phtf1
	Trmu
	Usp5
	Acp2
	D4Wsu53e
	Phc1
	Nsmaf
	D14Ertd668e
	Maged2
	Ptov1
	Ncaph2
	Madd
	Raf1
	5730403B10Rik
	Hace1
	Ilk
	Man2c1
	Sfr1
	Ikbkb
	Igf2

		Spag7
		Dpysl4
		Mamld1
		Slc7a4
		Flt3l
		Pank4
		Renbp
		Ssr4
		Fam50a
		Eif4a2
		Hirip3
		Slc22a17
		Pstpip1
		Dlk1
		Tead3
		Cdca3
		Prrc2a
		Npdc1
		Zfp873
		Hnrnpl
		Rif1
		Hsd3b7
		2310035K24Rik
		Aftph
		Aurkb
		Tmem44
		Cpne1
		Zbtb48
		Pms2
		Wdr75
		3110002H16Rik
		Adamtsl5
		Mrps2
		Smurf1
		Ydjc
		Anxa11
		Ppan
		Fus
		Rnf214
		1700021K19Rik
		Whrn
		Ebf4
		Pqlc3
		Pear1

	Adam33	
	Unc13a	
	Trappc6a	
	0610010K14Rik	
	Ccdc111	
	Sh2b3	
	Znrf1	
	Nfrkb	
	Dpp7	
	Dgkq	
	Eri2	
	Pigq	
	Lypla2	
	Pfas	
	Mis18bp1	
	Lztr1	
	Prdx5	
	Tbc1d17	
	Vldlr	
	Eno2	
	2610507B11Rik	
	Hdac6	
	Cul5	
	Fchsd1	
	Sned1	
	Atg16l1	
	Meis3	
	Nol9	
	Nae1	
	Cdc7	
	Dvl3	
	Sbf1	
	St7	
	Shroom3	
	Abhd11	
	Gramd4	
	Slc2a3	
	Tmed4	
	Atat1	
	Arl2	
	Dapk1	
	Cstf2	
	Maf1	
	Chrd	

	2610039C10Rik	
	Dtx2	
	Slc2a8	
	Crocc	
	Mapre3	
	Itga2b	
	Zfpl1	
	Afap1l1	
	Tank	
	Alx4	
	Sestd1	
	Ndor1	
	1500010J02Rik	
	Mtmr2	
	Trmt2b	
	Trabd	
	Ager	
	Gm7964	
	Ncapg	
	Rpp21	
	Rapgef3	
	Atp1a3	
	Gria3	
	Crtc2	
	Clk1	
	2410002F23Rik	
	Tmem134	
	5830418K08Rik	
	Rint1	
	Dmpk	
	Luc7l	
	Trmt2a	
	Spag5	
	Nle1	
	Clcn3	
	Tmem208	
	Clcf1	
	Stk11	
	Txn2	
	Dcxr	
	Guf1	
	Leprel2	
	BC017158	
	Pcnxl3	

	Setdb1 Aasdh Podn Mat2a Cnot6 Ift80 Eps15 Slc26a10 Tmem209

SE sensitive to HP1γ KO in Females gene symbols (12 genes)	**RI sensitive to HP1γ KO in Females** gene symbols (8 genes)
Aak1 Celf4 Dennd1a Fam171a1 Kcnt2 Lmbr1 Mbp Mtf2 Rims1 Scube1 Sft2d1 Tdp2	Dpysl4 Igf2 Ikbkb Mamld1 Man2c1 Pi16 Sfr1 Spag7

Fig S14. List of genes of which alternative splicing was sensitive to HP1γ KO in males and females respectively. *There are 34 and 12 (skipped exon event) and 258 and 8 genes (retained intron event) that were identified to be affect by HP1γ KO in males and females respectively.*

SE - genes were corrected by HP1γ in Males	RI - genes were corrected by HP1γ in Males
0610011L14Rik	0610037L13Rik
2210015D19Rik	1110034B05Rik
2700081O15Rik	1110038D17Rik
4933431E20Rik	1600027N09Rik
Abi3bp	1810074P20Rik
Apbb2	2400003C14Rik
Armcx1	4930471M23Rik
Ccdc46	5730403B10Rik
Cpa6	9430008C03Rik
Fam73b	Acaa1a
Hsf1	Acad9
Inca1	Acp2
Mrps10	Actr5
Pan2	Adam15
Pif1	Adam8
Rbm39	Adamts10
Sdcbp	Adrbk1
Slc29a3	Adsl
Slco4a1	Aifm1
Srsf11	Alad
Srsf3	Alkbh6
Srsf6	Ampd2
St7	Anapc2
Tcf3	Ankzf1
Tsc2	Arfrp1
Usf2	Arhgap4
Vmn1r90	Arhgef1
Whrn	Arhgef2
Zcrb1	Armcx2
Zfp277	Arrb2
	Arrdc1
	Atg4b
	Atp13a2
	Atp6v0a1
	Baz2b
	Bcas2
	Bcl6
	Becn1
	Brd8
	Ccdc59
	Ccnl2
	Cdc25b

		Cdk16
		Cdk4
		Celf1
		Cenpa
		Cep110
		Chd8
		Chkb
		Ciz1
		Clk2
		Cnbp
		Cnot3
		Cope
		Copg
		Cpsf3l
		Cpsf4
		Ctdsp1
		Ctsa
		Cxcl16
		D4Wsu53e
		Ddx39
		Ddx5
		Ddx55
		Dgkz
		Dmap1
		Dmxl2
		Dom3z
		Dus1l
		Dvl1
		Edc4
		Emg1
		F630028O10Rik
		Fam53a
		Farsa
		Fastk
		Fbxl20
		Fxc1
		Gba2
		Gdi1
		Gnb2
		Golga1
		Gpc2
		Gpn3
		Gtpbp2
		H2-Q4

		H2-T23
		Hace1
		Haus5
		Hdac10
		Hdac3
		Heatr7a
		Hmgn3
		Hps1
		Hps5
		Htra2
		Idh3g
		Ilk
		Ing4
		Ino80e
		Ints2
		Ipo8
		Irf3
		Jtb
		Kdelc1
		Klhdc4
		Lig3
		Lrdd
		Lrrc56
		M6pr
		Madd
		Maged1
		Maged2
		Map4k2
		Map4k5
		Mapk7
		Mars
		Mettl17
		Mib2
		Mllt3
		Mms19
		Mrps10
		Mrps17
		Mrps26
		Msh3
		Mtx1
		Mum1
		Mus81
		Nagk
		Ncaph2

		Ncf1
		Nek8
		Neu1
		Nfatc4
		Nfx1
		Nob1
		Npepl1
		Npr2
		Nr1h2
		Nrbp1
		Nsmaf
		ORF61
		Orc3
		Pafah1b1
		Pak1ip1
		Parp3
		Pcyt2
		Pddc1
		Pdlim7
		Phb2
		Phc1
		Phkg2
		Phtf1
		Pick1
		Pnkp
		Pnpt1
		Polr2e
		Polr2i
		Ppid
		Ppox
		Ppp1cc
		Ppp2r4
		Ppp5c
		Pqlc2
		Prkcd
		Prpf40b
		Psmc5
		Psmd4
		Psrc1
		Ptov1
		Qars
		Rab4b
		Rabep2
		Rabl2

		Raf1
		Rasal3
		Rbmx
		Rfx5
		Rpl10a
		Rpl30
		Rrp9
		Rtel1
		Samhd1
		Scnm1
		Sdccag3
		Sec11c
		Sec63
		Sfrs18
		Sft2d1
		Sgsm3
		Sh3glb2
		Sharpin
		Sirt7
		Skiv2l
		Skp2
		Slc25a22
		Slc30a9
		Slc35b4
		Slc50a1
		Smox
		Snapc4
		Snf8
		Snx5
		Spag9
		Srp19
		Srrm1
		Srsf5
		Stab1
		Stk25
		Stx4a
		Stx5a
		Sugp2
		Surf2
		Taz
		Tbrg1
		Tbxas1
		Tcirg1
		Tctex1d2

	Tecpr1
	Tfe3
	Thoc2
	Tia1
	Tial1
	Timm44
	Tle2
	Tmem198b
	Tmem214
	Tmem87b
	Tnip2
	Top3b
	Trafd1
	Trim28
	Trmt1
	Trmu
	Trp53
	Ttc12
	Tubgcp3
	Txlna
	U2af1l4
	Ufd1l
	Uros
	Use1
	Usp5
	Utp11l
	Vill
	Wbp1
	Wdr11
	Wdr54
	Wdr77
	Wdr8
	Wipi2
	Zfp326
	Zfp384
	Zfp523
	Zranb2

SE - genes were corrected by HP1γ in Females	RI - genes were corrected by HP1γ in Females
Apbb2	0610010K14Rik
Ccdc46	0610037L13Rik
Cdc25c	1110034B05Rik
Cnot2	1110038D17Rik
D6Wsu116e	1500010J02Rik
Enox	1600027N09Rik
Fam73b	1810074P20Rik
Gfra4	2400003C14Rik
Ggnbp1	2410002F23Rik
Inca1	2610039C10Rik
Mprip	2610507B11Rik
Pan2	3110002H16Rik
Pde7a	4930471M23Rik
Prdm5	5830418K08Rik
Rbm39	9430008C03Rik
Sgip1	Acaa1a
Slc29a3	Acad9
Slco4a1	Acp2
Srsf11	Actr5
Srsf6	Adam15
Tpm1	Adam33
Tsc2	Adam8
U2af1l4	Adamts10
Vmn1r90	Adrbk1
Whrn	Adsl
Zfp277	Afap1l1
	Aifm1
	Alad
	Alkbh6
	Ampd2
	Anapc2
	Ankzf1
	Anxa11
	Arfrp1
	Arhgap4
	Arhgef1
	Arhgef2
	Armcx2
	Arrb2
	Arrdc1
	Atat1
	Atg16l1

	Atg4b	
	Atp13a2	
	Aurkb	
	BC017158	
	Baz2b	
	Bcas2	
	Bcl6	
	Becn1	
	Brd8	
	Ccdc59	
	Ccnl1	
	Ccnl2	
	Cdc25b	
	Cdc7	
	Cdca3	
	Cdk16	
	Cdk4	
	Celf1	
	Cenpa	
	Cep250	
	Chd8	
	Chkb	
	Ciz1	
	Clcf1	
	Clk1	
	Clk2	
	Cnbp	
	Cnot6	
	Cope	
	Copg	
	Cpne1	
	Cpsf3l	
	Cpsf4	
	Crocc	
	Crtc2	
	Cstf2	
	Ctdsp1	
	Ctsa	
	D14Ertd668e	
	D4Wsu53e	
	Ddx39	
	Ddx5	
	Ddx55	
	Dgkq	

	Dgkz
	Dmap1
	Dmpk
	Dmxl2
	Dom3z
	Dpp7
	Dtx2
	Dus1l
	Dvl1
	Dvl3
	Edc4
	Eif4a1
	Emg1
	Eps15
	Eri2
	F630028O10Rik
	Fam53a
	Farsa
	Fastk
	Fbxl20
	Fchsd1
	Fxc1
	Gba2
	Gdi1
	Gnb2
	Golga1
	Gpc2
	Gpn3
	Gramd4
	Gtpbp2
	Guf1
	H2-Q4
	H2-T23
	Hace1
	Haus5
	Hdac10
	Hdac3
	Hdac5
	Hdac6
	Heatr7a
	Hmgn3
	Hnrnph1
	Hps1
	Hps5

	Htra2	
	Idh3g	
	Ift80	
	Ilk	
	Ing4	
	Ino80e	
	Ints2	
	Ipo8	
	Irf3	
	Jtb	
	Kdelc1	
	Klhdc4	
	Leprel2	
	Lig3	
	Lrdd	
	Lrrc56	
	Lypla2	
	M6pr	
	Madd	
	Maged1	
	Maged2	
	Map4k2	
	Map4k5	
	Mapk7	
	Mapre3	
	Mars	
	Mat2a	
	Mettl17	
	Mib2	
	Mllt3	
	Mms19	
	Mrps10	
	Mrps17	
	Mrps26	
	Msh3	
	Mthfsd	
	Mtmr2	
	Mtx1	
	Mum1	
	Mus81	
	Nae1	
	Nagk	
	Nat10	
	Ncapg	

	Ncaph2	
	Ncf1	
	Nek8	
	Nfatc4	
	Nfrkb	
	Nfx1	
	Nob1	
	Nol9	
	Npdc1	
	Npepl1	
	Npr2	
	Nr1h2	
	Nrbp1	
	Nsmaf	
	ORF61	
	Orc3	
	Parp3	
	Pcnxl3	
	Pcyt2	
	Pddc1	
	Pdlim7	
	Pfas	
	Phb2	
	Phc1	
	Phkg2	
	Phtf1	
	Pick1	
	Pms2	
	Pnkp	
	Pnpt1	
	Polr2e	
	Polr2i	
	Ppan	
	Ppid	
	Ppox	
	Ppp1cc	
	Ppp2r4	
	Ppp5c	
	Pqlc2	
	Pqlc3	
	Prkcd	
	Prpf40b	
	Psmc5	
	Psmd4	

	Psrc1
	Ptov1
	Qars
	Rab4b
	Rabep2
	Rabl2
	Raf1
	Rapgef3
	Rasal3
	Rbmx
	Rcbtb2
	Rfx5
	Rif1
	Rnf214
	Rpl10a
	Rpl30
	Rpp21
	Rtel1
	S100pbp
	Saal1
	Samhd1
	Sbf1
	Scnm1
	Sdccag3
	Sec11c
	Setdb1
	Sfrs18
	Sft2d1
	Sgsm3
	Sh3glb2
	Sharpin
	Sirt7
	Skiv2l
	Skp2
	Slc25a22
	Slc2a8
	Slc30a9
	Slc35b4
	Slc50a1
	Slc7a4
	Smox
	Smpd4
	Smurf1
	Snapc4

	Sned1	
	Snf8	
	Spag5	
	Spag9	
	Srp19	
	Srrm1	
	Srsf5	
	St7	
	Stab1	
	Stk11	
	Stk25	
	Stx4a	
	Stx5a	
	Sugp2	
	Surf2	
	Tank	
	Taz	
	Tbc1d17	
	Tbrg1	
	Tbxas1	
	Tcirg1	
	Tctex1d2	
	Tead3	
	Tecpr1	
	Tfe3	
	Thoc2	
	Tial1	
	Timm44	
	Tle2	
	Tmed4	
	Tmem134	
	Tmem198b	
	Tmem209	
	Tmem214	
	Tmem44	
	Tmem87b	
	Tnfaip2	
	Tnip2	
	Top3b	
	Tor1b	
	Trabd	
	Trafd1	
	Trappc6a	
	Trim28	

	Trmt1
	Trmt2b
	Trmu
	Trp53
	Tubgcp3
	Txlna
	U2af1l4
	Ubc
	Ufd1l
	Uros
	Usp5
	Utp11l
	Vill
	Vldlr
	Wbp1
	Wdr11
	Wdr54
	Wdr77
	Wdr8
	Wdr83
	Wipi2
	Zbtb17
	Zbtb48
	Zfp326
	Zfp384
	Zfp523
	Zfpl1
	Zranb2

Fig S15. Genes that were equalized with respect to SE between the sexes in males and genes that acquired difference between the sexes in females with respect to SE upon HP1γ KO. *There is a reduction in the number of genes that are sexually dimorphic spliced in males and in females there is an increase in the number of genes that are still sexually dimorphic spliced. These gene lists were obtained by comparing between Venn diagrams illustrated in Fig 4.3.6 vs Fig 4.3.7 and Fig 4.3.6 vs Fig 4.3.8.*

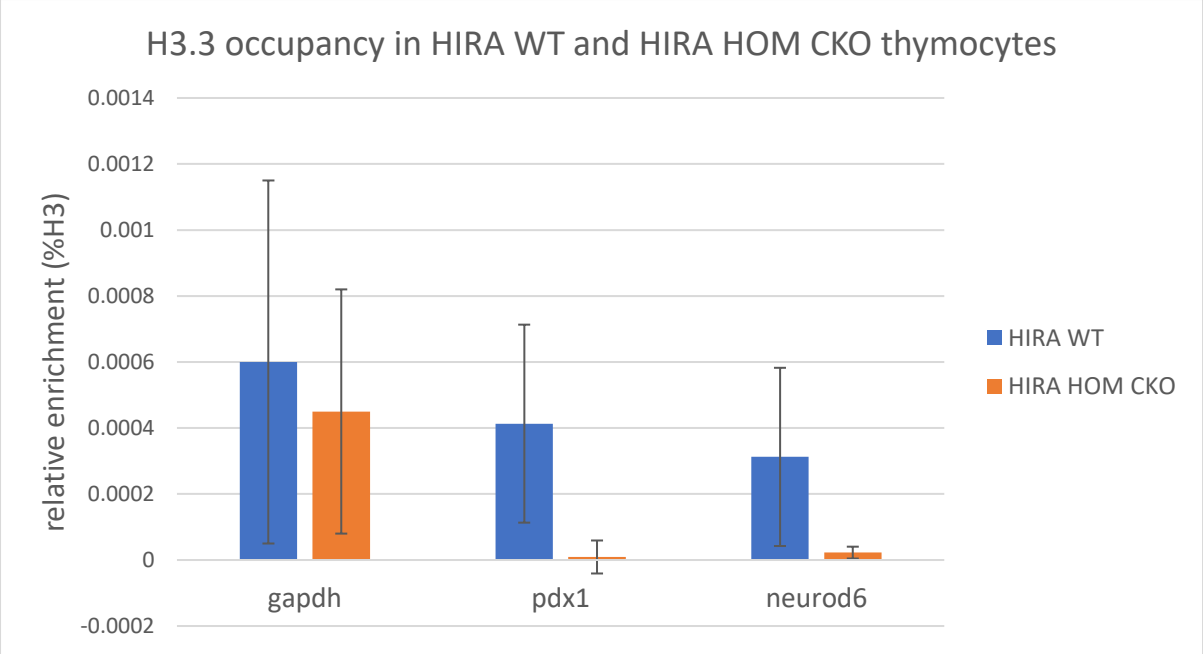

Fig S16. ***Relative enrichment of H3.3 on Gapdh, Pdx1 and Neurod6 genes in HIRA WT and HIRA HOM CKO thymocytes as revealed by ChIP.*** *Upon HIRA KO, the enrichment of H3.3 was reduced. But this anti-H3.3 antibody gave a very signal on all genes and the big error bar indicates that the variation between biological samples is big. Error bars: SEM. n=4 (biological replicates). Error bars: SEM.*